

TUM School of Engineering and Design

**Material Properties of Bacterial Biofilms and Bioinspired  
Synthetic Hydrogels**

a thesis presented by

Martin Kretschmer



Technische Universität München





Technische Universität München

TUM School of Engineering and Design

# **Material Properties of Bacterial Biofilms and Bioinspired Synthetic Hydrogels**

Martin Kretschmer

Vollständiger Abdruck der von der  
TUM School of Engineering and Design der Technischen Universität München  
zur Erlangung eines Doktors der Ingenieurwissenschaften (Dr.-Ing.)  
genehmigten Dissertation.

Vorsitz: Prof. Dr. techn. Peter Mayr

Prüfer\*innen: 1. Prof. Dr. rer. nat. Oliver Lieleg

2. Prof. Dr.-Ing. habil. Aldo R. Boccaccini

Die Dissertation wurde am 29.11.2021 bei der Technischen Universität München eingereicht und durch die TUM School of Engineering and Design am 01.04.2022 angenommen.



## Summary

Bacterial biofilms exhibit complex properties, many of which serve the purpose to protect the embedded bacterial cells against external influences, such as mechanical stress, toxic substances, and desiccation. To fulfill these tasks, the biofilm matrix is composed of a variety of different molecules and can exhibit a complex internal structure and surface topography. For humans, biofilms can be desired or undesired, depending on the bacterial species and the location of biofilm growth. On the one hand, undesired biofilms cause problems for human health and are a burden for industrial facilities. On the other hand, desired biofilms can be used to produce certain substances, to treat wastewater, to support plant growth in agriculture, or to alter the properties of construction materials (e.g. mortar). For both, biofilm removal and cultivation, it is important to be aware of their material properties and to find possibilities to adjust them. Moreover, by understanding the molecular mechanisms responsible for the biofilm material behavior, it is possible to design synthetic materials (e.g. hydrogels) with similar properties; then, those bio-inspired gels can fulfill tasks in technical applications which cannot be accomplished by simple hydrogels.

In the first part of this thesis, the material properties of bacterial biofilms are investigated. The erosion stability, rheology, and wetting behavior of *Bacillus subtilis* NCIB 3610 biofilms are analyzed to investigate inter-dependencies between these material properties. Furthermore, for *Bacillus subtilis* NCIB 3610 biofilm mutants that lack one of the major matrix components (i.e. the exopolysaccharides, TasA, or BslA), a reduced erosion resistance is observed, which seems to be due to a reduced biofilm hydrophobicity and stiffness. Also the effects of certain metal cations, that increase the stiffness of biofilms, are examined in regard to the erosion stability: biofilms with an increased stiffness exhibit an increased erosion resistance; however, also other factors, such as the adhesion and wetting behavior of biofilms is found to play a role.

To investigate the microscopic mechanisms by which cations increase the biofilm stiffness and to clarify why only certain cations show this effect, further tests with *Bacillus subtilis* B-1 and *Azotobacter vinelandii* biofilms are conducted. The obtained results suggest that, most likely, the observed stiffness increase is due to ionic cross-links of polyanionic biomacromolecules that are major components of the biofilm matrix. These relevant biomacromolecules are  $\gamma$ -PGA for *B. subtilis* B-1 biofilms, and alginate for *A. vinelandii* biofilms. Two parameters seem to decide whether biofilm stiffening occurs or not: the ionic size and the configuration of the polyanionic biomacromolecules.

To investigate the biofilm detachment behavior and to analyze the influence of biofilm adhesion and cohesion on this phenomenon, a new measurement setup was developed. This measurement setup is based on a commercial rheometer and allows for applying "pure" normal forces to a biofilm to analyze its detachment behavior *in situ*. By analyzing the biofilm material transfer,

conclusions are drawn about the dominant mode of fracture: biofilms with a high stiffness and high water repellency are less prone to material transfer in such a detachment event and thus tend to show adhesive failure rather than cohesive failure.

In a fourth study, a bioreactor is developed to cultivate *Bacillus subtilis natto* biofilms in a continuous, autonomous manner. *B. subtilis natto* biofilms can be used as additives to cementitious materials to increase their water repellency; thus, high amounts are needed. Moreover, the cultivation of *B. subtilis* biofilms requires specific conditions, such as a moisture and nutrient supply provided from the growth substrate. With this novel bioreactor, which is based on a rotating cylinder, these conditions can be fulfilled, and biofilm can be cultivated on a membrane surface at the solid/gas interface. It is shown, that the biofilm produced with this reactor exhibits similar material properties compared to conventional *B. subtilis natto* biofilm cultivated in petri dishes, and that the harvested biofilm increases the water repellency of mortar as expected.

In the second part of this thesis, the viscoelastic properties of synthetic hydrogels that are inspired by biological systems, are investigated. First, the linear and non-linear behavior of two different carbodiimide fueled Fmoc-peptide systems (*i.e.* Fmoc-AAD and Fmoc-AVD) are examined. It is shown, that the viscoelastic behavior of the formed gels is tunable by the amount of fuel and by an alteration of the peptide sequence. Moreover, the concentration of the reaction waste product is identified to influence the behavior of these chemically fueled hydrogels. In another study, the self-healing properties of Fmoc-AAD hydrogels are investigated. Here, it is observed, that - due to their dynamic character - these gels show a certain ability to recover their initial stiffness after their disruption by high shear forces.

Together, these findings help unravelling the underlying principles governing the material properties of bacterial biofilm and how they influence each other; such insights help identifying new strategies to support biofilm removal and cultivation. Moreover, the presented bioinspired synthetic hydrogels show the potential to be used as temporary programmable sealings for applications, in which they are challenged by mechanical forces, such as in microfluidic systems or as components in micro-robotics.

## Zusammenfassung

Bakterielle Biofilme weisen komplexe Eigenschaften auf, welche in erster Linie dem Schutz der eingebetteten Bakterien gegen äußere Einflüsse dienen. Dies umfasst den Schutz vor mechanischen Belastungen, toxischen Substanzen und Austrocknung. Um diese Anforderungen zu erfüllen ist die Biofilmmatrix aus einer Vielzahl an unterschiedlichen Molekülen aufgebaut und kann eine komplexe innere Struktur sowie Oberflächenbeschaffenheit aufweisen. Je nachdem um welche Bakterienart es sich handelt und wo diese auftreten, können Biofilme für den Menschen sowohl erwünscht als auch unerwünscht sein. Unerwünschte Biofilme können gesundheitliche Probleme beim Menschen hervorrufen, aber auch problematisch für industrielle Anwendungen werden. Andererseits können nützliche Biofilme bestimmte Substanzen produzieren, Biofilme können der Abwasseraufbereitung dienen und es können mit der Zugabe von Biofilmen die Eigenschaften von Baustoffen wie Mörtel verbessert werden. Sowohl für die Bekämpfung als auch für die Kultivierung von bakteriellen Biofilmen ist es wichtig deren Materialeigenschaften zu verstehen und Möglichkeiten zu finden, mit denen diese verändert werden können. Darüber hinaus ermöglicht die detaillierte Kenntnis der molekularen Mechanismen, welche den Materialeigenschaften von Biofilmen zugrunde liegen, die Entwicklung künstlicher Materialien (z. B. synthetische Hydrogele), mit vergleichbaren Eigenschaften. Solche bioinspirierten Gele könnten Aufgaben in technischen Anwendungen erfüllen, die von einfachen Hydrogelen nicht geleistet werden können.

Im ersten Teil dieser Dissertation werden die Materialeigenschaften von bakteriellen Biofilmen untersucht. Der Erosionswiderstand, die Rheologie und das Benetzungsverhalten von *Bacillus subtilis* NCIB 3610 Biofilmen werden analysiert um mögliche Abhängigkeiten zwischen diesen Materialeigenschaften entschlüsseln zu können. Für Mutanten von *Bacillus subtilis* NCIB 3610 Biofilmen, die einen bestimmten Hauptbestandteil (d. h. die Exopolysaccharide, oder die Proteine TasA oder BslA) nicht enthalten, wird ein reduzierter Erosionswiderstand festgestellt. Die Ursache hierfür scheint die verringerte Hydrophobizität und Steifigkeit dieser Biofilmmutanten zu sein. Darüber hinaus wird der Effekt von Metallkationen auf den Erosionswiderstand der Biofilme untersucht. Bestimmte Metallkationen führen zu einer Erhöhung der Biofilmsteifigkeit und somit auch zu einem höheren Erosionswiderstand. Allerdings spielen auch andere Faktoren, wie das Benetzungsverhalten und die Adhäsion der Biofilme, hierbei eine Rolle.

Um zu untersuchen welche Mechanismen dazu führen, dass die Steifigkeit von Biofilmen durch die Zugabe bestimmter Metallkationen erhöht wird, werden weitere Versuche mit Biofilmen der Bakterienarten *Bacillus subtilis* B-1 und *Azotobacter vinelandii* durchgeführt. Die Ergebnisse legen nahe, dass die Steifigkeitserhöhung auf ionischen Quervernetzungen der polyanionischen Biomakromoleküle beruht, welche Hauptbestandteile der Biofilmmatrix sind. Als relevante Biomakromoleküle werden  $\gamma$ -PGA für den Biofilm von *B. subtilis* B-1 und Alginat für den Biofilm von

*A. vinelandii* identifiziert. Dabei scheinen zwei Parameter zu entscheiden, ob eine Steifigkeitserhöhung bei Kontakt mit Metallkationen auftritt oder nicht: der Ionenradius und die Struktur der polyanionischen Biomakromoleküle.

Um den individuellen Einfluss der Biofilmadhäsion und -kohäsion auf das Ablösungsverhalten von Biofilmen zu bestimmen, wird ein neuartiger Messaufbau entwickelt. Das Messverfahren basiert auf einem kommerziellen Rheometer und ermöglicht es „reine“ Normalkräfte auf die Biofilmprobe aufzubringen um das Ablösungsverhalten und die dafür notwendige Kraft *in situ* zu bestimmen. Durch die Analyse des Materialtransfers der Biofilmprouben ist es möglich Rückschlüsse über die vorherrschende Bruchart zu ziehen: Biofilme mit einer hohen Steifigkeit und starken wasserabweisenden Eigenschaften zeigen in den Versuchen nur einen geringen Materialtransfer und neigen somit eher zu Adhäsionsbrüchen als zu Kohäsionsbrüchen.

In einer vierten Studie wird ein Bioreaktor für die kontinuierliche Kultivierung von *Bacillus subtilis natto* Biofilmen entwickelt. Biofilme dieser Bakterienart können als Zusatzstoffe für zementöse Werkstoffe verwendet werden um deren wasserabweisenden Eigenschaften zu verbessern. Hierfür werden jedoch größere Mengen des Biofilms benötigt, und die Kultivierung dieses Biofilms stellt spezielle Anforderungen, z. B. eine Feuchtigkeits- und Nährstoffzufuhr über das Bodensubstrat. Dies kann mit dem neuartigen Bioreaktor erfüllt werden, welcher auf einer rotierenden Walze basiert. Der Biofilm wird hier auf einer Membranoberfläche an der Grenzfläche zwischen Festkörper und Luft kultiviert. Es konnte gezeigt werden, dass der mit dem Bioreaktor produzierte Biofilm vergleichbare Materialeigenschaften aufweist, wie konventionell in Petrischalen gezüchteter *B. subtilis natto* Biofilm. Zudem führt der mit dem Reaktor produzierte Biofilm, entsprechend der Erwartung, auch zu einer Erhöhung der wasserabweisenden Eigenschaften von Mörtel.

Im zweiten Teil dieser Dissertation werden die viskoelastischen Eigenschaften von synthetischen Hydrogelen untersucht, die von biologischen Systemen inspiriert sind. Zunächst wird das lineare und nicht-lineare Verhalten von zwei unterschiedlichen Fmoc-Peptidsystemen (Fmoc-AAD und Fmoc-AVD) untersucht. Durch Selbstassemblierung sind diese Peptidsysteme dazu in der Lage, unter Verbrauch eines Carbodiimid-Treibstoffes Hydrogele zu bilden. Es wird gezeigt, dass das viskoelastische Verhalten dieser Hydrogele durch die Menge an Treibstoff und eine Änderung der Peptidsequenz eingestellt werden kann. Darüber hinaus wird festgestellt, dass die Konzentration des Abfallproduktes der Aktivierungsreaktion das Gellierungsverhalten und die Materialeigenschaften dieser Hydrogele beeinflusst.

In einer weiteren Studie werden die selbstheilenden Eigenschaften von Fmoc-AAD Hydrogelen untersucht. Hier wird festgestellt, dass diese Hydrogele eine gewisse Fähigkeit aufweisen ihre Steifigkeit nach einer mechanischen Belastung wiederherzustellen. Diesem Phänomen liegt der



dynamische Reaktionszyklus zugrunde, der zu einer ständigen Aktivierung und Deaktivierung der Peptidassemblierung führt, solange Treibstoff im System vorhanden ist.

Zusammengenommen helfen diese Untersuchungen die Prinzipien zu verstehen, welche den Materialeigenschaften von bakteriellen Biofilmen zugrunde liegen; ferner geben sie Aufschluss, wie die unterschiedlichen Eigenschaften der Biofilme miteinander zusammenhängen. Diese Erkenntnisse können helfen, neue Strategien für die Bekämpfung und Kultivierung von bakteriellen Biofilmen zu finden. Darüber hinaus zeigen die vorgestellten bioinspirierten, synthetischen Hydrogele das Potential als temporäre programmierbare Abdichtungen in Anwendungen zu dienen, in welchen sie mechanischen Belastungen ausgesetzt sind. Möglich sind hier Anwendungen in Mikrofluidiksystemen oder der Einsatz als Komponenten in der Mikrorobotik.



# Contents

1.	Introduction.....	1
1.1	Biofilm formation .....	1
1.2	Biofilm material properties and composition .....	2
1.3	Bacterial biofilms in natural and man-made environments .....	4
1.4	Biofilm characterization methods .....	6
1.5	Biofilm-inspired biological and synthetic hydrogels .....	7
1.6	Key findings of this thesis .....	8
2.	Materials.....	11
2.1	Bacterial biofilms.....	11
2.2	Polyanionic biomacromolecules.....	11
2.3	Metal ions.....	12
2.4	Fmoc based hydrogels.....	13
3.	Theoretical background and methods .....	15
3.1	Biofilm cultivation .....	15
3.2	Bioreactors .....	16
3.3	Rheology.....	17
3.3.1	Measurement basics .....	17
3.3.2	Determination of the frequency dependent shear behavior.....	19
3.3.3	Determination of gelation behavior.....	20
3.3.4	Non-linear rheology.....	21
3.4	Detachment tests .....	23
3.5	Biofilm wetting behavior .....	24
4.	Summaries of publications .....	27
4.1	Importance of the biofilm matrix for the erosion stability of <i>Bacillus subtilis</i> NCIB 3610 biofilms 27	
4.2	Chelate chemistry governs ion-specific stiffening of <i>Bacillus subtilis</i> B-1 and <i>Azotobacter vinelandii</i> biofilms .....	29
4.3	Biofilm adhesion to surfaces is modulated by biofilm wettability and stiffness.....	31
4.4	A rotating bioreactor for the production of biofilms at the solid-air interface .....	33
4.4.1	Abstract .....	33
4.4.2	Introduction .....	33
4.4.3	Materials and Methods .....	34
4.4.4	Results and Discussion .....	39
4.4.5	Conclusion .....	50

4.5	Viscoelastic behavior of chemically fueled supramolecular hydrogels under load and influence of reaction side products.....	51
4.6	Self-healing fiber network formed by chemically fueled self-assembly .....	53
5.	Discussion .....	61
6.	Outlook .....	71
	Appendix.....	73
A.	Full text of publications presented in this thesis .....	75
A.1	Importance of the biofilm matrix for the erosion stability of <i>Bacillus subtilis</i> NCIB 3610 biofilms .....	75
A.1.1	Supplementary information for: Importance of the biofilm matrix for the erosion stability of <i>Bacillus subtilis</i> NCIB 3610 biofilms .....	84
A.2	Chelate chemistry governs ion-specific stiffening of <i>Bacillus subtilis</i> B-1 and <i>Azotobacter vinelandii</i> biofilms .....	89
A.2.1	Supplementary information for: Chelate chemistry governs ion-specific stiffening of <i>Bacillus subtilis</i> B-1 and <i>Azotobacter vinelandii</i> biofilms .....	100
A.3	Biofilm adhesion to surfaces is modulated by biofilm wettability and stiffness .....	107
A.3.1	Supplementary information for: Biofilm adhesion to surfaces is modulated by biofilm wettability and stiffness .....	120
A.4	Viscoelastic behavior of chemically fueled supramolecular hydrogels under load and influence of reaction side products.....	133
A.4.1	Supplementary information for: Viscoelastic behavior of chemically fueled supramolecular hydrogels under load and influence of reaction side products.....	143
B.	Licenses for publications .....	157
B.1	Importance of the biofilm matrix for the erosion stability of <i>Bacillus subtilis</i> NCIB 3610 biofilms .....	157
B.2	Chelate chemistry governs ion-specific stiffening of <i>Bacillus subtilis</i> B-1 and <i>Azotobacter vinelandii</i> biofilms .....	163
B.3	Biofilm adhesion to surfaces is modulated by biofilm wettability and stiffness.....	169
B.4	Viscoelastic behavior of chemically fueled supramolecular hydrogels under load and influence of reaction side products.....	175
C.	Full list of publications.....	177
C.1	Peer-reviewed .....	177
C.2	Not peer-reviewed yet .....	177
D.	Bibliography .....	179
E.	Acknowledgements .....	191

# 1. Introduction

Bacteria are ubiquitous and occur on almost every surface in the natural and man-made environment [1]. They can exist as planktonic cells in liquid media, or they embed themselves into self-produced extracellular polymeric substances (EPS) as protection against external influences. The resulting slimy and sticky substances are called biofilms. On the one hand, biofilms can be problematic for human health and industrial facilities, as they can lead to disease and high economic costs [2, 3]. On the other hand, biofilms can also have beneficial functions, such as in the agriculture or for wastewater treatment [4-7]. Both, for combating unwanted biofilms and for the specific cultivation of beneficial biofilms, it is important to be aware of their material properties and the underlying physical and chemical principles. However, due to the biological and biochemical complexity of biofilms, these principles are not well understood.

The majority of bacteria tend to form biofilms on solid surfaces, depending on the species either at the solid/gas or solid/liquid interface [1]. Another form of bacterial communities are pellicles, which are formed on liquid surfaces. The biofilm matrix protects the bacteria against certain antibiotics, biocides and metal cations, ultra violet radiation, shear stress, and desiccation [8]. For instance, the resistance against certain antibiotics, biocides and chemicals can be up to 1500 times higher for biofilm bacteria than for planktonic bacterial cells [9]. In natural environments, biofilms can be found on rocks, plant roots, teeth, and in the soil [10-12]. Technical materials that are prone to biofilm formation are metals, ceramics, construction materials, and plastics (e.g., on ship hulls, harbor installations, pipes, tubes, implants, and catheters) [13-17]. To grow on a surface, a sufficient nutrient supply, moisture, and a certain temperature level are most important for the bacteria. However, bacteria can also survive in extreme conditions, such as at very low temperatures below the freezing point of water or in dry periods. In these circumstances, their metabolism is shut down: As spores, bacterial cells can survive over long time periods without any metabolic activity; as soon as the conditions become better, their metabolism is reactivated [18, 19].

A well investigated bacterial species is *Bacillus subtilis*, including its subspecies *Bacillus subtilis* NCIB 3610, *Bacillus subtilis natto* and *Bacillus subtilis* B-1 [20-22]. These bacteria form biofilms preferably at the solid/gas or liquid/gas interface. Thus, in nature, they occur predominantly as pellicles on stagnant water or as terrestrial biofilms in the soil and on plant roots [1, 20, 23]. Another bacterial species that forms biofilms on plant roots is *Azotobacter vinelandii* [5]. In contrast to these species, marine bacteria, e.g. those of the genus *Roseobacter*, form biofilms in aqueous conditions at solid surfaces submerged in water [13, 24].

## 1.1 Biofilm formation

Biofilm formation on solid surfaces is a multistage mechanism that is initiated by the adhesion of individual bacterial cells. As soon as the bacteria attach to the surface, they start to produce

EPS to embed themselves. Thereby, the bacterial cells connect to each other and establish a permanent colony on the substrate [1, 8, 9]. Here, different bacterial cells of the same species can perform different tasks and secrete different biomolecules. Cells that produce EPS are stationary and do not separate. In addition to these cells, also motile cells and spores are present in a biofilm [1]. During maturation, a biofilm can reach thicknesses of several millimeters and is able to spread laterally. Lateral spreading is enabled by the EPS that generates osmotic pressure gradients [1]. Some biomacromolecules, *e.g.* TasA and BslA in *B. subtilis* NCIB 3610 biofilms, are known to self-assemble and lead to complex biofilm architectures and topographical structures. Mature biofilms can even exhibit channels and pores to support nutrient intake [8, 25, 26]. The morphology of a biofilm can be smooth and flat, rough, fluffy, or filamentous and depends on different factors such as hydrodynamic conditions, nutrient supply, bacterial motility, and inter-cellular communication [8]. In the last step of biofilm development, certain parts are dispersed and thus individual bacterial cells and spores are released into the surrounding medium to colonize new surfaces [1, 8, 9]. This mechanism is triggered by the bacteria themselves, which degrade their own matrix; this can be necessary due to the accumulation of metabolic products or other toxic substances in the biofilm [8, 25, 26]. For this, enzymes and small molecules such as dextran, inulin, levan and D-amino acids are secreted by some bacterial cells [1, 8, 27, 28]. D-amino acids detach the cells from the matrix and thus lead to the release of cells into the environment. Also the formation of channels within the biofilm is achieved by matrix degrading molecules such as D-amino acids. Examples of biofilms in which D-amino acids are produced for its degradation are *B. subtilis* and *Pseudomonas aeruginosa* [27].

### *1.2 Biofilm material properties and composition*

The EPS of bacterial biofilms is composed of a variety of different molecules, which are largely responsible for the architecture and material properties of the biofilm. The main components of typical biofilm matrices are lipids, proteins, polysaccharides, nucleic acids and water [8]. In most biofilms, only 10% of the dry weight corresponds to bacterial cells, whereas the EPS constitutes 90% [8]. However, the exact compositions vary strongly in dependence of the bacterial species and growth conditions.

The internal forces of the biofilm, that hold the EPS molecules and bacterial cells together (thus providing cohesion) are mainly established by polysaccharides, proteins and eDNA (**Figure 1**) [8]. This cohesion affects the viscoelastic properties of a biofilm and determines its resistance against shear forces, erosion and gravity induced material flow. For *B. subtilis* NCIB 3610 bacteria, the structural development and consistency of the formed biofilm is largely influenced by exopolysaccharides (*i.e.*, gene products of the *epsA-O* operon) in combination with the fiber forming protein TasA [1, 8, 29, 30]. The latter is mainly responsible for connecting the bacterial cells with each other [1, 30, 31]. A major component of *B. subtilis* B-1 biofilm is the polyanionic polypeptide gamma-poly-DL-glutamic acid ( $\gamma$ -PGA), and this molecule influences the biofilm

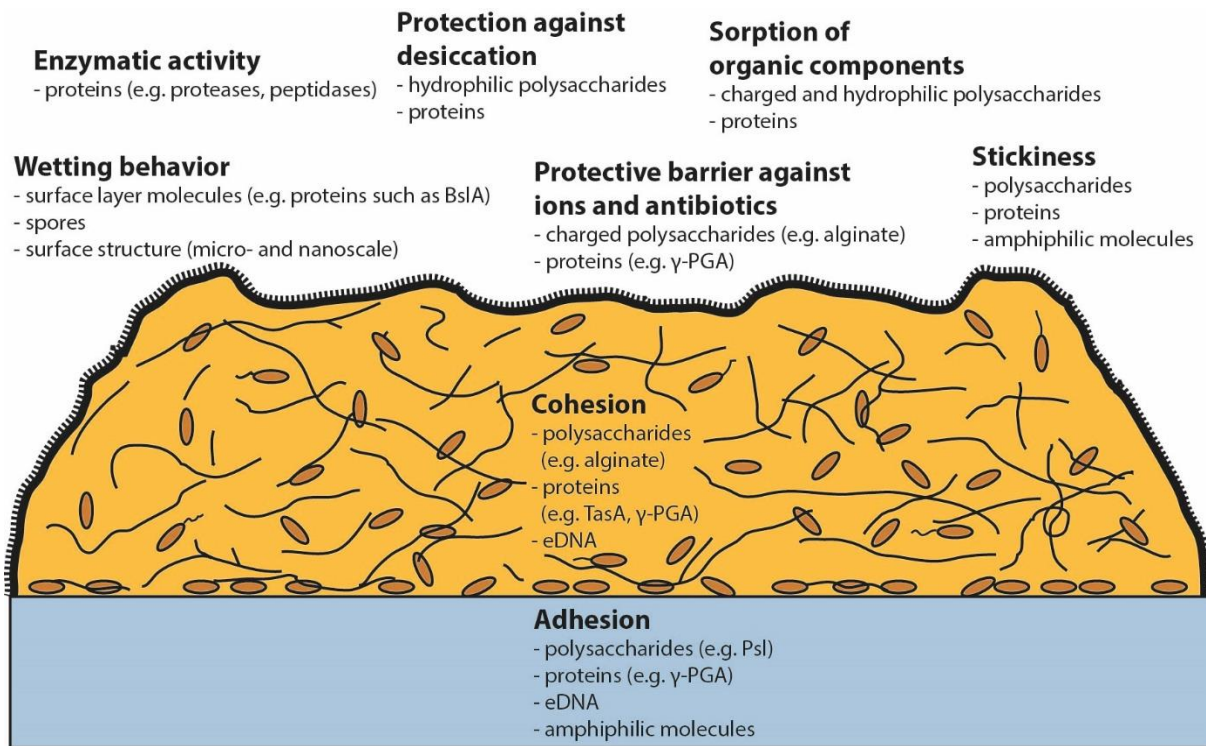
consistency here [1, 32, 33]. Another polyanionic biomacromolecule that is important for the viscoelastic properties of certain biofilms, is the polysaccharide alginate. This macromolecule is produced by *A. vinelandii*, *P. aeruginosa* and other bacteria from the genus *Pseudomonas* [34, 35].

The interactions between molecules and/or cells, that are responsible for the cohesion of the biofilm, are mostly hydrogen bonds, van der Waals interactions, electrostatic attractive forces (e.g. chelate complexes), dipole-dipole interactions and mechanical interactions [8, 36]. In most cases, natural biofilms can be described as viscoelastic solids and exhibit stiffness values between a few hundred Pa to several kPa (depending on the bacterial species). However, the biofilm stiffness can be increased up to 1000-fold, by exposure to certain metal ions [33, 37-39]. Also in the non-linear viscoelastic regime, the material behavior can vary for different bacterial species. For biofilm of *Bacillus subtilis* 168 and *P. aeruginosa*, strain weakening was observed in the non-linear viscoelastic regime [38, 40], whereas the biofilms of *Klebsiella pneumoniae* and *Staphylococcus epidermidis* show a strain hardening response [41]. A curious material property of biofilms is their ability to self-heal. Here, the material regains its initial viscoelastic properties (i.e. its stiffness) autonomously after it was disrupted by mechanical forces. Such a behavior was observed for *P. aeruginosa* biofilms [38].

However, the excellent resistance of biofilms against normal- and shear forces cannot be explained by their good cohesion alone; the adhesion behavior of biofilms is equally important for their ability to resist these mechanical forces. Adhesion is mainly established by polysaccharides, proteins, eDNA and amphiphilic molecules (**Figure 1**) [8]. For example, in *Bacillus cereus* biofilms, adhesion is mainly brought about by eDNA [42], and for *P. aeruginosa*, the exopolysaccharide Psl is involved in biofilm adhesion [43]. For *B. subtilis* biofilms,  $\gamma$ -PGA is reported to increase the surface adhesion of bacterial cells [36, 44].

Also the surface properties of biofilms, such as the wetting behavior and stickiness towards objects from the environment, are crucial for the bacterial communities. These properties are defined by molecules located close to the surface and the surface structure. Certain biofilms are able to repel a broad range of fluids ranging from water to oils [37, 45, 46]. Hydrophobic molecules at the surface in combination with a micro- and nanoscale roughness can even lead to superhydrophobic biofilms [47]. The hydrophobic properties of *B. subtilis* NCIB 3610 biofilms are largely dependent on the surface protein BslA, which is an amphiphilic protein that self-assembles at the biofilm surface [48]. Furthermore, spores can be responsible for the hydrophobicity of biofilms as well [49]. The level of protection against erosion and toxic substances (such as solutions of antibiotics or metal ions) is enhanced when the biofilm wetting resistance is high [33, 37, 46, 50]: When a biofilm is poorly wetted, its interactions with liquids and dissolved molecules are considerably reduced [46, 50]. However, even when bacterial biofilms are well wetted, the diffusive entry of molecules still can be prevented [51-53]. Here, the macromolecules of the

EPS are responsible: some macromolecules can specifically bind and thus inactivate certain ions or molecules. Such binding events can be established by different components of the EPS, which can feature apolar regions, groups with hydrogen-bonding potential, anionic groups (e.g. in proteins or polysaccharides) and cationic groups (e.g. in amino sugars) (Figure 1) [8, 54]. For example, the polyanionic biomacromolecules  $\gamma$ -PGA and alginate are suspected candidates of the EPS involved in regulating the diffusive entry and penetration of molecules [33, 34].



**Figure 1:** Central properties of bacterial biofilms and the corresponding matrix components [8, 48, 54].

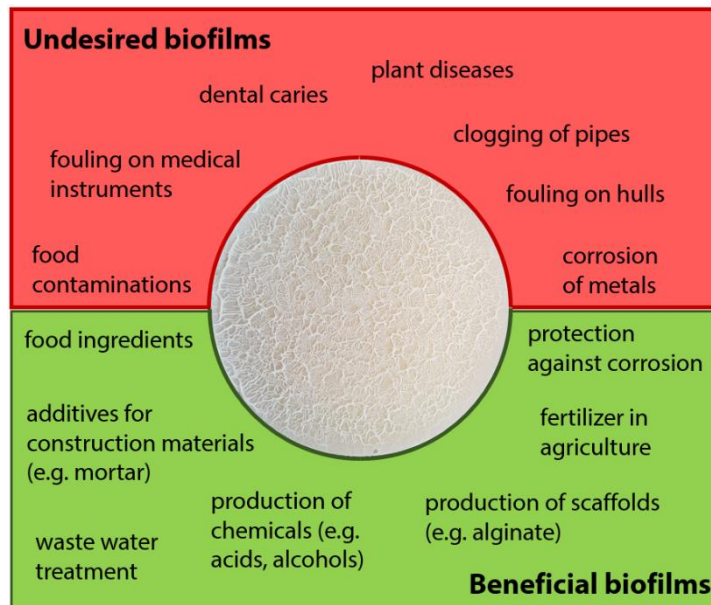
### 1.3 Bacterial biofilms in natural and man-made environments

In many cases, biofilms are undesired, since they can pose a threat for human health and lead to economic costs for the industry (Figure 2). Pathogenic biofilms can cause different diseases [2, 55]: Biofilm formation on medical instruments, such as catheters, can induce infections, and biofilms are also responsible for dental caries [2, 11, 16, 17, 44]. Moreover, cystic fibrosis is caused by the biofilm forming bacteria *P. aeruginosa* [56]. Also in industrial facilities, biofilms can cause problems, since they can promote corrosion of metals, plug tubes and pipes and the formation of biofilms on hulls increases the fuel consumption [3, 13, 57]. Furthermore, biofilms can lead to contaminations during food production and plant pathogens are problematic for agriculture [58-64]. Therefore, it is often required to combat these biofilms efficiently or to prevent their formation in the first place.

However, it can also be desirable to cultivate bacterial biofilms for certain purposes (Figure 2). The bacterial communities in the human gastro-intestinal system are essential for our metabo-



lism and immune system [65-67], bacteria can be used as food additives, and probiotic bacteria support human digestion [68, 69]. In the traditional Japanese dish nattō, *B. subtilis natto* forms a biofilm and ferments soy beans [70]. In agriculture, bacteria are used to increase the harvest yield, since some bacterial species (such as *B. subtilis* and *A. vinelandii*) live in symbiosis with certain plants. Here, the bacteria form biofilms on the roots and secrete antimicrobial compounds to protect the plants from pests such as pathogenic bacteria (e.g. *Erwina* and *Pseudomonas* strains), fungi and nematodes [1, 4, 5, 23, 44, 71, 72]. In industrial facilities, selected biofilms can be used to reduce the corrosion rates of steel [73, 74]: For example, biofilm of *Bacillus brevis* 18-3 is capable of reducing the corrosion of mild steel by inhibiting sulfate-reducing and iron-oxidizing bacteria [73]. Another application of biofilms is wastewater treatment. Here, the biofilms are submerged in water and secrete specific molecules and enzymes (e.g. proteases and peptidases) that clean the water [1, 6-8, 44, 75, 76]. Bacteria and bacterial biofilms are also used to produce substances such as vinegar, acids, alcohols and scaffolds (e.g. made of alginate or cellulose) [44, 77-80]. Moreover, biofilms can be used as additives for materials to establish specific properties. For example, the addition of bacterial biofilms from the genus *Bacillus subtilis* to mortar or other cementitious materials can induce a reduced wettability and water uptake of these materials [81-83]. This enhances the resistance against moisture and thus their lifetime. Usually, the cultivation of large biofilm amounts (for example for wastewater treatment) occurs in bioreactors [84]. Here, the biofilms are attached to fixed or fluidized surfaces or particles and submerged in water [85, 86]. However, to cultivate specific biofilms, such as those from the bacterial species *B. subtilis* (which can be used as an additive to mortar) these common bioreactors are not suitable. For *B. subtilis* biofilms, a dedicated bioreactor is necessary, in which the biofilm is cultivated at the solid/gas interface with a nutrient and moisture supply provided from the growth substrate, since *B. subtilis spec.* does not tend to form biofilms on surfaces submerged in water [20]. Technical solutions for this particular type of bioreactor are, however, scarce.



**Figure 2:** Overview of different environmental and industrial sectors in which biofilms either cause problems or offer beneficial impacts.

### 1.4 Biofilm characterization methods

Both, for the removal and the specific cultivation of bacterial biofilms, it is crucial to be aware of their material properties and to understand the underlying physical and chemical principles. Due to different compositions and architectures of biofilms from different bacterial species, their properties can vary strongly. Moreover, even biofilms created by an individual species can have properties that vary dependent on the growth conditions. This makes a prediction of biofilm properties difficult, which is why – at least at the moment - it is still necessary to examine biofilms in detail.

A variety of different methods have been established to characterize biofilm properties. For characterizing the mechanical properties of biofilms, common methods are rheology, microfluidics, particle tracking, atomic force microscopy and nano-indentation [38, 87]. The surface topography and three-dimensional architecture of bacterial biofilms can be investigated with microscopy methods, such as scanning electron microscopy, confocal laser scanning microscopy and light profilometry [47, 48, 88]. To investigate the adhesion properties of bacterial biofilms, however, only a few methods have been established yet. Most established methods used to determine the adhesion of technical materials such as synthetic glues are not directly transferrable to investigate biofilms. In some methods, that were specifically developed to determine the adhesion forces of biofilms, the biofilms are scraped from a surface with a spatula or removed by capillary forces [89, 90]. However, in none of these characterization methods, the biofilm is exposed to normal forces only. By a setup that applies controlled normal forces to the biofilm, a homogeneous stress distribution can be achieved and depending on the fracture behavior, determinations of the adhesion and cohesion forces are possible. Furthermore, biofilms are ex-

posed to surfaces in their natural environment in many scenarios (e.g., when a foreign surface is pushed onto them). Finally, the wetting behavior of biofilms can be characterized by determining the resulting contact angle, when a water drop is placed onto a biofilm, or by determining the contact angle hysteresis [47, 91].

### *1.5 Biofilm-inspired biological and synthetic hydrogels*

Not only biofilms themselves can be used for human purposes, it is also possible to use certain macromolecules produced by bacteria for different applications. Due to their specific properties and good biocompatibility, bacterial cellulose, alginate and  $\gamma$ -PGA are frequently used for different industrial applications, e.g. in the food industry as a thickening agent [34, 92-94]. In the medical sector, bacterial cellulose and alginate scaffolds can be used for enhanced wound healing [77, 95]. Here, these biomacromolecules are often used to generate hydrogels. The gel formation of alginates and  $\gamma$ -PGA can be induced by the addition of certain metal cations, which lead to the formation of chelate complexes [34, 96-98]. In contrast to that, bacterial cellulose can be crosslinked by high amounts of hydrogen bonds [99].

Furthermore, it is possible to design synthetic molecules to generate hydrogels with specific properties that are inspired by natural systems. In many cases, the formation of supramolecular structures that are found in nature is based on the self-assembly of molecular units. For example the surface layer of *B. subtilis* NCIB 3610 biofilms is formed by the self-assembly of BslA due to hydrophobic interactions [48, 100]. Moreover, the structural integrity of *B. subtilis* NCIB 3610 biofilm is supported by the fiber forming protein TasA, which specifically binds to the cell walls of the bacteria by the protein TapA and thus forms a network between the bacterial cells [30, 31, 101]. However, not only in bacterial biofilms, self-assembly mechanisms can be found, also the formation of filamentous actin is based on a fuel-driven self-assembly. Here, monomeric actin self-assembles into filamentous actin by the conversion of ATP into ADP [102-107]. Yet, the self-assembly of actin filaments can also be mimicked by chemically fueled synthetic materials which exist in their non-equilibrium state [108-111]. Fluorenylmethyloxycarbonyl (Fmoc)-based peptides are capable to self-assemble into supramolecular structures and thus form dynamic hydrogels by using carbodiimide based fuels, which drive the reaction cycle [110-115]. The morphologies of supramolecular structures that can be achieved by Fmoc-based peptides include colloids, vesicles, and fibers [116-118]. In aqueous solution, the anionic peptides repel each other due to electrostatic forces generated by the dicarboxylate groups. However, the fuel-driven reaction cycle leads to the conversion of the Fmoc-precursors into their anhydride state. In this state, electrostatic repulsive forces are eliminated and the peptides can agglomerate into supramolecular structures due to hydrophobic interactions [110]. In aqueous solution, these structures are not stable: A hydrolysis reaction forces them to disassemble spontaneously and they convert back into their precursor state. When enough fuel is present, the reaction cycle can be initiated again and a gel can be maintained dynamically outside of its thermodynamic equilibrium. These

dynamic hydrogels offer the possibility to adjust their properties (such as stiffness and lifetime) by varying the conjugated amino acid sequence and fuel concentration [110, 115]. Moreover, these materials exhibit the potential for self-healing due to their dynamic character. The ability for self-healing was also observed for bacterial biofilms, however, here the underlying mechanisms are mostly unknown [38]. Also certain hydrogels based on filamentous actin were shown to exhibit self-healing properties [119], however, these biological materials are very expensive and thus not suitable for technical applications in a large scale. Therefore, synthetic fuel-driven hydrogels based on Fmoc-based peptides with the ability to self-heal could be beneficial for technical applications.

### *1.6 Key findings of this thesis*

In the scope of the present dissertation, the properties of bacterial biofilms and hydrogels are investigated to obtain a better understanding of their principles and possibilities for modifications. The viscoelastic properties of *B. subtilis* B-1 biofilms were already investigated in previous work [33] and it was shown there, that certain positively charged metal ions lead to an increased stiffness of these biofilms. However, it remains unclear, which component of the biofilm plays the key role for this effect and why only some metal cations have a stiffening effect on the biofilm. In the present dissertation, it is shown, that the ionic properties, such as size and possible coordination number in a chelate complex, as well as the structure of the polyanionic biomacromolecules of the biofilms EPS are relevant.

In further studies, the detachment behaviors of different bacterial biofilms in dependence of their material properties (such as viscoelasticity and wetting behavior) are investigated. Here, it is demonstrated, that a high biofilm stiffness and a hydrophobic biofilm surface lead to reduced material transport in the detachment tests. For this study, a novel measurement method based on commercial rheometers is developed. With this method, it is possible to differentiate between different modes of fracture (*i.e.* adhesion fracture, cohesion fracture, and mixed fracture).

In a third project, the continuous production of *B. subtilis* biofilms is addressed. In recent years, the demand of these bacterial biofilms as a resource has increased strongly, since they can be used as additives for construction materials [81, 82]. Common bioreactors, however, are not suitable for biofilm cultivation at the solid/gas interface. For the production of *B. subtilis* biofilms, a rotating bioreactor is developed in this study, which enables the cultivation at atmospheric conditions with a nutrient and moisture supply from the growth substrate. The properties of biofilms cultivated with this bioreactor (*i.e.* the viscoelastic properties and wetting behavior) are comparable with the properties of biofilms cultivated conventionally in petri dishes. Moreover, the harvested biofilm from the bioreactor increases the water repellency of mortar as well.

Finally, the viscoelastic properties of dynamic non-equilibrium hydrogels are investigated to generate hydrogels with adjustable viscoelastic properties inspired by natural biological systems.

In these hydrogels, the material properties such as stiffness and lifetime are broadly tunable by the fuel concentration and peptide configuration. By using large amplitude oscillatory shear (LAOS) measurements, the non-linear viscoelastic behavior of these synthetic hydrogels is investigated. It is shown, that these hydrogels feature certain self-healing properties after they were exposed to large shear forces. Moreover, the effects of reaction waste products, which accumulate over time in the hydrogel, are examined. It is shown, that those waste products and molecules with comparable properties, are able to disintegrate the hydrogel and thus limit its lifetime. In addition, this finding also offers the possibility to destroy the hydrogel in a controlled manner.



## 2. Materials

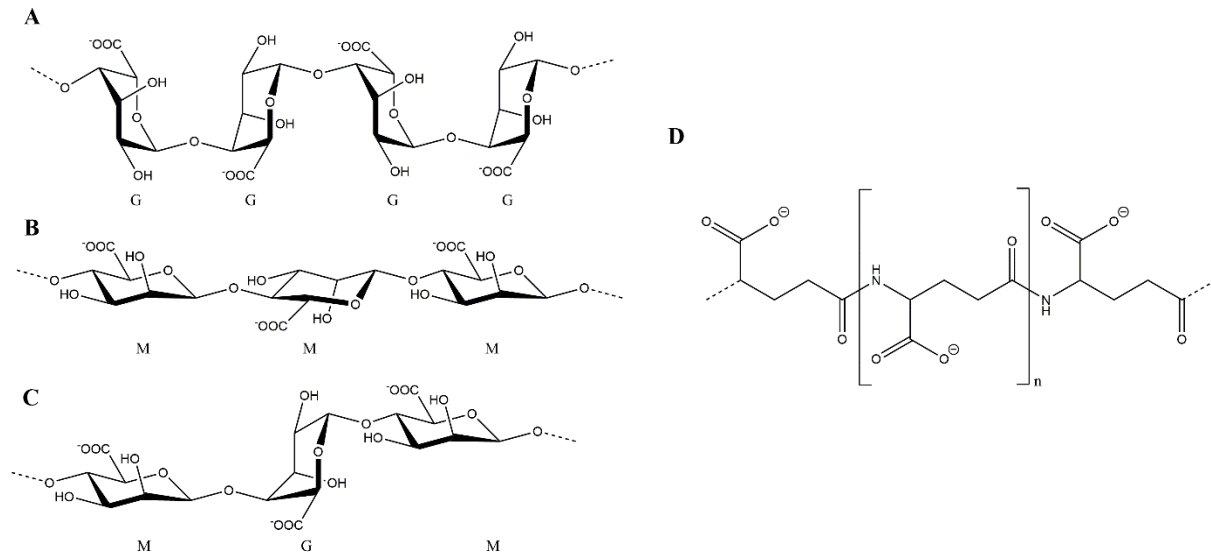
### 2.1 Bacterial biofilms

Bacterial communities can exist in different forms. Bacteria can survive as freely flowing planktonic cells in liquid media, or they can produce extracellular polymeric substances (EPS) to embed themselves into a slimy matrix. The latter can occur on liquid and solid surfaces. Bacterial slime that forms thin layers on liquid surfaces is called a "pellicle". When bacteria attach permanently to solid surfaces and embed themselves into EPS, these slimy bacterial communities are called biofilms. Depending on the bacterial species, these biofilms develop at the interface between solid and liquid (aquatic biofilms) or at the interface between solid and gas (terrestrial biofilms). Examples of bacterial species that are able to form biofilms at the solid/air interface are *B. subtilis* NCIB 3610, *B. subtilis natto*, *B. subtilis* B-1 and *A. vinelandii*. These biofilms exhibit a slimy consistency and can be classified as viscoelastic materials. The EPS protects the embedded bacteria against external influences such as shear forces, toxic substances, or dehydration. The main components of the EPS are proteins, polysaccharides, lipids, nucleic acids, and water [8]. However, the exact composition of bacterial biofilms varies depending on the bacterial species. The biofilm matrix of *B. subtilis* NCIB 3610 is mainly composed of the fiber forming protein TasA, the exopolysaccharides produced by the gene products of the *epsA-O* operon, and the matrix protein BslA, which self-assembles at the biofilm surface and creates a hydrophobic coat [29, 30, 48]. In contrast, the biofilm matrix of *B. subtilis* B-1 contains a high amount of the polyanionic polypeptide  $\gamma$ -PGA, which, to some extent, can also be found in *B. subtilis natto* biofilms [44]. Finally, the biofilm matrix of *A. vinelandii* mainly contains the polyanionic polysaccharide alginate [120]. The composition and structure of biofilms influences their material properties such as the viscoelasticity, stickiness and wetting behavior.

### 2.2 Polyanionic biomacromolecules

Polyanionic macromolecules can be found in multiple biological systems. Alginate, for example, can be produced by different algal and bacterial species such as *A. vinelandii*, *P. aeruginosa*, and *Pseudomonas putida* [34]. Depending on the biological source, the structure of its molecular chains can vary (**Figure 3**): Alginate is composed of  $\alpha$ -L-guluronate (G) and  $\beta$ -D-mannuronate (M) monomers in varying amounts and sequences. Only the alginate of *A. vinelandii* and some algal species contains sequences of  $\alpha$ -L-guluronate only, so called G-blocks. The alginates of other bacterial species, such as *P. aeruginosa* and *P. putida*, either contain M- blocks only, or possess alternating sequences of M- and G-monomers [97]. Alginates are able to form chelate complexes with certain metal cations, which lead to crosslinks between the alginate chains. Whether and how strong a chelate complex is formed depends on the structure of alginate as well as the ion type [34].

Another anionic biomacromolecule that can be produced by bacteria is  $\gamma$ -PGA, which is the main component of *B. subtilis* B-1 biofilms [44].  $\gamma$ -PGA is a polyanionic polypeptide that – similar to alginate – is able to form chelate complexes with certain positively charged metal ions as well [121].



**Figure 3:** Chemical structures of alginate composed of  $\alpha$ -L-guluronate residues forming G-blocks (A), of alginate composed of  $\beta$ -D-mannuronate residues forming M-blocks (B), of alginate composed of an alternating sequence of M- and G-monomers (C) and of  $\gamma$ -PGA (D).

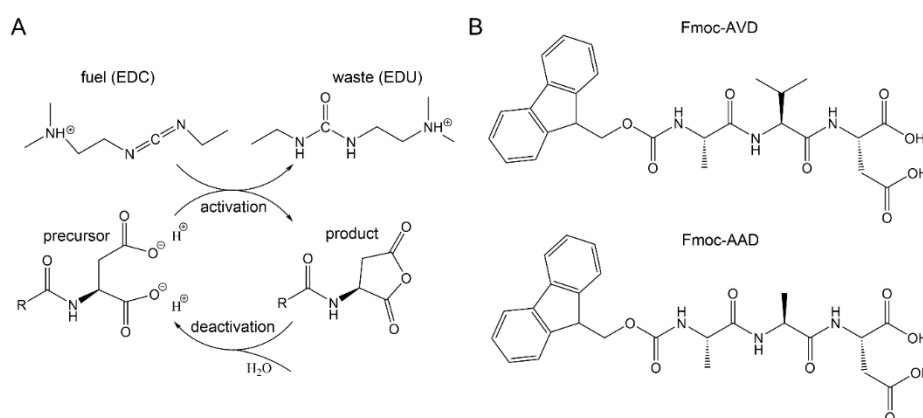
### 2.3 Metal ions

In natural conditions, metal ions always tend to release their valence electrons and thus form positively charged cations that tend to bind to negatively charged atoms or molecules. In direct contact with many microorganisms such as bacteria, metal ions can be toxic [33], and they influence the charge distribution and conductivity of solutions. When certain metal cations come in contact with polyanionic macromolecules such as alginate or  $\gamma$ -PGA, they form chelate complexes and thus cross-link the macromolecules [34, 121]. This effect can then lead to the formation of hydrogels. However, depending on the properties of the macromolecular chelating agent and the metal cation, a chelate complex cannot always be formed. On the side of the chelating agent, the molecular structure and denticity has an influence; on the side of the metal cation, the valence, ionic size and the possible coordination numbers might play a role. However, a determination of the individual dependencies is difficult, since many of these properties correlate with each other: When the valence increases, electrons are released and thus the ion becomes smaller. Moreover, it is impossible to measure the ionic size directly. It only can be measured when the ions are bound in a crystal lattice, and the result depends on the coordination number and measurement technique (*e.g.* X-ray diffraction) [122]. Within the scope of this dissertation, the effect of certain metal ions on the material properties (*i.e.* viscoelasticity, detachment behavior and wetting behavior) of *B. subtilis* B-1 and *A. vinelandii* biofilms was investigated.



## 2.4 Fmoc based hydrogels

Chemically materials based on fluorenylmethyloxycarbonyl (Fmoc)-protected peptides are able to self-assemble, driven by a chemical fuel [110]. These dynamic materials differ from in-equilibrium materials as a driving force is necessary to obtain and maintain their non-equilibrium state. The self-assembly can be driven by the fuel 1-ethyl-3-(3-dimethylaminopropyl)carbodiimid-hydrochlorid (EDC) and leads to the formation of supramolecular structures. By a variation of the conjugated amino acid sequence and the amount of available fuel, the properties such as size, shape and lifetime of these structures are tunable [110, 123]. When the Fmoc-protected peptide derivatives are solubilized in a suitable aqueous buffer solution, the anionic peptides repel each other due to the electrostatic forces generated by the dicarboxylate groups. The reaction with the fuel leads to a conversion of the precursor into its corresponding anhydride state and generates the waste product 1-[3-(dimethylamino)propyl]-3-ethylurea (EDU) (**Figure 4A**). In the anhydride state, the electrostatic repulsion between the molecules is eliminated, which results in their assembly due to hydrophobic interactions. In an aqueous environment, the activated anhydride state is not stable and will spontaneously hydrolyze and retransform into its precursor state and this destabilizes the self-assembled structures [110]. The range of dynamic assemblies that can be obtained by this mechanism contains colloids, vesicles, droplets and fibres [116-118]. With the assembly of Fmoc-peptides into supramolecular structures, hydrogels can be formed as well. Two possible peptide sequences that enable such self-assembly of Fmoc-peptide-conjugates into supramolecular structures are Fmoc-alanine-valine-aspartic acid (Fmoc-AVD) and Fmoc-alanine-alanine-aspartic acid (Fmoc-AAD) (**Figure 4B**).



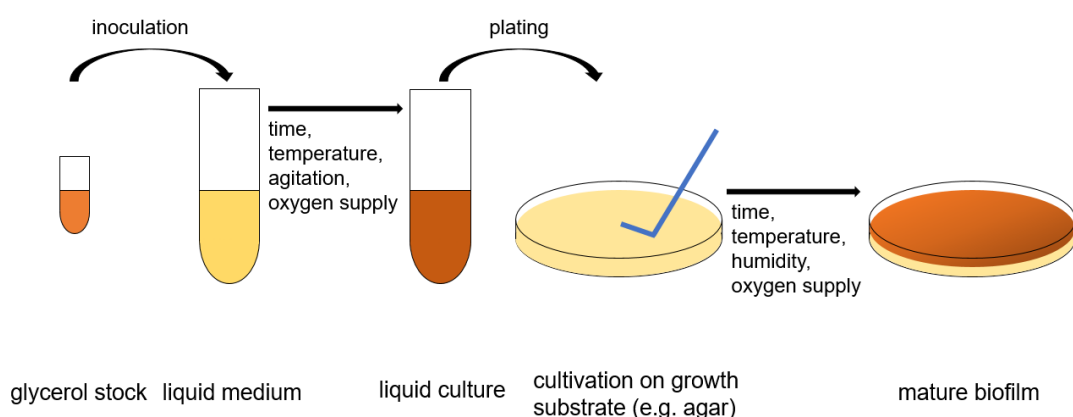
**Figure 4:** A: Schematic illustration of the reaction cycle of a precursor peptide, that reacts with a fuel (here: EDC) and is converted into the corresponding anhydride product. In aqueous solution it will hydrolyze spontaneously and retransform into its precursor state. B: The structures of Fmoc-AVD and Fmoc-AAD.



### 3. Theoretical background and methods

#### 3.1 Biofilm cultivation

The cultivation of bacterial biofilms requires multiple steps (**Figure 5**). To store bacteria, they can be kept deep-frozen (at  $-80\text{ }^{\circ}\text{C}$ ) as glycerol stocks. At these temperatures, their metabolism is inactivated. Due to the glycerol, the formation of ice crystals is prevented, which would destroy the bacterial cells otherwise. To cultivate the bacteria, small pieces of a frozen glycerol stock are immersed into a liquid medium that is enriched with nutrients. As soon as the temperature reaches a certain level, the bacterial metabolism is activated and the bacteria start to multiply as freely flowing planktonic cells in the liquid medium. After 16 – 18 hours, at rotatory motion, controlled oxygen supply and temperature (e.g.,  $37\text{ }^{\circ}\text{C}$  for *B. subtilis* NCIB 3610), a concentrated bacterial solution is obtained. To quantify the amount of bacterial cells in this culture, it is possible to measure the optical density. This can be conducted with a spectrophotometer that measures the light absorbance of the bacterial culture. In the next step, a small amount of the bacterial culture (e.g.  $1.6\text{ }\mu\text{L cm}^{-2}$ ) is placed onto a solid growth substrate (e.g. agar enriched with nutrients) and homogeneously distributed with a plate spreader. At controlled oxygen supply, humidity (e.g. 80% - 90% for *B. subtilis* NCIB 3610) and temperature (e.g.  $37\text{ }^{\circ}\text{C}$  for *B. subtilis* NCIB 3610), a biofilm develops on the substrate surface within 24 h. For further investigations, e.g. to characterize the viscoelastic properties, the biofilm can be harvested from the surface by manually scraping with a spatula. For the liquid culture and growth on a solid substrate, different media and substrates (depending on the bacterial species) can be used. For the cultivation of *B. subtilis* NCIB 3610, *B. subtilis natto* and *B. subtilis* B-1, lysogeny broth (LB) medium and LB agar are commonly used. For the cultivation of *A. vinelandii*, however, a special *azotobacter* medium based on glucose and mannose is needed.

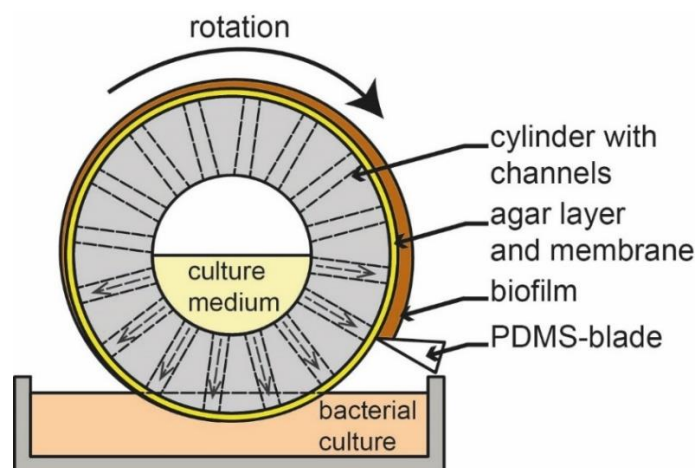


**Figure 5:** Individual steps of the biofilm cultivation. First, small pieces of a glycerol stock are inoculated in a liquid medium. At controlled temperature, agitation and oxygen supply, a bacterial liquid culture will develop with time. This liquid culture is spread across the growth substrate (e.g. agar) with a plate spreader. Then, over time, and at controlled temperature, humidity and oxygen supply, a biofilm forms at the solid/air interface.

### 3.2 Bioreactors

To cultivate bacterial cultures or biofilms in a larger amount than for research purposes, bioreactors are used. The bioreactor regulates the growth conditions such as the temperature, humidity and oxygen supply for the bacteria and supports them with nutrients. Bioreactors can be categorized into reactors to cultivate planktonic bacteria, *i.e.* bacterial liquid cultures, and reactors that cultivate bacterial biofilms. For the latter, most bioreactors are designed to produce biofilms attached to a support material or directly on the bioreactor surface and submerged in a liquid medium, *i.e.* to cultivate aquatic biofilms. Bioreactors that use support materials include sequencing batch reactors, continuous stirred tank reactors, packed- or fluidized-bed reactors, and tickling bed reactors [86, 124-128]. In contrast, in rotating disc contractors and membrane bioreactors, the biofilm cultivation occurs directly on the bioreactor surface. In most of these bioreactors, the biofilms are used to perform a dedicated function *in situ*, such as for wastewater treatment or for the production of chemical substances, such as alcohols or acids [78, 79, 84, 129]. However, bioreactors that produce biofilm as a product are rather scarce.

In a novel approach that is introduced within the scope of this dissertation, bacterial biofilms can be cultivated continuously on a rotating cylinder and at the solid/air interface (**Figure 6**). Here, the rotating cylinder is equipped with an agar layer and a porous membrane as outer surface. At its lower apex, the cylinder is submerged into a bacterial liquid culture. Then, with a full rotation of the cylinder, the whole surface area becomes inoculated and the biofilm develops over time. The inside of the cylinder is filled with a nutrient medium, that diffuses through the agar layer and membrane, and thus supplies the bacteria on the membrane surface with nutrients and moisture. Finally, the mature biofilm can be automatically harvested by a blade.

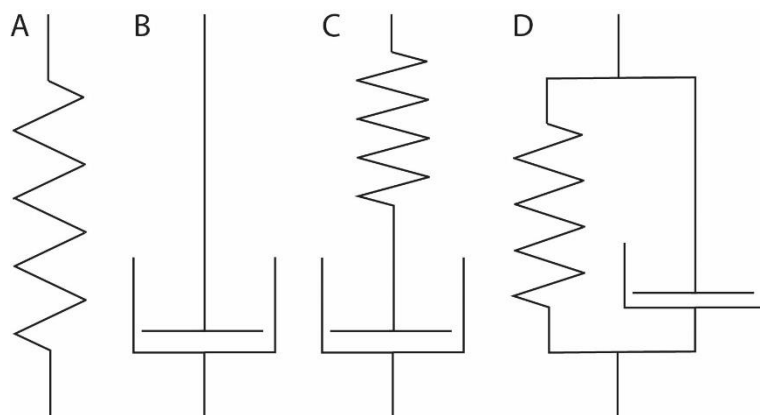


**Figure 6:** Schematic illustration of a rotating bioreactor for the cultivation of bacterial biofilms at the solid/air interface. The cylinder is immersed in a bacterial culture and with a rotation, the whole reactor surface becomes inoculated. The culture medium can penetrate the cylinder trough channels and the agar layer through diffusion to supply the biofilm with nutrients and moisture. The mature biofilm is automatically harvested by a blade.

### 3.3 Rheology

#### 3.3.1 Measurement basics

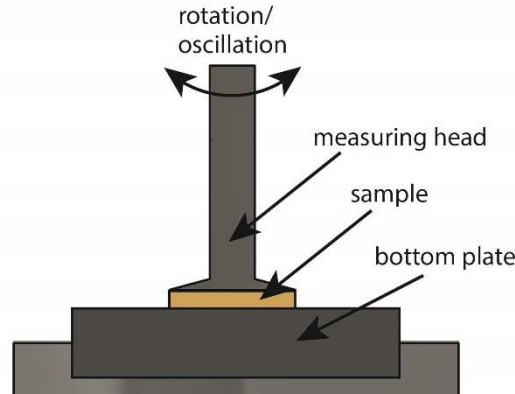
Materials can be classified based on their response behavior towards external forces. In a purely elastic material, the applied energy is completely stored by the material as potential energy and fully released again as soon as the applied force is removed. This material behavior is described by the Hook element (**Figure 7A**). In purely viscous materials, the energy of the applied force is completely dissipated by the deformation, and the material is unable to deform back. The Newton element corresponds to this material behavior (**Figure 7B**). Viscoelastic materials, such as suspensions, gels or polymeric melts show both, a partially elastic and partially viscous behavior. When the viscous parts dominate the material behavior, the materials are classified as viscoelastic liquids; when the elastic parts dominate, they are referred to as viscoelastic solids. The material behavior of viscoelastic liquids is modelled by the Maxwell model which represents a Hook and Newton element in a serial connection (**Figure 7C**). Viscoelastic solids are described by the Kelvin-Voigt model which combines a Hook and Newton element in a parallel connection (**Figure 7D**) [130].



**Figure 7:** Overview of different models to describe viscoelastic behavior. A: Hook element, B: Newton element, C: Maxwell model, D: Kelvin-Voigt model.

With a rheometer, the material behavior of viscoelastic materials and liquids can be characterized. Typically, the rheometer applies a shear stress to the sample via a measuring head (Searle method). The sample is placed between the measuring head and the bottom plate and should completely fill the measuring gap (**Figure 8**). The measuring head is set in rotational or oscillatory motion by a motor and either the resulting force or torque is determined via the operating current. The resulting displacement of the measuring head can then be measured precisely with an incremental rotary transducer. To enable the detection of small deflections, even if the sample exerts high normal forces, the measuring head is equipped with an air bearing. A requirement for a precise measurement is, that the plates do not slide off the sample and that the sample is deformed homogeneously.

To characterize a sample, different measurement geometries can be used. For viscosity dominated materials, cone-plate geometries are commonly used, whereas plate-plate geometries are used for stiff elasticity dominated samples. Also coaxial cylindrical measurement systems are well-established, especially for liquids with a very low viscosity.



**Figure 8:** Schematic illustration of a rheology a setup with plate-plate geometry. The sample fills the measuring gap between the measuring head and bottom plate and is stressed by a rotatory or oscillatory motion of the measuring head.

Oscillatory rheology is suitable to investigate the viscoelastic behavior of nearly all kind of materials, from liquid materials with a very low viscosity up to rigid materials with a high stiffness. The oscillating measuring head applies a sinusoidal wave onto the sample and thus induces shear forces. In a typical measurement, the torque / force is applied, and the displacement amplitude is measured. From these measured data, further parameters such as the stress ( $\tau$ ), strain ( $\gamma$ ) and complex shear modulus ( $G^*$ ) can be calculated. When the measurement is conducted in strain controlled mode, using a software based feedback loop to keep the strain constant, the shear strain for viscoelastic materials is calculated with **Equation 1**. When the shear stress is controlled within the measurement, the shear strain can be calculated according to **Equation 2** [130].

$$\tau(t) = \tau_A \sin(\omega t + \delta) \quad \text{(Equation 1)}$$

$$\gamma(t) = \gamma_A \sin(\omega t + \delta) \quad \text{(Equation 2)}$$

With:  $\tau(t)$  = shear stress [Pa];  $\gamma(t)$  = deformation [%];  $\tau_A$  = shear stress amplitude [Pa];  $\gamma_A$  = deformation amplitude [%];  $\omega$  = angular frequency [rad/s];  $t$  = time [s];  $\delta$  = phase shift angle [°].

Another central parameter is the complex shear modulus  $G^*$ , which can be calculated with **Equation 3** [130].  $G^*$  represents the stiffness of the sample and thus resistance against deformation.

$$G^* = \frac{\tau(t)}{\gamma(t)} \quad \text{(Equation 3)}$$

With:  $G^*$  = complex shear modulus [Pa];  $\tau(t)$  = shear stress [Pa];  $\gamma(t)$  = deformation [%].

As long as the test is conducted in the linear viscoelastic regime (LVE regime),  $G^*$  is clearly defined by sinusoidal waves in  $\tau$  and  $\gamma$ . Then,  $G^*$  can be split into the storage modulus  $G'$  and the loss modulus  $G''$  (**Equation 4**). The storage modulus describes the elastic properties of the sample behavior and is calculated with **Equation 5**. The loss modulus characterizes the viscous properties of the sample response and is calculated with **Equation 6**. Both viscoelastic moduli are dependent on the phase shift angle  $\delta$ . The phase shift angle equals  $0^\circ$  for purely elastic materials and  $90^\circ$  for purely viscous materials. Viscoelastic solids exhibit a phase shift angle between  $0^\circ$  and  $45^\circ$ ; here, the storage modulus dominates the material properties, accordingly. For viscoelastic liquids,  $\delta$  ranges between  $45^\circ$  and  $90^\circ$  and the loss modulus is dominant [130].

$$G^* = G' + iG'' \quad \text{(Equation 4)}$$

$$G' = \frac{\tau_A}{\gamma_A} * \cos(\delta) \quad \text{(Equation 5)}$$

$$G'' = \frac{\tau_A}{\gamma_A} * \sin(\delta) \quad \text{(Equation 6)}$$

With:  $G^*$  = complex shear modulus [Pa];  $G'$  = storage modulus [Pa];  $G''$  = loss modulus [Pa];  $\tau_A$  = shear stress amplitude [Pa];  $\gamma_A$  = deformation amplitude [%];  $\delta$  = phase shift angle [°].

### 3.3.2 Determination of the frequency dependent shear behavior

To investigate the frequency dependent shear behavior of viscoelastic materials, frequency sweeps are applicable. These are conducted in oscillatory mode and within the LVE regime, so that the sample is not damaged during the measurement. Therefore, the displacement amplitude has to be appropriately small. When the LVE regime of the sample is unknown, this has to be determined by a pretest. In such a pretest, a small torque (e.g.  $0.5 \mu\text{Nm}$ ) is applied to the sample and the resulting deformation is measured. As displacement amplitude in the frequency sweeps conducted in this thesis, the measured deformation is multiplied by a factor (e.g. 1.5). This displacement amplitude then represents the "ideal" deformation, since it is high enough to be measured accurately and small enough, so that the LVE regime is not exceeded. In addition, no gelation processes are allowed to take place within the sample and environmental influences, such as the temperature, have to be kept constant to ensure constant sample properties during the whole experiment.

A frequency sweep is typically conducted in a frequency range between 0.1 Hz and 10 Hz. In the regime of high and low frequencies, measurement artefacts may distort the results. Such measurement artefacts can occur at high frequencies due to the moment of inertia resulting from the mass of the measurement head. At low frequencies, slow movements of the measuring head can cause artefacts since external vibrations have a higher impact when more time is needed to generate a measuring point. Thus, results are not reliable when the measured signal fluctuates strongly in these regimes.

Whether a sample depicts a strong frequency dependence or not, gives insights into the intrinsic material characteristics. The properties of loosely entangled polymers that are not cross-linked are dictated by steric interactions and movements of these molecules. In these materials, the macromolecules are able to slowly disentangle and rearrange. This results in a dependency on the frequency [130]. Especially at low frequencies, the molecules have enough time to diffuse through their environment – a phenomenon that is called reptation. Thus even loosely entangled polymers with many steric interactions, that show an elastically dominated behavior at intermediate frequencies, exhibit a viscosity dominated behavior in the low frequency regime. When the frequency is increased, it is possible, that the molecules either lock each other, resulting in an increased stiffness; or the molecules align in flow direction and thus the stiffness is reduced [130]. At very high frequencies, single filament fluctuation occurs. In this case, friction forces, that occur due to undulatory bending of the molecular chains leads to the dissipation of energy, which results in a dominance of the loss modulus in this regime [38, 131].

The material behavior of crosslinked polymer networks differs from that described above. Here, the crosslinks prevent diffusion and shift of the molecular chains as long as the junctions are not destroyed. Therefore, only the molecular chains themselves can be deformed in the LVE regime. The extent of the possible deformation is dependent on the mesh size and degree of cross-links. When the polymers are densely cross-linked, both viscoelastic moduli show only weak frequency dependence for a wide range. Only weak cross-linked polymers show a broad frequency dependency. Here, the stiffness increases with an increasing frequency, since the molecules have less time to deform [130]. However, at very high frequencies, even for strongly cross-linked polymeric networks, single filament fluctuation can occur, and thus  $G''$  exceeds  $G'$  in this regime [131]. For the differentiation with loosely entangled polymers, the low frequency regime can be taken in account. In loosely entangled polymers, the storage modulus decreases continuing, whereas this does not occur even for weak crosslinked polymers. The molecular crosslinks hinder the movements and thus lead to a plateau value of the storage modulus at low frequencies. Reptation is not possible in cross-linked polymers [130].

### 3.3.3 *Determination of gelation behavior*

To determine the gelation behavior of a sample over time (*e.g.* as result of a temperature increase), the viscoelastic properties are measured in the LVE regime and in oscillating mode as well. However, here, a constant frequency and torque needs to be applied. When the measurement is conducted in torque controlled mode, the deflection amplitude is continuously adjusted according to the changing material behavior of the sample due to gelation and no pretest is necessary. As soon as the storage modulus reaches the loss modulus, the sample transits from a viscoelastic liquid to a viscoelastic solid. This event is classified as "gel point" [130].

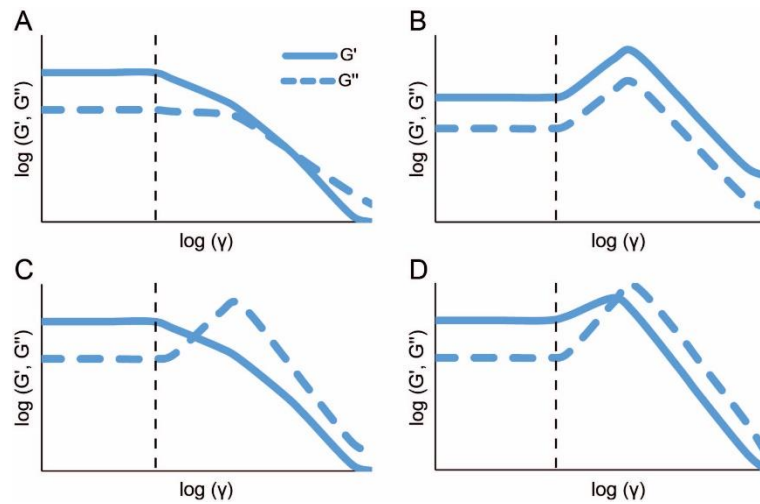


### 3.3.4 Non-linear rheology

To characterize the non-linear behavior of viscoelastic solids, oscillatory measurements can be conducted with a rheometer as well and are known as large amplitude oscillatory shear (LAOS) tests. These are of great importance to predict the material behavior at high mechanical load. In these tests, the strain amplitude is increased at a constant probing frequency - up to the end of the LVE regime and beyond. To display the obtained results, the viscoelastic moduli (in Pa) are typically depicted as a function of the shear strain (in %). In the LVE regime (*i.e.* when the strain amplitude is sufficiently small), both viscoelastic moduli are independent of the applied strain amplitude. For viscoelastic solids, Hook's law applies in this regime: the ratio  $\frac{\tau_A}{\gamma_A}$  is constant and the oscillatory stress response is sinusoidal. In the non-linear viscoelastic regime, however, both moduli are dependent on the strain amplitude ( $G'(\gamma_A)$ ;  $G''(\gamma_A)$ ); now, the resulting measurement signal becomes distorted and is not sinusoidal anymore. Therefore, the viscoelastic moduli are not clearly defined in the non-linear viscoelastic regime.

For calculating the viscoelastic moduli from a non-sinusoidal waveform, the most common method uses a Fourier transform analysis of the first harmonic measurement signal [132]. If material failure occurs and the structure of the sample becomes irreversibly altered, both viscoelastic moduli start to differ from the plateau value (by showing decreasing or increasing values). To define the limit of the linear regime and the onset of the non-linear regime, a common method is to set a certain deviation from the plateau value (*e.g.* 1%, 5% or 10%) [130]. Then, as soon as the loss modulus falls below the storage modulus, a material failure can be assumed and the sample cannot be characterized as a viscoelastic solid anymore. When the sample is able to recover its elasticity dominated material behavior after the experiment, this property is classified as self-healing behavior [38].

In the non-linear regime, at least four different scenarios of material behavior can occur. They represent different effects of (irreversible) material failure and molecular rearrangements and depend on the sample material. These scenarios are strain weakening, strain hardening, weak strain overshoot and strong strain overshoot [133]. Materials that obtain strain weakening behavior show a decrease of both viscoelastic moduli in the non-linear viscoelastic regime; this can be due to chain orientation, alignment of microstructures along the shear direction or the disruption of chemical or physical bonds (**Figure 9A**). This is the most common behavior in the non-linear regime and was observed for *Bacillus subtilis* 168 and *P. aeruginosa* biofilms for example [38, 40].



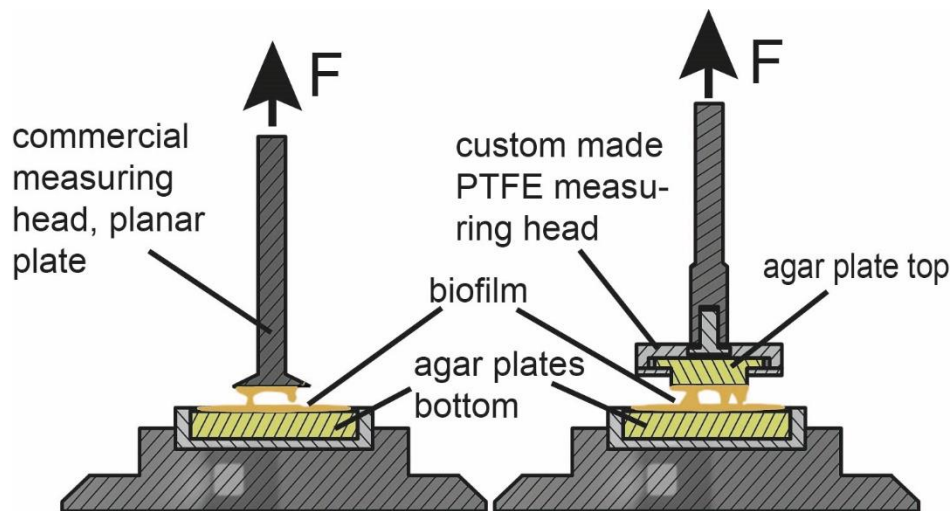
**Figure 9:** Exemplarily LAOS curves representing the different variants of material behavior in the non-linear regime: strain weakening (A), strain hardening (B), weak strain overshoot (C) and strong strain overshoot (D). The vertical, dashed lines represent the boundary between the linear viscoelastic regime at small strains (to the left) and the non-linear viscoelastic regime at high strains (to the right). Depicted are exemplary curves for the storage modulus (blue full lines) and loss modulus (blue dashed lines).

In contrast to this, when strain hardening occurs, both viscoelastic moduli increase before material failure sets in (**Figure 9B**). This can be due to interactions between the entangled molecules that hinder their movement and alignment. Strain hardening was observed for *Klebsiella pneumoniae* and *Staphylococcus epidermidis* biofilms [41]. In a weak strain overshoot,  $G'$  first decreases and  $G''$  increases; this feature is then followed by a decrease of both viscoelastic moduli (**Figure 9C**). Here, due to the mechanical load, new reinforcing interactions can arise in the material, and simultaneously, other network junctions become destructed. However, the rate of generating interactions is smaller than the loss of existing junctions. This leads to an increased energy dissipation, until the majority of the network junctions are destroyed and both moduli decrease [132]. Depending on the material, a rearrangement of unstable clusters [134] or the destruction of microstructures which develop during the test [135] can also lead to a weak strain overshoot. This material behavior can be observed in certain suspensions and soft hydrogel spheres dispersed in water [136-138]. A strong strain overshoot is characterized by an increase and subsequent decrease of both viscoelastic moduli (**Figure 9D**). This can occur when the rate of arising interactions exceeds the rate of vanishing interactions induced by the high shear strains [132]. This rare material behavior was observed in certain associative polymers [139].

### 3.4 Detachment tests

The detachment behavior of sticky and slimy substances such as bacterial biofilms is dominated by two material properties, the cohesion and adhesion behavior of the material. “Cohesion” represents the internal forces of the material that maintain the structural integrity of the substance, and “adhesion” represents the attachment process to external materials. In the case of bacterial biofilms, either the adhesion to the growth substrate or to an object that comes in contact with the biofilm surface can be of concern. For the investigation of the detachment properties of bacterial biofilms, only a few measurement techniques have been developed. For instance, it is possible to characterize the adhesion behavior of biofilms by removing them from their substrate with a spatula and measuring the lateral force occurring during this scraping process [89]. Another possible approach is to apply capillary forces to remove the biofilms from a surface and to measure the corresponding adhesion energy [90]. In contrast, there are different established tests to quantify the adhesion and cohesion behavior of synthetic materials such as glues [140]. These techniques either apply stretching forces in the vertical direction thus measuring the tensile strength of an adhesive connection (DIN EN 15870:2009-08), or large transversal shear forces are applied to the adhesive connection by single-lap shear tests (DIN EN 1465:2009-07; ISO 11003-2:2019-06). The application of torsional forces on the adhesive joint is used as well, *e.g.* by rotating two opposing surfaces relative to each other (ISO 10033-1:2011-04). However, these methods, which were developed for synthetic glues, cannot directly be used to investigate the adhesive strength of living materials such as bacterial biofilms, since the biofilm would need to be removed from the surface prior to the measurement. This disrupts its structure and thus can affect the result of the adhesion measurement. Moreover, with such pre-collected and thus potentially altered material, a characterization of the biofilm adhesive strength to its growth substrate is not possible anymore.

In a custom-made setup introduced within the scope of this dissertation (section **4.3**), the detachment behavior of bacterial biofilms can be investigated *in situ*. The measurement setup is based on a commercial rheometer, which applies normal forces to the biofilm material and measures the force that is needed for the detachment process. For this, the measuring head is vertically removed from the sample at slow speeds ( $100 \mu\text{m s}^{-1}$ ). By analyzing the amount of biological material that was transferred between the two test surfaces and evaluating the fracture surfaces, it is possible to differentiate between an adhesive and cohesive failure of the bio-material. With this setup it is possible to conduct the detachment process with different material pairings, such as metal-on-biofilm and biofilm-on-biofilm (**Figure 10**).



**Figure 10:** Illustration of the custom-made measuring setup to investigate the detachment behavior of bacterial biofilms *in situ* with the use of a commercial rheometer. On the left side, the material pairing metal-on-biofilm is depicted and on the right side the material pairing biofilm-on-biofilm.

### 3.5 Biofilm wetting behavior

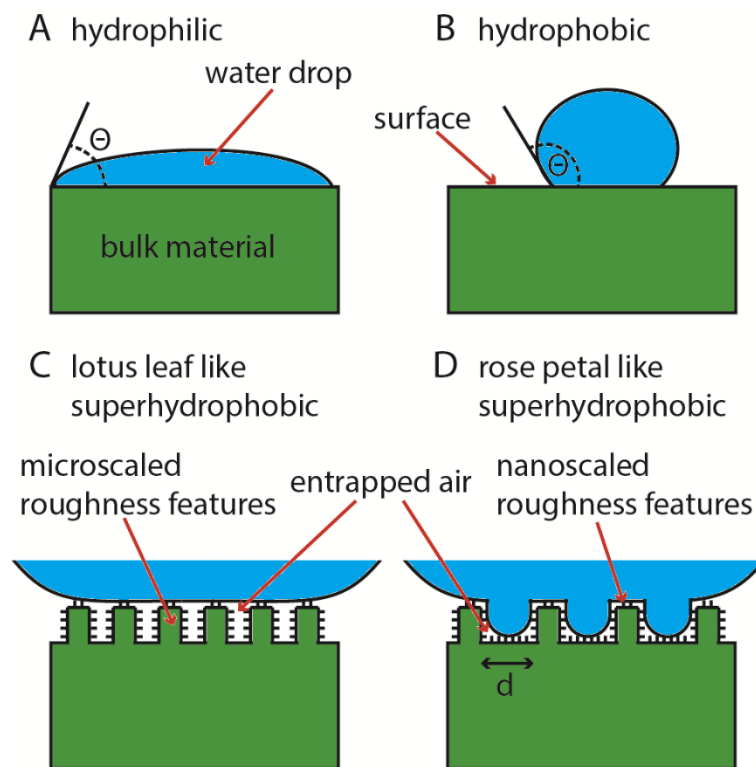
The wetting behavior of surfaces with water and aqueous solutions is dependent on the polarity of the surface material and its surface texture *i.e.* its roughness. Surfaces can be categorized into hydrophilic and hydrophobic, according to their wetting behavior (**Figure 11A** and **Figure 11B**). As a measure of the wetting behavior, the contact angle ( $\theta$ ) of a water drop on the surface is used. For hydrophilic surfaces, the material is easily wetted; the water drop distributes well over the surface and the contact angle is smaller than  $90^\circ$ . On hydrophobic surfaces, however, the drop tends to form a sphere; thereby, the contact area is reduced and the contact angle ( $\theta$ ) becomes greater than  $90^\circ$ . For hydrophobic materials, both, the micro- and nanoscaled roughness play an important role for the wetting behavior. With an increase of the roughness, a hydrophobic material can become superhydrophobic.

A superhydrophobic surface exhibits contact angles greater than  $120^\circ$  or even greater than  $150^\circ$  (depending on the definition) [141]. Superhydrophobic surfaces can be differentiated into lotus leaf like and rose petal like (**Figure 11C** and **Figure 11D**). For lotus leaf like superhydrophobic surfaces, a Cassie-Baxter state is present. Here, air is entrapped between the microscaled features of the rough surface, which leads to a very low contact area [141, 142]. For rose petal like superhydrophobic surfaces, an impregnated Cassie state is present. Here, the distance between the microscaled features of the surface is higher than for lotus leaf like surfaces. Thus, water is able to penetrate the space between microscaled roughness features and air is entrapped only between the nanoscaled roughness features [143].

When the surfaces are tilted, a water drop on a lotus leaf like surface will roll off, whereas the drop will stick to a rose petal like surface. To quantify this difference in behavior, it is possible to measure the contact angle hysteresis. Here, a small drop volume is placed onto the surface and

this volume is first incrementally increased and subsequently decreased. For every increment, the contact angle is determined. For lotus leaf like surfaces, the contact area of the water drop to the surface increases and decreases in parallel to the increase and decrease of the drop volume. Accordingly, the advancing and receding contact angles are nearly constant during the whole measurement. However, for rose petal like surfaces, the contact area increases with increasing drop volume but stays nearly constant, when the volume is reduced. Thus, the advancing contact angle stays constant and the receding contact angle decreases [47, 143].

Within the scope of this dissertation, the wetting behavior of *B. subtilis* NCIB 3610, *B. subtilis natto* and *B. subtilis* B-1 biofilms was determined in dependence of the growth conditions and after treatments with metal salts. Here, the aim was to find dependencies between the wetting behavior and the biofilm adhesion and detachment behavior.



**Figure 11:** A: Wetting behavior of a hydrophilic surface with a contact angle ( $\theta$ )  $< 90^\circ$ . B: Wetting behavior of a hydrophobic surface with a contact angle ( $\theta$ )  $> 90^\circ$ . C Detailed view of the interface of a lotus leaf like superhydrophobic surface with air entrapped between microscaled roughness features of the surface (Cassie-Baxter state). D: Detailed view of the interface of a rose petal like superhydrophobic surface with air entrapped only between the nanoscaled roughness features (impregnated Cassie state). The distance (d) between the microscaled roughness features is higher than for lotus leaf like surfaces.



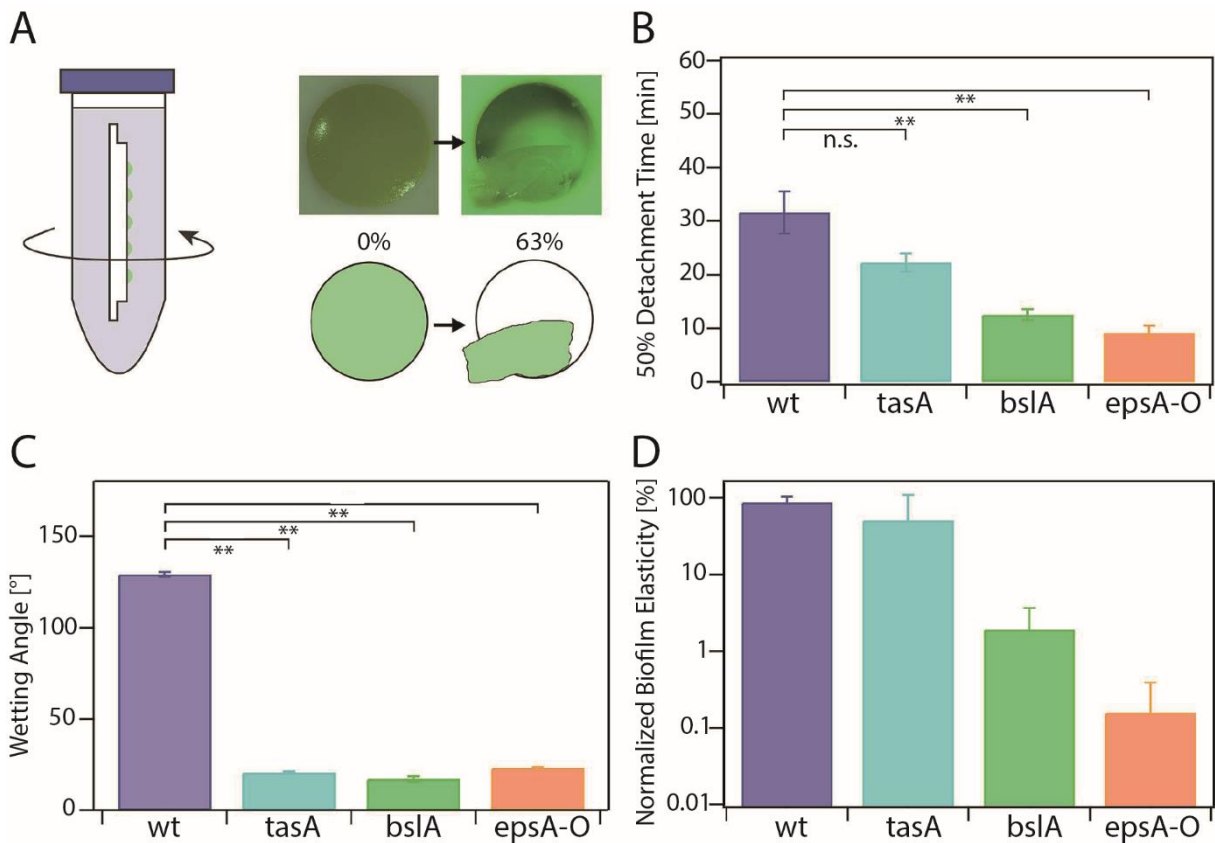
## 4. Summaries of publications

### 4.1 Importance of the biofilm matrix for the erosion stability of *Bacillus subtilis* NCIB 3610 biofilms

M. Klotz, M. Kretschmer, A. Goetz, S. Ezendam, O. Lieleg and M. Opitz [144]

The erosion stability is a central property of bacterial biofilms. In many cases, biofilms are not desired and need to be removed from surfaces such as from implants placed into the human body. In other cases, a strong attachment is desired to keep the biofilms on certain surfaces where they fulfill special functions such as wastewater treatment. The erosion resistance of a biofilm depends on its viscoelastic properties, its adhesion as well as its wetting behavior. Previous studies showed, that it is possible to alter this erosion stability by the addition of chemical substances, such as metal cations or antibiotics. However, it is unclear how the individual biofilm matrix components contribute to the erosion behavior of *Bacillus subtilis* NCIB 3610 biofilms. The most important components of the *B. subtilis* NCIB 3610 biofilm matrix are the exopolysaccharides produced by the gene products of the *epsA-O* operon, the fiber forming protein TasA, and the protein BslA. The latter is a hydrophobin which self-assembles at the surface of the biofilm.

In this study, the erosion resistances of *B. subtilis* NCIB 3610 and mutant strain biofilms were investigated. Biofilms were cultivated on agar and immersed in pure water or water containing either antibiotics or metal cations. To generate a water flow that leads to shear stresses and thus erosion, this setup was set in rotational motion. Additionally the wetting behavior as well as the viscoelastic properties of the biofilms were analyzed. It was found that the absence of each matrix component decreases the erosion stability of *B. subtilis* NCIB 3610 biofilms in water. Especially the lack of the exopolysaccharides and BslA weakened the biofilm. Most likely, this is due to a reduced stiffness and a loss of hydrophobicity which was observed in both biofilm mutants (**Figure 12**). Upon addition of certain positively charged ions, the stiffness of the biofilm can be increased, which results in enhanced erosion resistance. This increase appears to be independent of the biofilm content and thus seems to be based on unspecific cross-linking of the different biofilm components. Moreover, when adding  $\text{Ca}^{2+}$ ,  $\text{Na}^+$ , or the antibiotic ciprofloxacin, the biofilm stiffness was not enhanced, yet its erosion resistance increased significantly nevertheless. Maybe, an increase of the adhesion properties of the biofilm can explain this result, yet this property is difficult to measure.



**Figure 12:** Erosion stability and properties of *B. subtilis* NCIB 3610 biofilm. (A) Schematic representation of the erosion experiment. Left: Carrier slide containing biofilm covered agar patches inserted into a test tube filled with testing solution and set in rotational motion. Right: Images and sketches of agar patches covered with biofilm, before (0% biofilm removal) and during (63% biofilm removal) an erosion experiment. (B) Time-point of 50% detachment for *B. subtilis* NCIB 3610 and mutant strains in water. (C) Wetting behavior of *B. subtilis* NCIB 3610 and mutant strains. (D) Normalized biofilm elasticity of *B. subtilis* NCIB 3610 and mutant strains as determined by rheology. All data depicted represent mean values with corresponding standard deviation of at least three independent samples.

In conclusion, this study demonstrates that *B. subtilis* NCIB 3610 biofilm only possesses full erosion resistance when all matrix components are present. As soon as only one biofilm component is missing, the erosion resistance is strongly reduced. However, it is to date unknown, how the different components interact with each other.

Individual contributions of the candidate: I contributed to the design and implementation of the experiments, the data analysis, and the writing of the article.



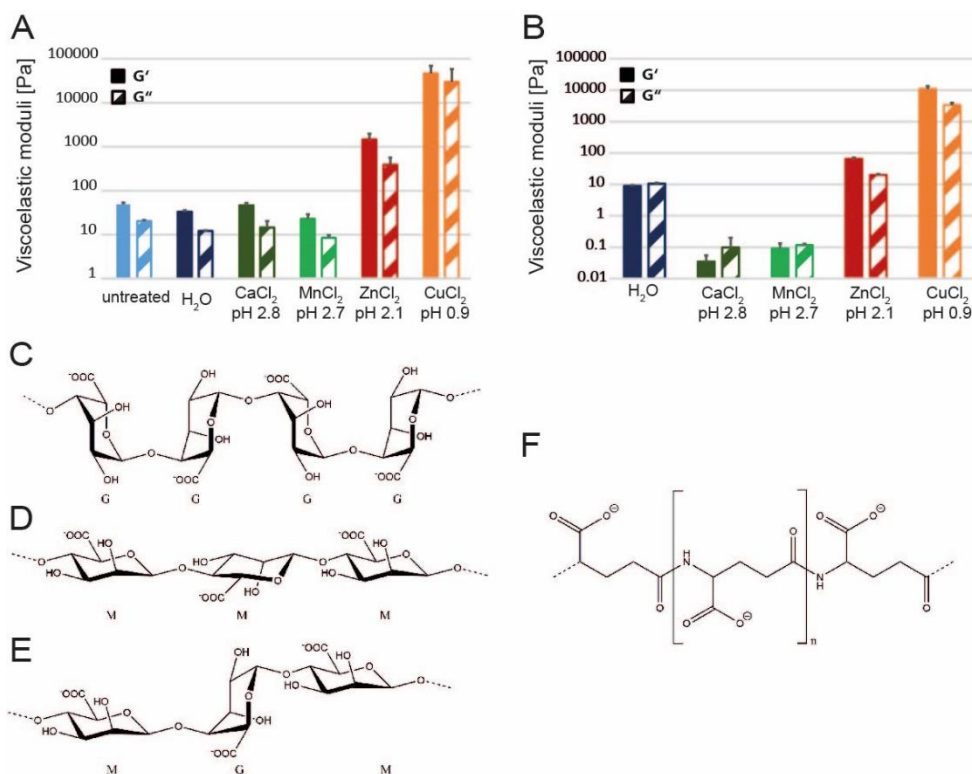
## 4.2 Chelate chemistry governs ion-specific stiffening of *Bacillus subtilis* B-1 and *Azotobacter vinelandii* biofilms

M. Kretschmer and O. Lieleg [145]

The viscoelastic properties of bacterial biofilms can vary strongly, depending on the bacterial species, environmental conditions and presence of chemical substances. In many cases, biofilms can cause severe problems for industry and human health. To be able to combat bacterial biofilms or to use them for human purposes it is important to understand the physical and chemical principles, which the material properties of bacterial biofilms rely on.

In this study, the effect of positively charged metal ions on the stiffness of biofilms from the species *Bacillus subtilis* B-1 and *Azotobacter vinelandii* was investigated. A main component of *B. subtilis* B-1 biofilm is the polyanionic biomacromolecule  $\gamma$ -PGA. When *B. subtilis* B-1 biofilm was exposed to certain divalent and trivalent ions, its stiffness increased strongly, whereas other divalent ions did not lead to this effect (**Figure 13A**). Interestingly, exactly the same ions led to the formation of a gel, when added to a solution of  $\gamma$ -PGA that was extracted from *B. subtilis* B-1 liquid culture (**Figure 13B**). This indicates that the ionic crosslinking of these biomacromolecules is responsible for the increased stiffness of the biofilms. A different trend was observed for *A. vinelandii* biofilm, which does not contain  $\gamma$ -PGA, but can contain alginate instead (depending on the cultivation method). When alginate is present in the biofilm, all tested divalent ions lead to an increased stiffness, whereas this effect cannot be observed when the biofilm does not contain this biomacromolecule. Here, different ions than for *B. subtilis* B-1 stiffen the biofilm. However, the same ions that lead to an increased stiffness of *A. vinelandii* biofilm, also lead to the formation of a gel, when added to solutions of alginate that was extracted from liquid cultures of this bacterium. This suggests that here, alginate is the crucial component for the stiffening effect by the addition of positively charged ions. Those results were interpreted such that the ions lead to the formation of chelate complexes with the respective biomacromolecules in *B. subtilis* B-1 and *A. vinelandii* biofilms. Alginate and  $\gamma$ -PGA have in common, that they are both polyanionic, however due to the different structures (**Figure 13C - Figure 13F**), different ions are able to initiate the formation of chelate complexes. In addition, alginate can occur in different conformations depending on its biological source. Alginate from *A. vinelandii* and from algae can contain G-blocks, whereas the alginate of other bacteria, such as *Pseudomonas aeruginosa* is only composed of M-blocks or an alternating sequence of M- and G-Monomers. As it is not possible to form chelate complexes with divalent cations and alginates that only possess M-blocks, *P. aeruginosa* biofilm cannot be stiffed by divalent cations (as reported in previous studies). It remains not fully understood, why different divalent ions lead to different effects on the biofilm of *B. subtilis* B-1. An analysis of the data obtained here in combination with results from the literature indicates that the ionic size plays a crucial role here. However, the ionic size cannot be measured directly and varies depending on the binding partner resulting in different

literature values. Nevertheless, it seems that smaller ions such as  $\text{Cu}^{2+}$  lead to the formation of chelate complexes with the biomacromolecules more easily than larger ones such as  $\text{Ca}^{2+}$ .



**Figure 13:** Viscoelastic moduli of *B. subtilis* B-1 biofilms (A) and  $\gamma$ -PGA solutions (B) after exposure to different aqueous solutions containing metal ions. Full bars denote the storage modulus,  $G'$ , and striped bars the loss modulus,  $G''$ . The error bars represent the standard deviation as obtained from at least three independent samples. The possible structural conformations of different alginate- and  $\gamma$ -PGA chains are shown in C-F. An alginate chain can be composed of  $\alpha$ -L-guluronate residues forming G-blocks (C), of  $\beta$ -D-mannuronate residues forming M-blocks (D) or they can comprise an alternating mixture of both (E). The structure of a  $\gamma$ -PGA chain is shown in (F).

In conclusion, this study demonstrates, that formations of chelate complexes with the respective biomacromolecules of biofilms are crucial for obtaining a stiffness increase when the biofilms are exposed to certain cations. These central biomacromolecules are  $\gamma$ -PGA for *B. subtilis* B-1 biofilms and alginate for *A. vinelandii* biofilms. Due to different structures of the biomacromolecules, different cations are able to form a chelate complex. On the side of the cations, their size seems to be the determining factor whether a chelate complex is formed or not. These findings contribute to the understanding of the viscoelastic behavior of biofilms and the molecular principles governing their properties. They are useful to increase the biofilm strength for applications, where the biofilms are used for human purposes, as in bioreactors or for wastewater treatment.

Individual contributions of the candidate: I contributed to the conception of this study, the design and implementation of the experiments, and the writing of the article. I was fully responsible for conducting the experiments and data analysis.

### 4.3 Biofilm adhesion to surfaces is modulated by biofilm wettability and stiffness

M. Kretschmer, C. A. Schüßler and O. Lieleg [146]

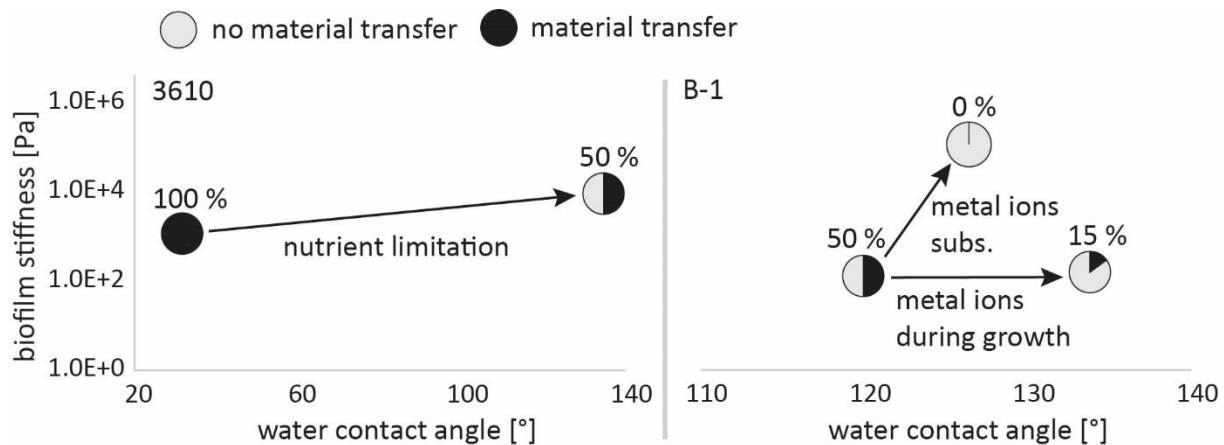
The attachment of bacterial biofilms to surfaces is important for biofilm formation and thus central to cultivate or combat them. However, it is not trivial to measure biofilm adhesion directly, since biofilm attachment is dependent on different properties; especially a clear differentiation from biofilm cohesion is challenging. When biofilm attachment is measured indirectly, for example by determining the erosion resistance, not only the adhesion, but also the viscoelastic properties and the wetting behavior play a role. For technical materials such as glues, a variety of different methods are established to quantify these properties individually. However, biofilms are living materials that actively form on surfaces. Thus, standardized measurement methods for the characterization of the cohesion and adhesion of biofilms grown *in situ* are scarce.

In this study a method was introduced, which enables the characterization of the adhesion and cohesion properties of bacterial biofilms *in situ*. The method is based on a commercial rheometer, which applies normal forces to a biofilm on its growth substrate without the need of disrupting the biofilm prior to the measurement, and then measures the detachment force. It enables the investigation of different material pairings, such as biofilm/metal or biofilm/biofilm. By analyzing the detachment behavior and material transfer of biofilms tested in different configurations, conclusions about the adhesion and cohesion properties can be drawn. In the detachment tests conducted here, four different modes of "fracture" can occur: One mode of fracture is the complete detachment of the biofilm from its growth substrate in which the whole biofilm is transferred from one side to another and the biofilm adhesion to its growth substrate is measured. Another possibility is the complete separation of the two surfaces without any material transfer; here the adhesion between those surfaces is measured. The third mode is the cohesion fracture, in which the biofilm is completely ruptured apart and the biofilm cohesion is determined by the rheometer. Also here, material transfer can occur, however compared to the mode of fracture mentioned first, in a lower extent. And lastly, a mixed fracture can occur, where only parts of the biofilm are ruptured and transferred. In this case, no clear disentanglement of the individual effects is possible.

With this setup, the detachment behavior of biofilms, generated by *B. subtilis* NCIB 3610, *B. subtilis natto* and *B. subtilis* B-1 bacteria, was investigated. Whereas the detachment behavior of *B. subtilis* B-1 biofilms was dominated by adhesion forces, the failure behavior of the other two biofilms was dominated by cohesion forces. In contrast to *B. subtilis* B-1 biofilm, which is very soft and hydrophobic, the biofilms of *B. subtilis* NCIB 3610 and *B. subtilis natto* are hydrophilic and exhibit a higher stiffness. Thus, the obtained results suggested, that the viscoelastic properties and wetting behavior play a major role for the detachment behavior of the biofilms. In further tests, the influence of these two properties on the adhesion and cohesion behavior of bio-

films was investigated in more detail. The biofilms were modified to alter these two properties: The addition of certain positively charged ions to the biofilm growth substrate leads to an alteration of the wetting behavior and stiffness of *B. subtilis* B-1 biofilms. In contrast, with the addition of  $\text{Cu}^{2+}$  to mature *B. subtilis* B-1 biofilms, the stiffness could be strongly increased without changing the wetting behavior. Finally, the cultivation of *B. subtilis* NCIB 3610 under nutrient limitation changed the wetting behavior of the biofilm from hydrophilic to rose petal-like hydrophobic and increased the stiffness as well.

With these investigations, it could be concluded, that biofilms with a low stiffness and hydrophilic properties tend to show material transfer during the detachment process and thus mostly cohesion fractures. In contrast, biofilms with a high stiffness and hydrophobic properties tend to exhibit no material transfer and thus adhesion fractures (**Figure 14**). Overall, these measurements showed that the method introduced here is suitable for the characterization of the adhesion and cohesion behavior of bacterial biofilms *in situ*. One advantage of this method is the application of a uniform stress distribution to the biofilm. Moreover a characterization of both, the adhesion and cohesion behavior is feasible by analyzing the fracture mode. In addition, the modular setup enables the investigation of a variety of different material pairings such as ceramics, polymer materials, hydroxyapatite and tissue samples. Also the environmental conditions can be changes; by extending the experimental setup with a chamber, that enables the immersion of the biofilms during the detachment process.



**Figure 14:** Relation between the biofilm stiffness and wetting behavior of the investigated biofilms and the occurrence of material transfer during the detachment tests in which two biofilm surfaces of the same kind were pressed against each other for *B. subtilis* NCIB 3610 (left) and *B. subtilis* B-1 (right). Black color denotes samples where material transfer occurred; gray colors denote samples which did not show such material transfer.

Individual contributions of the candidate: I contributed to the conception of this study; I was responsible for the design and implementation of the experiments and the data analysis, and I contributed to the writing of the article.

## 4.4A rotating bioreactor for the production of biofilms at the solid-air interface

Unpublished manuscript – in review process

### 4.4.1 Abstract

Conventional bioreactors are typically developed for the production of planktonic bacteria or submerged biofilms. In contrast, reactors for the continuous production of biofilms at the solid-air interface are scarce, and they require specific conditions since the bacteria need to attach firmly to the surface and require a permanent supply of moisture and nutrients from below. Recently, research from the field of civil engineering has pinpoint an increased need for the production of terrestrial biofilms: several variants of *Bacillus subtilis* biofilms have been shown to be useful additives to mortar that increase the water repellency and thus the lifetime of the cementitious material. The bioreactor introduced here allows for the continuous production of such bacterial biofilms at the solid/air interface, and they have virtually identical properties as biofilms cultivated via classical microbiological techniques. This is made possible by equipping a rotating cylinder with a porous membrane that acts as a solid growth substrate the bacterial biomass can form on. In this configuration, nutrient supply is enabled via diffusive transport of a suitable growth medium from the core volume of the cylindrical reactor to the membrane surface. In addition to cultivating bacterial biofilms, the versatile and adaptable setup introduced here also enables the growth of other microbial organisms including the yeast *Saccharomyces cerevisiae* and the fungus *Penicillium chrysogenum*.

### 4.4.2 Introduction

According to Yin and Yang philosophy, there is something “bad” in every “good” and vice versa. Similarly, bacterial biofilms, which are typically considered to be highly undesirable contaminants in industrial or medical setups, can have their perks as well. Indeed, for many biotechnological applications, this persistent form of bacterial communities is actually preferred over planktonic cells [44, 84, 147] – and this can be attributed to the same astonishing material properties that render biofilms annoying when found on surfaces such as pipes or implants: they can be sticky [90, 146], sturdy and resilient [148, 149] and liquid-repellent [45, 46]. Recent research efforts have identified a broad range of beneficial applications where bacterial biofilms can serve as interesting components, and example areas include agriculture, biomedicine, (environmental) biotechnology, electricity generation, and construction engineering [37].

The latter application area might seem the most surprising – even though biological additives to construction materials were already explored by the ancient Egyptians and Romans and during the Qing dynasty [150, 151]. Recently, the idea of using bacterial biofilms as additives to cementitious materials has been rediscovered, and the resulting hybrid mortar has been shown to possess highly interesting water-repellent properties [81, 82]. Of course, for such a bio-enhanced material to be used in real construction engineering efforts, larger biofilm amounts

are required than can be grown in the lab using classical microbiological assays. However, there are only few examples of dedicated bioreactors that produce bacterial biofilms – and in those kinds of bioreactors, the bacteria are either attached to (suspended or packed) support materials or directly to the bioreactor surface. Examples of biofilm bioreactors using support materials include sequencing batch reactors [124, 152, 153], continuous stirred tank reactors [125, 154-156], packed- or fluidized-bed reactors [126, 157-160], and trickling bed reactors [127, 128, 161]. Rotating disc contractors or membrane bioreactors are common examples where biofilm production occurs on the bioreactor surface, and those are typically used in wastewater treatment plants [129, 162-164]. The latter bioreactor variant also comes with the advantage to easily separate the biofilm after usage and to enhance biofilm attachment and growth by chemically modifying the reactor surface [165-167].

In most of these bioreactors, the biofilms perform a dedicated function in situ: The bacteria attach to organic or inorganic support materials, generate a biofilm, then catalyze reactions within the bioreactor, and finally are removed or inactivated once their task is fulfilled [168]. For an application in construction engineering, however, the biofilm itself is the desired product that needs to be harvested from the bioreactor. Thus, for the bioreactor to be sustainable, the support material used for biofilm cultivation needs to be reusable.

Here, we introduce a novel type of bioreactor that allows for cultivating bacterial biofilms on a solid substrate. This reactor makes use of a cylindrical geometry such that the substrate inoculation with bacteria and the biofilm harvesting step are conducted at different locations of the cylinder surface. Nutrient supply is guaranteed via a combination of diffusion and convection effects that drive a nutrient solution from the core of the cylinder to its outer surface. Here, a combined agar/membrane layer supports the growth of different bacterial biofilms as well as yeast and fungus biofilms. As a consequence of this particular design, when selecting a sufficiently low rotation speed, a continuous biofilm growth/harvest cycle is enabled. We show that *B. subtilis natto* biofilms harvested from this bioreactor have virtually identical material properties and hydrophobicity-conveying abilities to mortar as when they are grown in a classical microbiological manner, *i.e.*, on agar-filled petri dishes.

#### 4.4.3 Materials and Methods

##### 4.4.3.1 Microorganisms and growth conditions

Two different bacterial stains were used in this study: *Bacillus subtilis natto* (27E3), obtained from the Bacillus Gene Stock Center (BGSC, USA) and *Bacillus subtilis* 3610, obtained from the lab of Roberto Kolter (Harvard Medical School, USA). Additionally, the yeast *Saccharomyces cerevisiae* (Dr. Oetker, Bielefeld, Germany) and the fungus *Penicillium chrysogenum* DSM 848 (DSMZ, Germany) were used. For the cultivation of bacterial biofilm on agar plates and membranes, liquid cultures of *B. subtilis natto* and *B. subtilis* 3610 were generated by incubating small pieces of a

frozen glycerol stock in 10 mL of 2.5% (w/v) LB medium (Luria/ Miller; Carl Roth GmbH, Karlsruhe, Germany) at 37 °C while shaking at 300 rpm for ≈18 h. For biofilm growth experiments conducted on the bioreactor, the same liquid cultures were prepared in 500 mL of 2.5% (w/v) LB medium at 37 °C while shaking at 100 rpm for ≈18 h.

Yeast liquid cultures were prepared by inoculating a small piece of dried yeast into 10 mL of yeast extract peptone dextrose (YEPD) medium, which contains 1% yeast extract (Carl Roth GmbH, Karlsruhe, Germany), 2% peptone (Carl Roth GmbH, Karlsruhe, Germany) and 2% glucose (Sigma-Aldrich Corp., St. Louis, USA). The culture was incubated at 30 °C while shaking at 300 rpm for ~18 h.

To cultivate fungus, a potato/dextrose medium was prepared. In brief, 200 g potato was peeled and sliced into small cubes. After boiling those pieces in 1 L distilled water for 1 h, the infusion cleared by sieving, 20 g glucose was added to the infusion and the volume was adjusted to 1 L. Then, a piece of frozen glycerol stock of *P. chrysogenum* was inoculated in 10 mL of this potato dextrose medium, and the culture was incubated at 24 °C while shaking at 300 rpm for 3 days.

#### 4.4.3.2 Microbial cultivation on membranes and agar

To find an optimal substrate for the growth of different microorganisms (bacteria, yeast, fungus), several commercial membranes with a pore size of 0.2 µm each were tested: cellulose nitrate (obtained from analytical funnels for microbiology, Sigma-Aldrich Corp., St. Louis, USA), surfactant-free cellulose acetate (SFCA; Nalgene™ Rapid-Flow™ Membrane, Thermo Fisher Scientific, Waltham MA, USA), hydrophilic polyvinylidene difluoride (hydrophilic PVDF; Microlab Scientific Co., Ltd, Shanghai, China), hydrophobic polyvinylidene difluoride (hydrophobic PVDF; Immobilon-PSQ Membrane, Merck KGaA, Darmstadt, Germany) and polycarbonate (PC; ipPore™ Track Etched Membrane, it4ip S.A., Louvain-la-Neuve, Belgium) membranes. Additionally, to hydrophilize the commercial hydrophobic PVDF membranes, these membranes were immersed into isopropyl alcohol (i-PrOH, HPLC grade > 99.9%, Sigma-Aldrich Corp.) for 12 h. Afterwards, the samples were immersed into deionized water for 6 h to replace most of the alcohol with water. The success of this hydrophilization procedure was verified by determining the contact angle formed by a small water droplet (4.5 µL) on the membranes using the video-based optical contact angle measuring system Drop Shape Analyzer (Krüss - Easy Drop) and the software ADVANCE - sessile drop. Those measurements were repeated 5 times on each membrane.

For bacterial growth tests, round samples with a diameter of 3 cm were cut out from each membrane variant and sterilized by exposure to UV-light for at least 15 min. Then, these sterile membranes were placed onto 1.5% (w/v) agar gel patches of the same diameter having a thickness of ~2.4 mm. The membrane-covered agar patches were inserted into tailored PTFE holders with large holes, which then were placed into the wells of a 6-well plate. Each well was filled with ~8 mL of LB medium, YEPD medium and potato/dextrose medium, respectively. Afterwards, the

amount of added liquid media was adjusted until direct contact with the agar patches was achieved. Then, 13  $\mu\text{L}$  of an overnight culture (diluted to an OD of 0.7) of either bacteria (*B. subtilis natto* and 3610) or yeast (*S. cerevisiae*) were distributed across these membrane pieces. To grow *P. chrysogenum* biofilms on the membranes, the same procedure was followed yet without diluting the fungal overnight culture. The 6-well plate was then covered and a sterile towel was placed between the samples and the cover to prevent condensate water from dropping onto the growing biofilms. To promote the diffusion of nutrients from the medium reservoir towards the upper membrane surface, a temperature gradient was created by incubating the inoculated 6 well-plates on a heating plate at 37 °C for 2 days (with the top of the plates exposed to room temperature). Owing to the different conditions required for fungus growth, the fungus biofilms were grown at room temperature (without using a heating plate) for 4 days. For all samples, the liquid medium was refreshed daily. After the respective incubation time, the formed biofilms were harvested from the membrane surfaces by collecting them with a spatula and their mass was determined by weighing (Balance XSE205 DualRange, Mettler Toledo GmbH, Gießen, Germany).

As control samples that allow for assessing putative diffusion-hindering effects of the different membrane variants, all microorganisms were also inoculated directly onto agar patches and incubated at the same conditions as described above. A second set of control samples was created to quantify putative growth retardation effects arising from the diffusion-limited nutrient supply present in those membrane-covered agar patches (which resembles the final condition on the bioreactor). For this purpose, standard agar plates with a diameter of 90 mm were prepared and enriched with 2.5% LB medium; thus, in those samples, the nutrients were readily available at the surface of the agar layer at the start of microbial inoculation. Then, 100  $\mu\text{L}$  of *B. subtilis natto* culture (diluted to an OD of 0.7) were distributed on these LB-enriched agar plates and incubated in an incubator at 37 °C for 2 days.

For each microorganism/substrate combination, three independent samples were prepared from each growth batch, and all experiments were repeated three times using a different growth batch each time.

#### 4.4.3.3 Bacterial cultivation on the bioreactor

To grow *B. subtilis natto* biofilm on the bioreactor, the bioreactor was fully assembled and an agar layer was applied to the outer surface of the cylinder. To do so, the cylinder was manually rotated while partially immersed into a bath of liquid agar (1.5% (w/v) agar-agar, Carl Roth GmbH) heated to a temperature of  $\approx 60$  °C; a full rotation was conducted, then the cylinder was removed from the agar bath until the applied agar layer had solidified. This procedure was repeated three times, after which an agar layer of  $\approx 3 - 5$  mm thickness was obtained. Additionally, 2 mL liquid agar was inserted into each hole of the cylinder (from its inside) to create an addi-



tional resistance that helped preventing the liquid medium filled into the core volume of the cylinder from leaking out.

A hydrophilic polyvinylidene fluoride (PVDF) membrane (Microlab Scientific Co., Ltd, Shanghai, China) was then added on top of the agar layer and fixed as follows: A 10 mM solution of 1% DOPA (dopamine hydrochloride, Sigma-Aldrich Corp., St. Louis, USA; dissolved in pH 8.5 TRIS buffer; Illinois Tool Works Inc., Glenview, USA) was applied in circular lines onto the agar surface to glue the membrane to the agar layer; in addition, a DOPA-hyaluronic acid conjugate was used to glue the membrane overlap regions to each other. For this DOPA-hyaluronic acid conjugate, a solution of 1% HA (hyaluronic acid sodium salt, Streptococcus equi, 91%, ThermoFisher GmbH, Kadel, Germany), 0.1% EDC (1-Ethyl-3-(3-dimethylaminopropyl) carbodiimide-hydrochlorid, 99%, Carl Roth GmbH) and 0.1% NHS (N-hydroxysuccinimide, 98%, Sigma-Aldrich Corp.) was prepared in 10 mM MES and buffered to pH 5. The HA solution and EDC/NHS solution were dissolved separately. Additionally, a solution of 1% DOPA (dopamine hydrochloride, Sigma Aldrich Corp.) was prepared in PBS buffer at pH 8. After stirring overnight, the solutions were mixed and dialyzed for 72 h at 4 °C using a dialysis membrane (Spectra/Por®7 Dialysis membrane Pre-treated RC tubing, MWCO: 50 kD, Spectrum Chemical Mfg. Corp., New Brunswick, USA). The dialyzed solution was frozen at 80 °C and lyophilized (Alpha 1-2 LDplus, Martin Christ Gefriertrocknungsanlagen GmbH, Osterode am Harz, Germany). In a final step, the freeze dried DOPA-conjugate was dissolved at 8 mg mL<sup>-1</sup> in ddH<sub>2</sub>O, poured in a petri dish and dried at 60 °C to generate a thin adhesive film.

To supply the bacteria on the outer membrane surface with nutrients, the inside of the cylinder was infused with 5% (w/v) LB medium (Luria/ Miller; Carl Roth GmbH). For the first ≈24 h, the reactor was run without bacteria to ensure that the liquid medium has enough time to diffuse from the inside to the outer surface of the cylinder. Subsequently, the cylinder was partially immersed (2 – 3 cm) into a bacterial bath, *i.e.*, a liquid culture of planktonic *B. subtilis natto* bacteria having an optical density of 0.1 - 0.15. After 24 hours, the bacterial bath was renewed and the PDMS blade was installed to initiate the biofilm harvesting process.

To examine the microbial composition of the cultivated biofilm (*i.e.*, to test for contaminations with other bacteria), we collected biofilm samples from three different areas of the cylinder and determined their mass by weighing. Then, these biofilm sample were added to 2 mL of a physiological saline solution (0.9% w/v NaCl), and then rigorously stirred at ~2500 rpm for 20 min followed by a short vortexing step. The such obtained bacterial solution was serially diluted until a dilution of 10<sup>-6</sup> was obtained. Then, 100 µL of each diluted solution was inoculated on LB agar plates in duplicates and distributed by adding glass beads and shaking the plates. The inoculated agar plates were then incubated at 37 °C for 24 hours. For each dilution step, the grown colonies were evaluated regarding their morphological appearance, and the number of viable bacteria within the initial biofilm (CFU/mg biofilm) was calculated from the last two dilutions.

#### 4.4.3.4 Rheology

To compare the viscoelastic properties of biofilms cultivated under the different conditions described above (*i.e.*, on agar filled petri dishes and on the membrane surface of the bioreactor), rheological measurements were conducted. For this purpose, a commercial shear rheometer (MCR 302; Anton Paar) equipped with a 25 mm steel measuring head (PP25) and a plate–plate geometry was employed. The plate separation was set to 0.3 mm, and a solvent trap was installed to prevent sample drying during the measurements that were realized at 21 °C and in strain-controlled mode. To ensure linear material response, small strains corresponding to a torque of  $\approx 0.5 \mu\text{Nm}$  (this corresponds to a shear stress of  $\approx 0.1 \text{ Pa}$ ) were applied. In every rheological experiment, both the storage and loss modulus were determined over a frequency range of 0.1–10 Hz. Since, in all cases described in this study, the moduli obtained for a given biofilm sample were only weakly dependent on frequency, the obtained storage moduli were averaged over the complete measured frequency spectrum to obtain the bar plots shown in the manuscript. Obvious outliers resulting from measuring artefacts were excluded from calculating these mean values. For each sample type, at least three samples were tested, which were obtained from different locations of the reactor surface and from different agar plates, respectively.

#### 4.4.3.5 Biofilm-enriched mortar samples

Sample preparation:

To cultivate biofilm on agar plates, 100  $\mu\text{L}$  of a bacterial overnight culture were plated onto each agar plate (1.5% v/w, Agar Agar, Kobe I, Carl Roth GmbH; enriched with LB medium (2.5% v/w)) and incubated at 37 °C for 24 h. From those agar plates, the grown biofilm was harvested by manually scraping the plates. On the bioreactor, biofilm was grown as described above and manually collected from the PDMS blade. Both biofilm variants were freeze-dried for three days, and afterwards ground into a fine powder having an average particle size of  $\sim 500 \mu\text{m}$ . In full analogy to previous experiments with such freeze-dried biofilms [81], the biofilm concentration added to mortar is described by the parameter *bc* (biofilm content), which describes the ratio of fresh biofilm with respect to the mass of dry cement used for mortar sample generation. Using the mass loss factor, which is defined as the ratio of fresh biofilm with respect to the mass of lyophilized biofilm, the required amount of lyophilized biofilm can be calculated to match the respective amount of fresh biofilm.

Water repellency tests:

To evaluate the wetting resistance of different mortar samples, small mortar samples were prepared by mixing a 3:1 mixture of CEN standard sand (NORMENSAND GmbH, Beckum, Germany) and cement (Portland cement CEM 42.5 N, Schwenk Zement KG, Ulm, Germany) with a suspension of biofilm powder in the respective amount of water. All mortar samples were prepared with a w/c ratio of 0.5 and cured for 3 days at room temperature before contact angle meas-

urements were conducted. For measuring contact angles, a drop shape analyzer (DAS25S, Krüss GmbH, Hamburg, Germany) was used. Five 4  $\mu$ L droplets of ddH<sub>2</sub>O were placed onto each sample at different spots, and images were acquired from a lateral view using the built-in high-speed camera (CF04, Krüss GmbH, Hamburg, Germany). The contact angle was then evaluated using the software ADVANCE (Krüss GmbH, Hamburg, Germany).

For capillary water uptake experiments, samples were prepared according to DIN EN 196-1 using an automatic laboratory mortar mixer (ToniMix, Zwick Roell, Ulm, Germany). Cement and biofilm powder were added to the desired amount of water within 10 s, and the mixing process was immediately started at a stirring speed of 140 rpm. After 30 s, sand was added within a time window of 30 s, and the mixture was stirred at a stirring speed of 285 rpm for an additional 30 s. Then, the mixing process was stopped for 90 s. During this break, mortar adherent to the stirring head and/or the upper part of the bowl was transferred back to the bottom of the bowl using a rubber scraper, and the stirring process was continued for additional 60 s at a stirring speed of 285 rpm. The prepared mortar was then poured into the desired mold within 120 s, while being compacted using a vibrating table.

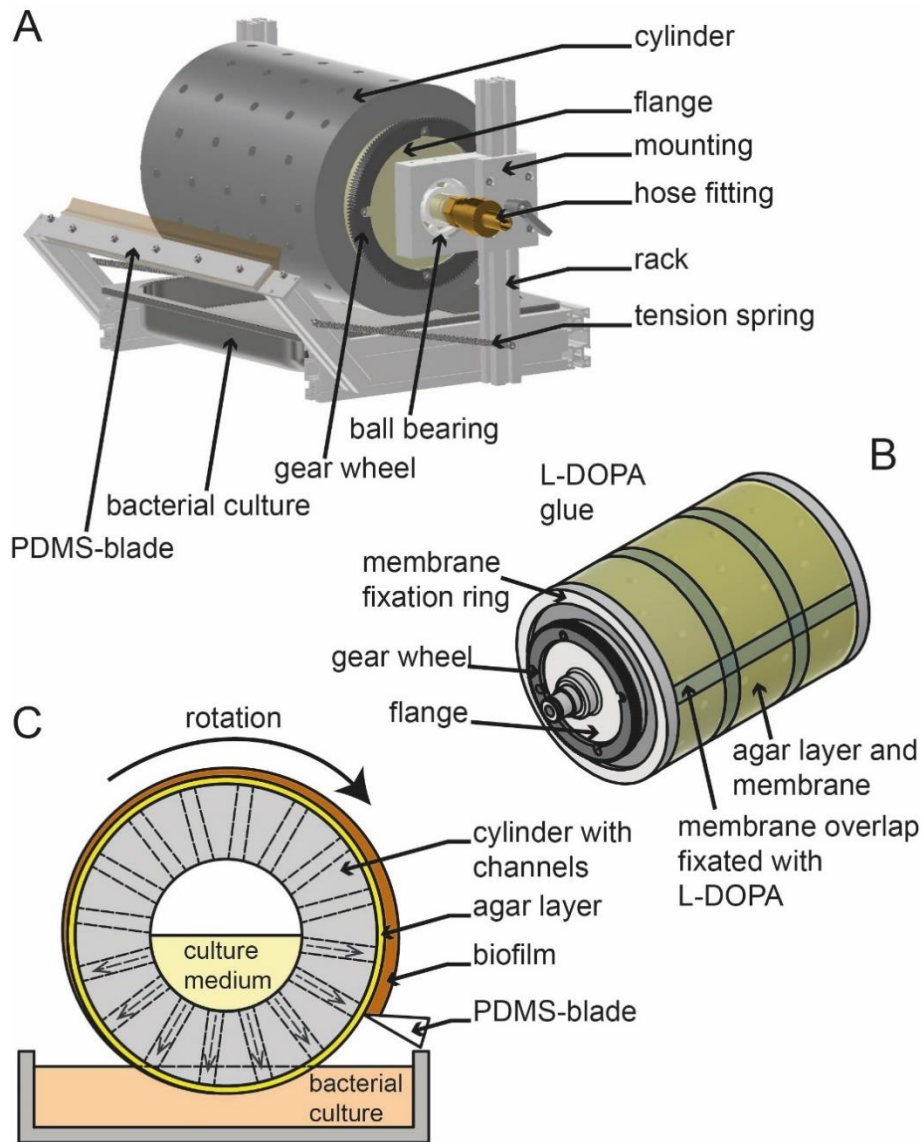
#### 4.4.4 Results and Discussion

##### 4.4.4.1 Bioreactor design

*Bacillus subtilis* biofilms form at the solid/air or liquid/air interface, and they require a moisture and nutrient supply from their growth substrate. For instance, a thin biofilm layer – so called pellicles – can be formed on the surface of standing liquids. Yet, here, the generated biomass is very low. The most common laboratory procedure to cultivate *B. subtilis* biofilm makes use of agar-filled petri dishes, where the nutrients (typically LB medium) are added to the agar layer. However, due to the nutrient depletion from the agar substrate during biofilm growth, this procedure does not allow for a continuous biofilm cultivation. Moreover, biofilm harvesting from such agar plates needs to be conducted manually and carefully to ensure that only biofilm is removed during the harvesting procedure while avoiding contaminations of the bacterial biomass with small agar pieces. Owing to those limitations, this traditional biofilm cultivation process is very material- and work-intensive and thus not suitable for the production of larger biofilm amounts.

To solve those limitations, we here introduce a new type of bioreactor that meets the requirements mentioned above but allows for a continuous growth/harvesting cycle of biofilm on/from the same substrate. The basic principle of this new bioreactor is depicted in **Figure 15**. It comprises a hollow cylinder that is rotated along its long axis. At its lower apex, the cylinder is immersed into a bacterial liquid culture which – during rotation – applies a bacterial coat to the cylinder surface. This cylinder has a length of 26.8 cm and an outer diameter of 19.9 cm, which results in an outer surface area of 1675 cm<sup>2</sup>. It is suspended horizontally by a framework, which

allows for adjusting the z-position of the cylinder (**Figure 15A**). As a material for this cylinder, we selected hydrophilic polypropylene (PP-H AlphaPlus, Simona AG, Kirn, Germany). This material was chosen as it can be autoclaved (for sterilization) and offers mechanical properties suitable for machining. However, growing biofilms directly on this PP material is very difficult; thus, a membrane layer is added on top to facilitate bacterial attachment and growth (*vide infra*).

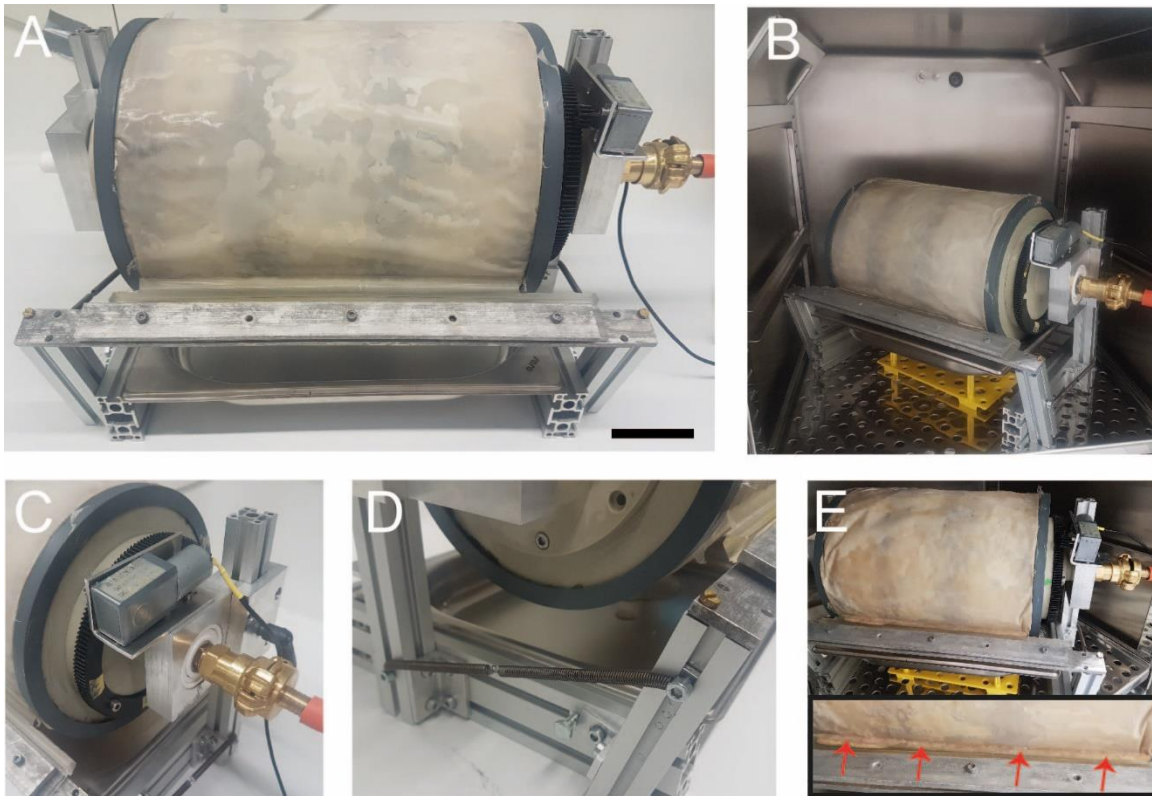


**Figure 15:** Schematic representations of the bioreactor. (A) A cylindrical, hollow central unit can be positioned at different z-levels such that it is partially immersed into a bacterial liquid culture located in a tray. (B) The cylinder is covered with an agar layer and a membrane to support microbial attachment and growth. (C) The growth medium located in the core of the cylinder reaches the membrane surface through channels in the cylinder wall by a combination of diffusion and convection effects. During a full rotation of the cylinder, the whole surface becomes inoculated with the bacterial liquid culture, and the grown biofilm is automatically harvested by a PDMS-blade.

Nutrient supply to this membrane layer is enabled by a combination of two measures: first, cylindrical holes with a diameter of 1 cm are drilled into the PP cylinder; this allows a nutrient solu-

tion added to the inner volume of the cylinder to reach the outer surface. Resupply of this nutrient solution is guaranteed by connecting the inner volume of the cylinder to a tank via tubings. Second, an agar layer of 3 – 5 mm (1.5%, Carl Roth GmbH) is sandwiched between the cylinder and the membrane; during this step, the holes in the cylinder are filled with agar as well. This agar layer acts as a sponge-like structure that guarantees nutrient transport to the membrane surface via capillary forces while preventing uncontrolled leakage of the nutrient solution from the bottom part of the bioreactor. The membrane is fixated to this agar layer in two ways: at the edges of the cylinder, two rigid PVC rings clamp the membrane to the cylinder; in addition, thin lines of L-DOPA glue the membrane to the agar substrate and stabilize the membrane/membrane overlap region (**Figure 15B**).

The last structural component of the bioreactor is responsible for biofilm harvesting: We installed a PDMS-blade, which is brought into mechanical contact with the membrane surface via elastic springs (spring rate:  $0.7 \text{ N mm}^{-1}$ ; **Figure 15A**). Images of the fully assembled bioreactor are shown in **Figure 16**. With this configuration – once the bioreactor is set into rotation – the PDMS-blade can collect the cultivated biofilm from the membrane surface without damaging the membrane (**Figure 15C** and **Figure 16A**). Such rotation is enabled by a 12 V direct current motor (BQLZR DC 12V 0.6RPM, Shenzhen, China; **Figure 16C**), and the rotation speed is chosen to be slow enough that a continuous biofilm layer can form during 5/6 of a full rotation (*i.e.*, a full rotation requires 12 h to conclude). To implement this slow speed, the rotational movement is clocked, so that the cylinder rotates for  $60^\circ$  and then pauses again. Once the harvesting step is completed, the membrane surface is immersed again into the bacterial liquid culture, and the cycle starts over. The whole bioreactor is placed into an incubator (CB-S 170, Binder GmbH, **Figure 16B**), where the temperature (typically,  $37^\circ\text{C}$ ) and the relative humidity (we here selected 80% - 90%) can be controlled. The biofilm harvested from the reactor by the PDMS blade that is slightly pressed against the membranes by springs (**Figure 16D** and **Figure 16E**) can then manually be collected from this blade, *e.g.*, once every 24 h.



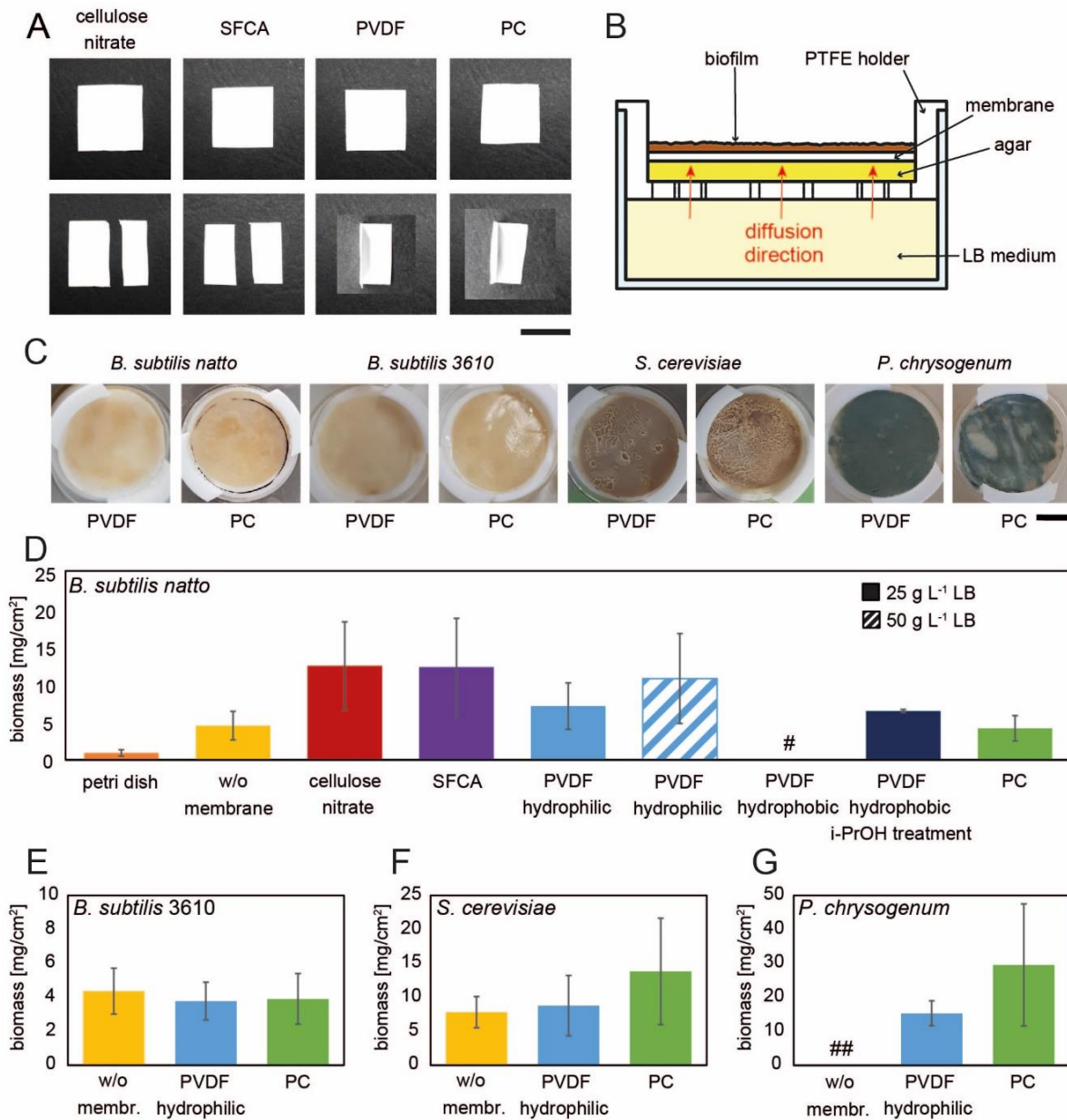
**Figure 16:** Detail images of the assembled bioreactor. (A) Side view depicting the membrane-covered cylinder and the PDMS blade used for biofilm collection. The bioreactor is placed into an incubator (B) and connected to an outside reservoir (containing growth medium) via tubings. A 12 V motor moves the cylindrical reactor in a rotational manner (C). A spring system ensures that the PDMS blade used for biofilm collection is in contact with the membrane surface (D). After a minimum of one full rotation, the biofilm material grown on the membrane surface is automatically harvested by the PDMS blade (E, red arrows indicate the collected biofilm material). The scale bar in (A) corresponds to 5 cm.

#### 4.4.4.2 Membrane selection for microorganism cultivation

To cultivate microorganisms on the cylinder, a membrane layer is used. Employing such a membrane surface is preferred over direct cultivation on the agar layer since such membranes are more durable than the brittle agar; thus, the membranes should be able withstand multiple harvesting cycles without being damaged. To identify a membrane material that combines suitable material properties with good microbial growth behavior on its surface, we compare the performance of four different membranes, which were reported in the literature to allow for microbial cultivation [169, 170]: a cellulose nitrate membrane, a surfactant-free cellulose acetate (SFCA) membrane, two polyvinylidene difluoride (PVDF) membranes (hydrophilic and hydrophobic, respectively), and a polycarbonate (PC) membrane (**Figure 17A**) – and all those membrane variants were selected to have a pore size of 0.2  $\mu\text{m}$  each to prevent inoculated bacteria from penetrating the membrane layer.

In a first step, the membranes are inoculated with *B. subtilis natto* bacteria and then incubated to allow for biofilm formation. For those growth tests, a custom-made setup is chosen (see **Fi-**

**gure 17B)** to mimic the growth conditions present on the surface of the bioreactor. In brief, with this setup, nutrient supply to the membrane surface is enabled by a combination of diffusion and convection effects (see section **4.4.3.2** for details). After an incubation time of 2 days, we find equal or even higher amounts of *B. subtilis natto* biofilm on almost all membrane variants than when bacterial inoculation is conducted directly on agar (**Figure 17C**). Only on hydrophobic PVDF membranes, biofilm formation is negligibly low. However, after treating those hydrophobic PVDF membranes with i-PrOH, the membranes become slightly hydrophilic as verified by an alteration of the contact angle from  $149.31^\circ \pm 5.30^\circ$  to  $83.93^\circ \pm 9.01^\circ$ ; consistently, biofilm growth on these hydrophilized membranes is comparable with the growth on commercial hydrophilic PVDF membranes which obtain a contact angle of  $34.65^\circ \pm 5.05^\circ$ .



**Figure 17:** Experimental tests for membrane selection. (A) Photographic images of the different membrane materials before (upper row) and after (lower row) folding. (B) Experimental setup of the growth experiments, in which the microorganisms are cultivated on top of a membrane and supplied by nutrients from a liquid reservoir by diffusion through a porous agar patch. (C) Photographic images of different microorganisms cultivated on PVDF and PC membranes using the setup depicted in (B). (D) Harvested biomass of *B. subtilis natto* biofilms; they were either cultivated on standard agar plates or with the growth setup depicted in (B); for the latter, different membrane materials and, for the hydrophilic PVDF membrane, two different nutrient concentrations (25 g L<sup>-1</sup> and 50 g L<sup>-1</sup>) were investigated. With the same membrane-based setup, the amount of harvested biomass obtained on hydrophilic PVDF and PC membranes, respectively, is shown for *B. subtilis 3610* biofilms (E), *S. cerevisiae* cultivation (F) and *P. chrysogenum* cultivation (G). #: no biofilm growth; ##: biofilm growth occurred, but harvesting was impossible without destroying the substrate. Scale bars in (A) and (C) correspond to 1 cm. Data shown in (D) – (G) represents the mean and the standard deviation as obtained from at least 6 independent samples from at least 2 growth batches.



Importantly, 'classical' cultivation of this biofilm on standard agar plates (where the agar layer has the same agar thickness as in the diffusion experiments but the nutrients are added to the agar layer during its production) returns less biomass than growth on the different membrane layers. We attribute this finding to a limitation of nutrients in those classical agar plates: here, as soon as all the accessible nutrients from the agar layer are consumed by the bacteria, biofilm growth will come to an end. In contrast, owing to the ongoing replacement of the growth media in the liquid reservoir used for the diffusion experiments with membrane layers (which imitates the continuous nutrient resupply that will be enabled on the rotating bioreactor), nutrient limitation is not an issue there. However, also for biofilm cultivation those membranes, a boost of the biomass output can be obtained if the nutrient concentration in growth medium is increased (**Figure 17D**).

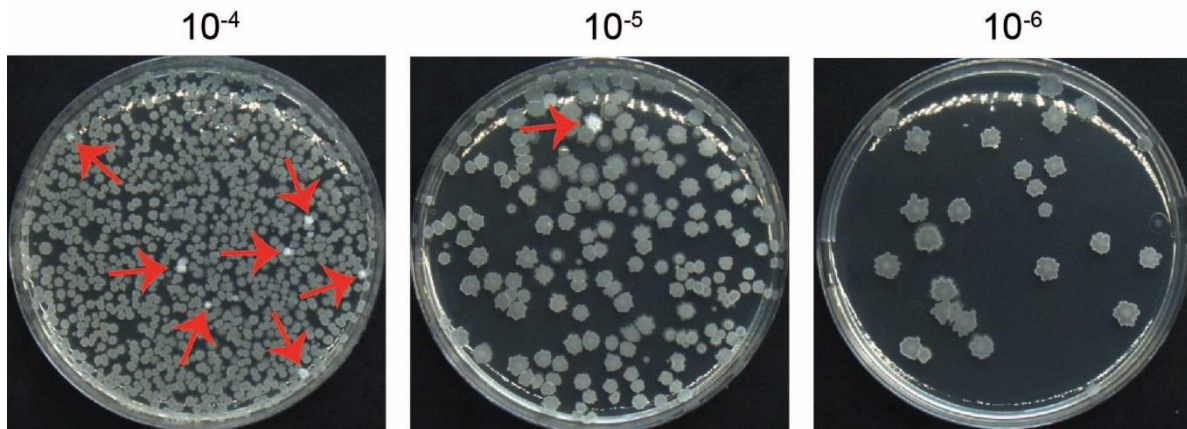
When handling those different membrane variants, it becomes apparent that the cellulose nitrate and SFCA membranes are not ideal for the use intended here: when they are folded, they break apart. This indicates that their life time on a rotating bioreactor, where the membrane layer will be continuously challenged by mechanical forces (arising from scraping), will be rather limited. In contrast, PVDF and PC membranes are more robust, which is why further experiments were conducted with those two membrane variants only.

In a next step, another biofilm variant, *i.e.*, biofilm created by the bacterium *B. subtilis* 3610, is cultivated on the two membranes. This biofilm variant is selected here as it has been shown before to be suitable to increase the hydrophobicity of mortar as well – which is why it is of similar interest for applications in construction engineering. With the same setup and conditions as used for *B. subtilis natto* cultivation, we obtain similarly high biofilm amounts on PVDF and PC membranes as for their direct cultivation on agar (**Figure 17D**). Importantly, successful cultivation of microbial biomass is not limited to bacteria: the yeast *S. cerevisiae* can be grown on both membrane variants as well (**Figure 17E**); only the liquid growth medium needs to be changed to fit the needs of this particular microorganism (see section 4.4.3.1). Finally, even a fungal biofilm can be cultivated on those two membranes when the growth medium and growth conditions are adjusted (see section 4.4.3.1): *P. chrysogenum*, which can be employed for the production of penicillin, can be successfully grown on and harvested from both membranes using the same setup as described before (**Figure 17F**). In contrast, whereas cultivation of *P. chrysogenum* on bare agar surfaces works out well, it is impossible to remove the fungal biomass without destroying the agar layer (the fungus tends to grow its mycelial network into the substrate, and harvesting the fungal biomass breaks the brittle agar layer apart). Because of this problem, **Figure 17F** does not list a value for harvestable biomass in this particular case. This result underscores the great advantage brought about by using porous membranes as a growth substrate: they are very suitable for cultivating a broad range of different microorganisms and greatly simplify the harvesting process of the generated biomass.

#### 4.4.4.3 Material properties of biofilm collected from the bioreactor

As the results described above show, the basic principle used by the bioreactor, *i.e.*, cultivating microorganisms at the interface between a solid substrate and air while supplying a nutrient solution from the substrate via diffusion, is indeed suitable to grow a variety of different microorganism. Moreover, this strategy comes with the advantage to easily adjust the type of nutrient source and to harvest the microbial biomass from the growth substrate. In previous research, bacterial biofilm – in addition to other bacterial additives [83] – has already been proven its value as a hydrophobizing agent in mortar [81, 82]. However, the classical microbiological production process of biofilm, *i.e.*, its cultivation on sterile petri dishes and the subsequent manual harvesting step, is time consuming and not economical. With the presented biofilm reactor, those issues are mitigated – provided that the bacterial material produced on the reactor has properties comparable to biofilm generated via the ‘classical’ method.

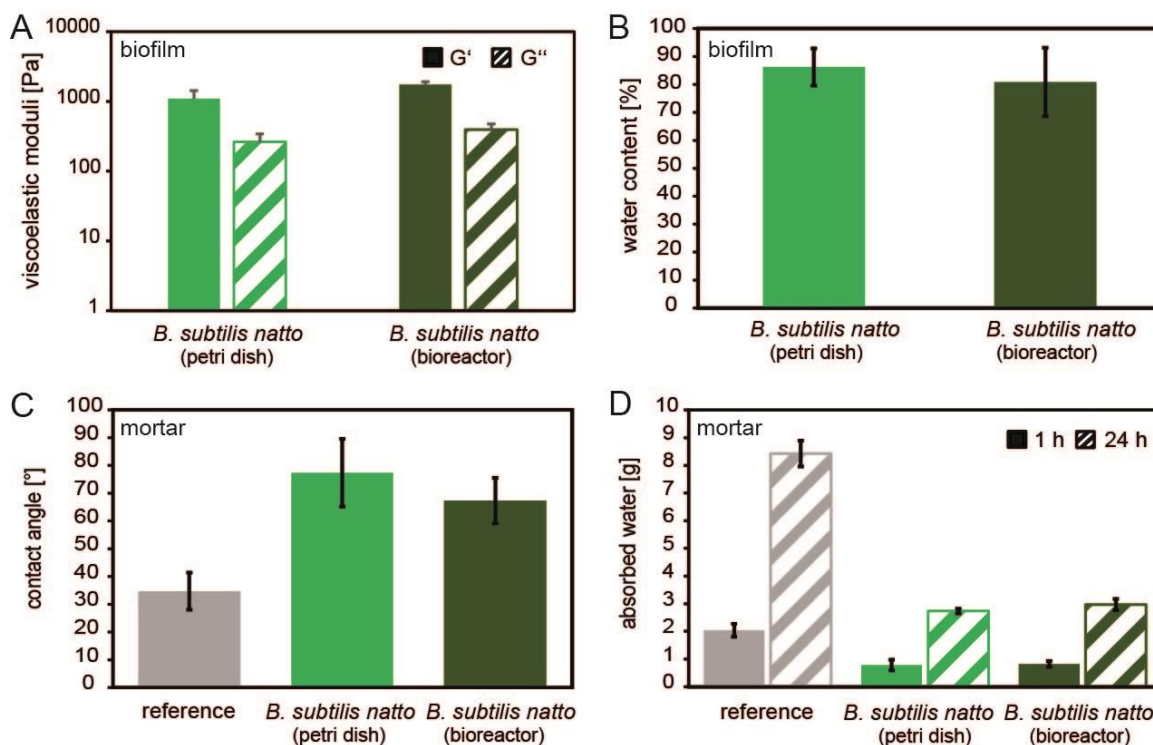
To assess this, we first verify that the microbial product grown on the bioreactor is indeed composed of the bacteria of choice; this is not trivial as – different from the ‘classical’ cultivation on agar plates – the biofilm develops on the bioreactor in a non-sterile environment. Since there are typically other bacterial spores in the air (*e.g.*, other *Bacillus* variants than the one used for biofilm production), a contamination of the reactor with other bacterial strains might compromise the quality of the grown biomass. However, as results from a contamination study conducted with serially diluted biofilm pieces collected from the bioreactor show (**Figure 18**), such contaminations are rare: we find mostly colonies with a morphology typical for *B. subtilis natto* colonies grown at the conditions selected here – and it is this particular strain that was used for the liquid culture (and thus biofilm growth) in those contamination tests.



**Figure 18:** Microbial composition of biofilm cultivated on the bioreactor. To test the *B. subtilis natto* biofilm harvested from the reactor for microbial contamination, a serial dilution assay was conducted (see section 4.4.3.3). The bacterial colonies marked with red arrows represent such contaminations, which are rare and established by spores of a different *B. subtilis* strain (*B. subtilis B-1*) used in the same lab where the bioreactor was set up. The number of colony forming units (cfu) from this biofilm sample was determined to be  $8.8 \times 10^7$  cfu/mg.

We attribute this positive finding to the high number of planktonic bacteria present in the liquid culture that is used to inoculate the bioreactor and the relatively short time interval (12 h) between two individual inoculation cycles.

Accordingly, we also expect the material properties of the *B. subtilis natto* biofilms cultivated on either, agar plates or the biofilm reactor, to be very similar. We test this expectation by determining the viscoelastic properties (**Figure 19A**) and water content (**Figure 19B**) of the two biofilm variants.



**Figure 19:** Material properties and hydrophobizing abilities of biofilm grown on the bioreactor. The viscoelastic properties of *B. subtilis natto* biofilms (A) as well as their water (B) is compared for biofilm cultivation on the bioreactor (dark green) and ‘classical’ cultivation on agar-filled petri dishes (bright green). For biofilm-enriched mortar samples, the obtained water-repellent properties are quantified by contact angle measurements (C) and capillary water uptake tests (D) after partial immersion into a water bath for 1 h (full bars) and 24 h (striped bars), respectively. Standard mortar samples devoid of biofilm additives (grey) are shown as controls. Error bars denote the standard deviation.

*B. subtilis natto* biofilm cultivated on agar-filled petri dishes exhibits a viscoelastic behavior that is clearly dominated by elastic properties (**Figure 19A**). This is an important property for the biofilms to be successfully cultivated on the rotating biofilm reactor as it prevents the bio-material to flow off the reactor surface during rotation. Moreover, similar to the manual harvesting process applied to collect the biofilm from agar plates, this viscoelastic material behavior enables the biofilm to be automatically collected from the cylinder by a PDMS blade. Moreover, the rheological characterization reveals that the two variants of *B. subtilis natto* biofilm show very similar absolute values of viscoelastic moduli, *i.e.*, stiffnesses in the range of ~1 kPa each (**Figure 19A**).

With this result in mind, it is also not surprising that both biofilm variants exhibit a very similar water content of 80-90% (**Figure 19B**) – a parameter this is intimately related to the absolute stiffness of the biofilm. However, this result is not trivial: when grown in petri dishes with the lid closed, the biofilm is very well protected from dehydration. Our results suggest that placing the bioreactor into an incubator (which, in addition to covering the petri dishes, is also done when the ‘classical’ biofilm cultivation approach is chosen) is sufficient to control the temperature and humidity requirements during biofilm growth.

In a last step, we ask if biofilm material collected from the bioreactor is equally suitable in conveying water-repellent properties to mortar as biofilm generated on classical petri dishes. To answer this question, we compare hybrid mortar samples containing biofilm powder (*i.e.*, freeze-dried bacterial biofilm) of the bacterial strain *B. subtilis natto* cultivated on both, agar and the biofilm reactor, and we test the wetting resistance and capillary water uptake properties of those biofilm-enriched mortar samples (**Figure 19C** and **Figure 19D**). In addition, unmodified reference mortar samples are analyzed as a control group.

To assess the wetting resistance of the samples, water contact angles are determined on the surface of small mortar samples (see section **4.4.3.5**). For the unmodified reference samples, low contact angles of  $\sim 35^\circ$  (**Figure 19C**) are obtained, and this result represents strongly hydrophilic behavior. In contrast, for biofilm-enriched samples (either obtained from cultivation on petri dishes or from the biofilm reactor), the wetting resistance is considerably enhanced: here, we measure contact angles in the range of  $70^\circ - 80^\circ$ . Similarly, we obtain very good results in capillary water uptake tests (**Figure 19D**): here, the amount of invaded water is reduced from  $\sim 8.5$  g/day (measured for the control group) to  $\sim 3$  g/day (measured for either variant of biofilm-enriched mortar). In other words, when mortar samples are continuously exposed to water for 24 h, both variants of the produced *B. subtilis natto* biofilm powder can reduce the capillary water uptake of mortar by  $\sim 2/3$ .

#### *4.4.4.4 Further possible improvements to obtain an industrial scale bioreactor*

The bioreactor we introduce here is a lab-scale prototype that fulfills its envisioned task. However, to be able to produce biomass in large amounts as relevant for industrial applications, its dimensions would need to be increased. Then, placing the bioreactor into a lab incubator will not be feasible anymore. To still provide the correct temperature levels required for biofilm growth, it should be possible to heat the hollow cylinder from the inside – and changing the material of this cylinder into a material with good heat transport properties and corrosion resistance (*e.g.*, stainless steel) will be helpful to realize this modification.

As of now, we make use of an agar layer as an intermediate structure sandwiched between the cylinder and the membrane layer; this setup is completely suitable for a continuous cultivation of biofilms over several days, but it might turn out insufficient when the reactor is run for a longer period of time such as several weeks or months: since agar is a biological material, it will start to decompose at some point – and this will require a new layer to be applied to the reactor. Such a time-consuming maintenance step might be avoidable when a synthetic material is used to replace the agar layer. To guarantee a good diffusive transport of nutrients from the cylinder to the membrane layer, a hydrophilic and porous, sponge-like material is required. In addition, sufficiently high elastic properties are needed so that this intermediate layer is not squished by the mechanical scraping process used to harvest the biofilm layer. With those con-

siderations in mind, plastic foams (made from, *e.g.*, PU, PE, or PET) appear to be the most likely candidates for this purpose. These materials should be equally potent in preventing the liquid medium added to the core of the cylinder from leaking through the membrane layer while efficiently distributing the nutrients from the growth medium to the membrane surface.

Finally, we here identified two hydrophilic membrane variants as suitable support systems to facilitate the growth of different microbial organisms. Depending on the selected microorganism, however, another membrane variant might turn out to be even more efficient. Also, it is possible that applying a macromolecular coating to the membrane can further boost the biomass production of certain microbes by promoting their attachment to the membrane layer [171, 172], but such modifications certainly would need to be optimized for each targeted microorganism.

#### 4.4.5 Conclusion

As we demonstrate here, a membrane-covered rotating bioreactor can be used to successfully cultivate and harvest biomass generated by different microorganisms, such as bacteria, yeast and fungi, in a continuous manner. Importantly, the membrane layer not only provides this versatility, but also allows for obtaining more biomass compared to direct cultivation on bare agar layers and ensures an easy harvesting procedure. The latter aspect is especially important when fungi are cultivated as those microorganisms tend to grow into soft substrates such as agar, and this makes harvesting them from such agar substrates very difficult. In addition to antibiotic-producing fungi such as *P. chrysogenum* tested here (as well as others such as *Acremonium chrysogenum* [173], *Fusidium coccineum* [174], *Muscodor albus* [175, 176] or other endophytes [177, 178]), also other fungi such as *Trichoderma harzianum* [179, 180] and *Metarhizium anisopliae* [181, 182] (which have applications as a biocontrol agent in agriculture) could be interesting future targets for this bioreactor. Thus, bioproducts generated on this device could have applications in civil engineering, medicine, and agriculture.

Individual contributions of the candidate: I contributed to the conception of this study, the design and implementation of the experiments, the data analysis, and the writing of the article.

#### *4.5 Viscoelastic behavior of chemically fueled supramolecular hydrogels under load and influence of reaction side products*

M. Kretschmer, B. Winkeljann, B. A. K. Kriebisch, J. Boekhoven and O. Lieleg [183]

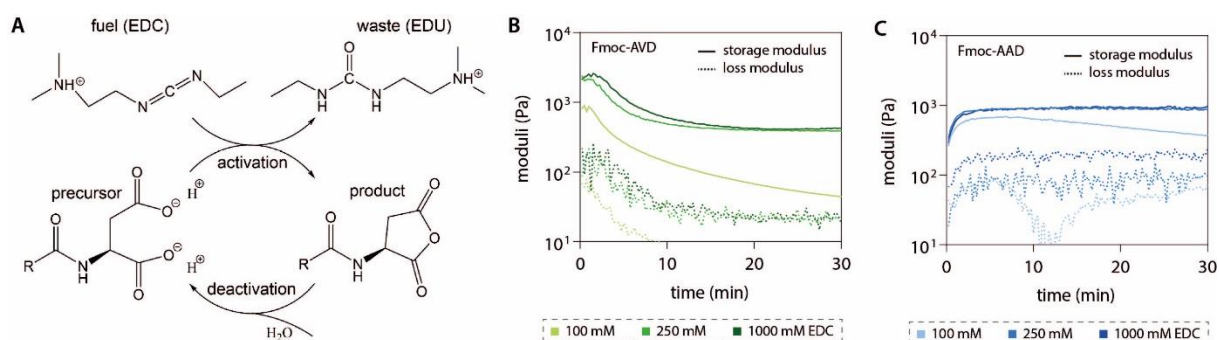
Hydrogels are soft materials that are used for a variety of different purposes in everyday life, such as body care, medical purposes and technical applications. In transient hydrogels, the supramolecular structures are built and disassembled dynamically. This offers possibilities to adjust their life-time and stiffness in a controlled way. Dynamic materials can be based on a fuel-driven reaction cycle that provides the driving force to obtain the materials and keep them in a non-equilibrium state. Examples for such materials can be found in nature; the building blocks of the actin cortex assemble into filaments by consuming energy provided by the hydrolysis of ATP. To mimic these properties, fluorenylmethyloxycarbonyl (Fmoc)-protected peptides can be used. In aqueous solution, the self-assembly of Fmoc-peptide-conjugates leads to the formation of hydrogels, which is driven by a carbodiimide fuel. Here, the properties of the material are tunable by varying the conjugated amino acid sequence. This amino acid sequence affects the reaction kinetics of the system as well as the shape, size, and lifetime of the generated supramolecular structures. For the usage of those transient gels in technical applications, it is essential to be aware of their exact lifetime and viscoelastic properties such as the stiffness and yield stress.

In this study, the viscoelastic properties of Fmoc-AVD and Fmoc-AAD hydrogels were investigated with a focus on their lifetime, linear and non-linear behavior, and the influence of waste products. To induce the self-assembly of the tripeptides, 1-Ethyl-3-(3-dimethylaminopropyl)carbodiimid-hydrochlorid (EDC) was used as a fuel, which was converted in '1-[3-(dimethylamino)propyl]-3-ethylurea (EDU) by the reaction cycle (**Figure 20A**). Simultaneously, the Fmoc-derivatives were converted into their anhydride state. Here, the electrostatic repulsion between the molecules was eliminated, which resulted in their assembly due to hydrophobic interactions. However, the anhydride product was not stable in aqueous conditions and disassembled spontaneously. Both Fmoc conjugates possess a hydrophobic character, which is less pronounced in Fmoc-AAD. This resulted in a different morphology of the assembled structures from wide, flat fibers (Fmoc-AVD) into thinner, more twisted helical structures (Fmoc-AAD). As a consequence, the reaction kinetics and viscoelastic properties of the hydrogels differed. Right after the addition of fuel, Fmoc-AVD gels obtain a distinct stiffness maximum and subsequently, the stiffness decreased until a plateau value was reached (**Figure 20B**). Fmoc-AAD gels obtained a stiffness plateau as well. However, it was on the same level as their maximum (**Figure 20C**). Overall, the stiffness of the Fmoc-AVD gels was higher than for Fmoc-AAD gels. In both systems, an increase of the gel stiffness was observed when the fuel amount was increased to an EDC concentration of 250 mM. Large amplitude oscillatory shear (LAOS) measurements revealed, that Fmoc-AVD as well as Fmoc-AAD gels showed strain weakening at strain

levels above  $\sim\gamma = 1 - 2\%$  independent of the fuel concentration. By applying normal loads to the gels, which was made possible by a custom-made fluidic system, a similar material behavior was observed. The maximal pressure resistance was higher for Fmoc-AAD conjugates, than for Fmoc-AVD conjugates; for both systems, this resistance increased with the EDC concentration analogous to the viscoelastic properties that were observed by rheology. This implied, that the failure of the hydrogel clogs occurred as soon as the linear elastic regime was left.

However, it was unclear, why further increasing the EDC concentration did not prolong the lifetime of the Fmoc-AVD gels. As one reason, the hydrophobic waste product EDU was identified. When EDU was mixed with either Fmoc-AVD or Fmoc-AAD solutions prior to gelation, the gel formation was completely inhibited. Tests with the EDU mimetic methyl 3-(dimethylamino)propionate (MDP), led to the same effect. This implied, that the hydrophobic and cationic carbon chain of EDU (or MDP) interacted with the Fmoc-systems such that its self-assembly process was disrupted. Even preformed Fmoc-AAD gels were dissolved by the addition of MDP. However, this was not possible for Fmoc-AVD gels. Most likely, this is due to the gel-stabilizing, hydrophobic properties of the peptides, which were weaker in the Fmoc-AAD conjugates.

In conclusion, these results showed that gels assembled from the chemically fueled peptide conjugates Fmoc-AVD and Fmoc-AAD offer tunable viscoelastic properties in the linear and non-linear regime as well as a tunable lifetime, and both parameters could be regulated by a variation of the peptide sequence and fuel concentration. Moreover, the effect of the waste product EDU was demonstrated, which offers additional possibilities to control the lifetime of the hydrogels. These multiple possibilities enable a broad range of future applications, such as the use as sealings for micro-fluidic systems, and as components in soft actuators or in micro robotics.



**Figure 20:** Reaction cycle of an Fmoc-based peptide precursor to its anhydrite state, driven by a carbodiimide fuel, and subsequent deactivation in aqueous solution (A). Viscoelastic properties of Fmoc-AVD (B) and Fmoc-AAD (C) hydrogels. The viscoelastic properties, depend on the fuel concentration for both hydrogel systems.

Individual contributions of the candidate: I contributed to the conception of this study, the design and implementation of the experiments, the data analysis, and the writing of the article.

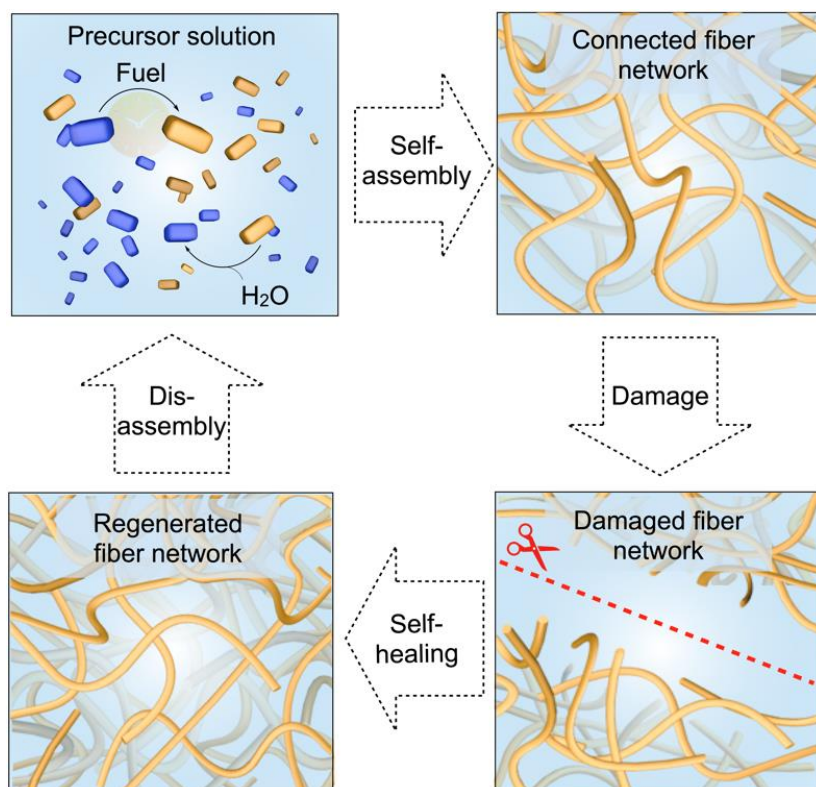


#### 4.6 Self-healing fiber network formed by chemically fueled self-assembly

Unpublished manuscript

In many natural systems, the formation of supramolecular structures is based on self-assembly. A prominent example of this phenomenon is the fuel-driven formation of actin fibers. Here, monomeric actin (G-actin) self-assembles into filamentous actin (F-actin) by the conversion of ATP into ADP [105-107]. This fuel-driven self-assembly process can be mimicked by chemically fueled peptides. Fmoc-protected tripeptides exhibit fuel-driven self-assembling possibilities that lead to the formation of fibers in a non-equilibrium state and thus form dynamic hydrogels [110, 117, 123, 184-186]. The underlying dynamic reaction cycle that leads to the continuous activation and deactivation of the peptide anhydride state, can be repeated as long as fuel is present in the system. Thus, such systems might have the (limited) ability to heal themselves. This means, that also when mechanical loads induce damages to the hydrogel, the structures might be able to reassemble driven by the consumption of chemical fuel, and this might recover the initial stiffness of the gel. Indeed, the self-regenerating character of chemically fueled dissipative materials has been reported before [187].

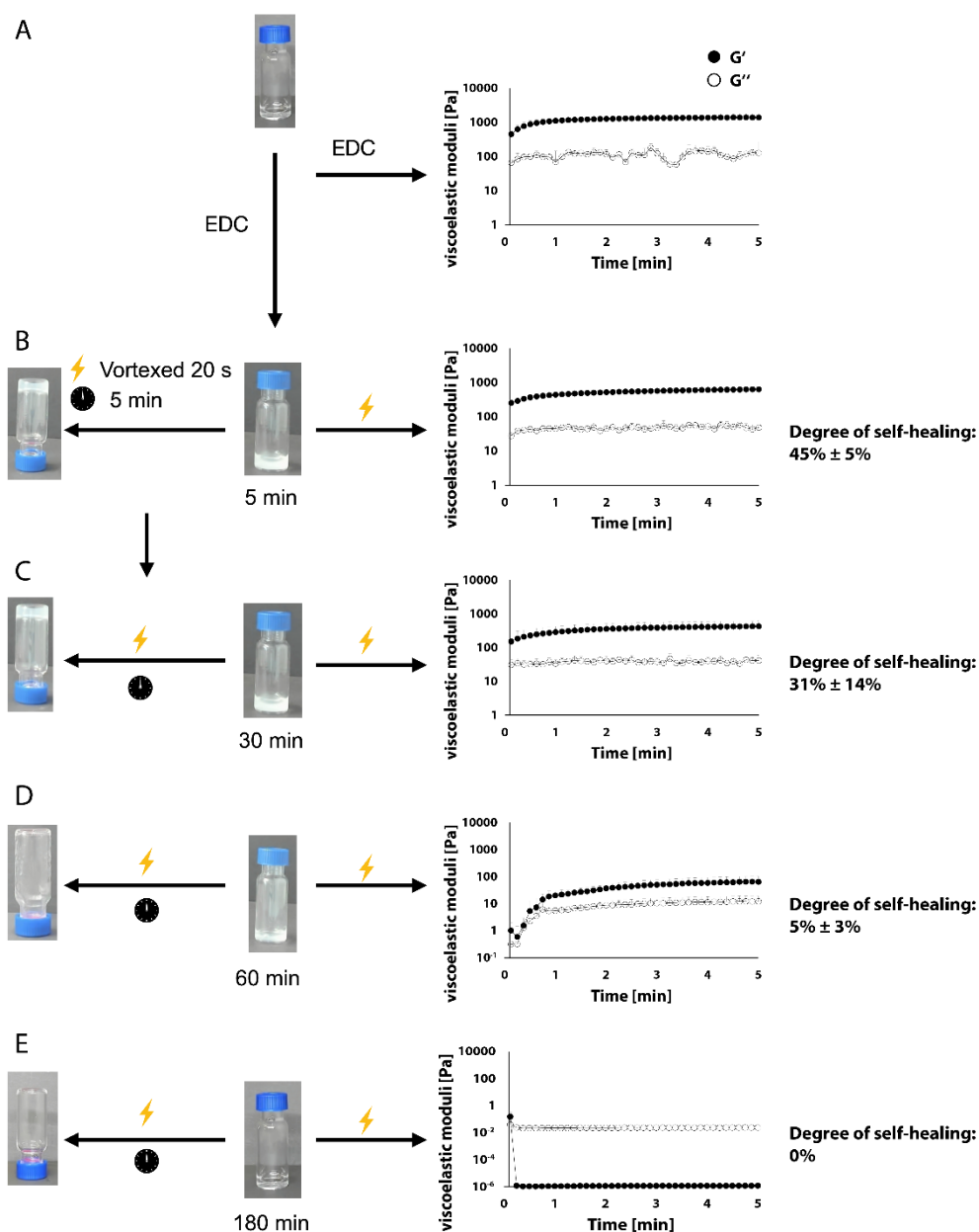
In this study, the self-assembling and self-healing mechanisms of fluorenylmethyloxycarbonyl-alanine-alanine-aspartic acid (Fmoc-AAD) hydrogels that are chemically fueled by 1-ethyl-3-(3-dimethylaminopropyl)carbodiimide-hydrochlorid (EDC) are investigated. In the precursor state, these peptides repel each other due to electrostatic repulsive forces. In the presence of a suitable fuel (here: EDC) the precursors are converted into their corresponding anhydride product, and a waste product (here: 1-[3-(dimethylamino)propyl]-3-ethylurea (EDU)) is generated. In the anhydride state, the electrostatic repulsive forces are eliminated; thus, the peptides can self-assemble into supramolecular structures (such as fibers) due to hydrophobic interactions (**Figure 21**) [123]. When such a fiber network is disrupted by shear forces, it is expected that the dynamic reaction cycle leads to a regeneration of the supramolecular structures (**Figure 21**). However, in aqueous solution, the anhydride is not stable and spontaneously transforms back into its precursor state. Only as long as fuel is available in the system, the activation cycle can be repeated and a hydrogel can be maintained. When the fuel is fully consumed, the fibers will partially disassemble (**Figure 21**). Moreover, as shown in section 4.5, the waste product EDU can influence the self-assembling kinetics of the Fmoc-peptides and can cause disassembly of the supramolecular structures [183]. A high performance liquid chromatography analysis (HPLC) of 10 mM Fmoc-AAD fueled with 500 mM EDC reveals, that 60 min after the addition of the fuel, 200 mM EDC is left and an anhydride concentration of more than 4 mM is present in the system; after 180 min, the EDC is fully consumed.



**Figure 21:** Model expectation of the fuel-driven self-assembly and self-healing behavior of Fmoc-protected tripeptides. Owing to the fuel-driven reaction cycle, the Fmoc-peptides self-assemble into fibers that form a network. Upon mechanical damage, the fibers are disrupted; however, due to the repeatable reaction cycle they are able to regenerate as long as fuel is present in the system. When the fuel is fully consumed, the fibers disassemble in aqueous solution with time.

To analyze the self-healing properties of Fmoc-AAD hydrogels, inverted tube tests and rheological characterizations were conducted (**Figure 22**). When 500 mM EDC is added to 10 mM Fmoc-AAD in MES buffered water (pH = 6.0), the sample turns turbid. This indicates the successful generation of supramolecular structures. Rheological measurements reveal, that the samples exhibit elasticity dominated properties as soon as the fuel is added to the precursor. In other words, the fuel turns the system into a viscoelastic gel (**Figure 22A**). To induce mechanical stress and thus to destroy the gel structure, the gel is vortexed for 20 s. Subsequently, the viscoelastic properties are monitored for 5 minutes. When the mechanical stress is applied 5 min after the addition of fuel to the precursor, the samples are able to recover their elasticity dominated properties, however, their stiffness remain reduced ( $45\% \pm 5\%$  of the original stiffness) (**Figure 22B**). Moreover, after a waiting time of 5 min subsequent to the disruption, the gels are able to resist gravity again and stay in place when the tubes are turned upside down (**Figure 22B**). When the mechanical stress is applied 30 min after the addition of fuel, the samples are able to re-form gels as well. However, compared to unchallenged hydrogels, their stiffness remains further reduced ( $31\% \pm 14\%$ ) (**Figure 22C**). A stress application 60 min after the fuel addition (**Figure 22D**) reduces stiffness of the hydrogels crucially ( $5\% \pm 3\%$ ), but the samples still recover their elasticity dominated properties. However, these samples starts to flow as soon as the tubes

are inverted, due to their low stiffness. For gels, in which the mechanical damage occurs 180 min (**Figure 22E**) after the addition of fuel, a different material behavior is observed: These samples are not able to form gels after the mechanical disruption anymore, thus no self-healing could be observed at all. Consistently, the samples start to flow as soon as the tubes are inverted. This indicates that, only in the first minutes after fuel addition, Fmoc-AAD gels are able to self-heal and their gel structure seems to recover for a certain extend. At later timepoints, this ability is more and more reduced. According to the kinetics of fuel consumption, however the fuel concentration should be high enough to regenerate the hydrogel even after 60 min. Thus, another parameter than the anhydride and fuel concentration has to be considered to explain the lack of self-healing potential observed at those later time points. One possibility for the reduced self-healing ability with time is the accumulation of the waste product EDU.

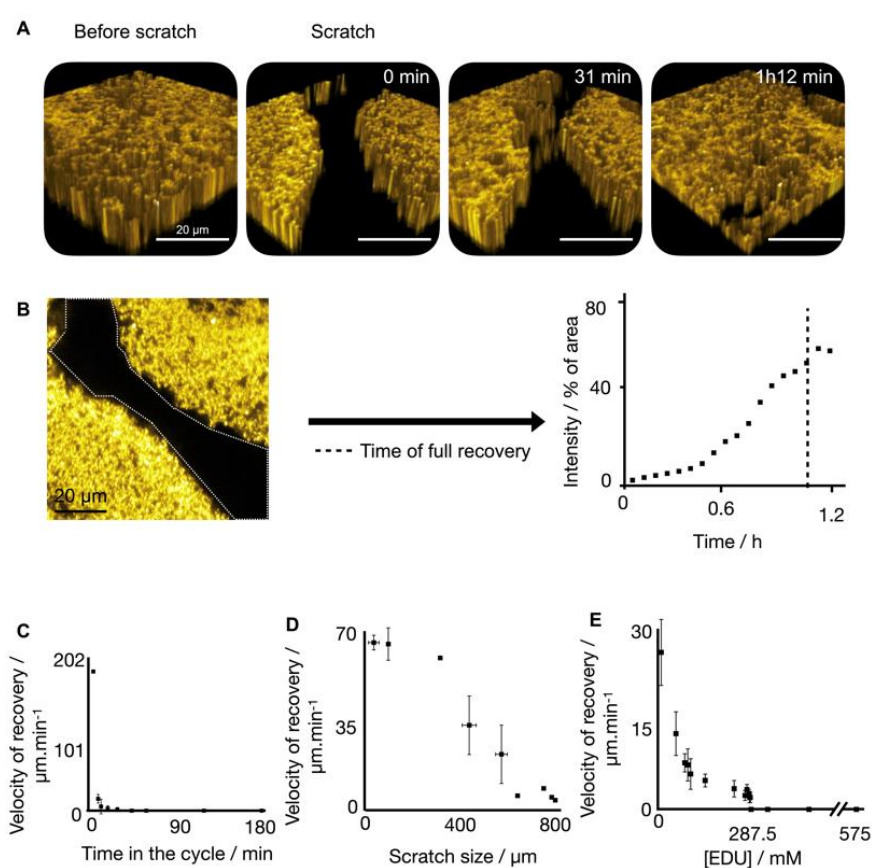


**Figure 22:** Inverted tube tests and rheology of 10 mM Fmoc-AAD hydrogels fueled with 500 mM EDC. The rheological behavior of the gelation process is depicted in (A). Inverted tube tests and rheology after a mechanical challenge by vortexing are depicted in (B-E). Vortexing was conducted at 5 min (B), 30 min (C), 60 min (D) and 180 min (E) after the addition of fuel. The depicted data represent the mean value of three independent samples with corresponding standard deviation.

In additional investigations, the self-healing ability of Fmoc-AAD is examined and visualized on a microscopic scale. By means of fluorescence confocal microscopy, the recovery of the gel after a mechanical disruption (induced by a scratch) is monitored (**Figure 23A**). Here, the gel is damaged by a scratch induced with a 0.2 mm thick needle using a micromanipulator setup. The resulting scratch exhibits a width of  $201.5 \mu\text{m} \pm 19 \mu\text{m}$ . When the scratch is applied 13 min after the addition of fuel, the fiber network is able to regenerate within 72 min (**Figure 23B**). When the scratch is performed earlier than 13 min after the fuel addition, the structural self-healing

actually occurs too fast to be monitored. When a scratch is performed much later than 13 min after the fuel addition, an incomplete and slow self-healing is observed (**Figure 23C**). Moreover, the self-healing ability is dependent on the scratch size. The fastest recovery of the induced damage is observed for scratches smaller than 200  $\mu\text{m}$ , whereas for scratches greater than  $\approx 300 \mu\text{m}$ , no regeneration of the fiber network can be observed (**Figure 23D**).

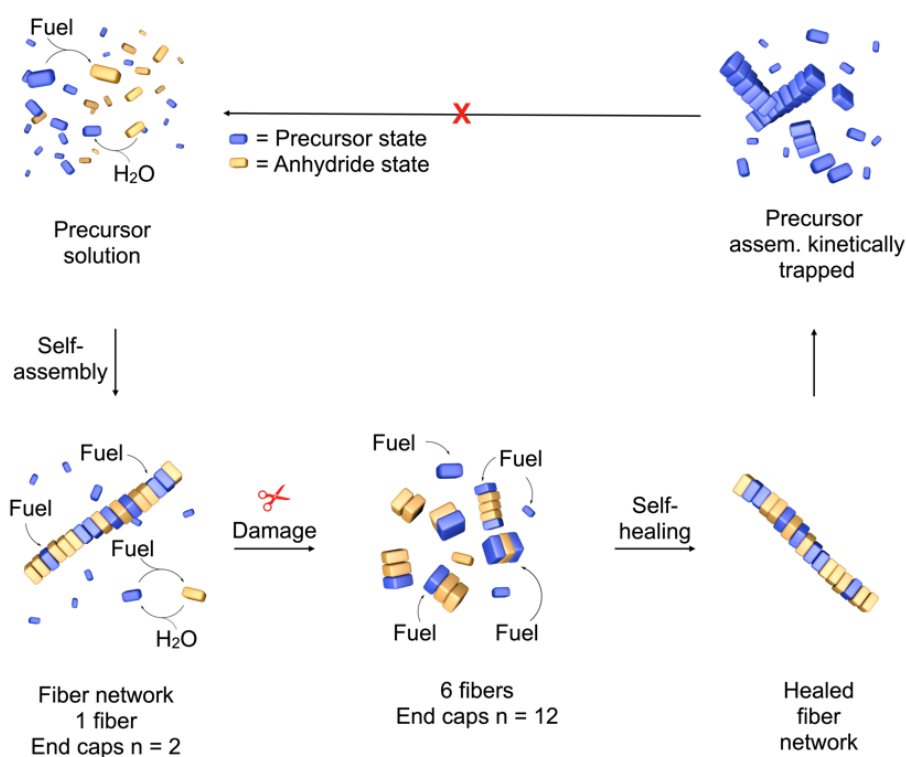
Furthermore, the effect of the reaction waste product EDU is investigated. Here, it is observed, that the self-healing ability of the system decreases with increasing EDU concentration (**Figure 23E**). When the EDU concentration is too high ( $> \approx 150 \text{ mM}$ ), no self-healing is present at all. This motivates the hypothesis that the decreasing ability to self-heal with time could be due to the increasing EDU concentration in the gel.



**Figure 23:** Fluorescence confocal microscopy images of 10 mM Fmoc-AAD fueled with 500 mM EDC before and after scratching with a 0.2 mm thick needle (A). When the scratch is executed 13 min after the fuel addition, a recovery of the gel structure within 72 min is observed (B). The depicted data in B represents an exemplarily sample. Furthermore, the velocity of recovery of 10 mM Fmoc-AAD fueled with 500 mM EDC in dependence of the gelation time (C), scratch size (D), and EDU concentration (E) are depicted. The depicted data in C-E represent the mean value of at least two independent samples with corresponding standard deviation.

Based on these observations, it can be hypothesized, that the fiber network is able to reassemble after a mechanical disruption by the consumption of EDC. The building blocks within a fiber undergo permanent activation and deactivation reactions, however, due to kinetic trapping, the

fibers can remain in their assembled state and do not disassemble immediately. Indeed, the fibers represent a co-assembly state combining building blocks in their precursor- and anhydride state (**Figure 24**), as confirmed by  $^1\text{H-NMR}$  spectroscopy.



**Figure 24:** Possible self-healing mechanism of Fmoc-AAD hydrogels after a mechanical damage. The initial fiber formation is generated by the fuel that leads to the conversion of the precursor into the anhydride product. Due to the permanent activation and deactivation reaction of the Fmoc-peptides as long as fuel is available, some building blocks are present in the precursor state and others in the anhydride state within one fiber. When a mechanical stress is induced, the fibers are disrupted and break into pieces. When the fiber end caps are reactivated by the fuel, new building blocks can assemble and thus the fiber is regenerated. Due to kinetic trapping, the fibers can be maintained for a certain extent, even when the fuel is fully consumed.

When the fibers are mechanically ruptured apart, new fiber end caps are created (**Figure 24**). When the building blocks of the fiber ends are reactivated by EDC, it seems that new Fmoc-anhydrides can assemble at the fiber ends. This leads to the reconstruction of the fiber network and thus to the recovery of the gel stiffness (**Figure 24**). However, due to the accumulation of EDU, which influences the assembling kinetics of the Fmoc-AAD peptides, self-healing is only possible within the first minutes after fuel addition. As soon as the EDU concentration exceeds a certain threshold, the self-healing ability is reduced, or even fully inhibited. This effect can be due to electrostatic or hydrophobic interactions established by the waste product. To extend the self-healing capability of these hydrogels, it is imaginable to continuously remove the EDU from the system by diffusion, similar to what was shown for the waste product of other systems [188].

For applications in technical fields, the self-healing ability of the presented hydrogels is advantageous. For gels, that exhibit no self-healing capability, their application and transfer is difficult, since mechanical stress can destroy them irreversibly as soon as they are gelled. However, for hydrogels that are able to self-heal after gelation, high shear forces are unproblematic, since the gels are able to regenerate their stiffness autonomously. This offers the possibility to inject them or to pass them through a hose for application.

Individual contributions of the candidate: I contributed to the design and implementation of the experiments, the data analysis, and the writing of the article.



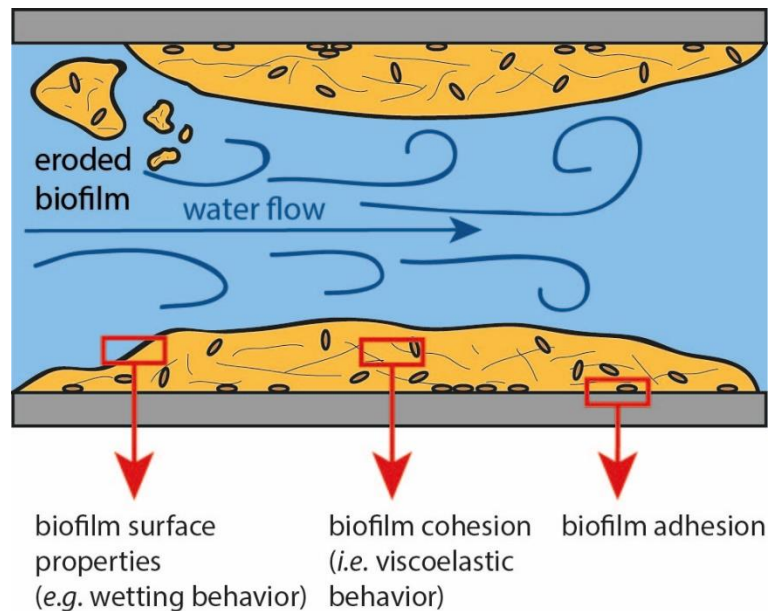


## 5. Discussion

Bacterial biofilms exhibit extraordinary properties, such as the capability to self-assemble certain molecular structures and the ability for self-healing [38, 48, 100]. Furthermore, the EPS fulfills a variety of different tasks and enables the bacteria to survive even in challenging conditions. To obtain these properties, biofilms are composed of a variety of different molecules and feature a complex internal structure and topography [1, 8, 189]. Problematic bacterial biofilms are responsible for many issues in human health, in the food sector, and in the industry [2, 3, 55, 57-60]. Because of this, the formation of these biofilms needs to be prevented, or they have to be removed efficiently. However, due to the biofilms viscoelastic material behavior, self-healing ability, resistance against toxic substances, such as ions and antibiotics, and wetting behavior (which can be superhydrophobic), this task is challenging [33, 38, 46, 47]. In contrast to those examples, bacterial biofilms can also be beneficial for humans and can fulfill important tasks, such as the production of certain substances, removal of toxins during wastewater treatment, or serving as additives for construction materials [6, 7, 75, 78-83]. For these applications, it is important to cultivate biofilms with dedicated properties. Thus, in both cases (when biofilms need to be efficiently removed or cultivated), it is necessary to be aware of the biofilm material properties such as the erosion stability, viscoelasticity, adhesion behavior, and wetting behavior. The detailed characterization of these biofilm properties helps to understand the chemical and physical principles on which they are based on. Furthermore, these insights offer the possibility to modify biofilm properties as desired and to mimic them with artificial materials (e.g. in synthetic hydrogels).

An important biofilm property is their erosion resistance, which determines the attachment to a surface submerged in liquids when shear forces are applied to the biofilm by water streams (e.g., in pipes or fluidized-bed reactors) [33, 46]. In previous work, it was shown that the erosion resistance of biofilms (such as those generated by *B. subtilis* B-1 and *B. subtilis* NCIB 3610) can be altered by different chemical treatments or biological additives, especially by the addition of certain metal cations or biopolymers [33, 190]. As described in section 4.1, for *B. subtilis* NCIB 3610 biofilms, the exopolysaccharides that are the gene product of the *epsA-O* operon seem to play a crucial role for the erosion resistance. However, only *B. subtilis* NCIB 3610 biofilms that produce this polysaccharide as well as BslA and TasA exhibit an optimal erosion resistance. When *B. subtilis* NCIB 3610 biofilms lack one of these components, the erosion resistance is reduced, which can be rationalized by a reduced stiffness and a loss of hydrophobicity as observed in these biofilms. Apart from that, the erosion resistance of these biofilms can also be increased, for example by exposure to certain metal cations, which enhances the biofilm stiffness. This indicates a certain inter-dependency of these two material properties. Another possibility to increase the erosion resistance of biofilms is the addition of certain polymers such as

PGA, alginate, or PEG to the biofilm matrix during biofilm growth. Here, in contrast to ionic treatments, the addition of these polymers does not alter the biofilm elasticity [190]. This example nicely illustrates that, due to dependencies of the erosion stability on other biofilm properties (such as the stiffness, wetting behavior and adhesion) (**Figure 25**), a characterization of one property alone is not sufficient to understand the complex biofilm behavior.



**Figure 25:** Illustration of a bacterial biofilm attached to the inner surface of a pipe. Shear forces generated by a water flow can erode the biofilm. However, some biofilm are able to resist certain shear forces. Here, their material properties, especially the combination of the biofilm surface properties, cohesion and adhesion play an important role.

The consistency of biofilms is described by the viscoelasticity, which can be very complex and relies mainly on the interactions between the molecules of the biofilm matrix. The most important interactions, that hold the biofilm matrix and cells together are steric interactions, van der Waals forces, electrostatic forces (including ionic cross-links), hydrogen bonds, and dipole-dipole interactions (**Figure 26**) [8, 33]. The viscoelastic behavior of biofilms is typically dominated by the elastic properties. Natural biofilms are rather soft but are able to resist gravity and do not flow by themselves [33, 38, 40, 191, 192]. However, the viscoelastic properties of bacterial biofilms can be altered by different additives: By the addition of citric acid, biofilms can be weakened [38], and biofilms can be stiffened by the addition of certain biomacromolecules (e.g. eDNA) and metal cations [33, 193]. With the latter modification, biofilms can be stiffened by up to three decades, as observed for *B. subtilis* B-1 biofilm for example [33]. A major component of this particular biofilm is the polypeptide  $\gamma$ -PGA that also largely affects the viscoelastic properties. As described in section 4.2, when solutions of  $\gamma$ -PGA are exposed to certain metal cations, hydrogels are formed, which is most likely due to the formation of chelate complexes. By interactions between the metal cations and the polyanionic  $\gamma$ -PGA, the molecules become cross-linked and thus form a network. It was shown, that the same set of metal ions that increase the

biofilms stiffness, also lead to hydrogels when added to solutions of  $\gamma$ -PGA. This finding strongly indicates, that  $\gamma$ -PGA is the critical component that is mainly responsible for the ion-induced stiffening effect observed for *B. subtilis* B-1 biofilm.

Also other polyanionic biomacromolecules are able to form chelate complexes with certain metal cations: the polysaccharide alginate, which can be produced by *A. vinelandii*, forms chelate complexes upon exposure to  $\text{Ca}^{2+}$  [34, 97, 98]. Thus, it is possible to form alginate hydrogels by adding certain metal cations. However, not all alginate variants can be crosslinked by  $\text{Ca}^{2+}$ , and it is a set of different ions than for  $\gamma$ -PGA that lead to hydrogel formation. As a reason for this discrepancy, different molecular architectures of alginate (that can vary depending on the biological source) were identified to be responsible. Only alginates that contain G-blocks are able to form chelate complexes with  $\text{Ca}^{2+}$  [97]. For both, *A. vinelandii* biofilm and the alginate produced by this bacterium, the same set of ions lead to an increased stiffness or the formation of a gel respectively. This indicates that alginate is the most important component of *A. vinelandii* biofilms responsible for stiffening after exposure to certain metal cations. However, it remains somewhat curious, why only some metal cations are able to form chelate complexes with  $\gamma$ -PGA and alginate. Potential factors for this question are the ionic size and the possible coordination number in the formed chelate complex, and the experiments conducted in this dissertation indicate, that the ionic size indeed plays an important role: smaller ions (e.g.  $\text{Cu}^{2+}$ ) tend to form chelate complexes with a higher propensity than bigger ions (e.g.  $\text{Ca}^{2+}$ ).

Such a formation of chelate complexes with metal cations offers various advantages for biofilms although, for planktonic bacteria, high concentrations of these metal cations are toxic [33]. When these cations are bound by the biofilm matrix, they become immobilized and their toxic effect for the bacteria is reduced. At the same time, as the stiffness of the biofilm is increased by the ionic cross-links generated upon binding, the biofilm can resist higher normal forces and shows increased erosion resistance [33].

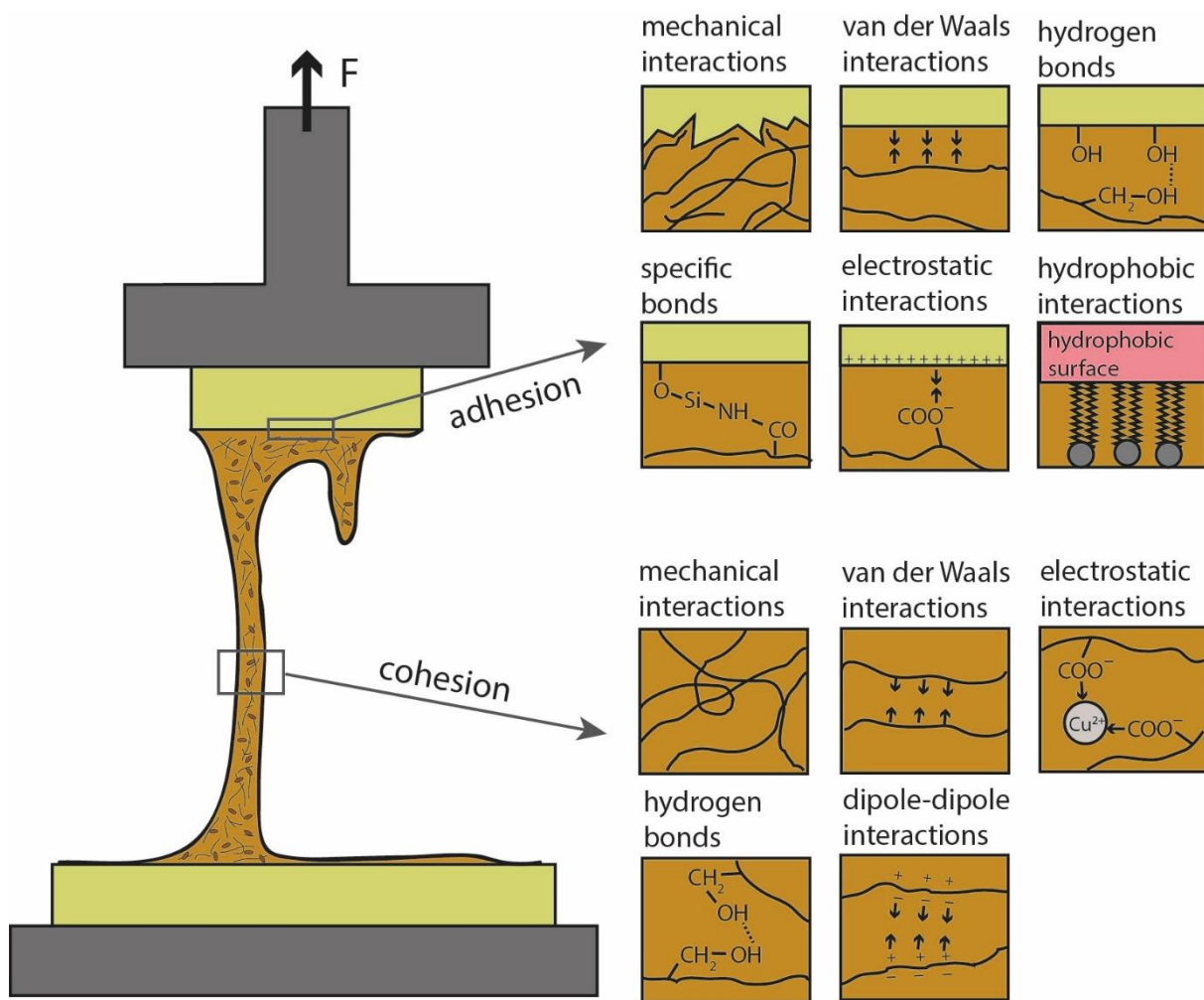
In addition to the viscoelastic properties, also the adhesion behavior of biofilms is of great interest for their removal and cultivation: The adhesion of biofilms to surfaces determines (in combination with the biofilm viscoelasticity) their resilience against shear- and normal forces. In several previous studies, the attachment and growth of biofilms on a variety of different surfaces has been investigated either to prevent biofilm growth [194-198] or to enhance it [171, 172, 199, 200]. Biofilm adhesion can be established by specific and non-specific interactions between the biofilm matrix and the surface. Common contributions are mechanical interactions with rough surfaces, van der Waals interactions, hydrogen bonds, specific interactions (e.g. peptide bonds), electrostatic interactions, and hydrophobic interactions (**Figure 26**) [172, 201]. However, there are only a few methods to investigate the adhesion properties of bacterial biofilms [89, 90], and

neither of them can determine adhesion in response to normal forces only. Thus, in section 4.3 a novel measurement method was described that allows for investigating the detachment behavior of bacterial biofilms exposed to such normal forces. With this method, it is possible to differentiate between different modes of fracture (*i.e.*, adhesion fracture, cohesion fracture, and mixed fracture). It is observed that the detachment behavior is influenced by the adhesion forces to the substrate, the biofilm stiffness (cohesion), and the biofilm wetting behavior. The results obtained in this dissertation indicate that, in such detachment events, biofilms are more prone to material transfer (and to fail via cohesion fractures) when they exhibit a low stiffness and hydrophilic surfaces properties. In contrast, a biofilm with a high stiffness and hydrophobic surface tends to not show material transfer and thus is more prone to adhesion failures.

These findings imply, that it is easier to remove a hydrophilic biofilm with a low stiffness from surfaces (*e.g.* in pipes). When a naturally grown biofilm does not exhibit these properties, it can be possible to reduce its stiffness by treatment with citric acid [38] and to reduce its water repellency via treatment with either a concentrated saline solution or a concentrated glucose solution [46]. The former reduces ionic cross-links from the biofilm matrix whereas the latter flattens the surface roughness of the biofilm by osmotic deflation effects. Biofilms with a lotus like hydrophobicity can be rendered rose-like hydrophobic (*e.g.* by treatment with NaCl-solution or glucose solution), and rose-like hydrophobic biofilms can be turned hydrophilic (*e.g.* by treatment with KCl-solution) [46]. For the cultivation of biofilms (*e.g.* for waste water treatment), a high attachment of the biofilm to the substrate and thus a high stiffness and water repellency is desired. Here, the stiffness can be increased by treating the biofilm with certain metal cations as described in Grumbein *et al.* (2014) [33] and in this thesis. The water repellency can be increased by specific culture conditions (such as by cultivation with nutrient limitation [47]) or by the addition of polymers (*e.g.* PGA, alginate, or PEG) during biofilm growth [190].

However, depending on the bacterial species, the cultivation of biofilms comes with distinct demands that limit the cultivation possibilities. Thus, dedicated approaches are necessary to cultivate biofilms with desired properties. Many biofilms, such as those of *Acinetobacter calcoaceticus* and *Comamonas denitrificans* that are used for wastewater treatment, form biofilms on surfaces submerged in water [202], whereas other bacterial species, such as *B. subtilis spec.* do not. Bacterial cells from the latter genus either tend to form pellicles or biofilms on solid surfaces at the solid/gas interface. Common bioreactors are used to cultivate biofilms submerged in water; here, the nutrient supply can easily be realized and for, certain applications such as wastewater treatment, such direct contact with the medium is required. However, also the cultivation of *B. subtilis* biofilms (such as those of *B. subtilis natto*) is desired since those biofilms can be used as additives to increase the water repellency of mortar [81, 82]: cementitious materials are commonly used for a wide range of applications in the construction industry in which the materials are exposed to challenging conditions, such as moisture and ice. With an increased

water repellency, the lifetime of cementitious materials can be increased [82, 203, 204]. However, for this purpose, large amounts of biofilm are necessary. In this dissertation, a cylindrical bioreactor was introduced, which enables the continuous production of *B. subtilis natto* biofilms at the solid/gas interface (as described in section 4.4). Here, the biofilm is cultivated on the outer surface of a rotating cylinder, which is covered by a membrane; the nutrients are supplied by diffusion from the cylinder core. To cultivate biofilms with this reactor, the biofilm needs to be a sufficiently strong viscoelastic solid, so that it can stay on the rotating cylinder and does not flow off by itself. For the same purpose, the attachment of the biofilm needs to be strong enough, but also weak enough to allow for efficient biofilm removal. The tests conducted in this thesis revealed, that *B. subtilis natto* biofilm cultivated with the novel bioreactor shows similar properties as biofilm cultivated in petri dishes: Not only the viscoelasticity and wetting behavior were found to be similar, it was also possible to remove the biofilm automatically with a PDMS-blade, and an increased water repellency of mortar was achievable with biofilm harvested from this reactor as well. Thus, for usage as an additive to mortar, the biofilm cultivated with this bioreactor is suitable and offers the advantage that it can be produced continuously in larger amounts. A stronger attachment of the bacterial cells to the reactor surface could increase the biofilm yield further. An improved binding of bacterial cells to the reactor surface during inoculation could be achieved by modifications of the growth substrate: To promote bacterial attachment, it is possible to activate the surface (e.g. chemically or physically), or to coat it with polyelectrolytes or silanes [171, 172].



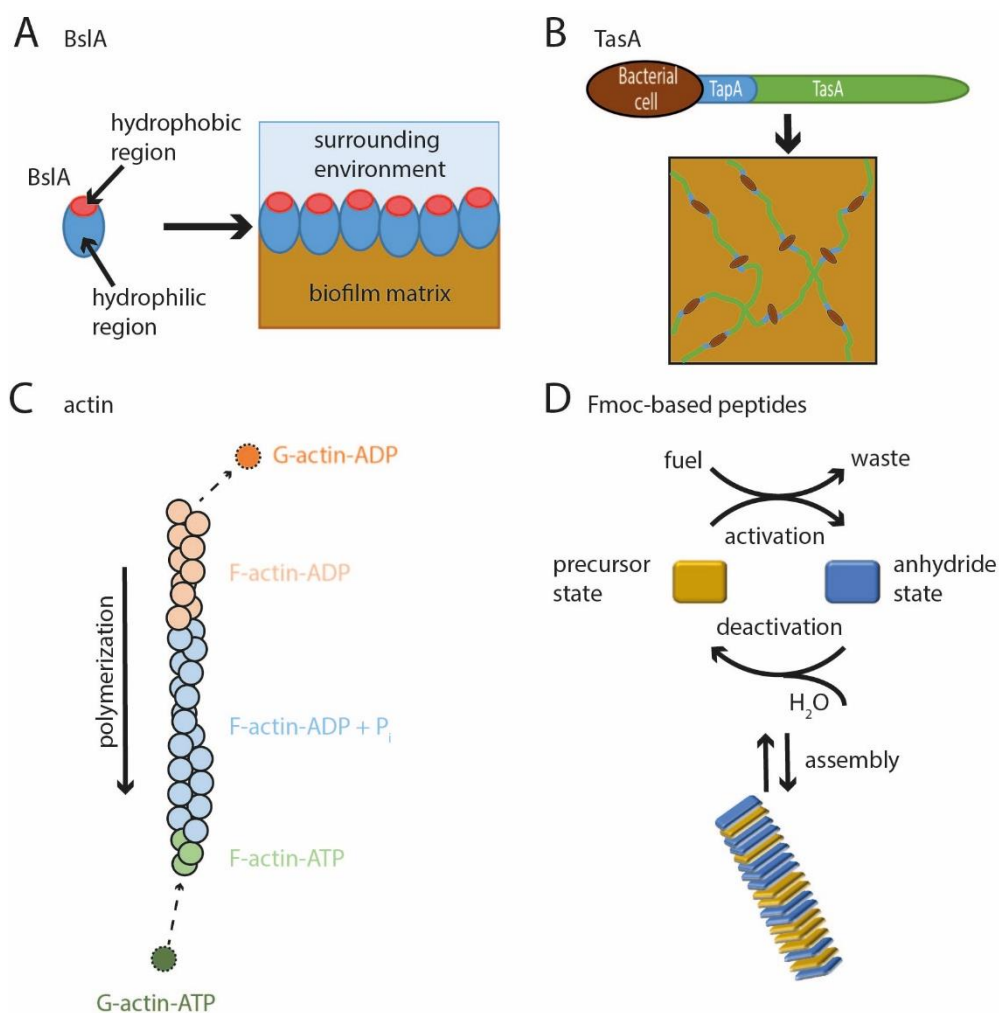
**Figure 26:** Overview of different physico-chemical interactions that determine the adhesion and cohesion of biofilms. Biofilm adhesion is defined by interactions between the surface and the biofilm matrix. Mechanical interactions are possible with irregularities of rough surfaces. Adhesion is also affected by van der Waals interactions, hydrogen bonds, specific bonds (e.g. peptide bonds), and electrostatic interactions. In aqueous environments, also hydrophobic interactions with hydrophobic surfaces can occur. Biofilm cohesion, and thus its viscoelastic properties, is defined by interactions between the biofilm molecules and/or bacterial cells. Possible interactions include mechanical interactions, van der Waals interactions, electrostatic interactions (including ionic-cross-links), hydrogen bonds, and dipole-dipole interactions. Especially ionic cross-links can greatly increase the biofilm stiffness [8, 33, 172, 201].

In a second part of this dissertation, the viscoelastic properties of synthetic hydrogels that were inspired by biological systems were investigated. The curious properties of bacterial biofilms make them unique materials: Biofilms are known to recover their stiffness after exposure to large shear strains [38]. This phenomenon is called "self-healing" and biofilms even exhibit this property when stiffened by metal cations. However, the molecular mechanisms that are responsible for this behavior are widely unknown; it is particularly curious, that bacterial biofilms exhibit this property, whereas ionically crosslinked alginate and  $\gamma$ -PGA gels do not. Another interesting property is the self-assembling ability of certain biofilm molecules into complex structures; examples are the amphiphilic surface protein BslA and the amyloid fiber forming protein TasA [30,

31, 48, 100]. BslA consists of a hydrophobic and a hydrophilic region that are diametrically located. In biofilms, amphiphilic BslA is capable to self-assemble into a stable surface layer. At the interface between the biofilm and the surrounding environment (e.g. air), BslA polymerizes and orientates itself with its hydrophobic cap towards the environment. This assembly occurs without the aid of another protein or carbohydrate partner (**Figure 27A**) [48, 100]. TasA assembles into amyloid fibers that specifically bind to the bacterial cell wall associated protein TapA. Thus, a protein scaffold is formed that holds the cells together (**Figure 27B**) [1, 30, 31, 101]. In combination with the exopolysaccharides, these fibers mainly account for the mechanical stability of *B. subtilis* NCIB 3610 biofilms. Self-assembling supramolecular structures are also found in other natural systems such as eukaryotic cells. Here, the self-assembly of actin filaments is driven by the chemical fuel adenosine 5'-(tetrahydrogen triphosphate) (ATP). Monomeric actin (G-actin) forms filamentous actin (F-actin) through a reversible, noncovalent self-association. During this polymerization, the monomeric G-actin (to which an ATP molecule is noncovalently bound) hydrolyzes the ATP into adenosine 5'-(trihydrogen diphosphate) (ADP) and free inorganic phosphate ( $P_i$ ) in two steps. First, ATP becomes cleaved and F-actin-ADP +  $P_i$  is formed. In a second step the inorganic phosphate is released to the surrounding environment. The polymerization and depolymerization results in the continued hydrolysis of ATP and thus a dynamic fiber can be maintained (**Figure 27C**) [105-107]. For the cohesion of the actin monomers within one fiber, hydrophobic interactions play a role [107, 205]. The self-assembly process as well as the self-healing properties of these different biological systems can be mimicked artificially by Fmoc-protected peptides (**Figure 27D**) [110, 117, 123]. As described in section 4.5, supramolecular structures of Fmoc-protected peptides can be maintained in a non-equilibrium state by carbodiimide based fuels such as EDC. As a consequence, transient hydrogels are generated. For Fmoc-precursor, the molecular assembly is prevented by repulsive electrostatic interactions. With an activation reaction driven by a carbodiimide fuel, the Fmoc-precursor transform into their anhydride state. In the anhydride state, the repulsive forces are eliminated and thus the molecules assemble due to hydrophobic attractive forces into supramolecular structures such as fibers. Thus, the cohesion of the molecular building blocks is based on hydrophobic interactions, similar to BslA and actin fibers. In aqueous solution, the anhydride state of the Fmoc-peptides is not stable and they transform back into their precursor state. Thus, both states are simultaneously present in the fibers. As long as fuel is available in the system and the concentration of the waste product is low enough, these supramolecular structures can be maintained in the non-equilibrium state [110, 117, 123]. These dynamic hydrogels offer the possibility to tune their material properties by varying the peptide sequence and fuel concentration. It was observed here that, with this approach, the stiffness, lifetime and yield point of the gels can be altered. Furthermore, the waste product EDU (which is generated by the reaction cycle and accumulates in the gel) influences the assembly of the supramolecular structures. By adding this waste product

to the system, it is possible to prevent gel formation, and it is even possible to destroy the gel in a controlled manner.

In further studies, the self-healing properties of these hydrogel systems were investigated. When Fmoc-AAD hydrogels are disrupted by large shear forces, they are able to recover their stiffness – at least to a certain extent. Most likely, this is due to the ongoing reaction cycle of the system, which enables a reassembly of the supramolecular structures. However, the degree of self-healing remains low in comparison to biological systems such as biofilms. A possible reason for this might be the accumulation of the waste product EDU in the system. With further optimizations, these gels, inspired by natural systems, have the potential to be used as pre-programmable sealings for (micro)-fluidic systems, or as components in soft actuators and micro-robotics.



**Figure 27:** Self-assembly mechanisms of different natural and synthetic systems. A: BslA self-assembles into a stable surface layer at the interface of the biofilm and surrounding environment (e.g. air) due to its amphiphilic character [48, 100]. B: The amyloid fiber forming protein TasA specifically binds to the cell wall associated protein TapA and thus forms a scaffold [30, 31, 101]. C: ATP driven self-assembly of actin filaments [105-107]. D: Carbodiimide fuel driven self-assembly of Fmoc-based peptides into transient fibers [110, 117, 123].



In conclusion, this thesis gives insights into the molecular mechanisms and relations that determine the material properties of bacterial biofilms and bioinspired synthetic hydrogels. These findings contribute to developing improved strategies to remove or cultivate bacterial biofilms. However, due to the high complexity and diversity of bacterial biofilms, several questions remain unsolved, such as, how biofilms are able to almost fully recover their mechanical strength after exposure to high shear stresses, even when they are ionically crosslinked by certain metal cations. Furthermore, new methods to investigate and cultivate bacterial biofilms have been demonstrated in this thesis. A dedicated method to investigate the detachment behavior of bacterial biofilms enables the characterization of their adhesion and cohesion properties *in situ* by the application of well-controlled normal forces. Moreover, the development of a novel bioreactor enables the continuous cultivation of *B. subtilis natto* biofilms at the solid/gas interface. In addition, the characterization of bioinspired synthetic hydrogels in dependence of the used peptide sequence, as well as fuel and waste concentration offers possibilities to finely tune their viscoelastic properties, such as stiffness, lifetime and yield point. The self-assembly process of these hydrogels is based on a fuel-driven reaction cycle that is inspired by the self-assembly of actin fibers. These dynamic hydrogels even exhibit certain self-healing properties (similar to biofilms) and have the potential to be used in different technical applications, for instance, as temporal and programmable sealings.



## 6. Outlook

The dynamic character of the synthetic hydrogels presented here can be beneficial for certain applications: it allows us to program the properties of transient hydrogels, and the self-healing capability of those materials enables advanced application possibilities (e.g. injection). Gels with self-healing abilities can also be very useful in certain biomedical applications, such as for controlled drug delivery, 3D bio-printing and tissue regeneration [206]. However, for these applications, not only good biocompatibility is necessary - in some applications (e.g. for wound healing), also gels with constant properties are needed. Yet, in such passive gels, the self-healing possibilities are limited. A biological material that exhibits constant properties and simultaneously a very high ability for self-healing are bacterial biofilms. Thus, it is of great interest to mimic these biofilm properties by synthetic hydrogels. However, the detailed mechanisms that are responsible for the self-healing ability of bacterial biofilms remain enigmatic: It is unclear, why bacterial biofilms are able to regenerate their stiffness after a mechanical disruption, even when the matrix is strongly ionically crosslinked. Confusingly, it is possible to crosslink the biomacromolecules alginate and  $\gamma$ -PGA with metal cations as well, but these hydrogels do not exhibit the ability to self-heal after a mechanically induced disruption. However, in this thesis it was shown, that these molecules are involved in the stiffening effect of bacterial biofilms when the biofilms are exposed to certain metal cations. Most likely, the formation of chelate complexes induces the increased stiffness here. Thus, one reason for the self-healing abilities of biofilms might be hidden in certain interactions with other biofilm components.

Interestingly, it is possible to obtain hydrogels capable of self-healing based on chelate chemistry. For instance, the ability to self-heal was observed for different gels based on polymers (e.g. polyethylene glycol (PEG), hyaluronic acid (HA), and polyacrylic acid (PAA)) that are functionalized with certain ligands (e.g. catechols, bisphosphonates, histidines, thiolates, and carboxylates) [206-212]. Gels based on L-DOPA-conjugated polymers (e.g. PEG or HA), were shown to exhibit good self-healing properties due to chelate complexes of the catechol groups with certain metal cations [213-215]. In contrast to bacterial biofilms, the self-healing properties of L-DOPA are pH-dependent: only at high pH (~9-12) a strong gel with self-healing properties is obtained [213]. However, this indicates, that it should be possible to obtain hydrogels with self-healing properties by using biofilm components.

Moreover, in further studies, it would be of great interest to identify the biofilm components that are responsible for their self-healing properties. The ability to self-heal was observed in biofilms of different bacterial strains that strongly differ in their composition, such as *P. aeruginosa* and *B. subtilis* B-1 [38, 145]. To identify the responsible biofilm components, alginate and PGA hydrogels could be enriched with further biofilm components until a system with self-healing abilities is obtained. With this method, step by step, a reconstituted biofilm can be recreated artificially. In this context, it is also possible, that the bacterial cells themselves play a role

for the self-healing ability of biofilms. However, it was observed, that biofilms are also able for self-healing, when the bacterial cells are not viable [38]. Thus, the self-healing ability of biofilms is a passive material property, independent of an active bacterial metabolism. To investigate the influence of bacterial cells on the biofilm self-healing properties, it is also possible to use bacterial strains that are not able to produce a biofilm matrix by themselves and to enrich these bacteria with respective matrix components. When an artificial biofilm with self-healing abilities can indeed be successfully created, this will also provide new insight into the molecular mechanisms that are responsible for this phenomenon occurring in natural biofilms and offers new possibilities to design artificial hydrogels with self-healing properties.

## **Appendix**

- A. Full-text of publications presented in this thesis
- B. Licenses for publications
- C. Full list of publications
- D. Bibliography
- E. Acknowledgements



## A. Full text of publications presented in this thesis

### A.1 Importance of the biofilm matrix for the erosion stability of *Bacillus subtilis* NCIB 3610 biofilms



RSC Advances

PAPER

View Article Online  
View Journal | View Issue



Cite this: *RSC Adv.*, 2019, 9, 11521

## Importance of the biofilm matrix for the erosion stability of *Bacillus subtilis* NCIB 3610 biofilms†

M. Klotz,<sup>a</sup> M. Kretschmer,<sup>b</sup> A. Goetz,<sup>a</sup> S. Ezendam,<sup>a</sup> O. Lieleg<sup>ib</sup> and M. Opitz<sup>ib\*</sup>

Production and secretion of biomolecules can provide new emergent functionalities to the synthesizing organism. In particular, the secretion of extracellular polymeric substances (EPS) by biofilm forming bacteria creates a biofilm matrix that protects the individual bacteria within the biofilm from external stressors such as antibiotics, chemicals and shear flow. Although the main matrix components of biofilms formed by *Bacillus subtilis* are known, it remains unclear how these matrix components contribute to the erosion stability of *B. subtilis* biofilms. Here, we combine different biophysical techniques to assess this relation. In particular, we quantify the importance of specific biofilm matrix components on the erosion behavior of biofilms formed by the well-studied *Bacillus subtilis* NCIB 3610. We find that the absence of biofilm matrix components decreases the erosion stability of NCIB 3610 biofilms in water, largely by abolishing the hydrophobic surface properties of the biofilm and by reducing the biofilm stiffness. However, the erosion resistance of NCIB 3610 biofilms is strongly increased in the presence of metal ions or the antibiotic ciprofloxacin. In the first case, unspecific ionic cross-linking of biofilm components or individual bacteria seems to be responsible for the observed effect, and in the second case there seems to be an unspecific interaction between the antibiotic and the biofilm matrix. Taken together, our results emphasize the importance of the biofilm matrix to reduce biofilm erosion and give insights into how the specific biomolecules interact with certain chemicals to fulfill this task.

Received 14th March 2019  
Accepted 2nd April 2019

DOI: 10.1039/c9ra01955c

rsc.li/rsc-advances

## Introduction

The production and secretion of extracellular polymeric substances (EPS) by biofilm forming bacteria provides the biofilm forming community with new emergent properties:<sup>1</sup> the bacteria are embedded within these exopolymers (the biofilm matrix), the resulting clusters protect them from the environment, antibiotics<sup>2,3</sup> and other chemicals,<sup>4</sup> and the structural rigidity provided by the biofilm matrix enables the community to withstand high shear forces or other mechanical stresses<sup>5</sup> and governs invasion resistance.<sup>6</sup> Although biofilm formation can be beneficial for industrial applications,<sup>7,8</sup> biofilms growing on heart valves or medical implants cause serious infections and device failure.<sup>9,10</sup> The biofilm matrix can be composed of different exopolymeric substances such as proteins, polysaccharides, DNA or lipids.<sup>11–13</sup> One finds an accumulation of multiple substances like eDNA, proteins, lipids, water and sugar within the assembled biofilms. However, not all bacterial cells produce these biopolymers that determine the structure of bacterial biofilms;<sup>14</sup> instead, one observes a division of labor of

secreting and non-secreting cells and a high physiological heterogeneity in biofilms.<sup>15</sup> Although the biofilm matrix composition is understood for many bacterial species,<sup>16,17,18,19–21</sup> it is largely unknown how the individual biopolymers contribute to the biofilm properties, e.g. which of them provide the biofilm with its high mechanical stability. Only recently, technical advances in high-resolution optical microscopy<sup>22</sup> and scanning electron microscopy allowed the investigation on how specific matrix components affect biofilm structure. For biofilms formed by *Escherichia coli* it was shown, that cellulose serves as an architectural element and that a network of curli fibers forms the outer biofilm layer.<sup>23,24</sup> Similarly, the function of specific proteins for cell–cell adhesion and cell encasement within *Vibrio cholerae* biofilms was described.<sup>25,26</sup> However, further studies are needed to understand the role of single matrix components for certain (physical) biofilm properties. In this study, we focus on the soil bacterium *Bacillus subtilis* that forms biofilms on solid nutrient surfaces in air, or at liquid–air interfaces.<sup>21–25</sup> The biofilm matrix of the *B. subtilis* strain NCIB 3610 used in this work is mainly composed of an exopolysaccharide produced by the gene products of the *epsA-O* operon<sup>26</sup> and an amyloid fiber forming protein TsaA.<sup>27,28</sup> A second biofilm matrix protein, BslA,<sup>29,30</sup> is a self-assembling hydrophobin that is primarily found on the surface of *B. subtilis* NCIB 3610 biofilms.

<sup>a</sup>Center for NanoScience, Faculty of Physics, Ludwig-Maximilians-Universität München, Munich, Germany. E-mail: opitz@physik.uni-muenchen.de

<sup>b</sup>Munich School of BioEngineering and Department of Mechanical Engineering, Technische Universität München, Garching, Germany

† Electronic supplementary information (ESI) available. See DOI: 10.1039/c9ra01955c

In the past years many studies have investigated physical properties of *B. subtilis* biofilms including biofilm erosion,<sup>4</sup> biofilm elasticity<sup>21,22</sup> and surface properties.<sup>23,24–26</sup> However, only recently direct correlations between the biofilm matrix composition and specific biofilm properties could be determined.<sup>24,26,27</sup> Importantly, it was shown that the surface layer protein BslA is important for the surface stiffness and surface roughness<sup>24</sup> of NCIB 3610 biofilms, and this protein also strongly affects the biofilm wettability.<sup>29,33,38</sup> Both for *B. subtilis* B-1 biofilms and biofilms generated by *Pseudomonas aeruginosa*<sup>39</sup> it was shown that multi-valent ions protect the biofilms from erosion. However, if and how these ions interact with biopolymers within the biofilm matrix to provide this stability remains elusive.

Using a set of deletion mutants, we here investigate the importance of selected biofilm matrix components on the erosion stability of *B. subtilis* NCIB 3610 biofilms. In addition, we show that – similar to biofilms created by strain B-1 – also biofilms generated by strain NCIB 3610 are protected from erosion in the presence of metal ions. In contrast to our expectations, this effect does not stem from interactions between a specific matrix component with these ions, but seems to be due to unspecific cross-linking effects – either between some matrix components or between the bacterial cells themselves. Finally, we report that the antibiotic ciprofloxacin increases the erosion resistance of NCIB 3610 biofilms – an effect that is surprising but appears to be specific rather than generic for antibiotics.

## Materials and methods

### Strains and growth conditions

The *B. subtilis* strains used in this study are NCIB 3610, CA017, ZK3660 and N24, as described in Table 1. LB medium (Luria/Miller; Carl Roth GmbH, Karlsruhe, Germany) served as complex medium for all *B. subtilis* strains and contained the corresponding antibiotic (Table 1). Bacteria were cultivated overnight in 5 ml medium at 37 °C and 300 rpm agitation. The cultures were then diluted to an OD<sub>600</sub> of 0.05 and grown until an OD<sub>600</sub> of 0.1 was reached, representing the beginning of the exponential growth phase. The cultures were again diluted to an OD<sub>600</sub> of 0.05 for the erosion assay. Sterile polytetrafluorethylene (PTFE) chips (Fig. 1a) containing 10 chambers (*i.e.*, cylindrical holes of 6 mm diameter and 3 mm depth) were filled with hot LB-agar as growth medium for the biofilms. After cooling of the medium 5 µl of the diluted cultures were applied on each agar patch and the chips were then incubated at 37 °C lying flat in sterile Petri dishes without agitation for 24 h for biofilm growth.

These chips were then transferred to the prefilled falcon tubes used in the erosion assays as described below.

### Erosion assay

To conduct the erosion tests, 45 ml of a testing liquid was prepared and filled into falcon tubes. Depending on conditions specific for the different experiments, either double deionized water, ionic solution or antibiotic solution was used as testing liquid. The PTFE chips were placed into the falcon tubes (Fig. 1a) which in turn were mounted onto a lab shaker (Innova 4200, New Brunswick Scientific). The lab shaker was then set into rotation at 300 rpm for defined time intervals, which generated a shear stress of approximately 180 mPa. The shear stress was calculated by measuring the rotation speed inside the falcon tubes and using the appropriate calculation presented in Grumbein *et al.*, 2014.<sup>4</sup> After exposure to this shaking induced shear force, images of the biofilm-covered agar patches were acquired (Fig. 1a) using a stereomicroscope (Nikon SMZ1000).

Images were then analyzed using the freeware ImageJ (version 1.48) and a graphic tablet (Wacom Intuos Art M) by manually marking the area of each patch that was covered with biofilm for all measured time steps. The detached area fraction was determined by dividing the area covered at each time step with the area covered at the beginning ( $t = 0$  min).

Measurements with antibiotic agents were performed for three different antibiotics at the following concentrations: vancomycin 0.75 µg ml<sup>-1</sup> (Van); ciprofloxacin 0.25 µg ml<sup>-1</sup> (Cipro); spectinomycin 64 µg ml<sup>-1</sup> (Spec). In order for the antibiotic agents to be able to penetrate the biofilm/the cells, the measurements protocols were adapted as follows: a reference image for time  $t = -15$  min was taken. Then the biofilm slides were placed into a falcon tube filled with 45 ml of water (containing the antibiotic in the concentrations described above) for 15 minutes. After that, the slides were taken out of the falcon tubes and an image was taken of all biofilm patches ( $t = 0$  min) and the measurements were then performed as described before.

### Rheological characterization

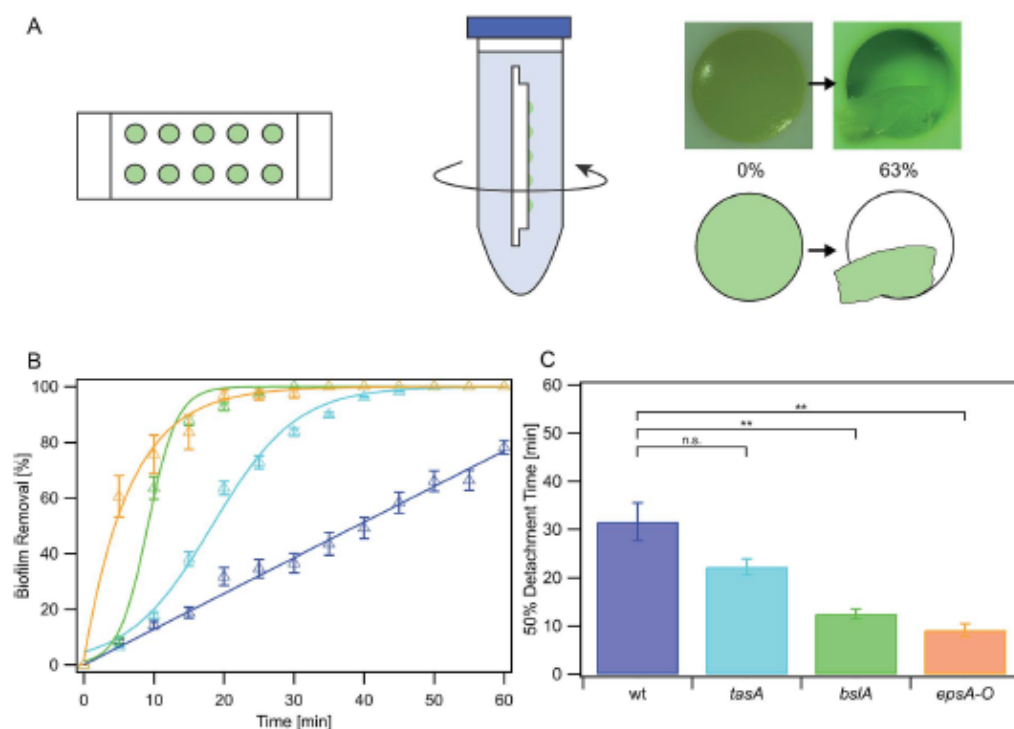
Biofilms were cultivated in Petri dishes on LB-agar for 24 h using similar growth conditions as described above. The two following differences in the growth protocol were applied to obtain large amounts of biofilm as needed for rheology: cultivation overnight was executed in 10 ml LB medium, and 100 µl of this liquid culture was applied and homogeneously distributed on a Petri dish filled with LB-agar. The biofilms were incubated with different salt solutions (50 mM FeCl<sub>3</sub>, 50 mM

Table 1 Strains used in this study

Strain	Genotype	Remaining main matrix composition	Antibiotic and concentration	Reference
NCIB 3610	Wild-type	Proteins TsaA & BslA, exopolysaccharide	None	53
CA017 <sup>a</sup>	<i>tsaA::kan</i>	Protein BslA, exopolysaccharide	Kanamycin, 50 µg ml <sup>-1</sup>	28
N24 <sup>a</sup>	<i>bslA::cat</i>	Protein TsaA, exopolysaccharide	Chloramphenicol, 5 µg ml <sup>-1</sup>	29
ZK3660 <sup>a</sup>	<i>epsA-O::tet</i>	Protein TsaA	Tetracycline, 12.5 µg ml <sup>-1</sup>	54
BD630	Wild-type	Unable to produce a proper biofilm matrix	None	55

<sup>a</sup> These strains are non-isogenic derivatives of strain NCIB 3610.





**Fig. 1** Erosion stability of NCIB 3610 biofilms. (A) Schematic representation of the erosion experiment. Left: a PTFE slide containing 10 biofilm-covered agar patches is inserted into a tube which is then filled with a testing solution (middle). Shear forces are induced by setting the tube into rotational motion using a lab shaker. Right: images and sketch of biofilm-covered agar patches before (0% biofilm removal) and during (63% biofilm removal) an erosion experiment. Sometimes folding of the biofilm over the edge during detachment was observed. Consequently, only the biofilm free area was calculated as a measure for biofilm removal. (B) Biofilm erosion of biofilms formed by the NCIB 3610 wild-type strain and mutant strains in water. (NCIB 3610 is depicted in blue, the *tasA* mutant in turquoise, the *bslA* deletion mutant in green and the *epsA-O* mutant in orange). (C) Time-point of 50% detachment for NCIB 3610 and mutant strains in water.

CuSO<sub>4</sub>, 50 mM CaCl<sub>2</sub>, 250 mM NaCl, or double deionized water as a control) for one hour. For hydrophilic biofilms (*epsA-O*, *bslA*), 10 ml of the solutions were poured onto the biofilm; for hydrophobic biofilms (*B. subtilis* NCIB 3610, *tasA*) 20 ml were added, so that the liquids were able to cover the whole biofilm. After the incubation the solutions were discarded and the biofilms were harvested from the agar plates by manual scraping. Additionally, reference samples were prepared which were not incubated with liquids at all. Those reference biofilms were harvested directly after the growth period.

Rheological measurements were performed using a commercial shear rheometer (MCR 302; Anton Paar GmbH) equipped with a 25 mm plate–plate geometry. The plate separation was set to 0.4 mm for almost all samples; only for the samples incubated with FeCl<sub>3</sub> (which exhibited a very high stiffness) a larger plate separation of 0.7 mm had to be used. For a single measurement, biofilm from up to two agar plates had to be pooled to collect enough material to fill the measuring gap. A solvent trap was applied to prevent drying of the samples during the measurement. All measurements were conducted at 21 °C and in strain-controlled mode, and frequency sweeps were recorded in a frequency range of 0.1 Hz to 10 Hz. Small strains corresponding

to a constant torque of 0.5 μNm were applied to guarantee linear response. For each condition, three different samples were tested.

Within each rheological experiment, the storage and loss modulus were determined; however, for simplicity (as the loss moduli exhibited the same trends we describe for the storage moduli), only the storage modulus is discussed in the manuscript. Since the recorded moduli showed only a very weak frequency dependence, the obtained storage moduli were averaged over the complete measured frequency spectrum to obtain the bar plots shown in the manuscript. Obvious outliers resulting from measuring artefacts were excluded from calculating these mean values. This averaged storage modulus is referred to as biofilm stiffness ( $G_0$ ) in the manuscript. Error bars denote the standard deviation calculated from the mean values of three frequency sweeps.

#### Wetting assay

Here, the above described day cultures were diluted to an optical density of 0.05 in a 1.5 ml reaction tube containing 500 μl of LB medium before being spotted onto LB-agar plates. On each plate, five 5 μl spots were applied at equal distance and the plates were

incubated at 37 °C for 24 h. Then 10 µl drops of water were applied to the biofilm surface. An image of each droplet on the biofilm surface was acquired with a Canon PowerShot G12 digital camera and the contact angle was determined using the angle tool of ImageJ.

### Significance analysis

For significance analysis we performed a Wilcoxon rank test using the program Igor7Pro (version 7.04, WaveMetrics) as the samples were not normally distributed. The significance level was chosen as  $\alpha = 0.05$  (\*\*) and plotted in the corresponding figures and ESI Table 2.†

## Results

### Matrix components contribute to NCIB 3610 biofilm erosion stability

In a first set of experiments, we studied the erosion stability of biofilms formed by the *Bacillus subtilis* NCIB 3610 wild-type strain exposed to water (Fig. 1a). When challenged by fluid shear induced by shaking, biofilms formed by this strain detached from the agar patches on the PTFE chip within 65 min: the averaged erosion behavior of these wild-type strain biofilms was approximately linear (Fig. 1b, Table S1†), with 50% of the biofilm mass being detached from the agar surface after  $32 \pm 4$  min (Fig. 1c). This was in contrast to submerged control samples investigated in the absence of shear forces, which did not detach (data not shown). In a next step, we investigated the erosion stability of biofilms formed by several mutant strains each lacking one or two components of the biofilm matrix (Fig. 1b). The first deletion mutant, *tasA*, lacks the amyloid fiber forming protein TasA.<sup>27,28</sup> Biofilms formed by this mutant detached from the agar patches in a sigmoidal fashion (Fig. 1b and Table S1†) and faster than the wild-type strain biofilms: here 50% of the biofilm was already eroded after  $22 \pm 2$  min (Fig. 1c). Biofilms generated by a deletion mutant lacking the surface layer protein BslA<sup>29,30</sup> also detached in a sigmoidal fashion (Fig. 1b, Table S1†) with 50% of the biofilm mass being eroded within  $13 \pm 2$  min. The lowest erosion stability was observed for biofilms formed by a deletion mutant unable to produce the exopolysaccharide.<sup>26</sup> Here, biofilm removal was exponentially growing with time (Fig. 1b, Table S1†), with a 50% detachment value of  $9 \pm 2$  min (Fig. 1c). In this context, it is important to note that expression of the exopolysaccharide is necessary for the production of the BslA protein.<sup>29</sup> Consequently, this *epsA-O* mutant also lacks the BslA protein which might explain why this biofilm variant exhibits the highest sensitivity to erosion. From this data, we conclude that – among the conditions tested here – the absence of either BslA and/or the exopolysaccharide has a strong influence on the erosion stability of the biofilm.

To better understand the mechanisms by which the biofilm matrix components contribute to the biofilm erosion stability, we investigated two physical biofilm properties that could be relevant. First, we analyzed if the lack of certain biofilm matrix components

would affect the wettability of NCIB 3610 biofilms. This question was motivated by previous results on wild-type biofilms which demonstrated that a reduction of the biofilm surface hydrophobicity can enable faster erosion.<sup>40</sup> To assess the biofilm wettability, we determined contact angles: values greater than 90° indicate a hydrophobic surface, while contact angles smaller than 90° represent a hydrophilic surface. We found that the surface of biofilms formed by the wild-type strain was hydrophobic with a contact angle of  $(129 \pm 2)^\circ$  (Fig. 2a). In contrast, *bslA* and *epsA-O* mutant strains formed biofilms with hydrophilic surfaces as demonstrated by measured contact angles smaller than 35° (Fig. 2a). For *tasA* biofilms, the wetting properties were a bit more complicated. Here, the biofilm initially exhibited large contact angles in the range of  $(132 \pm 2)^\circ$ ; however, the droplet then spread and reached final contact angle values comparable to those obtained for the other mutant strain biofilms.

Overall, this agreed with previous results from the literature<sup>29</sup> and demonstrated that the absence of one or two biofilm matrix components strongly alters the wetting behavior of the biofilm, shifting it from hydrophobic to hydrophilic. Moreover, the differences in biofilm erosion stability described above agree well with the differences in biofilm wettability: the hydrophobic wild-type biofilm showed the strongest erosion resistance, the hydrophilic *bslA* and *epsA-O* biofilms (which both lack the hydrophobic surface protein BslA) showed the weakest erosion resistance, and the *tasA* biofilms exhibited both intermediate wetting and intermediate erosion properties.

A second possible biofilm property which could affect the biofilm erosion process is the biofilm bulk stiffness. Although previous experiments<sup>31</sup> showed that the stiffness of untreated wild-type biofilm is comparable to that of biofilms formed by the individual mutant strains, this could change after prolonged biofilm exposure to water (as it is the case in our erosion tests) – especially since the different biofilm variants exhibited differences in wettability. Indeed, after incubation with water, biofilms formed by the three mutant strains showed a decreased biofilm stiffness (Fig. 2b): this drop in biofilm stiffness was strong for the *epsA-O* mutant biofilm, weaker for the *bslA* mutant biofilms and virtually absent for (hydrophobic) *tasA* and wild-type biofilms. From this data, we conclude that softening of the biofilm matrix by prolonged exposure to water may also contribute to the erosion behavior of the biofilm – and that this softening effect is directly related to the biofilm wettability.

### Metal ions increase the erosion stability of NCIB 3610 biofilms

In Grumbein *et al.*, 2014<sup>4</sup> it was shown that selected metal ions increase the erosion stability of *Bacillus subtilis* B-1 biofilms, whose biofilm matrix is mainly composed of  $\gamma$ -polyglutamate. Consequently, we assessed if metal ions are also able to increase the erosion stability of NCIB 3610 biofilms which – as described above – possess a completely different biofilm matrix. We therefore tested the erosion behavior of NCIB 3610 biofilms in the presence of  $\text{Fe}^{3+}$ ,  $\text{Cu}^{2+}$  and  $\text{Ca}^{2+}$ ; those ions were chosen since they have been shown to induce a strong increase in erosion stability of B-1 biofilms.<sup>4</sup> In addition, we also tested the

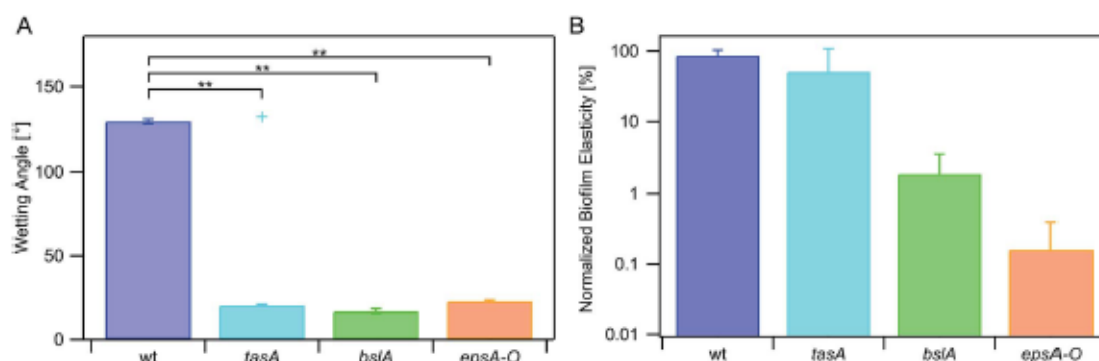


Fig. 2 Absence of biofilm matrix components affects wettability of the biofilm surface and biofilm stiffness. (A) Wetting behavior of NCIB 3610 wild-type and mutant strain biofilms. Turquoise +: corresponding contact angle right after application of water droplet (this value is not included in the significance analysis). (B) Biofilm stiffness given as the storage modulus obtained by macro rheology.

influence of the mono-valent ion  $\text{Na}^+$ , which had shown no effect on the erosion behavior of B-1 biofilms.

Indeed, we found that all three multi-valent ions  $\text{Fe}^{3+}$ ,  $\text{Cu}^{2+}$ , and  $\text{Ca}^{2+}$  strongly decreased erosion of NCIB 3610 biofilms (Fig. 3a); in case of the former two, biofilm erosion was almost totally inhibited. However, biofilm erosion was also decreased in the presence of the mono-valent ion  $\text{Na}^+$  (Fig. 3a). In a set of control experiments, we ensured that the pH of the ion solutions alone was not responsible for the observed increase in erosion stability (Fig. 4). Hence, we believe that the presence of the metal ions in our experiments is the main reason for the decreased biofilm erosion of the tested biofilms. Interestingly, the effect of metal ions to decrease biofilm erosion is not exclusively due to an increase in biofilm stiffness (Fig. 3b), although we did find an effect on both properties for  $\text{Fe}^{3+}$  and – albeit weaker – for  $\text{Cu}^{2+}$ .

#### Interaction of metal ions with biofilm matrix components

In a next set of experiments, we assessed the question if the tested metal ions interacted with specific components of the biofilm matrix, and if such an interaction was responsible for the observed increase in biofilm erosion stability. To do so, we repeated the erosion experiments with the ion solutions, but this time we applied the ion solutions to biofilms created by the mutant strains introduced above. We found that, in the presence of  $\text{Fe}^{3+}$ , biofilm erosion was almost completely inhibited for all mutant strains tested (Fig. 3a). At the same time, biofilm stiffness was increased to similar levels for all mutant strain biofilms as for the wild-type biofilm (Fig. 3b). Interestingly, a bacterial colony formed by a *B. subtilis* strain unable to produce any biofilm matrix (ESI Fig. 1†) was also completely protected from erosion in the presence of  $\text{Fe}^{3+}$ . From those experiments, we conclude that the  $\text{Fe}^{3+}$  ions do not interact with a single specific biofilm matrix component. Instead, the observed increase in biofilm stiffness and erosion resistance seems to be due to unspecific ionic cross-linking effects. Of course, the source of this unspecific cross-linking effect is difficult to pinpoint as it could occur either between different

matrix components, between matrix components and biofilm bacteria, or between individual bacterial cells themselves and/or the agar substrate.

In the presence of  $\text{Cu}^{2+}$ , we obtained a similar picture as for  $\text{Fe}^{3+}$ : biofilm erosion was decreased for all mutant strains; however, this effect was not always as strong as for the wild-type biofilm (Fig. 3a). As for  $\text{Fe}^{3+}$ , also for  $\text{Cu}^{2+}$ , we detected an increase in biofilm stiffness for all biofilm variants – albeit less pronounced than for  $\text{Fe}^{3+}$ . Taken together, this seemed to suggest that erosion sensitivity and biofilm stiffness are directly related for *B. subtilis* NCIB 3610 biofilms, and both can be affected by unspecific cross-linking effects induced by multi-valent ions.

Experiments conducted with solutions containing either  $\text{Ca}^{2+}$  or  $\text{Na}^+$ , challenged this picture. Here, we did not find combinations of ions and biofilms where the biofilm stiffness was increased compared to the control performed with pure water. Nevertheless, there were conditions where biofilm erosion was significantly decreased – even for  $\text{Na}^+$  (Fig. 3).

#### The antibiotic ciprofloxacin increases erosion stability of NCIB 3610 biofilms

In a last set of experiments, we investigated if specific antibiotics also affect the erosion stability of NCIB 3610 biofilms. Antibiotics represent an important medical treatment to counteract bacterial growth and are often applied in an aqueous environment. We tested three different antibiotics that differ in their mode of action: (i) vancomycin, which inhibits the production of the bacterial cell membrane<sup>44</sup> (ii) ciprofloxacin, that inhibits DNA replication<sup>42</sup> and (iii) spectinomycin, that inhibits protein synthesis.<sup>43</sup> All antibiotics were applied at concentrations that are above the individual minimal inhibitory concentration (MIC) proven to have an effect on single bacterial cells (ESI Fig. 2†). We find that biofilm erosion of the wild-type strain NCIB 3610 is not significantly affected in the presence of vancomycin and spectinomycin (Fig. 5a). The presence of ciprofloxacin, however, increased the erosion stability of NCIB

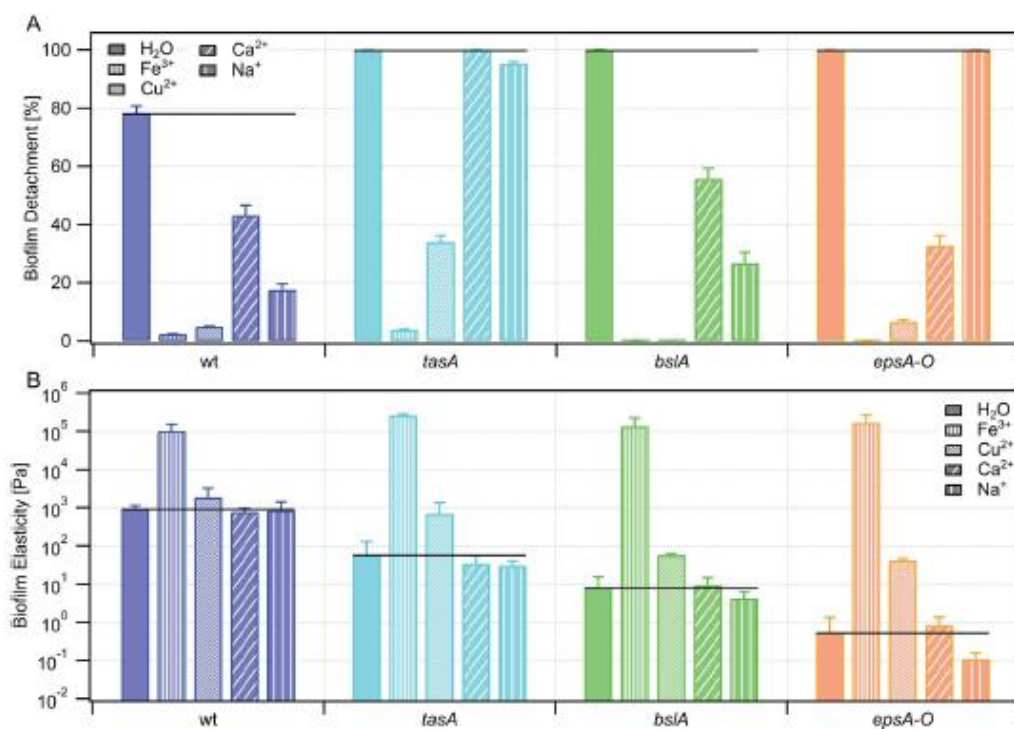


Fig. 3 Metal ions increase the erosion stability of NCIB 3610 biofilms. (A) Biofilm erosion of the NCIB 3610 wild-type and several mutant strains as mean fraction of removed biofilm from the agar patches compared to the fully covered patches at time  $t = 0$  min. (B) Biofilm stiffness of the NCIB 3610 wild-type and several mutant strains. (A and B) Black line indicates value of corresponding water treated sample.

3610 biofilms (Fig. 5a). Surprisingly, the presence of this antibiotic lead to a small decrease in biofilm stiffness (ESI Fig. 3†), which is the opposite trend as we described above for the metal ions. When we studied the erosion stability of the mutant strain

biofilms lacking one or two biofilm matrix components, and found that in the absence of one or two biofilm matrix components the protective effect of ciprofloxacin was strongly reduced (Fig. 5b).

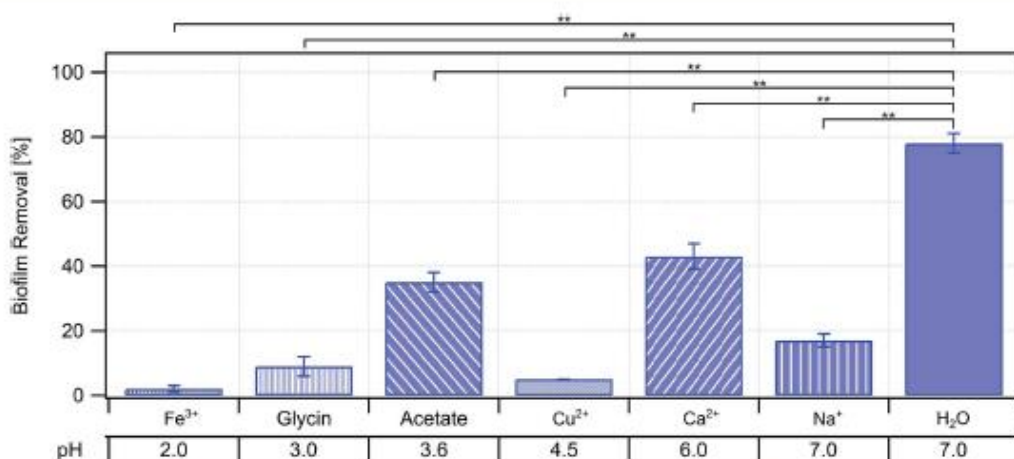


Fig. 4 Influence of pH on biofilm erosion. The pH of each tested ionic solution is given underneath the corresponding biofilm removal data of the wild-type strain.

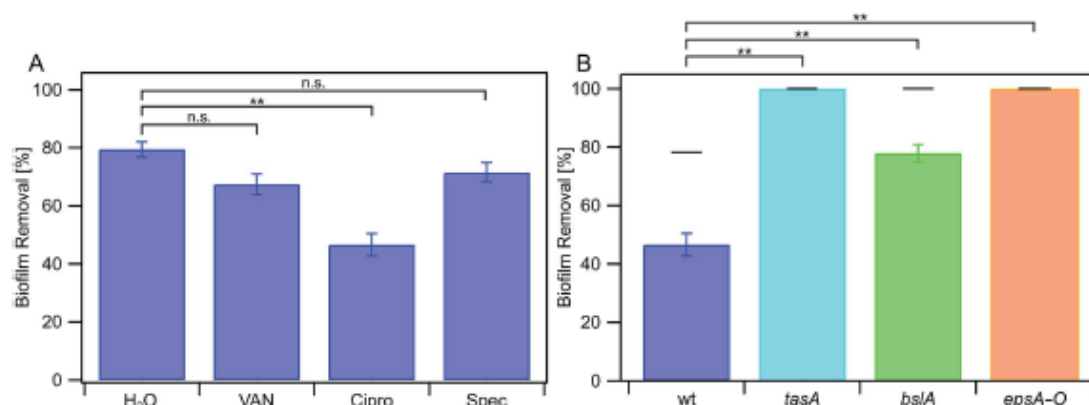


Fig. 5 Treatment with the antibiotic ciprofloxacin increases erosion stability of NCIB 3610 biofilms. (A) Biofilm erosion of the NCIB 3610 wild-type in water and three different antibiotics. (B) Biofilm detachment for NCIB 3610 and mutant strains in the presence of ciprofloxacin. Black lines indicate the biofilm removal of each strain in water.

## Discussion

In this study, we presented a quantitative time-resolved analysis on the erosion stability of *Bacillus subtilis* NCIB 3610 biofilms. In particular, we demonstrated the importance of the biofilm matrix in this regard and showed that the erosion kinetics differ for all strains studied ranging from linear erosion observed for the wild-type strain, over sigmoidal erosion kinetics for strains lacking the TasA protein in the biofilm matrix, to exponential erosion kinetics for the strain not able to produce the exopolysaccharide. Linear erosion kinetics were previously also found for a different *Bacillus subtilis* variant, i.e. *B. subtilis* B-1,<sup>4</sup> whose biofilm matrix is mainly composed of  $\gamma$ -polyglutamate.<sup>7</sup>

Different molecular factors might be important for the erosion stability of bacterial biofilms<sup>44–46</sup> such as biofilm composition or the distribution of molecules throughout the extracellular matrix. In this study, we addressed two physical biofilm properties influencing biofilm erosion. We showed that *B. subtilis* NCIB 3610 biofilms with a hydrophobic biofilm surface, as well as biofilms with a high biofilm stiffness exhibit an increased biofilm erosion stability, and that this erosion stability is strongly reduced if one or two biofilm matrix components are missing in the biofilm matrix. Thereby, the TasA protein seems to be of minor importance, while the surface layer protein BslA and the exopolysaccharide have a strong impact. However, the presence of all biofilm matrix components is necessary to achieve the full erosion stability of NCIB 3610 biofilms. It appears reasonable that a less hydrophobic biofilm would be more susceptible to softening induced by water ingress, and that a softer biofilm can be removed from a surface by shear forces more easily than a stiff biofilm variant. However, how the different biofilm matrix molecules work together to fine-tune both of those properties at the same time, cannot be disentangled at this point.

In our study, we also investigated the importance of certain chemicals on the erosion stability of *Bacillus subtilis* NCIB 3610 biofilms. First, we addressed the presence of metal ions on

biofilm erosion stability. Both, mono- and multi-valent metal ions are present in many fluid environments such as the human blood,<sup>47</sup> or in pipes and tubes of the food industry.<sup>48</sup> In contrast to biofilms formed by the *Bacillus subtilis* strain B-1<sup>4</sup> that were protected from erosion by multi-valent ions only, we here found that the erosion properties of biofilms formed by strain NCIB 3610 can also be modulated by the mono-valent ion Na<sup>+</sup>. At this point, we attribute this difference in biofilm response to differences in the composition of the biofilm matrix of these strains.<sup>7,44</sup> Similar to previous results obtained for *B. subtilis* B-1 biofilms,<sup>4</sup> here we also detected a stiffening of the biofilm upon exposure to Fe<sup>3+</sup> and Cu<sup>2+</sup> ions. However, specific interactions between a certain biofilm matrix component and these metal ions seem not to be required to obtain this effect. This finding appears to fit into a broader picture,<sup>49,50</sup> as an effect of selected metal ions on the erosion stability and/or stiffness was also described for *Pseudomonas aeruginosa*<sup>49,51</sup> (where the main biofilm component is alginate) and *Staphylococcus epidermidis* biofilms.<sup>52</sup> This suggests that protecting themselves from erosion by absorbing metal ions from the liquid environment might be a more generic principle that biofilms developed to optimize their survival in the presence of mechanical shear forces, and that different bacterial species make use of a distinct set of matrix molecules to achieve this effect.

Second, we investigated the effect of selected antibiotics on the erosion stability of biofilms. While the antibiotics vancomycin and spectinomycin had no effect, the presence of the antibiotic ciprofloxacin increased erosion stability of mature NCIB 3610 biofilms, that is attributed to an unspecific interaction with the biofilm matrix. However, biofilm stiffness was not considerably altered by the antibiotic ciprofloxacin, so we speculate the increase in biofilm erosion stability being due to an increase in biofilm adhesion. An effect of certain antibiotics on biofilm stiffness was also described for *S. epidermidis* and *P. aeruginosa*.<sup>49,50,52</sup> In the latter case, the antibiotic ciprofloxacin decreased biofilm stiffness. To our knowledge, no information is yet available on how these different types of chemicals (ions

or antibiotics) interact with the single biofilm matrix components to achieve the effects described above.

In summary, we have shown that the biofilm matrix composition is important for the erosion stability of NCIB 3610 biofilms and that this stability can be altered by certain chemicals such as mono- and multi-valent ions or the antibiotic ciprofloxacin.

## Conflicts of interest

There are no conflicts of interest to declare.

## Acknowledgements

We thank R. Kolter for *Bacillus subtilis* strains NCIB 3610, CA017 and ZK3660 and K. Kobayashi for strain N24. For technical assistance, we thank L. Kern, B. v. Bronk, M. Jung and N. Schäffler. This study was supported by the Deutsche Forschungsgemeinschaft through project B11 in the framework of SFB863. Additional financial support by the Center for Nanoscience (CeNS) is gratefully acknowledged.

## References

- H. C. Flemming, J. Wingender, U. Szewzyk, P. Steinberg, S. A. Rice and S. Kjelleberg, Biofilms: an emergent form of bacterial life, *Nat. Rev. Microbiol.*, 2016, **14**(9), 563.
- P. S. Stewart, Mechanisms of antibiotic resistance in bacterial biofilms, *Int. J. Med. Microbiol.*, 2002, **292**, 107–113.
- N. Høiby, T. Bjarnsholt, M. Givskov, S. Molin and O. Ciofu, Antibiotic resistance of bacterial biofilms, *Int. J. Antimicrob. Agents*, 2010, **35**, 322–332.
- S. Grumbein, M. Opitz and O. Lieleg, Selected metal ions protect *Bacillus subtilis* biofilms from erosion, *Metallomics*, 2014, **6**, 1441–1450.
- M. Irsfeld, B. M. Prüß and S. J. Stafslien, Screening the mechanical stability of *Escherichia coli* biofilms through exposure to external, hydrodynamic shear forces, *J. Basic Microbiol.*, 2014, **54**, 1403–1409.
- C. D. Nadell, K. Drescher, N. S. Wingreen and B. L. Bassler, Extracellular matrix structure governs invasion resistance in bacterial biofilms, *ISME J.*, 2015, **9**, 1700–1709.
- M. Morikawa, S. Kagihiro, M. Haruki, K. Takanashi, S. Branda, R. Kolter and S. Kanaya, Biofilm formation by a *Bacillus subtilis* strain that produces  $\gamma$ -polyglutamate, *Microbiology*, 2006, **152**, 2801–2807.
- T. L. Wood, R. Guha, L. Tang, M. Geitner, M. Kumar and T. K. Wood, Living biofouling-resistant membranes as a model for the beneficial use of engineered biofilms, *Proc. Natl. Acad. Sci. U. S. A.*, 2016, **113**, E2802–E2811.
- L. Hall-Stoodley, J. W. Costerton and P. Stoodley, Bacterial biofilms: from the natural environment to infectious diseases, *Nat. Rev. Microbiol.*, 2004, **2**, 95–108.
- P. Gupta, S. Sarkar, B. Das, S. Bhattacharjee and P. Tribedi, Biofilm, pathogenesis and prevention—a journey to break the wall: a review, *Arch. Microbiol.*, 2016, **198**, 1–15.
- Q. Wei and L. Z. Ma, Biofilm matrix and its regulation in *Pseudomonas aeruginosa*, *Int. J. Mol. Sci.*, 2013, **14**, 20983–21005.
- M. Marvasi, P. T. Visscher and L. Casillas Martinez, Exopolymeric substances (EPS) from *Bacillus subtilis*: polymers and genes encoding their synthesis, *FEMS Microbiol. Lett.*, 2010, **313**, 1–9.
- H. C. Flemming and J. Wingender, The biofilm matrix, *Nat. Rev. Microbiol.*, 2010, **8**, 623–633.
- L. Hobley, C. Harkins, C. E. MacPhee and N. R. Stanley-Wall, Giving structure to the biofilm matrix: an overview of individual strategies and emerging common themes, *FEMS Microbiol. Rev.*, 2015, **39**, 649–669.
- P. S. Stewart and M. J. Franklin, Physiological heterogeneity in biofilms, *Nat. Rev. Microbiol.*, 2008, **6**, 199–210.
- V. Berk, J. C. N. Fong, G. T. Dempsey, O. N. Develioglu, X. Zhuang, J. Liphardt, F. H. Yildiz and S. Chu, Molecular architecture and assembly principles of *Vibrio cholerae* biofilms, *Science*, 2012, **337**, 236–239.
- C. Hung, Y. Zhou, J. S. Pinkner, K. W. Dodson, J. R. Crowley, J. Heuser, M. R. Chapman, M. Hadjifrangiskou, J. P. Henderson and S. J. Hultgren, *Escherichia coli* Biofilms Have an Organized and Complex Extracellular Matrix Structure, *mBio*, 2013, **4**, 1–10.
- J. Valle, C. Latasa, C. Gil, A. Toledo-Arana, C. Solano, J. R. Penadés and I. Lasa, Bap, a Biofilm Matrix Protein of *Staphylococcus aureus* Prevents Cellular Internalization through Binding to GP96 Host Receptor, *PLoS Pathog.*, 2012, **8**(8), e1002843.
- K. Drescher, J. Dunkel, C. D. Nadell, S. van Teeffelen, I. Grnja, N. S. Wingreen, H. A. Stone and B. L. Bassler, Architectural transitions in *Vibrio cholerae* biofilms at single-cell resolution, *Proc. Natl. Acad. Sci. U. S. A.*, 2016, **113**, E2066–E2072.
- D. O. Serra, A. M. Richter and R. Hengge, Cellulose as an architectural element in spatially structured *Escherichia coli* biofilms, *J. Bacteriol.*, 2013, **195**, 5540–5554.
- D. O. Serra, A. M. Richter, G. Klauk, F. Mika and R. Hengge, Microanatomy at cellular resolution and spatial order of physiological differentiation in a bacterial biofilm, *mBio*, 2013, **4**, 1–12.
- J. K. Teschler, D. Zamorano-Sánchez, A. S. Utada, C. J. A. Warner, G. C. L. Wong, R. G. Lington and F. H. Yildiz, Living in the matrix: assembly and control of *Vibrio cholerae* biofilms, *Nat. Rev. Microbiol.*, 2015, **13**, 255–268.
- H. Vlamakis, Y. Chai, P. Beauregard, R. Losick and R. Kolter, Sticking together: Building a biofilm the *Bacillus subtilis* way, *Nat. Rev. Microbiol.*, 2013, **11**, 157–168.
- L. S. Cairns, L. Hobley and N. R. Stanley-Wall, Biofilm formation by *Bacillus subtilis*: new insights into regulatory strategies and assembly mechanisms, *Mol. Microbiol.*, 2014, **93**, 587–598.
- R. Gallegos-Monterrosa, E. Mhatre and Á. T. Kovács, Specific *Bacillus subtilis* 168 variants form biofilms on nutrient-rich medium, *Microbiology*, 2016, **162**, 1922–1932.

- 26 S. S. Branda, F. Chu, D. B. Kearns, R. Losick and R. Kolter, A major protein component of the *Bacillus subtilis* biofilm matrix, *Mol. Microbiol.*, 2006, **59**, 1229–1238.
- 27 D. Romero, C. Aguilar, R. Losick and R. Kolter, Amyloid fibers provide structural integrity to *Bacillus subtilis* biofilms, *Proc. Natl. Acad. Sci. U. S. A.*, 2010, **107**, 2230–2234.
- 28 H. Vlamakis, C. Aguilar, R. Losick and R. Kolter, Control of cell fate by the formation of an architecturally complex bacterial community, *Genes Dev.*, 2008, **22**, 945–953.
- 29 K. Kobayashi and M. Iwano, BslA(YuaB) forms a hydrophobic layer on the surface of *Bacillus subtilis* biofilms, *Mol. Microbiol.*, 2012, **85**, 51–66.
- 30 L. Hobley, A. Ostrowski, F. V. Rao, K. M. Bromley, M. Porter, A. R. Prescott, C. E. MacPhee, D. M. F. van Aalten and N. R. Stanley-Wall, BslA is a self-assembling bacterial hydrophobin that coats the *Bacillus subtilis* biofilm, *Proc. Natl. Acad. Sci. U. S. A.*, 2013, **110**, 13600–13605.
- 31 S. Kesel, S. Grumbein, I. Gümperlein, M. Tallawi, A. K. Marel, O. Lielég and M. Opitz, Direct comparison of physical properties of *Bacillus subtilis* NCIB 3610 and B-1 biofilms, *Appl. Environ. Microbiol.*, 2016, **82**, 2424–2432.
- 32 S. Grumbein, D. Minev, M. Tallawi, K. Boettcher, F. Prade, F. Pfeiffer, C. U. Grosse and O. Lielég, Hydrophobic Properties of Biofilm-Enriched Hybrid Mortar, *Adv. Mater.*, 2016, 8138–8143.
- 33 M. Werb, C. F. García, N. C. Bach, S. Grumbein, S. A. Sieber, M. Opitz and O. Lielég, Surface topology affects wetting behavior of *Bacillus subtilis* biofilms, *npj Biofilms and Microbiomes*, 2017, **3**(1), 11.
- 34 M. Asally, M. Kittisopikul, P. Rue, Y. Du, Z. Hu, T. Cagatay, A. B. Robinson, H. Lu, J. Garcia-Ojalvo and G. M. Suel, Localized cell death focuses mechanical forces during 3D patterning in a biofilm, *Proc. Natl. Acad. Sci. U. S. A.*, 2012, **109**, 18891–18896.
- 35 W. Zhang, Y. Wang, S. Bougouffa, R. Tian, H. Cao, Y. Li, L. Cai, Y. H. Wong, G. Zhang, G. Zhou, X. Zhang, V. B. Bajic, A. Al-Suwailem and P. Y. Qian, Synchronized dynamics of bacterial niche-specific functions during biofilm development in a cold seep brine pool, *Environ. Microbiol.*, 2015, **17**, 4089–4104.
- 36 A. K. Epstein, B. Pokroy, A. Semnara and J. Aizenberg, Bacterial biofilm shows persistent resistance to liquid wetting and gas penetration, *Proc. Natl. Acad. Sci. U. S. A.*, 2011, **108**, 995–1000.
- 37 S. Kesel, B. von Bronk, C. Falcón García, A. Götz, O. Lielég and M. Opitz, Matrix composition determines the dimensions of *Bacillus subtilis* NCIB 3610 biofilm colonies grown on IB agar, *RSC Adv.*, 2017, **7**, 31886–31898.
- 38 S. Arnaouteli, A. S. Ferreira, M. Schor, R. J. Morris, K. M. Bromley, J. Jo, K. L. Cortez, T. Sukhodub, A. R. Prescott, L. E. P. Dietrich, C. E. MacPhee and N. R. Stanley-Wall, Bifunctionality of a biofilm matrix protein controlled by redox state, *Proc. Natl. Acad. Sci. U. S. A.*, 2017, **114**, E6184–E6191.
- 39 O. Lielég, M. Caldara, R. Baumgärtel and K. Ribbeck, Mechanical robustness of *Pseudomonas aeruginosa* biofilms, *Soft Matter*, 2011, **7**, 3307–3314.
- 40 C. Falcón García, F. Stangl, A. Götz, W. Zhao, S. A. Sieber, M. Opitz and O. Lielég, Topographical alterations render bacterial biofilms susceptible to chemical and mechanical stress, *Biomater. Sci.*, 2019, **7**(1), 220–232.
- 41 C. Watanakunakorn, Mode of action and in vitro activity of vancomycin, *J. Antimicrob. Chemother.*, 1984, **14**, 7–18.
- 42 M. L. Fisher, J. M. Lawrence, I. C. Josty, R. Hopwell, E. E. C. Margerrison and M. E. Cullen, Ciprofloxacin and the fluoroquinolones, *Am. J. Med.*, 1989, **87**, 2–8.
- 43 J. Davies, P. Anderson and B. D. Davis, Inhibition of Protein Synthesis by Spectinomycin, *Science*, 1965, **149**, 5–8.
- 44 L. C. Simões, M. Simões and M. J. Vieira, Biofilm interactions between distinct bacterial genera isolated from drinking water, *Appl. Environ. Microbiol.*, 2007, **73**, 6192–6200.
- 45 O. E. Petrova and K. Sauer, Escaping the biofilm in more than one way: desorption, detachment or dispersion, *Curr. Opin. Microbiol.*, 2016, **30**, 67–78.
- 46 H. Jang, R. Rusconi and R. Stocker, Biofilm disruption by an air bubble reveals heterogeneous age-dependent detachment patterns dictated by initial extracellular matrix distribution, *npj Biofilms and Microbiomes*, 2017, **3**, 0–1.
- 47 G. E. Jackson and M. J. Byrne, Metal Ion Speciation in Blood Plasma: Gallium-67-Citrate and MRJ Contrast Agents, *J. Nucl. Med.*, 1996, 379–386.
- 48 A. Z. Aris, R. C. Y. Kam, A. P. Lim and S. M. Praveena, Concentration of ions in selected bottled water samples sold in Malaysia, *Appl. Water Sci.*, 2013, **3**, 67–75.
- 49 W. L. Jones, M. P. Sutton, L. McKittrick and P. S. Stewart, Chemical and antimicrobial treatments change the viscoelastic properties of bacterial biofilms, *Biofouling*, 2011, **27**, 207–215.
- 50 M. Tallawi, M. Opitz and O. Lielég, Modulation of the mechanical properties of bacterial biofilms in response to environmental challenges, *Biomater. Sci.*, 2017, **5**, 887–900.
- 51 V. Körstgens, H. Flemming, J. Wingender and W. Borchard, Influence of calcium ions on the mechanical properties of a model biofilm of mucoid *Pseudomonas aeruginosa*, *Water Sci. Technol.*, 2001, **43**(6), 49–57.
- 52 E. R. Brindle, D. A. Miller and P. S. Stewart, Hydrodynamic deformation and removal of *Staphylococcus epidermidis* biofilms treated with urea, chlorhexidine, iron chloride, or dispersinB, *Biotechnol. Bioeng.*, 2011, **108**, 2968–2977.
- 53 S. S. Branda, J. E. González-Pastor, S. Ben-Yehuda, R. Losick and R. Kolter, Fruiting body formation by *Bacillus subtilis*, *Proc. Natl. Acad. Sci. U.S.A.*, 2001, **98**, 11621–11626.
- 54 Y. Chai, P. B. Beauregard, H. Vlamakis, R. Losick and R. Kolter, Galactose Metabolism Plays a Crucial Role in Biofilm Formation by *Bacillus subtilis*, *mBio*, 2012, **3**(4), e00184-12.
- 55 M. Albano, J. Hahn and D. Dubnau, Expression of competence genes in *Bacillus subtilis*, *J. Bacteriol.*, 1987, **169**, 3110–3117.

*A.1.1 Supplementary information for: Importance of the biofilm matrix for the erosion stability of Bacillus subtilis NCIB 3610 biofilms*

**Supplementary Material for**

Title: Importance of the biofilm matrix for the erosion stability of *Bacillus subtilis* NCIB 3610 biofilms

M. Klotz<sup>1</sup>, M. Kretschmer<sup>2</sup>, A. Goetz<sup>1</sup>, S. Ezendam<sup>1</sup>, O. Lieleg<sup>2</sup> and M. Opitz<sup>1+</sup>

**Affiliations**

<sup>1</sup> Center for NanoScience, Faculty of Physics, Ludwig-Maximilians-Universität München, Munich, Germany

<sup>2</sup> Munich School of BioEngineering MSB and Department of Mechanical Engineering, Technische Universität München, Garching, Germany

+ corresponding author: [opitz@physik.uni-muenchen.de](mailto:opitz@physik.uni-muenchen.de).



## Supplementary Tables and Figures

### Supplementary Tables

**Table S1**

Linear fit	a+b x			
	a	b		
3610	0 ± 0	1.28 ± 0.03		
Sigmoidal fit	base+{ max/(1+exp((xhalf-x)/rate)) }			
	base	max	xhalf	rate
<i>tasA</i>	0 ± 0	100 ± 0	18.31 ± 0.46	6.02 ± 0.41
<i>bsIA</i>	0 ± 0	100 ± 0	9.13 ± 0.26	2.09 ± 0.25
Exponential fit	y0+A*exp(invTau*x)			
	y0	A	invTau	
<i>epsA-O</i>	100 ± 0	-98.19 ± 2.94	0.15 ± 0.01	

In this table, the fit parameter for Figure 1b are given. The wild-type strain shows a linear erosion kinetic. The mutants *tasA* and *bsIA* show a sigmoidal erosion kinetic. The mutant *epsA-O* shows an exponential erosion kinetic.

**Table S2**

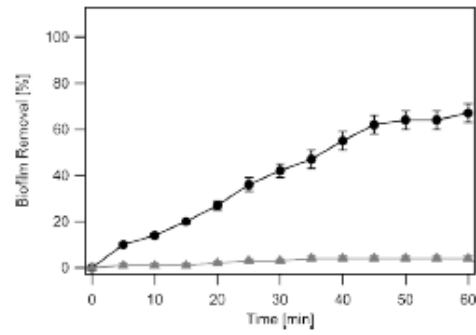
	<i>tasA</i>	<i>bsIA</i>	<i>epsA-O</i>
wt	**	**	**

	wt(Cipro)	<i>tasA</i> (Cipro)	<i>bsIA</i> (Cipro)	<i>epsA-O</i> (Cipro)
strain H <sub>2</sub> O	**	n.s.	*	n.s.

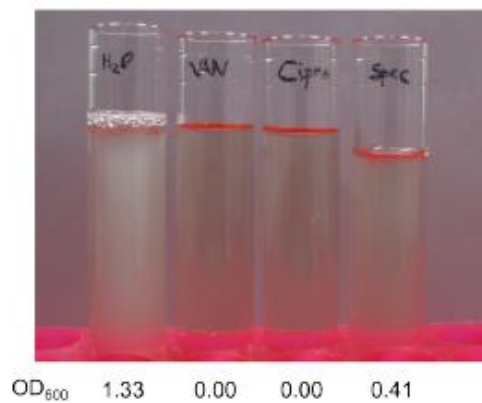
**Significance of biofilm detachment in the absence and presence of the antibiotic ciprofloxacin.** Significance levels from high to low significance: \*\*  $\alpha=0.01$ , \*  $\alpha=0.05$  and not significant: n.s. Top: significance between wild-type and mutants in the

presence of ciprofloxacin. Bottom: significance between each strain in the absence of ciprofloxacin and in the presence of the antibiotic.

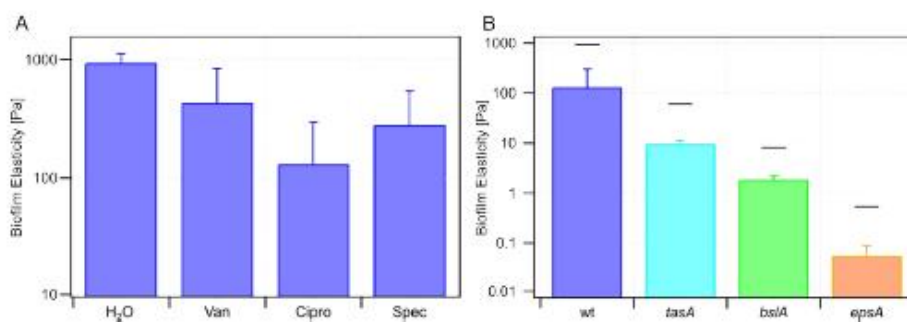
### Supplementary Figures



**Fig S1: BD630 erosion over time.** Biofilm detachment in water (black circles) and Fe<sup>3+</sup> solution (grey triangles).



**Fig S2:** Antibiotics tested in this study kill the bacteria in solution as long as no biofilm is formed. Overnight cultures of NCIB 3610 in LB medium with water or antibiotic agent added in concentrations used for erosion experiments (from left to right: H<sub>2</sub>O, VAN: 0.75µg/ml; Cipro: 64µg/ml; Spec: 0.25µg/ml).



**Fig S3:** Stiffness of biofilms does not change significantly with antibiotic treatment. A) Storage modulus of NCIB 3610 treated with water and 3 antibiotics. B) Storage modulus of NCIB 3610 wildtype and mutants treated with ciprofloxacin. Black lines indicate corresponding treatment values of elasticity measured in water.



## A.2 Chelate chemistry governs ion-specific stiffening of *Bacillus subtilis* B-1 and *Azotobacter vinelandii* biofilms

Biomaterials  
Science



PAPER

View Article Online  
View Journal



Cite this: DOI: 10.1039/c9bm01763a

### Chelate chemistry governs ion-specific stiffening of *Bacillus subtilis* B-1 and *Azotobacter vinelandii* biofilms†

Martin Kretschmer and Oliver Lieleg \*

Unwanted formation of bacterial biofilms can cause problems in both the medical sector and industrial settings. However, removing them from surfaces remains an ongoing challenge since biofilm bacteria efficiently protect themselves from external influences such as mechanical shear forces by embedding themselves into a matrix of extracellular polymeric substances. Here, we discuss microscopic principles, which are responsible for alterations in the viscoelastic properties of biofilms upon contact with metal ions. We suggest that it is a combination of mainly two parameters, that decides if biofilm stiffening occurs or not: the ion size and the detailed configuration of polyanionic macromolecules from the biofilm matrix. Our results provide new insights in the molecular mechanisms that govern the mechanical properties of biofilms. Also, they indicate that hydrogels comprising purified biopolymers can serve as suitable model systems to reproduce certain aspects of biofilm mechanics – provided that the correct biopolymer is chosen.

Received 31st October 2019,  
Accepted 27th January 2020  
DOI: 10.1039/c9bm01763a  
rsc.li/biomaterials-science

## 1. Introduction

Bacteria are able to live in a variety of conditions, even in hostile environments where mechanical or chemical challenges are present. This is made possible by the ability of bacteria to form biofilms, *i.e.*, colonies that settle on solid surfaces.<sup>1–6</sup> Biofilm formation is enabled by the secretion of extracellular polymeric substances which the bacteria use to embed themselves.<sup>7–9</sup> In such biofilms, the bacterial cells are protected from external influences such as shear forces, antibiotics or metal ions that are toxic for individual, planktonic bacteria.<sup>10–16</sup>

In industrial settings, biofilms can cause problems as they can clog pipes or promote corrosion.<sup>17</sup> Unwanted biofilm formation is also an issue in the food industry and in the medical sector;<sup>18,19</sup> when biofilms are not adequately dealt with, pathogenic bacteria can induce health problems.<sup>20,21</sup> Indeed, bacteria embedded into a biofilm matrix are much more difficult to remove or inactivate. To fight biofilms and to enable their removal from surfaces, it is crucial to understand the microscopic principles which dictate the mechanical properties of this biomaterial. Accordingly, there is increasing effort in

recent biofilm research to find treatment strategies to modify the mechanical properties of biofilms.<sup>22–26</sup>

Typically, biofilms exhibit a slimy consistency and can be classified as viscoelastic materials.<sup>27–29</sup> However, the material properties of biofilms can be drastically altered when they are exposed to certain substances such as antibiotics, enzymes, chelators or metal ions.<sup>30–34</sup> If and how the material properties of a bacterial biofilm are affected by a chemical substance seems to depend strongly on the bacterial species generating the biofilm.<sup>35,36</sup> For instance, whereas several bacterial biofilms, *e.g.*, those formed by *Pseudomonas aeruginosa*,<sup>33</sup> *Pseudomonas fluorescens*,<sup>34</sup> *Pseudomonas putida*<sup>34</sup> and *Bacillus subtilis* NCIB 3610<sup>37</sup> and *Bacillus subtilis* B-1<sup>38</sup> have been reported to show an increased stiffness upon exposure to certain metal ions, they do not all react to the same set of metal cations: whereas some divalent metal ions increase the stiffness of *B. subtilis* B-1 biofilms, other ions do not.<sup>38</sup> In contrast, *P. aeruginosa* biofilms seem to be virtually unaffected by divalent ions, but become stiffer when exposed to trivalent ions such as Al<sup>3+</sup> or Fe<sup>3+</sup>.<sup>34</sup>

Biofilms generated by different bacterial species not only differ regarding the bacteria residing in the biofilm matrix, they also comprise distinct sets of bi(o)macro)molecules. This even applies if biofilms are created by variants of the same genus, *i.e.*, if biofilms by *B. subtilis* NCIB 3610 and *B. subtilis* B-1, are compared. The former secretes a range of proteins<sup>39–42</sup> and a polysaccharide whereas the latter mainly comprises  $\gamma$ -polyglutamate ( $\gamma$ -PGA).<sup>43</sup> Of course, bacteria from other

Munich School of Bioengineering and Department of Mechanical Engineering,  
Technical University of Munich, 85748 Garching, Germany.  
E-mail: oliver.lieleg@tum.de; Fax: +49 89 289 10801; Tel: +49 89 289 10952

† Electronic supplementary information (ESI) available. See DOI: 10.1039/c9bm01763a

orders such as Pseudomonadales (e.g., *Pseudomonas aeruginosa* or *Azotobacter vinelandii*) differ fundamentally from *B. subtilis* and secrete, for example, alginate.<sup>44</sup> However, whereas the molecular composition of certain biofilms is (at least to some extent) understood, it remains an open question which component of the biofilm matrix is responsible for interacting with chemical substances such as metal ions.

Here, we study the influence of metal ions on the viscoelastic properties of biofilms generated by two selected soil bacteria, *B. subtilis* B-1 and *A. vinelandii*. We observe that, depending on the biofilm variant studied, different metal cations induce biofilm stiffening. Our results suggest that it is not the ion valency but rather the ion size which dictates whether biofilm stiffening occurs or not. For each biofilm variant, we demonstrate that solutions comprising the main macromolecular component of the respective biofilm matrix, i.e., either  $\gamma$ -PGA or alginate, show a stiffening response to the same subset of metal ions as the multi-component biofilm does. Moreover, we argue that the detailed spatial organization of anionic side groups of the polyanionic biopolymers is important for the successful formation of a chelate complex with the added metal ions.

## 2. Materials and methods

### Bacterial strains and growth conditions

The bacterial strains used in this study are *Bacillus subtilis* B-1<sup>45</sup> and *Azotobacter vinelandii* (DSMZ 13529). *B. subtilis* B-1 is a Gram-positive bacterium that is found in soil and the gastrointestinal tract of humans.<sup>46</sup> *B. subtilis* B-1 was isolated from an oil field and is able to form biofilms on solid surfaces.<sup>45</sup> *A. vinelandii* is a Gram-negative bacterium from the order of Pseudomonadales and is found in soil as well.<sup>47</sup> A liquid culture of *B. subtilis* B-1 was obtained by cultivating small pieces of a frozen glycerol stock in 10 mL LB medium (Luria/Miller; Carl Roth GmbH, Karlsruhe, Germany) at 37 °C and 300 rpm agitation for ~18 h. Then, biofilms were cultivated on LB agar (15 g L<sup>-1</sup> Agar-Agar Kobe I enriched with 25 g L<sup>-1</sup> LB; Carl Roth GmbH, Karlsruhe, Germany) by homogeneously distributing 100  $\mu$ L of this liquid culture across a Petri dish filled with 25 mL LB agar and incubating the agar plates for 24 h at 37 °C and high humidity (>80%).

To create liquid cultures of *A. vinelandii*, two different protocols were followed, and each of those made use of modified Burk's medium as described in Peña *et al.*<sup>48</sup> The difference between growth conditions was as follows: either, cultivation was realized in 50 mL medium at 35 °C and 200 rpm for 72 h (growth conditions #1) or at similar conditions as for *B. subtilis* B-1 (i.e., in 10 mL medium at 37 °C and 300 rpm for 42 h) (growth conditions #2). The latter set of growth parameters was chosen to reduce the bacterial alginate production to determine the effect of alginate on the material properties of the biofilms. *A. vinelandii* biofilms were also cultivated in Petri dishes filled with 25 mL agar; however, here, the agar was enriched with azotobacter medium (composition per liter:

agar, 15 g; glucose, 5 g; mannitol, 5 g; CaCl<sub>2</sub>·2H<sub>2</sub>O, 0.1 g; MgSO<sub>4</sub>·7H<sub>2</sub>O, 0.1 g; Na<sub>2</sub>MoO<sub>4</sub>·2H<sub>2</sub>O, 5 mg; K<sub>2</sub>HPO<sub>4</sub>, 0.9 g; KH<sub>2</sub>PO<sub>4</sub>, 0.1 g; FeSO<sub>4</sub>·7H<sub>2</sub>O, 0.01 g; CaCO<sub>3</sub>, 5 g). For generating *A. vinelandii* biofilms, 200  $\mu$ L of the liquid culture was homogeneously distributed across the agar plates and incubated for 24 h at 37 °C and high humidity (>80%).

### Extraction of $\gamma$ -PGA and alginate

$\gamma$ -PGA was extracted from *B. subtilis* B-1 liquid cultures based on a protocol published in Kaplan.<sup>49</sup> In brief, *B. subtilis* B-1 was cultivated in 10 mL medium E<sup>50</sup> at 30 °C and 100 rpm for 15 h. Subsequently, 5 mL of this liquid culture was added to 250 mL medium E in baffled Erlenmeyer flasks and incubated at 30 °C and 100 rpm until the static phase of bacterial growth was reached (this occurred after ~70 h). Then, the culture broth was mixed with ice in a volumetric ratio of 2 : 1, and the cold liquid was centrifuged at 3500g and 4 °C for 1 h. Afterwards, the supernatant was mixed with ice-cold ethanol in a ratio of 1 : 4 and incubated at -20 °C for 48 h. The resulting precipitate was dried at 37 °C, solved again in 100 mL ddH<sub>2</sub>O and dialyzed against ddH<sub>2</sub>O at 4 °C for 48 h using dialysis membranes with a MWCO of 12–14 kDa. Then, the polymer solution was centrifuged at 100 000g at 4 °C for 4 h, the supernatant was frozen at -20 °C and freeze-dried. The identity of the purified  $\gamma$ -PGA was verified using a combination of chromatography and spectroscopy (Fig. S1†).

Alginate was extracted from *A. vinelandii* liquid cultures according to the protocol outlined in Sabra *et al.*<sup>47</sup> The published procedure was followed step-by-step with one exception: here, the alginate producing culture was cultivated in 50 mL of Burk's medium in 250 mL unbaffled Erlenmeyer flasks at 35 °C and 200 rpm for ~72 h.

### Rheological measurements

To determine their rheological properties, biofilms generated by *B. subtilis* B-1 or *A. vinelandii* were harvested from the agar substrate by manual scraping; afterwards, they were treated with different salt solutions at defined pH or (as controls) with 0.6 M HCl and ddH<sub>2</sub>O, respectively. The unbuffered stock solutions of the different metal salts had concentrations (those are different due to differences in ion solubility) and pH values as follows: CaCl<sub>2</sub> (1 M; pH 2.8), MnCl<sub>2</sub> (1 M; pH 2.7), ZnCl<sub>2</sub> (1 M; pH 5.4), CuCl<sub>2</sub> (1 M; pH 0.9), MgCl<sub>2</sub> (0.4 M; pH 4.1), CrCl<sub>3</sub> (0.4 M; pH 0.1), FeCl<sub>3</sub> (0.4 M; pH 0.2); VCl<sub>2</sub> (0.4 M; pH 2.5). VCl<sub>2</sub> was dissolved in buffer containing a mix of glucose oxidase/catalase to slow down the naturally occurring oxidation process of the ions. Nevertheless, we expect that, at all conditions tested here, there is a mix of V<sup>2+</sup> and V<sup>3+</sup> ions present (which ratio changes over time as the ions oxidize). To assess the influence of pH on the outcome of the experiments, the pH of CaCl<sub>2</sub> and ZnCl<sub>2</sub> solutions was – for a subset of experiments – increased to 6.8 by adding 1 M Tris-buffer to the salt solution; for a similar purpose (as indicated in the caption of respective figure), the pH of the ZnCl<sub>2</sub> solution was reduced to 2.1 by adding of 32% HCl.

For a single measurement, biofilm from up to two agar plates had to be pooled to collect enough material to fill the measuring gap. The salt solutions were mixed with the biofilm such that the final concentration of the metal cations was adjusted to 0.25 M. The biofilms were treated with the salt solutions for 5 h before their rheological characterization was initiated.

These ion concentrations are much higher than what bacteria are exposed to in nature – in natural environments such as soil, the concentrations of metal ions can be up to 570 mg kg<sup>-1</sup> zinc and 750 mg kg<sup>-1</sup> copper.<sup>51</sup> However, the aim of this study is to unravel why certain metal ions induce biofilm stiffening whereas others do not. Because of that, also rather exotic metal ions such as Vanadium were investigated. Moreover, to minimize experimental uncertainties, the high ion concentrations were chosen here. With this strategy, unwanted side effects associated with inhomogeneous distributions of ions within the biofilm sample (which would be more likely for lower ion concentrations) were reduced.

Rheological measurements were performed using a commercial shear rheometer (MCR 302; Anton Paar GmbH, Graz, Austria) equipped with a 25 mm plate-plate geometry. For biofilm samples with a stiffness of  $G' < 10$  kPa, the plate separation was set to 0.3 mm. For biofilm samples with a higher stiffness, the plate separation had to be increased to 0.7 mm. A solvent trap was applied to prevent sample drying during the measurements, which were realized at 21 °C and in strain-controlled mode. To ensure linear material response (which is confirmed by large amplitude oscillation measurements, see Fig. S2 and S3†), small strains corresponding to a torque of  $\sim 0.5$   $\mu$ Nm (this corresponds to a shear stress of  $\sim 0.1$  Pa) were applied. For each condition, at least three samples were tested, which were obtained from one to two biological replicas.

Measurements with  $\gamma$ -PGA and alginate solutions were conducted at a final biopolymer concentration of 1.5% (w/v) each, and the final concentration of added metal cations was always set to 0.25 M. As reference, the biopolymer samples were mixed with ddH<sub>2</sub>O or 0.6 M HCl. The biomacromolecule solution was always placed first onto the bottom plate of the rheometer; then, either a salt solution, ddH<sub>2</sub>O or HCl was added onto this biomacromolecule layer without any additional mixing. This procedure was chosen since, when mixed outside the rheometer, phase separation occurred in several cases, which made a rheological evaluation of those samples impossible because parts of the sample will be lost during the transfer process. In contrast, when the sample is mixed directly on the rheometer, the ions lead to the formation of a skin-like film on the surface of the biopolymer sample and, here, this thin surface layer can be maintained for the measurement. Finally, the measuring head was lowered onto the sample, and after a waiting time of five minutes the measurement was initiated.

The sample volume used was 200  $\mu$ L for all samples, and the plate separation was set to 0.1 mm for all  $\gamma$ -PGA-samples as well as the alginate samples mixed with ddH<sub>2</sub>O and MnCl<sub>2</sub> and to 0.3 mm for all other alginate samples. For the smaller

plate separation, this caused excess sample to be squeezed out from the gap.

#### Data analysis

In every rheological experiment, both the storage and loss modulus were determined over a frequency range of 0.1 Hz to 10 Hz with 21 measuring points. Exemplary frequency spectra for both, biofilms and biopolymer solutions/gels (with and without exposure to a selected metal ion) are shown in the ESI (Fig. S4–S7†). Since, in all cases described in this paper, the moduli obtained for a given sample were only weakly dependent on frequency, they were averaged over the complete measured frequency spectrum and are referred to as plateau moduli ( $G_0$ ) in the manuscript. Obvious outliers resulting from measuring artefacts were excluded from calculating these mean values. Then, averaged values obtained from different repetitions of a sample were averaged again to obtain the bar plots shown in the manuscript.

Subsequent to the first frequency sweep, a strain ramp was executed for all biofilm samples. As a consequence of this strain ramp, the material was exposed to a shear strain as large as 1000%, which is sufficiently high to induce material failure/ yielding.<sup>34</sup> Afterwards, the sample was allowed to rest for 15 seconds; then, a second frequency sweep in the range of 0.5 Hz to 10 Hz was conducted. To determine the degree of self-healing, the average storage moduli of the first and second frequency sweep were determined in the frequency range of 0.5 Hz to 5 Hz, and the ratio of these two average values was calculated.

Error bars shown in Fig. 1, 3 and 4 denote the standard deviation as calculated from the mean values of at least three different samples.

### 3. Results and discussion

When exposed to certain metal ions, the viscoelastic properties of *B. subtilis* B-1 biofilms are significantly altered; previous results showed that a mechanical fortification of this biofilm (i.e., an increase of both viscoelastic moduli) can be achieved with Fe<sup>3+</sup> ions but not with Fe<sup>2+</sup>.<sup>38</sup> Whereas this finding seems to suggest that a certain ion valency might be required for obtaining such an effect, experiments conducted with other trivalent and divalent ions challenge this hypothesis: the addition of Cu<sup>2+</sup>, Zn<sup>2+</sup> and Cr<sup>3+</sup> leads to an increase in biofilm stiffness whereas adding other metal cations such as Ca<sup>2+</sup> and Mn<sup>2+</sup> does not (Fig. 1A). This shows that, at least among divalent ions, other parameters need to be considered.

One possible explanation for this somewhat puzzling result could be that the salt solutions containing the metal ions differ in terms of pH, and that those differences in pH are responsible for the different experimental outcomes. Indeed, at a concentration of 1 M of the respective metal cation, unbuffered aqueous solutions of CaCl<sub>2</sub>, MnCl<sub>2</sub>, CuCl<sub>2</sub> and CrCl<sub>3</sub> exhibit a strongly acidic pH below 3 (see Methods for details), whereas solutions containing ZnCl<sub>2</sub> are only mildly

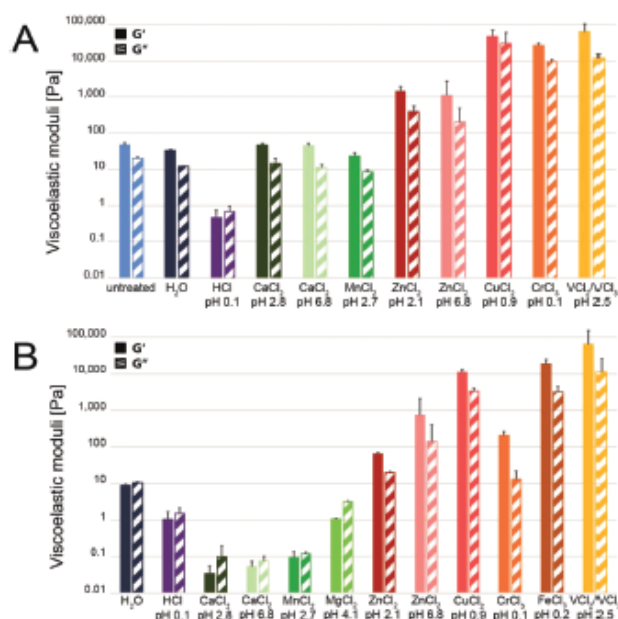


Fig. 1 Viscoelastic moduli of *B. subtilis* B-1 biofilms (A) and  $\gamma$ -PGA solutions (B) after exposure to different aqueous solutions at different pH levels as indicated (see Methods). Full bars denote the storage modulus,  $G'$ , and striped bars the loss modulus,  $G''$ . The error bars represent the standard deviation as obtained from at least three independent samples.

acidic (pH  $\sim$  5.4). However, as depicted in Fig. 1A, altering the pH of the salt solutions (*i.e.*, lowering the pH of the  $\text{ZnCl}_2$  solution to 2.1 or increasing the pH of either the  $\text{CaCl}_2$  or  $\text{ZnCl}_2$  solution to 6.8) does not qualitatively change the experimental outcome – only the degree of biofilm fortification is affected. Moreover, in additional control experiments, where the biofilm was exposed to a 0.6 M HCl solution (pH = 0.1) devoid of metal cations, the stiffness of the *B. subtilis* B-1 biofilm was even reduced. Together, this shows that the increase in biofilm stiffness observed after exposure to selected metal cations is due to ion specific effects.

There are at least three possible variants of ion-specific interactions, which could be considered to contribute to the observed biofilm stiffening: counter ion condensation,<sup>52</sup> Hofmeister effects,<sup>53</sup> or the formation of a chelate complex.<sup>54</sup> If counter ion condensation occurs, (metal) ions concentrate on polyanionic polymers and thereby alter the charge density on the polymer chain. This leads to conformational changes of the polymer, affects its interactions with other polymers and thus might alter the viscoelastic properties of a polymer network (such as a bacterial biofilm). For this effect to be relevant, Manning's criterion needs to be fulfilled, *i.e.*, the ratio of the Bjerrum length and the line charge of the polyanionic polymer should be well above 1. However, for the main polyanionic macromolecule of the matrix of *B. subtilis* B-1 biofilms,  $\gamma$ -PGA,<sup>43,55</sup> we calculate a value of  $\sim$ 0.9. Thus, Manning con-

denation is not likely to explain the observed biofilm stiffening.

The next possible scenario we consider are Hofmeister effects. According to Hofmeister theory, ions can be either kosmotropic or chaotropic: whereas kosmotropic ions induce protein precipitation ('salting-out') by enhancing hydrophobic interactions, chaotropic ions cause protein denaturation ('salting-in') by weakening hydrophobic interactions. Even though the main component of the *B. subtilis* B-1 biofilm matrix,  $\gamma$ -PGA, does not carry hydrophobic motifs, other biofilm components could be affected by alterations in hydrophobic interactions, and this might explain the observed changes in biofilm viscoelasticity. Hyde *et al.*<sup>56</sup> showed that both,  $\text{Mn}^{2+}$  and  $\text{Zn}^{2+}$ , have a kosmotropic effect on proteins, whereas  $\text{Cu}^{2+}$  has a chaotropic effect. However, we find that  $\text{Zn}^{2+}$  and  $\text{Cu}^{2+}$  increase the stiffness of *B. subtilis* B-1 biofilm, whereas  $\text{Mn}^{2+}$  does not. This disagreement already indicates that Hofmeister effects cannot rationalize the ion-specific increase in biofilm stiffness observed here.

Instead, it was suggested before, that di- and trivalent metal ions can induce ionic cross-linking in biofilms, and that this cross-linking is responsible for biofilm stiffening. Of course, for metal cations to act as cross-linking agents, they require a polyanionic target polymer, and the polyanionic macromolecule  $\gamma$ -PGA has already been described to be able to form chelate complexes with positively charged ions.<sup>57,58</sup> Thus, it is



reasonable to assume, that solutions of purified  $\gamma$ -PGA react to the same subset of metal cations as *B. subtilis* B-1 biofilms.

Of course, different from biofilms (which are viscoelastic solids, see Fig. S4†), 1.5% (w/v) solutions of  $\gamma$ -PGA are viscoelastic fluids (Fig. S5†) and thus are slightly dominated by their viscous properties (Fig. 1B). On a microscopic level, this can be explained by the absence of cross-links in a pure  $\gamma$ -PGA solution – entanglements alone are not sufficient for those flexible polymer chains to establish a pronounced elastic character. However, when  $\gamma$ -PGA polymers become cross-linked, for example by metal ions, the viscoelastic properties change and the storage modulus becomes dominant, *i.e.* gelation is induced. This is, *e.g.*, observed when  $\gamma$ -PGA is mixed with  $\text{ZnCl}_2$ , both at acidic and neutral pH. The latter result is important since experiments described in the literature indicated that strongly acidic conditions may induce gelation of  $\gamma$ -PGA solutions even in the absence of metal ions. However, at the conditions tested here, acidic gelation seems not to be relevant: when a  $\gamma$ -PGA solution is titrated to strongly acidic levels (by mixing with an HCl solution), both viscoelastic moduli are decreased below levels of 1 Pa. Moreover, exposure of  $\gamma$ -PGA solutions to  $\text{Cu}^{2+}$  or  $\text{Cr}^{3+}$  ions induces gelation (Fig. 1B) whereas the addition of  $\text{Ca}^{2+}$  or  $\text{Mg}^{2+}$  does not. These results correlate very well with the behavior we described for *B. subtilis* B-1 biofilms above: either a metal ion shows an effect on the viscoelastic properties of both materials or not at all. Together, this data underscores our assumption, that the biomacromolecule  $\gamma$ -PGA is the key player in governing the ion-specific stiffening behavior of B-1 biofilms.

Ionic cross-linking of polyanionic macromolecules typically occurs *via* the formation of a complex; however, whether or not such a chelate effect occurs depends on the properties of the macromolecule as well as on the properties of the cation, *i.e.* its valency, coordination number and size. Since the same subset of metal ions entails cross-linking in both systems, *i.e.*, multi-component biofilms and solutions of purified  $\gamma$ -PGA, this indicates that differences in the cation properties are responsible for the observed differences in biofilm stiffening.

A first obvious difference between the tested ions is their valency, and indeed  $\text{Fe}^{3+}$  and  $\text{Cr}^{3+}$  trigger biofilm stiffening and  $\gamma$ -PGA gelation whereas some divalent ions do not. However, as we already discussed above, considering the ion valency alone is not sufficient to understand biofilm stiffening since also some divalent ions can entail this effect.

The next parameter we consider is the coordination number, which different ions achieve in a chelate complex. According to Huheey *et al.*,<sup>59</sup> all ions tested here can form complexes with a coordination number of six, and many of the tested ions (with the exception of  $\text{Cr}^{3+}$ ,  $\text{V}^{2+}/\text{V}^{3+}$ , and  $\text{Ca}^{2+}$ ) can also assume a coordination of four (Fig. 2A). However, since  $\text{Cr}^{3+}$  and  $\text{V}^{2+}/\text{V}^{3+}$  induce gelation of  $\gamma$ -PGA but  $\text{Ca}^{2+}$  does not, no clear picture emerges from analyzing this parameter.

A third property, in which the cations differ, is their size. According to the same literature source we used for comparing the coordination numbers,<sup>59</sup>  $\text{Ca}^{2+}$  and  $\text{Mn}^{2+}$  are relatively large ions whereas the other cations, *i.e.*,  $\text{Zn}^{2+}$ ,  $\text{Cu}^{2+}$ ,  $\text{V}^{2+}/\text{V}^{3+}$  and  $\text{Cr}^{3+}$ ,

are reported to be comparably small (Fig. 2B). This seems to suggest that smaller ions are more likely than larger ones to induce the ion-specific biofilm stiffening and  $\gamma$ -PGA gelation we report here. To visualize this relation, we also plotted the individual results obtained for the storage moduli of the biofilm samples as a function of the radius of the added ions (see Fig. S8†).

This hypothesis is further supported by experiments conducted with  $\text{VCl}_2$ . In aqueous solutions, vanadium can spontaneously oxidize from  $\text{V}^{2+}$  to  $\text{V}^{3+}$  and even further to  $\text{V}^{4+}$ . Here, we tried to counteract this oxidation process by adding a glucose oxidase/catalase mix to the  $\text{VCl}_2$  stock solution. Still, a change in color of the  $\text{VCl}_2$  solution showed that the vanadium ions nevertheless slowly oxidized over the course of several hours (Fig. S9†). Interestingly, for this particular metal ion species, we also detected a biofilm stiffening response that became stronger over time: when a freshly prepared solution of  $\text{VCl}_2$  (*i.e.*, within the first hour after the solution has been prepared) was incubated with either *B. subtilis* B-1 biofilm or a  $\gamma$ -PGA solution for 5 h (as for the other metal ions tested). Here, we measured a well-defined stiffness increase of either sample to a final shear modulus of  $\sim 100$  kPa (Fig. 1A and B). Similarly high values were obtained if the incubation time of either sample was shortened to 5 min but when, at the same time,  $\text{VCl}_2$  solutions were used which were allowed to oxidize for at least 3 h (Fig. S10A†). Consistently, a short incubation of either, biofilm or  $\gamma$ -PGA solutions, with  $\text{VCl}_2$  solutions of lower age lead to a weaker (but also reproducible) increase in sample stiffness (Fig. S10A and S10B†). We interpret those findings as follows: when the vanadium ion oxidizes from  $\text{V}^{2+}$  to  $\text{V}^{3+}$  (or even to  $\text{V}^{4+}$ ), the ion radius decreases, and the propensity to create a chelate complex with  $\gamma$ -PGA is increased. This, in turn, leads to samples with more cross-links and thus with a higher shear elasticity.

Previous results obtained with *B. subtilis* B-1 biofilms exposed to  $\text{Mg}^{2+}$ ,  $\text{Fe}^{2+}$ ,  $\text{Fe}^{3+}$ , or  $\text{Al}^{3+}$  seem to agree with this picture reasonably well: whereas, there, the smaller ions  $\text{Fe}^{3+}$  and  $\text{Al}^{3+}$  induced biofilm stiffening, the somewhat larger cations  $\text{Fe}^{2+}$  and  $\text{Mg}^{2+}$  did not. A similar comparative analysis of the different ion radii using<sup>60</sup> as a reference returns a similar picture. However, due to the relatively large differences in the reported literature values for the different ion sizes, the agreement with our results remains imperfect. Thus, we further challenge this picture by exposing  $\gamma$ -PGA solutions to  $\text{Mg}^{2+}$  and  $\text{Fe}^{3+}$  as well, and find that – as expected – the large  $\text{Mg}^{2+}$  ion does not induce gelation whereas the smaller  $\text{Fe}^{3+}$  does (Fig. 1B).

Having analyzed the detailed requirements that lead to ion-specific stiffening of *B. subtilis* B-1 biofilms, we next ask if another property of those bacterial biofilms, *i.e.*, their ability to recover their initial mechanical strength after exposure to large shear forces, is affected by the metal cations.<sup>38</sup> Previous results had indicated that this so-called self-healing behavior of biofilms is very robust: the degree of mechanical recovery remained close to 100% after the biofilm is exposed to selected metal ions.<sup>38</sup> Here, we can confirm this result with the broad

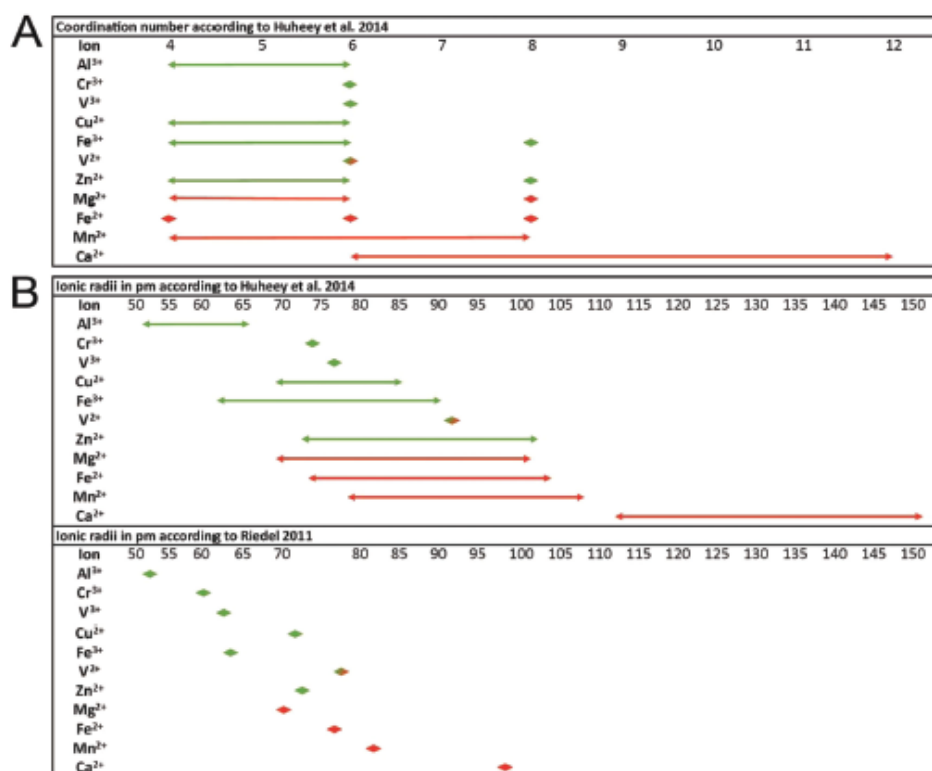


Fig. 2 Overview of the coordination numbers of certain metal cations (A) that can be achieved when a chelate complex is formed<sup>49</sup> and overview of the ionic radii in pm of the metal cations (B) according to Huheey et al.<sup>50</sup> and Riedel.<sup>50</sup> Green signs indicate a stiffening effect of the ions on the viscoelastic properties of *B. subtilis* B-1 biofilm and red signs indicate no such effect. Symbols related to V<sup>2+</sup> are shown in dual color as, here, it is not clear to what extent V<sup>2+</sup> and/or V<sup>5+</sup> ions are present in the experiment.

range of metal cations tested here (Fig. 3). Only biofilm samples exposed to Zn<sup>2+</sup> or Cr<sup>3+</sup> exhibit somewhat reduced self-healing capabilities with degrees of recovery below 80%; for all other conditions, the corresponding value is well above 80%.

The data discussed so far indicates that the polyanionic macromolecule  $\gamma$ -PGA, the key component of *B. subtilis* B-1 biofilms, is responsible for the ion-specific stiffening of this biological material. However, different bacteria make use of

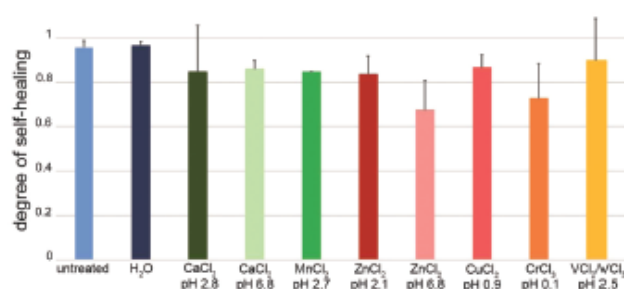


Fig. 3 Degree of self-healing for *B. subtilis* B-1 biofilms treated with different aqueous solutions containing selected metal cations. The degree of self-healing represents the ratio of the storage modulus obtained before and after the application of a shear ramp. For comparison, the self-healing abilities of untreated biofilms are shown. Error bars denote the standard deviation as obtained from at least three independent samples.

distinct biopolymers to construct their biofilm matrix. For instance, the soil bacterium *Azotobacter vinelandii*, which belongs to the order of Pseudomonadales and also forms biofilms on solid substrates, does not produce  $\gamma$ -PGA; however, when cultivated at the correct conditions (e.g., growth conditions #1, see Methods), *A. vinelandii* secretes alginate.<sup>44</sup> Similar to  $\gamma$ -PGA, also alginate is a polyanionic macromolecule, and it is well established, that alginates can be cross-linked with positively charged ions.<sup>61</sup> However, different from the results we obtained with *B. subtilis* B-1 biofilms, the stiffness of those alginate producing *A. vinelandii* biofilms is not only increased after exposure to  $\text{Cu}^{2+}$ , but also after exposure to  $\text{Ca}^{2+}$  and  $\text{Mn}^{2+}$  (Fig. 4A). Importantly, this effect is absent when growth conditions are used that do not promote alginate production (growth conditions #2, Fig. 4A).

In agreement with the picture discussed so far, solutions comprising alginate purified from *A. vinelandii* liquid cultures show a qualitatively similar behavior as the multi-component *A. vinelandii* biofilms obtained at alginate-producing growth conditions, i.e., they show an increased stiffness upon contact with either  $\text{Ca}^{2+}$ ,  $\text{Mn}^{2+}$ , or  $\text{Cu}^{2+}$ : in each case, gelation of the alginate solutions is induced, and their elastic modulus is increased by at least one order of magnitude compared to the treatment with water alone. Importantly, alginate solutions are

also turned into viscoelastic gels when they are exposed to strongly acidic conditions (Fig. 4B). Thus, we conducted control experiments where the stock solutions of  $\text{CaCl}_2$  and  $\text{MnCl}_2$  were prepared at a pH close to neutral conditions. Here, in the absence of acidic conditions, we still detected the formation of an alginate gel. Together, this demonstrates that metal ion induced alterations in the viscoelastic properties of alginate solutions agree well with similar alterations in the viscoelastic properties of *A. vinelandii* biofilms. This indicates that, also for *A. vinelandii* biofilms, the polyanionic biomacromolecule is the key component of the biofilm matrix that is responsible for the stiffening response of the multi-component biomaterial.

Of course, alginates are not only produced by *A. vinelandii* but also by various other bacterial species from the order Pseudomonadales and by certain algae. Depending on the biological source, however, the conformation of the alginate chains can be different (Fig. 5A–C): whereas alginate from algae such as *Laminaria hyperborea* contains so-called G-blocks,<sup>62</sup> alginate from most alginate-secreting bacteria, such as *Pseudomonas aeruginosa* or *Pseudomonas putida*, possesses either only M-blocks or exhibits an alternating chain sequence.<sup>63</sup> In fact, the conformation of alginate plays a major role whether or not ionic cross-linking can occur when these biomacromolecules are exposed to metal cations.<sup>63</sup>

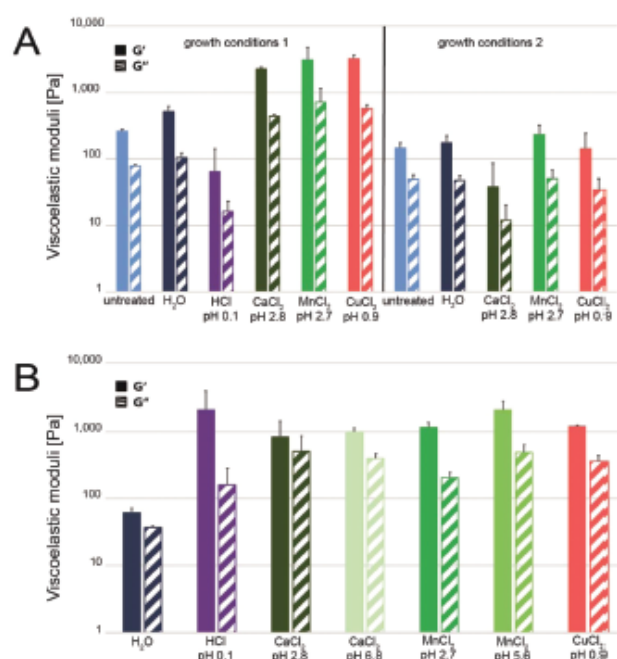


Fig. 4 Viscoelastic moduli of *A. vinelandii* biofilms (A) cultivated at two different growth conditions and purified alginate solutions (B). In both cases, samples are shown after exposure to different aqueous solutions at different pH levels as indicated (see Methods). Full bars denote the storage modulus,  $G'$ , and striped bars the loss modulus,  $G''$ . The error bars represent the standard deviation as obtained from three independent samples.

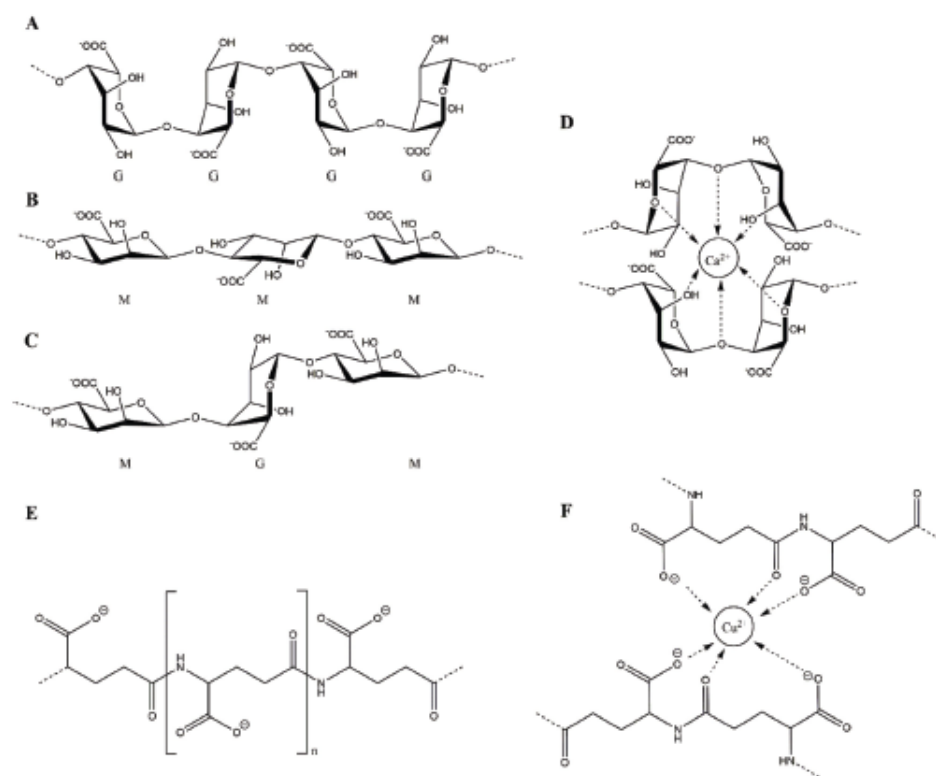


Fig. 5 Possible structural conformations of different alginate- and  $\gamma$ -PGA chains. An alginate chain can be composed of  $\alpha$ -L-guluronate residues forming G-blocks (A), of  $\beta$ -D-mannuronate residues forming M-blocks (B) or they can comprise an alternating mixture of both (C). An exemplary chelate complex between a calcium cation and two alginate-chains (G-block type) is depicted in (D). In this particular example, the coordination number of the calcium ion is six. The structure of a  $\gamma$ -PGA chain is shown in (E), and a possible configuration of a chelate complex between a copper cation and two  $\gamma$ -PGA chains is depicted in (F). In this example, the coordination number of the copper ion is six.

In this context, it is important to realize that the alginate from *A. vinelandii* comprises G-blocks with a density between 5% and 85%.<sup>63</sup> Thus, the results we obtain here with in-lab purified alginate solutions agree very well with data published on commercially purified alginate solutions obtained from algae<sup>61</sup> (which also contain G-blocks). There is, however, an important difference to the behavior of *Pseudomonas aeruginosa* biofilms: those biofilms (which contain M-block and MG-block alginate) show increased stiffness after exposure to trivalent ions such as  $\text{Fe}^{3+}$  or  $\text{Al}^{3+}$ , but not when exposed to divalent ions such as  $\text{Ca}^{2+}$  or  $\text{Cu}^{2+}$ .<sup>34</sup>

When alginate is present in a G-block configuration, it can achieve a coordination number of six or even higher (Fig. 5D). This is, however, not possible for alginate chains with an M-block configuration: in this particular configuration, owing to the very straight chain structure of the polypeptide, the anionic carboxyl groups face alternating sides of the polymer chain (Fig. 5E). Thus, only a few anionic side groups can interact with a given metal ion, so that the achievable coordi-

nation number might be too low to form a stable chelate complex.

According to Rehm,<sup>61</sup> also the mixed configuration (MG-blocks) of alginate should be able to form chelate complexes as MG-blocks are thought to be able to achieve a relatively high coordination number with a central cation. However, results from other research groups<sup>63</sup> challenge this idea – at least for  $\text{Ca}^{2+}$  ions. The current set of data suggests that, for this MG-configuration, only some metal ions are able to form a chelate complex – as it was also observed here for  $\gamma$ -PGA. Indeed, in Lieleg *et al.*,<sup>34</sup> it was observed, that only small trivalent ions such as  $\text{Al}^{3+}$  and  $\text{Fe}^{3+}$  lead to an increased stiffness of *P. aeruginosa* biofilms – and those biofilms contain alginates with M- and MG-blocks.<sup>2</sup>

From a molecular point of view, the following explanation might help rationalizing those observations: different from the M-block type alginate, in  $\gamma$ -PGA, the monomer units of the polymer can rotate relative to each other. Thus,  $\gamma$ -PGA might be able to achieve a coordination number, which is sufficiently

high to form a chelate complex with ions including smaller ones (Fig. 5F).

Together with the data we discussed so far, the following picture emerges: whether or not a bacterial biofilm shows increased stiffness after exposure to metal cations depends – to a large extent – on the ability of the biofilm components to form a complex with those cations. A biofilm, whose main macromolecular component is G-block-type alginate (e.g. *A. vinelandii* biofilm), can even form complexes with large cations such as  $\text{Ca}^{2+}$ . For biofilms making use of M-block-type alginate as a key component (e.g., *Pseudomonas aeruginosa* biofilm), this is not possible. Similarly, also for  $\gamma$ -PGA-based biofilms (e.g., *Bacillus subtilis* B-1 biofilm), the range of cations that induce an increase in biofilm stiffness is limited.

A possible benefit biofilms might experience from their ability to form chelate complexes is that the absorption of metal ions into the biofilm matrix and their stable arrangement into a chelate complex permanently removes these cations from the surrounding fluid – which is important for the biofilm bacteria when the free metal ions are toxic.<sup>38</sup> In addition, biofilms, which have absorbed metal cations, exhibit increased erosion resistance.<sup>37,38</sup> This is especially beneficial for biofilms grown on surfaces where they experience continuous shear forces, e.g. by flowing water. Of course, when biofilms develop in their natural environment, e.g., in pipes, soil or on the surface of medical devices or industrial equipment, they might already be exposed to metal ions during biofilm growth. In such a scenario, additional effects might come into play. For instance, we recently found that, when *B. subtilis* 3610 bacteria are grown on agar enriched with low concentrations (i.e., 0.5 mM to 1.5 mM) of either  $\text{CuSO}_4$  or  $\text{ZnCl}_2$ , the production of extracellular matrix components is reduced.<sup>64</sup> This effect seems not to be specific for a certain matrix component but rather appears to be a generic one affecting all matrix constituents across the board. How such a reduction of the extracellular matrix components affects the viscoelastic properties of the biofilm is, at this point of research, unclear, and needs to be addressed in future experiments.

## 4. Conclusions

Here, we demonstrated that the material behavior of biofilms generated by *B. subtilis* B-1 and *A. vinelandii* depends crucially on the biomacromolecule that primarily builds the biofilm matrix. These key biomacromolecules are  $\gamma$ -PGA in the case of *B. subtilis* B-1 and alginate in the case of *A. vinelandii*. For both biofilm types, the formation of a chelate complex seems to be responsible for the increased biofilm stiffness we observe upon exposure to certain metal cations.

Our results show that both, the properties of the biomacromolecule as well as those of the metal cations, determine whether a chelate complex can be formed. On the side of the biomacromolecule, the structure of the polymer chain and thus the orientation of the negatively charged side chains is crucial. On the side of the cross-linking metal cations, it

appears that it is mainly the ion size rather than other ion properties, which decides if complex formation is possible.

Of course, for many bacterial biofilms their molecular composition is only partially known – if at all. Thus, it remains very difficult to predict how such incompletely characterized biofilms will react when exposed to environments containing metal cations. However, a profound understanding of the mechanical behavior of biofilms and how this is regulated on a microscopic level is essential to efficiently combat unwanted biofilms or to prevent their formation in the first place.

## Author contributions

M. K. and O. L. planned the experiments, which were conducted and analyzed by M. K. The manuscript was written by M. K. and O. L.

## Conflicts of interest

There are no conflicts of interest to declare.

## Acknowledgements

We thank Marvin Ertelt for helpful discussions regarding chelate chemistry. This project was funded by the Deutsche Forschungsgemeinschaft (DFG, German Research Foundation) – SFB-863 – Project ID 111166240.

## References

- 1 G. O'Toole, H. B. Kaplan and R. Kolter, Biofilm Formation as Microbial Development, *Annu. Rev. Microbiol.*, 2000, **54**, 49–79.
- 2 H. Vlamakis, *et al.*, Sticking together: building a biofilm the *Bacillus subtilis* way, *Nat. Rev. Microbiol.*, 2013, **121**, 1–58.
- 3 H.-C. Flemming, *et al.*, Biofilms: an emergent form of bacterial life, *Nat. Rev. Microbiol.*, 2016, **14**(9), 563–575.
- 4 N. M. Oliveira, *et al.*, Biofilm Formation As a Response to Ecological Competition, *PLoS Biol.*, 2015, **13**(7), 1–23.
- 5 G. A. O'Toole and G. C. L. Wong, Sensational biofilms: surface sensing in bacteria, *Curr. Opin. Microbiol.*, 2016, **30**, 139–146.
- 6 L. S. Cairns, L. Hopley and N. R. Stanley-Wall, Biofilm formation by *Bacillus subtilis*: new insights into regulatory strategies and assembly mechanisms, *Mol. Microbiol.*, 2014, **93**(4), 587–598.
- 7 J. W. Costerton, P. S. Stewart and E. P. Greenberg, Bacterial Biofilms: A Common Cause of Persistent Infections, *Science*, 1999, **17**, 1318–1322.
- 8 R. D. Monds and G. A. O'Toole, The developmental model of microbial biofilms: ten years of a paradigm up for review, *Trends Microbiol.*, 2009, **17**, 73–87.

- 9 E. S. Gloag, *et al.*, Viscoelastic properties of *Pseudomonas aeruginosa* variant biofilms, *Sci. Rep.*, 2018, **8**, 1–11.
- 10 H. Cao, *et al.*, Revealing region-specific biofilm viscoelastic properties by means of a micro-rheological approach, *npj Biofilms Microbiomes*, 2016, **5**, 1–7.
- 11 J. Yan, *et al.*, Bacterial Biofilm Material Properties Enable Removal and Transfer by Capillary Peeling, *Adv. Mater.*, 2018, **30**, 1–10.
- 12 S. C. Booth, *et al.*, Effect of aluminium and copper on biofilm development of *Pseudomonas pseudoalcaligenes* KF707 and *P. fluorescens* as a function of different media compositions, *Metallomics*, 2013, **5**, 723–735.
- 13 H.-C. Flemming and J. Wingender, The biofilm matrix, *Nat. Rev. Microbiol.*, 2010, **8**, 623–633.
- 14 A. Bridier, *et al.*, Resistance of bacterial biofilms to disinfectants: a review, *Biofouling*, 2011, **27**, 1017–1032.
- 15 S. Aggarwal and R. M. Hozalski, Effect of Strain Rate on the Mechanical Properties of *Staphylococcus epidermidis* Biofilms, *Langmuir*, 2012, **28**, 2812–2816.
- 16 A. W. Cense, *et al.*, Mechanical properties and failure of *Streptococcus mutans* biofilms, studied using a microindentation device, *J. Microbiol. Methods*, 2006, **67**, 463–472.
- 17 R. M. Donlan, Biofilms: Microbial Life on Surfaces, *Emerging Infect. Dis.*, 2002, **8**, 881–890.
- 18 B. Carpentier and O. Cerf, Biofilms and their consequences, with particular reference to hygiene in food industry, *J. Appl. Bacteriol.*, 1993, **75**, 499–511.
- 19 M. Wilson, Bacterial biofilms and human disease, *Sci. Prog.*, 2001, **84**(3), 235–254.
- 20 T. Bjarnsholt, The Role of Bacterial Biofilms in Chronic Infections, *APMIS*, 2013, **121**, 1–58.
- 21 S. R. Shah, *et al.*, Evolving strategies for preventing biofilm on implantable materials, *Mater. Today*, 2013, **16**, 177–182.
- 22 E. N. Hayta and O. Lieleg, Biopolymer-enriched *B. subtilis* NCIB 3610 biofilms exhibit increased erosion resistance, *Biomater. Sci.*, 2019, **7**, 4675–4686.
- 23 M. Böl, *et al.*, Recent advances in mechanical characterization of biofilm and their significance for material modeling, *Crit. Rev. Biotechnol.*, 2013, **33**, 145–171.
- 24 D. N. Hohné, J. G. Younger and M. J. Solomon, Flexible Microfluidic Device for Mechanical Property Characterization of Soft Viscoelastic Solids Such as Bacterial Biofilms, *Langmuir*, 2009, **25**, 7743–7751.
- 25 H. Koo, *et al.*, Targeting microbial biofilms: current and prospective therapeutic strategies, *Nat. Rev. Microbiol.*, 2017, **15**(12), 740–755.
- 26 J. Masák, *et al.*, *Pseudomonas* biofilms: possibilities of their control, *FEMS Microbiol. Ecol.*, 2014, **89**(1), 1–14.
- 27 V. D. Gordon, *et al.*, Biofilms and mechanics: a review of experimental techniques and findings, *Appl. Phys.*, 2017, **50**, 1–12.
- 28 S. Kesel, *et al.*, Direct Comparison of Physical Properties of *Bacillus subtilis* NCIB 3610 and B-1 Biofilms, *Appl. Environ. Microbiol.*, 2016, **82**(8), 2424–2432.
- 29 B. Kundukad, *et al.*, Mechanical properties of the superficial biofilm layer determine the architecture of biofilms, *Soft Matter*, 2016, **12**, 5718–5726.
- 30 X. Chen and P. S. Stewart, Biofilm removal caused by chemical treatments, *Water Res.*, 2000, **9**, 4229–4233.
- 31 X. Chen and P. S. Stewart, Role of electrostatic interactions in cohesion of bacterial biofilms, *Appl. Microbiol. Biotechnol.*, 2002, **59**, 718–720.
- 32 M. Wloka, *et al.*, Structure and rheological behaviour of the extracellular polymeric substance network of mucoid *Pseudomonas aeruginosa* biofilms, *Biofilms*, 2005, **2**, 275–283.
- 33 W. L. Jones, *et al.*, Chemical and antimicrobial treatments change the viscoelastic properties of bacterial biofilms, *Biofouling*, 2011, **27**, 207–215.
- 34 O. Lieleg, *et al.*, Mechanical robustness of *Pseudomonas aeruginosa* biofilms, *Soft Matter*, 2011, **7**(7), 3307–3314.
- 35 M. Tallawi, M. Opitz and O. Lieleg, Modulation of the mechanical properties of bacterial biofilms in response to environmental challenges, *Biomater. Sci.*, 2017, **5**, 887–900.
- 36 B. W. Peterson, *et al.*, Viscoelasticity of biofilms and their recalcitrance to mechanical and chemical challenges, *FEMS Microbiol. Rev.*, 2015, **39**(2), 234–245.
- 37 M. Klotz, *et al.*, Importance of the biofilm matrix for the erosion stability of *Bacillus subtilis* NCIB 3610 biofilms, *Metallomics*, 2019, **9**, 11521–11529.
- 38 S. Grumbein, M. Opitz and O. Lieleg, Selected metal ions protect *Bacillus subtilis* biofilms from erosion, *Metallomics*, 2014, **6**(8), 1441–1450.
- 39 S. S. Branda, *et al.*, Fruiting body formation by *Bacillus subtilis*, *Proc. Natl. Acad. Sci. U. S. A.*, 2001, **98**, 11621–11626.
- 40 H. Vlamakis, *et al.*, Control of cell fate by the formation of an architecturally complex bacterial community, *Genes Dev.*, 2007, **22**, 945–953.
- 41 K. Kobayashi and M. Iwano, BslA(YuaB) forms a hydrophobic layer on the surface of *Bacillus subtilis* biofilms, *Mol. Microbiol.*, 2012, **85**, 51–66.
- 42 Y. Chai, *et al.*, Galactose Metabolism Plays a Crucial Role in Biofilm Formation by *Bacillus subtilis*, *mBio*, 2012, **3**(4), e00184-12.
- 43 M. Morikawa, Beneficial Biofilm Formation by Industrial Bacteria *Bacillus subtilis* and Related Species, *J. Biosci. Bioeng.*, 2006, **101**(1), 1–8.
- 44 G. Skjåk-Bræk, G. Hans and B. Larsen, Monomer sequence and acetylation pattern in some bacterial alginates, *Carbohydr. Res.*, 1986, **154**, 239–250.
- 45 M. Morikawa, M. Ito and T. Imanaka, Isolation of a new surfactin producer *Bacillus pumilus* A-1, and cloning and nucleotide sequence of the regulator gene, *psf-1*, *J. Ferment. Bioeng.*, 1992, **74**(5), 255–261.
- 46 H. A. Hong, *et al.*, *Bacillus subtilis* isolated from the human gastrointestinal tract, *Res. Microbiol.*, 2009, **160**, 134–143.
- 47 W. Sabra, *et al.*, Effect of oxygen on formation and structure of *Azotobacter vinelandii* alginate and its role in protecting nitrogenase, *Appl. Environ. Microbiol.*, 2000, **66**(9), 4037–4044.

- 48 C. Peña, N. Campos and E. Galindo, Changes in alginate molecular mass distributions, broth viscosity and morphology of *Azotobacter vinelandii* cultured in shake flasks, *Appl. Microbiol. Biotechnol.*, 1997, **48**, 510–515.
- 49 D. L. Kaplan, Introduction to biopolymers from renewable resources, in *Biopolymers from renewable resources*, Springer, Berlin, Heidelberg, 1998, pp. 1–29.
- 50 C. G. Leonard, R. D. Housewright and C. B. Thorne, Effects of some metallic ions on glutamyl polypeptide synthesis by *Bacillus subtilis*, *J. Bacteriol.*, 1958, **76**(5), 499–509.
- 51 M. Hiroki, Effects of Heavy Metal Contamination on Soil Microbial Population, *J. Soil Sci. Plant Nutr.*, 1991, **38**(1), 141–147.
- 52 G. S. Manning, Limiting Laws and Counterion Condensation in Polyelectrolyte Solutions I. Colligative Properties, *J. Chem. Phys.*, 1969, **51**(3), 924–933.
- 53 F. Hofmeister, Zur Lehre von der Wirkung der Salze, *Arch. Exp. Pathol. Pharmacol.*, 1888, **25**(1), 1–30.
- 54 G. Schwarzenbach, Der Chelateffekt, *Helv. Chim. Acta*, 1952, **35**(7), 2344–2359.
- 55 G.-H. Ho, *et al.*,  $\gamma$ -Polyglutamic Acid Produced by *Bacillus subtilis* (natto): Structural Characteristics, Chemical Properties and Biological Functionalities, *J. Chin. Chem. Soc.*, 2006, **53**, 1363–1384.
- 56 A. M. Hyde, *et al.*, General Principles and Strategies for Salting-Out Informed by the Hofmeister Series, *Org. Process Res. Dev.*, 2017, **21**(9), 1355–1370.
- 57 H. Takesada, H. Yamazaki and A. Wada, Nature of Cu(II)-poly(glutamic acid) complex in aqueous solution, *Biopolymers*, 1966, **4**(7), 713–721.
- 58 L. Shih and Y. T. Van, The production of poly( $\gamma$ -glutamic acid) from microorganisms and its various applications, *Bioresour. Technol.*, 2001, **79**(3), 207–225.
- 59 J. E. Huheey, E. A. Keiter and R. L. Keiter, *Anorganische Chemie*, Walter de Gruyter, Berlin, Boston, 2014.
- 60 E. Riedel, *Anorganische chemie*, Walter de Gruyter, Berlin, New York, 2011.
- 61 *Alginates: biology and applications*, ed. B. H. A. Rehm, Springer-Verlag, Berlin, Heidelberg, 2009.
- 62 Ý. A Mørch, *et al.*, Mechanical properties of C-5 epimerized alginates, *Biomacromolecules*, 2008, **9**(9), 2360–2368.
- 63 O. Smidsrød and G. Skjåk-Bræk, Alginate as immobilization matrix for cells, *Trends Biotechnol.*, 1990, **8**, 71–78.
- 64 C. Falcón García, *et al.*, Metal ions weaken the hydrophobicity and antibiotic resistance of *Bacillus subtilis* NCIB 3610 biofilms, *npj Biofilms Microbiomes*, 2020, **6**(1), 1–11.

A.2.1 Supplementary information for: *Chelate chemistry governs ion-specific stiffening of Bacillus subtilis B-1 and Azotobacter vinelandii biofilms*

Supplemental information for

Chelate chemistry governs ion-specific stiffening of  
*Bacillus subtilis B-1* and *Azotobacter vinelandii* biofilms

Martin Kretschmer and Oliver Lieleg<sup>#</sup>

Munich School of Bioengineering and Department of Mechanical Engineering,  
Technical University of Munich, 85748 Garching, Germany

<sup>#</sup>: Corresponding author:

Prof. Dr. Oliver Lieleg  
Department of Mechanical Engineering and Munich School of Bioengineering,  
Technical University of Munich,  
Boltzmannstraße 11, 85748 Garching, Germany  
e-mail: [oliver.lieleg@tum.de](mailto:oliver.lieleg@tum.de)  
phone: +49 89 289 10952, fax: + 49 89 289 10801

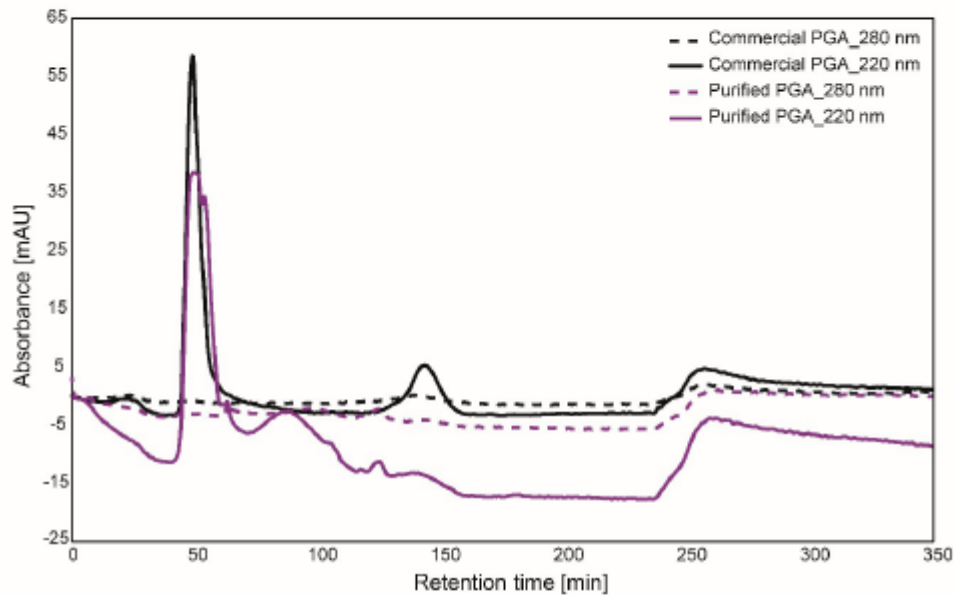
Keywords: Rheology, metal ions, alginate, polyglutamic acid



## 1. Purity of purified $\gamma$ -PGA

As in a previous study from our group [1], we purified  $\gamma$ -PGA from liquid cultures of *B. subtilis* B-1 bacteria following a purification procedure established for different bacteria of the genus *Bacillus*, such as *B. subtilis natto* [2].

As described there, the identity of  $\gamma$ -PGA can be verified spectroscopically by comparing it to commercial PGA (obtained from Sigma Aldrich, St. Louis, USA) as shown below:



**Figure S1: Gel filtration chromatograms of commercial and in-lab purified PGA.** The same amount of a commercial or purified PGA solution (concentration 0.05% (w/v)) was run through a Sepharose 6FF XK50/100 column, and the absorbance at 220 nm and 280 nm was compared. Both PGA variants give a strong peak at 220 nm and at the same retention time. Moreover, neither sample exhibits significant absorption at 280 nm, which shows that the purity of both samples is comparable.

## 2. Exemplary large amplitude oscillatory shear (LAOS) measurements

To determine the linear response range of both, soft (= treated with water) and stiff (= metal ion enriched) biofilm samples, LAOS measurements are conducted as shown below. The excellent reproducibility of those measurements also shows that surface slippage events do not occur with the slimy, sticky biofilm material.

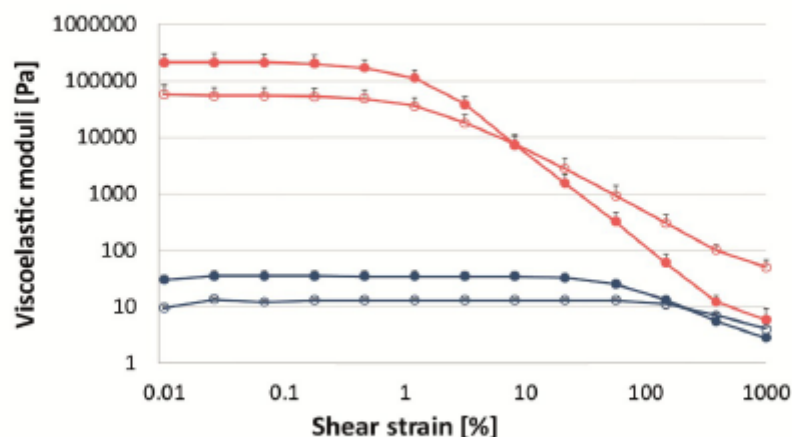


Figure S2: Viscoelastic behavior of *B. subtilis* B-1 biofilms at increasing oscillatory shear strain (LAOS measurements). Viscoelastic moduli are shown in dependence of the shear strain, and biofilm samples treated with water (blue symbols) and  $\text{CuCl}_2$  (pink, final concentration in the samples was 250 mM), respectively, are compared. Full symbols denote the storage modulus,  $G'$ , and open symbols denote the loss modulus,  $G''$ . The values shown represent the mean obtained from three independent measurements, and the error bars (which are sometimes smaller than the symbol size) represent the standard deviation.

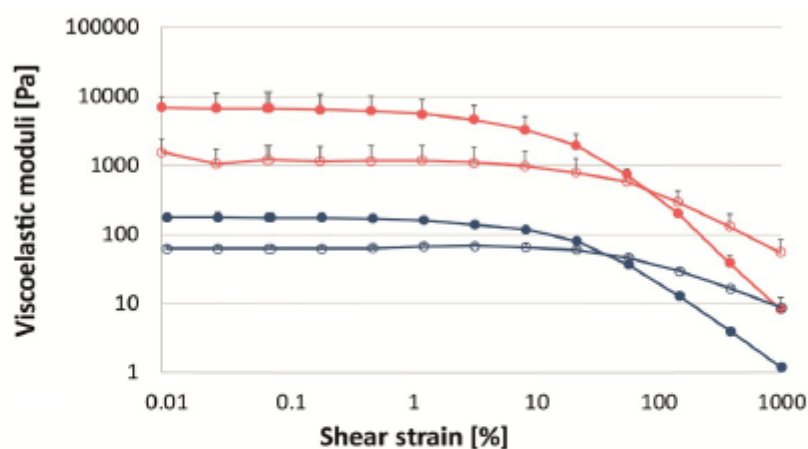


Figure S3: Viscoelastic behavior of *A. vinelandii* biofilms at increasing oscillatory shear strain (LAOS measurements). Viscoelastic moduli are shown in dependence of the shear strain, and biofilm samples treated with water (blue symbols) and  $\text{CuCl}_2$  (pink, final concentration in the samples was 250 mM), respectively, are compared. Full symbols denote the storage modulus,  $G'$ , and open symbols denote the loss modulus,  $G''$ . The values shown represent the mean obtained from three independent measurements, and the error bars (which are sometimes smaller than the symbol size) represent the standard deviation.

S3

### 3. Exemplary frequency spectra

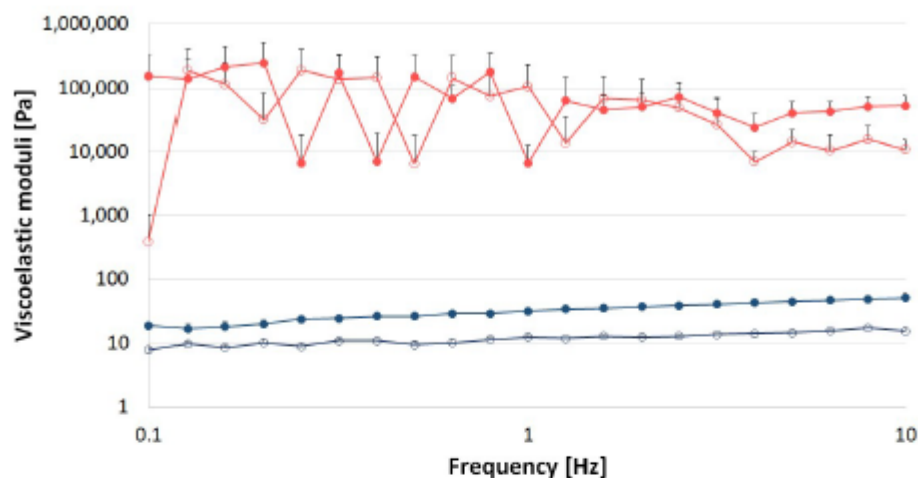


Figure S4: Viscoelastic response of *B. subtilis* B-1 biofilm with and without exposure to  $\text{CuCl}_2$ . Frequency spectra are shown for biofilm samples treated with water (blue symbols) and  $\text{CuCl}_2$  (pink), respectively. In the second case, the final concentration of  $\text{Cu}^{2+}$  ions in the biofilm was set to 250 mM (using a  $\text{CuCl}_2$  stock solution of 1 M which had a pH of 0.9). Full symbols denote the storage modulus,  $G'$ , and open symbols denote the loss modulus,  $G''$ . The values shown represent the mean obtained from three independent measurements and the error bars (which are sometimes smaller than the symbol size) represent the standard deviation.

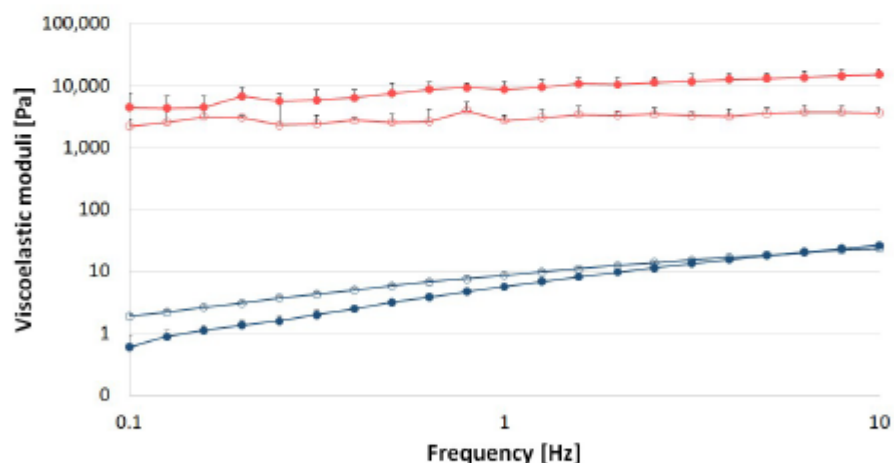


Figure S5: Viscoelastic response of a 1.5 % (w/v)  $\gamma$ -PGA solution with and without exposure to  $\text{CuCl}_2$ . Frequency spectra are shown for  $\gamma$ -PGA solutions treated with water (blue symbols) and  $\text{CuCl}_2$  (pink), respectively. In the second case, the final concentration of  $\text{Cu}^{2+}$  ions in the biofilm was set to 250 mM (using a  $\text{CuCl}_2$  stock solution of 1 M which had a pH of 0.9). Full symbols denote the storage modulus,  $G'$ , and open symbols denote the loss modulus,  $G''$ . The values shown represent the mean obtained from three independent measurements and the error bars (which are sometimes smaller than the symbol size) represent the standard deviation.

S4

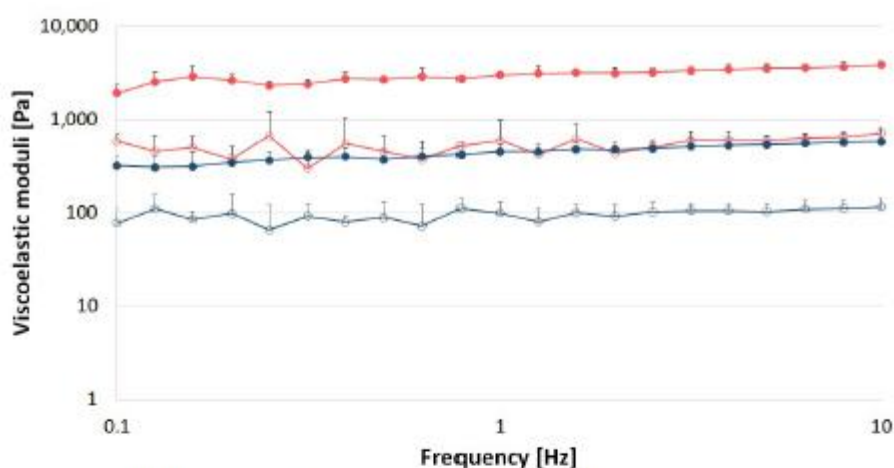


Figure S6: Viscoelastic response of an *A. vinelandii* biofilm with and without exposure to  $\text{CuCl}_2$ . Frequency spectra are shown for biofilm samples treated with water (blue symbols) and  $\text{CuCl}_2$  (pink), respectively. In the second case, the final concentration of  $\text{Cu}^{2+}$  ions in the biofilm was set to 250 mM (using a  $\text{CuCl}_2$  stock solution of 1 M which had a pH of 0.9). Full symbols denote the storage modulus,  $G'$ , and open symbols denote the loss modulus,  $G''$ . The values shown represent the mean obtained from three independent measurements and the error bars (which are sometimes smaller than the symbol size) represent the standard deviation.

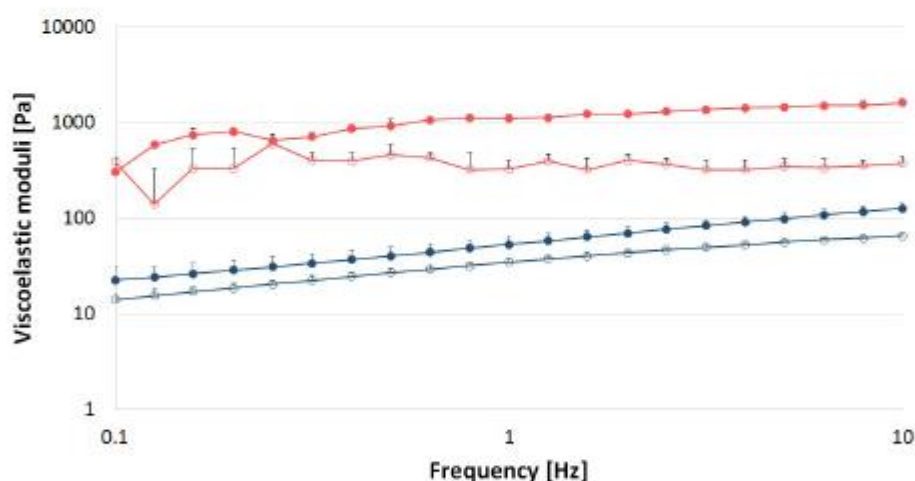


Figure S7: Viscoelastic response of 1.5 % (w/v) alginate solution with and without exposure to  $\text{CuCl}_2$ . Frequency spectra are shown for alginate solutions treated with water (blue symbols) and  $\text{CuCl}_2$  (pink), respectively. In the second case, the final concentration of  $\text{Cu}^{2+}$  ions in the biofilm was set to 250 mM (using a  $\text{CuCl}_2$  stock solution of 1 M which had a pH of 0.9). Full symbols denote the storage modulus,  $G'$ , and open symbols denote the loss modulus,  $G''$ . The values shown represent the mean obtained from three independent measurements and the error bars (which are sometimes smaller than the symbol size) represent the standard deviation.

## 1. Elastic modulus of metal-ion treated biofilms as function of the ionic radius

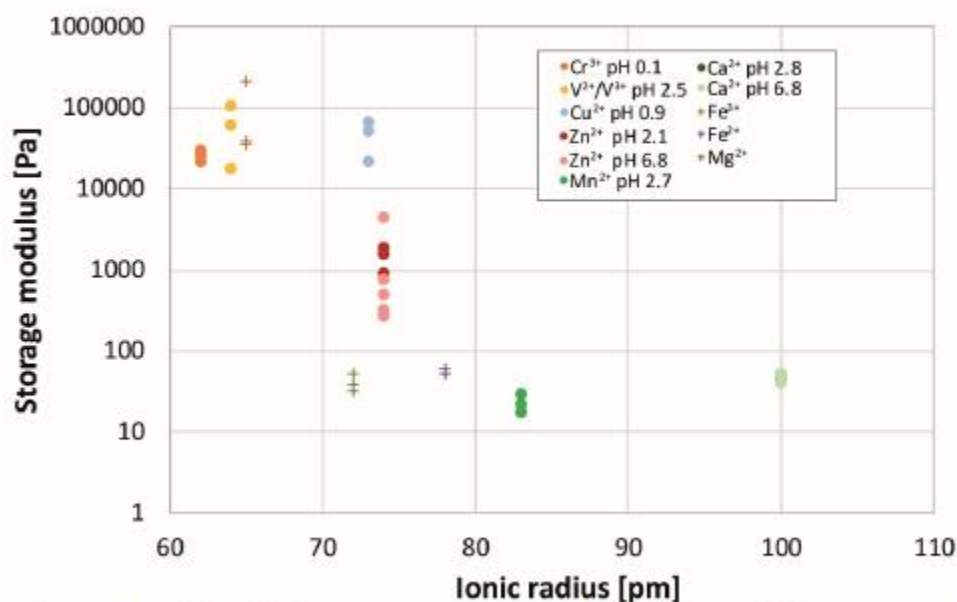


Figure S8: Plateau modulus of *B. subtilis* B-1 biofilms treated with different metal cations as a function of the ionic radius. Full circles denote the storage modulus,  $G'$ , in the plateau regime as obtained in this study for individual samples. The final concentration of metal ions in the biofilms was 250 mM for all measurements conducted in this study (data depicted as circles). In addition, data points from a previous study by Grumbein *et al.* [3] is added to the graph (cross symbols). Samples from this earlier study had a final metal ion concentration of 50 mM. The ionic radius shown on the x-axis was chosen according to Riedel [4].

## 2. Time dependent biofilm stiffening induced by vanadium chloride

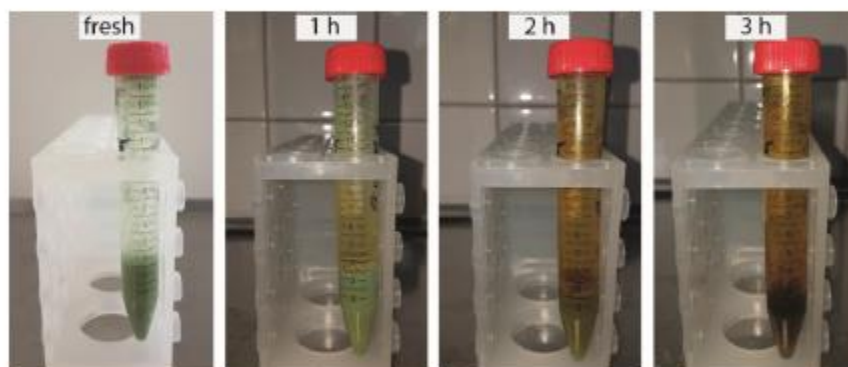
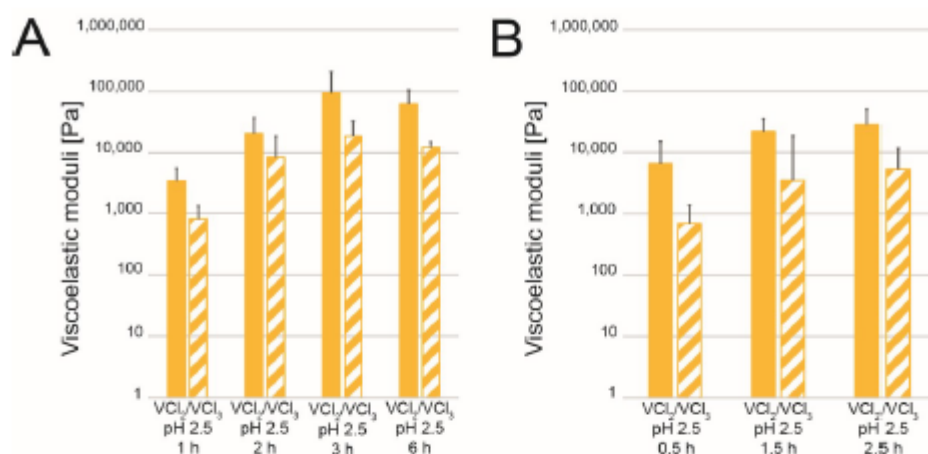


Figure S9: A vanadium chloride solution changes color as it oxidizes. A freshly prepared vanadium chloride solution (left) exhibits a mint-like, green color. Over time, this color changes into brown as the vanadium ions oxidize. The age of the solution is indicated above the respective image.



**Figure S10: Viscoelastic moduli of *B. subtilis* B-1 biofilm (A) and  $\gamma$ -PGA solutions (B) treated with aging vanadium(II) chloride solutions. Full bars denote the storage modulus,  $G'$ , and striped bars the loss modulus,  $G''$ . The samples were always treated for 5 minutes, only the age of the solution increased up to 6 hours. With increasing age of the vanadium(II) chloride solution, the ratio of  $V^{2+}$  and  $V^{3+}$  changes as  $V^{2+}$  oxidizes over time. The error bars represent the standard deviation as obtained from at least three independent samples.**

#### Cited Literature

1. Hayta, E., Nur and O. Lieleg, *Biopolymer-enriched B. subtilis NCIB 3610 biofilms exhibit increased erosion resistance*. *Biomater. Sci.*, 2019. 7: p. 4675-4686.
2. Kaplan, D., L., *Biopolymers from renewable resources*. 1998, Berlin, Heidelberg: Springer.
3. Grumbein, S., M. Opitz, and O. Lieleg, *Selected metal ions protect Bacillus subtilis biofilms from erosion*. *Metallomics*, 2014. 6(8): p. 1441-1450.
4. Riedel, E., *Anorganische chemie*. 2011, Berlin, New York: Walter de Gruyter.

# Biofilm Adhesion to Surfaces is Modulated by Biofilm Wettability and Stiffness

Martin Kretschmer, Carina Anke Schüßler, and Oliver Lieleg\*

Although many surfaces in industry and medicine are colonized by bacterial biofilms, little is known about the physical principles that govern the adhesion properties of such bacterial communities. In part, this is due to the technical challenge associated with the characterization of a biofilm directly on the substrate it is grown on. Moreover, distinguishing between the cohesive and adhesive properties of a (bio)material requires information on the amount of material transferred between the interacting surfaces, which is not easily possible in existing measurement techniques applied in biofilm research. Here, a new method is introduced which allows for characterizing the detachment process of biofilms *in situ* and makes it possible to identify the dominant mode of fracture. As a countersurface in those detachment tests with biofilm layers, either a synthetic/inorganic material surface or another biofilm layer can be used. By comparing results obtained with different biofilms generated at distinct cultivation conditions, how two selected material properties, i.e., the biofilm wettability and the biofilm stiffness, contribute to the detachment process can be shown. The novel measurement approach demonstrated here can easily be adapted further to enable adhesion/detachment measurements with a broad range of other biofilms including those grown at submerged conditions.

include pipes, ship hulls, teeth or medical implants.<sup>[20–25]</sup> Biofilms contain not only bacteria but also extracellular polymeric substances (EPS) secreted by them.<sup>[16–18]</sup> Typically, the EPS comprises polysaccharides, proteins and extracellular DNA.<sup>[19–22]</sup> Whereas many studies have investigated the adhesion of individual bacterial cells to surfaces,<sup>[23–27]</sup> less is known how the biofilm matrix contributes to this phenomenon.<sup>[28–31]</sup> There are, however, strong indications that the biofilm matrix polymers play an important role here as well.<sup>[32,33]</sup> cross-linking of the biofilm matrix by, e.g., metal ions, has been shown to strongly alter the viscoelastic properties, cohesion strength and erosion resistance of biofilms;<sup>[34–37]</sup> it appears likely that those material properties are closely related to the adhesion behavior of biofilms.

Different techniques have already been established to quantify certain material properties of biofilms. For instance, macrorheology is very well suited to investigate the shear stiffness and yielding behavior of viscoelastic materials such as biofilms<sup>[38–41]</sup>—and such measurements allow for drawing conclusions on the cohesion behavior of these slimy substances. Classical macrorheological measurement protocols, however, cannot assess the surface adhesion properties of biofilms, and standardized procedures to characterize this surface adhesion behavior of biofilms do not exist yet.

In contrast, for synthetic materials such as glues, there are well-defined protocols for quantifying their adhesion and cohesion strength.<sup>[42]</sup> Those either apply stretching forces in the vertical direction thus measuring the tensile strength of a material,<sup>[43]</sup> or they make use of large shear forces to study the internal yielding behavior of a glue.<sup>[44,45]</sup> Other methods apply torsional forces to a sample to generate a defined shear stress, e.g., by rotating the two opposing surfaces relative to each other.<sup>[46]</sup> With the latter protocols (which can, in similar form, easily be implemented in a standard rheometer), however, drawing conclusions on the adhesion properties of a material is not easily possible. In addition, standard procedures developed for testing synthetic glues would require a biofilm (prior to its characterization) to be removed from the substrate it was grown on—and this can significantly affect the result of an adhesion measurement.


There are, however, a few examples of dedicated setups which allow for investigating the adhesive properties of biofilms *in situ*. For instance, Chen et al. characterized the adhesion

## 1. Introduction

Bacteria form slimy substances, so-called biofilms; this allows them to settle permanently on surfaces<sup>[1–4]</sup> and to protect themselves from external challenges, such as temperature differences, toxic substances or shear loads.<sup>[5–9]</sup> Biofilms are able to adhere to nearly any surface in a wet environment; examples

M. Kretschmer, C. A. Schüßler, Prof. O. Lieleg  
 Department of Mechanical Engineering and Munich School  
 of Bioengineering  
 Technical University of Munich  
 Boltzmannstraße 11, 85748 Garching, Germany  
 E-mail: oliver.lieleg@tum.de

M. Kretschmer, C. A. Schüßler, Prof. O. Lieleg  
 Center for Protein Assemblies (CPA)  
 Technical University of Munich  
 Ernst-Otto-Fischer Straße 8, 85747 Garching, Germany

 The ORCID identification number(s) for the author(s) of this article can be found under <https://doi.org/10.1002/admi.202001658>.

© 2021 The Authors. Advanced Materials Interfaces published by Wiley-VCH GmbH. This is an open access article under the terms of the Creative Commons Attribution-NonCommercial License, which permits use, distribution and reproduction in any medium, provided the original work is properly cited and is not used for commercial purposes.

DOI: 10.1002/admi.202001658

behavior of biofilms by removing them from their substrate with a spatula and measuring the lateral force occurring during this scraping process.<sup>[47]</sup> A different approach was chosen by Yan et al., who employed capillary forces to remove biofilms from a surface to measure the corresponding adhesion energy.<sup>[48]</sup> With this method, the biofilm layer remains intact can be transferred to a different substrate and—potentially—be characterized further. In spite of this considerable progress made in the area of biofilm adhesion, there is no clear picture yet if and how biofilm detachment from a surface is linked to other material properties of this bacterial substance.

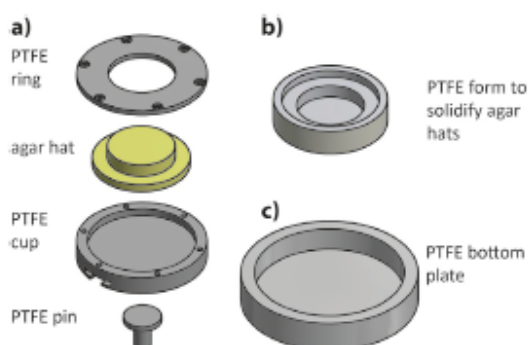
Here, we present a measurement setup based on a commercial rheometer, which applies normal forces to the biofilm material and allows for characterizing the detachment process of biofilms from the substrate they are grown on. Since we can analyze both, the force–distance curves measured during the detachment process and the amount of biological material transferred between the two test surfaces, we can differentiate between an adhesive and cohesive failure of the biomaterial. Moreover, we are able to test this detachment process in two different configurations, i.e., in a metal-on-biofilm and a biofilm-on-biofilm setup. We compare biofilms generated by three different variants of the soil bacterium *Bacillus subtilis* and alter the biofilm properties by modulating the nutrient conditions during biofilm growth or exposing the biofilm to cross-linking metal ions. Our results demonstrate that the wetting properties of a biofilm and—to a lesser extent—the biofilm stiffness dictate the detailed detachment behavior of biofilms by deciding whether adhesion or cohesion failure dominates.

## 2. Experimental Section

### 2.1. Development of a New Measurement Method to Characterize the Adhesion and Cohesion of Mature Biofilms In Situ

The technique introduced here allows for quantifying the adhesive properties of a biofilm toward a second surface, which can either be a metal surface (here aluminum) or another biofilm layer. This is made possible by equipping a commercial rheometer (MCR 302; Anton Paar GmbH, Graz, Austria) with a custom-made measuring head (Figure 1a) and sample holder (Figure 1c). Technical drawings of the custom-made components for the detachment test are shown in the Supporting Information (Figures S1–S5, Supporting Information).

The dedicated measuring head is used when a biofilm-on-biofilm configuration is tested; otherwise, a commercial planar measuring head (made from aluminum) with a diameter of 25 mm is used (D-PP25/Al/S07, No. 10637, Anton Paar). The custom-made measuring head comprises three components made from polytetrafluoroethylene (PTFE): a ring, a cup and a connector pin. The ring can be attached to the cup with six screws and the pin is slid into the bottom side of the cup where it locks in the center. With the connector pin, the three-component measuring head is attached to a commercial measuring shaft (shaft for disposable measuring systems, D-CP/PP7, No. 10636, Anton Paar) of the rheometer. In between the PTFE ring and cup, an agar layer is inserted. This agar layer is produced in a hat-like geometry using a special PTFE mold (Figure 1b). Because of the



**Figure 1.** Schematic representation of the custom-made components required for the detachment tests conducted on a commercial rheometer. a) Individual parts of the dedicated measuring head; the ring, cup and pin are made of PTFE, and a hat-shaped agar layer can be inserted in between the cup and the ring. The ring is attached to the cup with screws, and the pin can be slid into the cup and allows for connecting the fully assembled measuring head to the shaft of the rheometer. b) PTFE form used for the preparation of the hat-shaped agar layers. c) PTFE bottom plate that can be filled with an agar layer so that a biofilm can be cultivated on its surface.

hat-like shape, the upper part of this agar piece (having a diameter of 25 mm) protrudes the ring structure of the sample holder; this ensures that only the surface, where the biofilm is cultivated on, is in contact with the bottom plate of the rheometer measuring setup during a measurement. As a bottom plate holding a biofilm sample, a PTFE bowl was designed (Figure 1c); also here, the cavity can be filled with agar onto which biofilm cultivation is easily possible. The cavity in this PTFE bowl has a diameter of 55.2 mm and a height of 9 mm, and the bowl is clamped into the rheometer bottom plate (P-PTD200/80/1, No. 81664467, Anton Paar) for the detachment measurements. CAD models and the images of the custom-made components for the detachment tests were created with Autodesk Inventor Professional 2020 (Autodesk Corp., San Rafael, USA).

### 2.2. Bacterial Strains and Growth Conditions

Three different *B. subtilis* strains were used in this study: *B. subtilis* 3610<sup>[49]</sup> was obtained from the lab of Roberto Kolter (Harvard Medical School, USA); *B. subtilis* B-1<sup>[50]</sup> was obtained from Masaaki Morikawa (Hokkaido University, Japan); *B. subtilis natto* (27E3)<sup>[51]</sup> was obtained from the Bacillus Genetic Stock Center (BGSC, USA). *B. subtilis* 3610 is found in soil and common used as model bacteria for the properties of bacterial biofilms.<sup>[49]</sup> *B. subtilis* B-1 is also found in soil, it was isolated from an oil field.<sup>[50]</sup> *B. subtilis natto* is known from the traditional Japanese dish natto where it leads to the fermentation of soybeans.<sup>[51]</sup> All of the investigated bacterial strains are able to form biofilms on solid surfaces. A liquid culture of each bacterial strain was generated by cultivating small pieces of a frozen glycerol stock in 10 mL of 2.5% (w/v) LB medium (Luria/ Miller; Carl Roth GmbH, Karlsruhe, Germany) at 37 °C and at agitation (300 rpm) for ~18 h. Before the planktonic bacteria were plated onto agar, their OD<sub>600</sub> was measured with a spectrophotometer (GeneQuantpro, No. 1715,



Amersham Biosciences, Little Chalfont, United Kingdom) and set to 0.5 by diluting the bacterial liquid culture with fresh LB medium. Then, the bacterial suspension was inoculated on 1.5% (w/v) agar-agar (Carl Roth GmbH) by distributing  $1.6 \mu\text{L cm}^{-2}$  of the diluted liquid culture homogeneously over the agar plates. In detail, 100  $\mu\text{L}$  of the liquid culture were added to a commercial petri dish, 40  $\mu\text{L}$  to the custom-made PTFE bowls and 8  $\mu\text{L}$  to the agar hats.

Commercial petri dishes with a diameter of 8.8 cm were used to cultivate biofilm for rheological measurements (for those measurements, larger biofilm amounts were required). Custom made PTFE bowls with a diameter of 5.5 cm were used to cultivate biofilm to determine the biofilm wetting properties and were also used as bottom part of the detachment measurements. For the top part of the detachment tests, agar hats with a diameter of 2.5 cm were used. The thickness of the agar layers in commercial petri dishes, custom-made PTFE bowls and agar hats was always set to  $\approx 8$  mm by filling the respective reservoirs with 50, 19, and 6 mL of agar medium, respectively. This ensured that the thickness of biofilm cultivated on those three substrate variants was comparable. The inoculated agar samples were all incubated for 24 h at 37 °C and at high humidity (>80%).

For the tests described in the results section, biofilms were cultivated on different agar media, which differed in the content of nutrients; as “standard” growth conditions, agar enriched with 2.5% (w/v) LB medium (Carl Roth GmbH) was used. For some experiments, the agar substrate was enriched with 0.5 mmol of a selected metal salt by adding sterile-filtered metal salt solutions to autoclaved LB agar at a temperature of 60 °C. The salts used in this study were  $\text{CaCl}_2$ ,  $\text{CuCl}_2$ ,  $\text{ZnCl}_2$ ,  $\text{AlCl}_3$  (Carl Roth GmbH), and  $\text{FeCl}_3$  (Sigma Aldrich Corp., Missouri, USA). To examine the influence of metal ion exposure to mature biofilms, biofilms were cultivated at standard conditions as described above. Then, the mature biofilm layer was treated with a solution of  $\text{CuCl}_2$  (250 mmol) as follows: for the bottom plates, the  $\text{CuCl}_2$  solution was poured onto the biofilm layer such, that the whole biofilm surface was covered with liquid. Biofilm cultivated on the agar hats were stored upside down (with the biofilm layer facing downward) and immersed into the  $\text{CuCl}_2$  solution. In either case, the incubation time was 1 h; then the  $\text{CuCl}_2$  solution was discarded, and the biofilm layer was allowed to dry at room temperature for 10 min so that liquid remnants on the surface could evaporate. In preliminary experiments, it was shown that the different treatment procedure of the petri dishes and agar hats have the same effect on the biofilm properties (Figure S6, Supporting Information). For simulating limiting nutrient conditions, biofilm was cultivated on MSgg agar (0.5% glycerol, 0.5% K-glutamate, 5 mmol K-phosphate, 100 mmol MOPS, 2 mmol  $\text{MgCl}_2$ , 0.7 mmol  $\text{CaCl}_2$ , 0.05 mmol  $\text{MnCl}_2$ , 0.05 mmol  $\text{FeCl}_3$ , 0.001 mmol  $\text{ZnCl}_2$ , 0.002 mmol thiamine, 50  $\mu\text{g mL}^{-1}$  L-tryptophan, 50  $\mu\text{g mL}^{-1}$  L-phenylalanine, 50  $\mu\text{g mL}^{-1}$  threonine), which was prepared at pH 7.0 according to Branda et al.<sup>[49]</sup>

### 2.3. Biofilm Wetting Tests

To determine the wetting behavior of the different biofilm samples, a 10  $\mu\text{L}$  droplet of  $\text{ddH}_2\text{O}$  was placed onto the biofilm

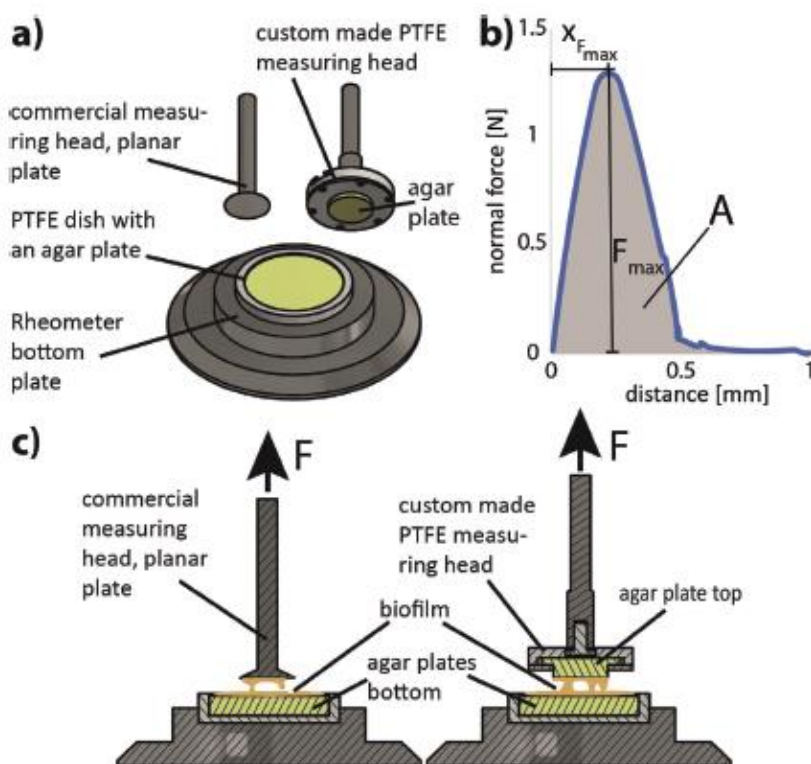
surface. Then, a transversal image of the liquid–solid interface was captured right afterward using a high-resolution camera (Point Gray Research, Richmond, Canada). The static contact angle value was determined from such pictures, using the software ImageJ and the “drop snake” plug-in.<sup>[52]</sup> Afterward, superhydrophobic biofilm samples (i.e., those with static contact angles >120°) were tilted and the response of the liquid droplet was observed to distinguish between rose petal (high adhesion: droplet sticks) and lotus-like (low adhesion: droplet rolls off) hydrophobicity. In addition, contact angle hysteresis measurements were conducted as described and summarized in the Supporting Information.

### 2.4. Rheological Measurements

To determine the rheological properties of the different biofilms, the biofilms were cultivated as described above and harvested from the agar substrate by manual scraping. Rheological measurements were performed using a commercial shear rheometer (MCR 302; Anton Paar) equipped with a 25 mm aluminum measuring head (PP25) and a plate–plate geometry. The plate separation was set to 0.3 mm. A solvent trap was applied to prevent sample drying during the measurements that were realized at 21 °C and in strain-controlled mode. To ensure linear material response, small strains corresponding to a torque of  $\approx 0.5 \mu\text{N m}$  (this correlates to a shear stress of  $\approx 0.1$  Pa) were applied. In every rheological experiment, both the storage and loss modulus were determined over a frequency range of 0.1–10 Hz. Since, in all cases described in this study, the moduli obtained for a given biofilm sample were only weakly dependent on frequency (exemplary frequency spectra for different biofilm samples are shown in the Supporting Information; Figure S7, Supporting Information), only the moduli obtained at a frequency of 1 Hz were considered for obtaining the bar plots in the manuscript. For each condition, at least six samples were tested, which were obtained from two biological replica. For those shear measurements, standard deviations were chosen as error bars, since biological variations between different replicates of the bacterial biofilms always dominate the technical uncertainties/inaccuracies of the measurements. In fact, the technical error, which can be obtained from repeated rheological measurements of the same sample (e.g., a 1.5% (w/v) agar hydrogel), amounts to only <5%: five frequency sweeps conducted with the same agar sample in a range from 0.1 to 10 Hz return a storage modulus of 5058 Pa  $\pm$  199 Pa (determined at an intermediate frequency of 1 Hz).

### 2.5. Detachment Tests

In the presented study, the two material pairings biofilm/aluminum and biofilm/biofilm were investigated. As reference measurements, the material pairings agar/aluminum and agar/agar were used. For both measuring heads, the contact area had a diameter of 25 mm. In each detachment test, first the measuring head was moved down onto the bottom plate at a speed of 100  $\mu\text{m s}^{-1}$  until a normal force of 1 N was reached. This force level was chosen since pretests had shown, that such a normal



**Figure 2.** Overview of the two configurations used in the detachment tests. a) The custom-made bottom plate is paired with either a commercial measuring head or the custom-made measuring head described in the main text. b) Typical examples of a force–distance curve obtained during a detachment test. Relevant parameters obtained from such a curve are the maximal force ( $F_{\text{max}}$ ), the distance at which this maximal force occurs ( $x_{F_{\text{max}}}$ ) and the area  $A$  below the force–distance curve, which corresponds to the separation work. c) Experimental setup for the two material pairings used in this study, i.e., biofilm/aluminum (left) and biofilm/biofilm (right).

force level is sufficient to obtain full contact between the two surfaces without damaging the agar substrate. When this normal force was reached, the position was maintained for 60 s; this allowed the normal force to relax and reach a plateau value. Afterward, the measuring head was lifted up again at a speed of  $100 \mu\text{m s}^{-1}$ , and the force occurring during this pulling process was recorded at a measuring point density of  $10 \text{ s}^{-1}$  until the measured force dropped to zero (Figure 2b). The rheometer used here has a normal force resolution of 0.5 mN, which is valid in a normal force range between 5 mN and 50 N. The measured peak force values of the investigated biofilms range between 50 mN and 3 N, which is at least tenfold larger than the normal force resolution of the device. In addition to these force measurements, the biofilm areas exposed to this normal force treatment were also analyzed optically by imaging them with a digital camera (Samsung Galaxy S7, Samsung Group, Seoul, South Korea). Moreover, after each detachment test, the biofilm layers from the tested surface areas were removed by scraping with a polydimethylsiloxane spatula and weighed with a microbalance (XSE205 Dual Range,  $d = 0.01 \text{ mg}/0.1 \text{ mg}$ , Mettler Toledo, Columbus, USA). Those amounts were then compared to those collected from untested samples created at the same conditions

by calculating the ratio of treated/untreated samples (using average values of six samples generated from two biological replicates). The material transfer values reported in the results section denote percentage values differences, i.e., a material transfer of 15% corresponds to a loss (or gain) of 15% of biofilm mass on one of the surfaces tested in the respective material pairing.

## 2.6. Data Evaluation

All error bars shown in the figures denote the standard deviation as calculated from the mean values. In this study, standard deviations were chosen as error bars since, for measurements conducted on naturally grown, biological materials such as bacterial biofilms, the biological variations occurring between different samples always dominate the technical uncertainties/inaccuracies—especially when the tested biofilms were cultivated on different days (which is typically done to explore this biological variability arising from sample generation). For the calculation of all mean values and the corresponding standard deviations, Microsoft Excel 2016 (Microsoft Corporation, Redmond, USA) was used.

### 3. Results and Discussion

To conduct adhesion/cohesion experiment with bacterial biofilms, a customized sample chamber (see Figure 2a) was developed as described in detail in the Methods section. With this customized setup, it is possible to perform measurements with biofilms grown on either (or both), the lower and upper part of the two-component measuring setup. In the following, if detachment tests are conducted between biofilm and aluminum, biofilm is cultivated only on the bottom part of the measuring setup (Figure 2c, left). In contrast, if detachment tests with two biofilm surfaces are performed, also the upper part of the sample holder contains a biofilm-grown agar layer (Figure 2c, right).

#### 3.1. Measurement Procedure and Possible Modes of Rupture

To assess the reproducibility of the customized setup, we first conduct reference measurements, where the bottom part of the sample holder contains agar only. Detachment tests performed on this agar layer using an aluminum surface as a countermaterial on the measuring head returns maximal adhesion forces, which are well within the range of normal forces the rheometer can accurately determine. In detail, we find  $F_{\text{max,aha/agar}} = (0.53 \pm 0.15)$  N (Figure S8a, Supporting Information) at a separation distance of  $(0.14 \pm 0.03)$  mm (Figure S8b, Supporting Information). When an agar surface is used as a countermaterial on the upper part of the measuring setup, the corresponding values are only slightly higher: now, we measure  $F_{\text{max,agar/agar}} = (0.61 \pm 0.12)$  N (Figure S8c, Supporting Information) at an average separation distance of  $(0.37 \pm 0.11)$  mm (Figure S8d, Supporting Information). The small fluctuations in the maximal forces determined in those reference measurements can be due to two technical challenges: first, variations in the moisture content of the agar plates can be responsible; second, an imperfect alignment of the bottom part of the sample holder and the upper part (the measuring head) may contribute as well. However, as the sample-to-sample variations in those reference measurements are all rather small, we conclude that the in-house crafted sample holders are functional and that the measuring method is suitable for conducting more complex measurements involving biofilms.

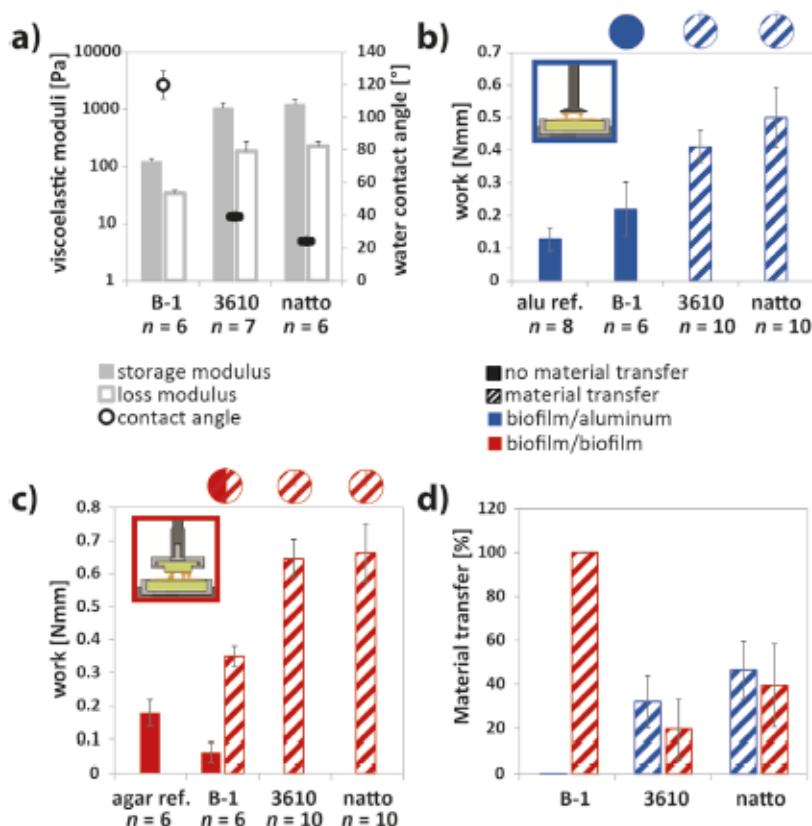
When slimy substances such as biofilms are examined with the method presented here, it is important to distinguish between the different types of fractures that can occur at a biofilm/agar, biofilm/aluminum or biofilm/biofilm interface (Table S1, Supporting Information). One possible scenario is that the measuring head detaches from the biofilm layer (grown on the bottom plate) without damaging the biofilm. In this case, the biofilm will be stretched but remains attached on the agar substrate. The resulting normal force corresponds to the adhesion properties between the biofilm surface and the surface of the measuring head (i.e., either aluminum or biofilm). A second possibility is that the biofilm layer is completely removed from the agar layer it was grown on (i.e., from either the bottom plate or the measuring head); now, transfer of biological material to the other surface should occur at rate of close to 100%. In this case, the reported normal forces describe the

adhesion strength of the biofilm to the substrate on which it was cultivated (here: agar). The third option is that the biofilm layer is partially torn apart; then, after a separation experiment, biofilm material should be present on both surfaces, i.e., on the measuring head as well as on the bottom plate. In this scenario, where the biofilm itself is ruptured, the measured normal forces will depend on the internal cohesion strength of the biofilm layer.

With those considerations in mind, we will not only record and compare the peak forces occurring during the different rupture processes, we will also determine the amount of biofilm material transferred to the second surface involved in the detachment test. Together, this approach should allow us to differentiate the three possible fracture types outlined above.

#### 3.2. Viscoelastic Properties and Wetting Behavior of the Studied Biofilms

Before we conduct the first set of detachment experiments with different *B. subtilis* biofilms, we determine the viscoelastic properties and wetting behavior of the three biofilm variants we plan to compare. Our rationale for doing this is that both of those material properties are likely to affect the adhesion behavior of the biofilms. As shown in Figure 3, the biofilms we grow from *B. subtilis* 3610 and *B. subtilis natto* are very similar to each other in terms of both, viscoelasticity and wetting (Figure 3a); we measure storage moduli around 1 kPa and hydrophilic surfaces with contact angles between  $25^\circ$  and  $40^\circ$ . In contrast, biofilms grown from *B. subtilis* B-1 bacteria are much softer (here,  $G' \approx 100$  Pa) and have strongly hydrophobic surfaces with contact angles as high as  $125^\circ$  (Figure 3a). In detail, these *B. subtilis* B-1 biofilm exhibit rose petal-like hydrophobicity: a wetting water droplet sticks to the surface and does not roll off when the biofilm sample is tilted or turned upside down. In addition to this qualitative method to determine the type of superhydrophobicity, contact angle hysteresis measurements were conducted on all hydrophobic biofilms (Figure S9, Supporting Information). Here, the difference between the contact angles determined at the first and last step of those dynamic wetting tests (ACA) was calculated (Table S2, Supporting Information). Furthermore, the topographical structure of the biofilms, which is crucial for the detailed mode of wetting was investigated with laser scanning profilometry (Figure S10, Supporting Information) for each biofilm variant, and the respective metrological roughness parameters (Sq and Sdr values) were calculated (Table S3, see the Supporting Information for details). In full agreement with previous results, we found large differences between hydrophilic biofilms (which exhibit a very smooth and unstructured surface) and the hydrophobic biofilms (which show multiscale roughness on the micro- and nanolevel in addition to mesoscopic waviness).<sup>[53]</sup> For the detailed wetting behavior of the biofilms (i.e., the type of hydrophobicity: lotus- or rose-like), the roughness features on the micro- and nanoscale are very important; in contrast, the mesoscopic waviness is less relevant, although it contributes to the calculated metrological parameters (for more detailed information, see the Supporting Information).



**Figure 3.** Material properties and detachment behavior of *B. subtilis* B-1, *B. subtilis* 3610 and *B. subtilis* natto biofilms. Data obtained for “empty” material pairings (where no biofilms were grown on the agar layers) are depicted as references. a) Viscoelastic properties and wetting behavior of the biofilms. Full bars denote the storage modulus and open bars the loss modulus. The contact angle is depicted with open circles when rose petal-like hydrophobic behavior is observed, and with filled symbols for hydrophilic behavior. The separation work measured is depicted for the material pairing biofilm/aluminum b) and for the material pairing biofilm/biofilm c). Full bars denote absence of material transfer whereas striped bars indicate that material transfer did occur. The pie charts above the bars visualize how often material transfer occurred for a given sample type. The amount of biofilm material transferred during a detachment test is summarized in d). All data shown represent mean values; error bars denote the standard deviation. The number of different samples analyzed per condition is specified in the respective subfigures.

Interestingly, we also find differences between the three biofilm variants when we compare results from the detachment measurements. For both types of material pairing, i.e., for biofilm/aluminum (Figure 3b) and biofilm/biofilm (Figure 3c) configurations, the measurements conducted with *B. subtilis* 3610 and *B. subtilis* natto biofilms return higher values for the work needed to achieve full separation of the two surfaces than for *B. subtilis* B-1 biofilm. In detail, the maximal force occurring during the detachment test as well as the distance, at which this force peak is located, is higher for *B. subtilis* 3610 and *B. subtilis* natto biofilms than for *B. subtilis* B-1 biofilm (Figure S8, Supporting Information).

When we examine the material transport occurring as a consequence of the detachment process (Figure 3d), again *B. subtilis* B-1 biofilms stand out. For the material pairing biofilm/aluminum, *B. subtilis* 3610 and *B. subtilis* natto biofilms show such material transport (and at comparable levels), but B-1

biofilms do not. This indicates that the first two biofilm variants exhibit cohesive failure when probed with an aluminum surface, whereas, in the case of B-1 biofilms, adhesive failure dominates. For the material pairing biofilm/biofilm, we find similar levels of material transfer for *B. subtilis* 3610 and *B. subtilis* natto biofilms as for the biofilm/aluminum pairing. This indicates that, also here, a cohesion failure occurs. However, also in this biofilm/biofilm configuration, *B. subtilis* B-1 biofilms return a different result: Here, two different scenarios are observed: Either the two B-1 biofilm surfaces are separated from each other without any material transfer or there is a complete material transfer from one side to the other. In either case, this indicates an adhesion failure, which takes place between the two biofilm layers (=no material transfer) or between the biofilm layer and the agar substrate (=full material transfer).

These first results allow us to conclude that the viscoelastic properties as well as the wetting behavior of biofilms seem to

be relevant for rationalizing the observed differences in the detachment tests conducted with *B. subtilis* 3610 and *B. subtilis natto* biofilms on the one hand and *B. subtilis* B-1 biofilms on the other hand. It seems that hydrophilic biofilms exhibit stronger adhesion to foreign surfaces than hydrophobic biofilms, and that they are more likely to stick to each other. However, the higher shear stiffness of *B. subtilis* 3610 and *B. subtilis natto* biofilms could also result in stronger cohesion of these biofilms, which can influence the detachment tests as well.

To disentangle the influence of these two biofilm properties on the adhesion and detachment process, we conduct further experiments where we attempt to alter only one of those properties for a given biofilm variant without modifying the other one. To achieve this, we repeat detachment tests with *B. subtilis* B-1 biofilm, but generate the biofilm such that its viscoelastic properties are modified. *B. subtilis* B-1 biofilms are chosen for this purpose since previous studies<sup>[34,37]</sup> have already shown that the stiffness of those biofilms can be drastically changed by metal cations. This can be achieved by either treating mature biofilms with aqueous solutions containing such metal cations (which leads to a formation of chelate complexes between the cations and the biomacromolecules from the biofilm matrix thus inducing biofilm stiffening) or by enriching the growth medium used for biofilm generation with metal ions; the latter approach affects the stiffness and/or wettability of biofilms by influencing the production of biofilm matrix components. Another method to alter the stiffness and/or wettability of a biofilm is to cultivate the biofilm with different growth media, e.g., on MSgg agar.<sup>[54,55]</sup> In the following, we explore those three options to obtain biofilms with altered wetting behavior and/or viscoelastic properties.

### 3.3. Exposure to Metal Cations during Biofilm Growth

We first study *B. subtilis* B-1 biofilms cultivated on LB agar in the presence of metal cations. To ensure that the added ions have no toxic effect on the bacteria so that they are still able to form a proper biofilm, the ion concentrations are kept at low levels, i.e., at 0.5 mmol. As expected, the addition of those metal ions has an influence on both, the viscoelastic properties and the wetting behavior of the biofilms (Figure 4a). The addition of  $\text{Cu}^{2+}$  and  $\text{Zn}^{2+}$  slightly increases the storage modulus of the biofilm, whereas the addition of  $\text{Fe}^{3+}$  slightly reduces the biofilm stiffness. The other two tested ions,  $\text{Al}^{3+}$  and  $\text{Ca}^{2+}$  do not influence the viscoelastic properties of B-1 biofilms. Regarding the wetting behavior of the biofilms, we find that—overall—the strongly hydrophobic surface properties of the biofilm are maintained. Yet, the contact angles we measure on biofilms cultivated on metal ion-enriched agar substrates are all slightly higher than those we determine when standard agar substrates are used. In addition, for biofilm grown on  $\text{Cu}^{2+}$  or  $\text{Al}^{3+}$  enriched agar, the mode of superhydrophobicity is affected; here, a lotus-like behavior is developed—at least on some parts of the biofilm surface. In other words, now, there are areas on the biofilm surface where a water drop easily rolls off when the biofilm sample is tilted.

In addition to those differences in the viscoelastic and wetting properties, we also find differences in the adhesion

behavior of those biofilms grown in the presence of metal ions. For the material pairing biofilm/aluminum, we observe a reduction in the separation work for all those modified biofilms (Figure 4b). Interestingly, we find the strongest reduction of the separation work for biofilms grown in the presence of  $\text{Cu}^{2+}$  and  $\text{Zn}^{2+}$ —and among the cations we test here, those two increase the stiffness of B-1 biofilms. Moreover, no material transfer occurs in any of these new tests conducted with modified B-1 biofilms. This suggests that, now, adhesion failure is the dominant mechanism during the detachment process.

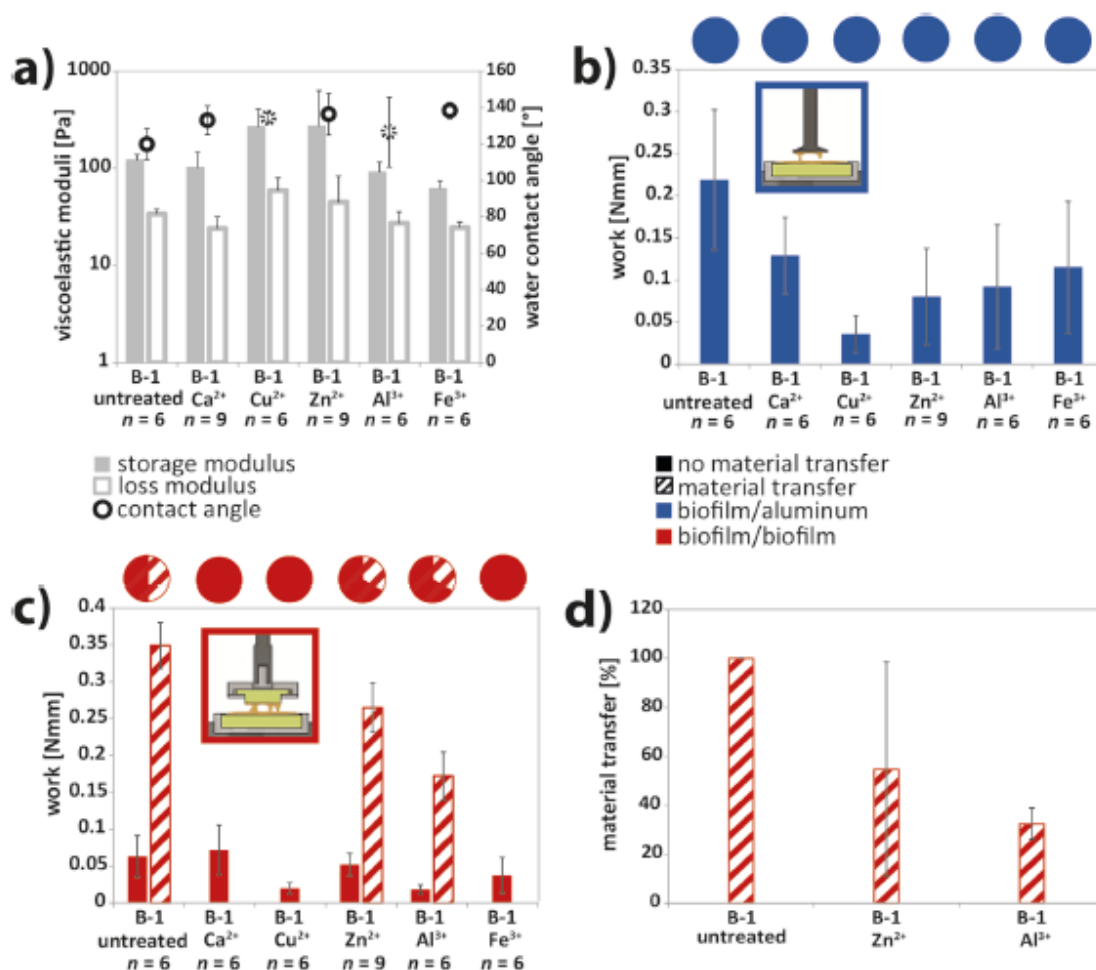
We interpret this finding such that—with an increased biofilm stiffness—two parameters relevant for the mechanical failure process are affected: first, the material can endure larger forces until it ruptures; second, the biofilm material can transfer the externally applied stretching/pulling forces to its substrate more efficiently thus rendering an adhesion failure more likely. Of course, also the alteration of the biofilm surface properties we observe could, in principle, contribute to the observed differences in the detachment tests. However, as the countersurface used in this set of experiments is hydrophilic aluminum, the subtle change in the mode of biofilm superhydrophobicity we find here appears to be a rather unlikely candidate for rationalizing the absence of material transfer we describe above.

When we test the same set of metal-ion exposed biofilms in the biofilm/biofilm configuration, the mode of fracture changes. Untreated biofilms show either complete material transfer or no material transfer at all—and both outcomes are similarly likely. In both cases, an adhesion failure takes place; in the first scenario, it occurs on the substrate, whereas, in the second scenario, it occurs between the two biofilm surfaces. For biofilms exposed to metal ions, material transfer events occur less frequently (Figure 4c). Only biofilms exposed to  $\text{Al}^{3+}$  or  $\text{Zn}^{2+}$  exhibit partial material transfer events (Figure 4d), and only in  $\approx 1/3$  of the conducted tests. As we argued above, such a partial material indicates a mixed detachment event combining adhesion and cohesion failure. This finding is in agreement with our observation that ionic cross-linking of the biofilm matrix as brought about by the metal cations slightly increases the biofilm stiffness. In addition, such cross-linking effects are also likely to increase the cohesive strength of the biofilm matrix thus rendering a cohesion failure less likely.

Consistent with this picture, we also find a reduction of the separation work for almost all biofilm variants exposed to metal ions. We observe the strongest effect for biofilms cultivated on LB agar enriched with  $\text{Cu}^{2+}$  and  $\text{Al}^{3+}$ —and these are the biofilms, where we also find an alteration in their mode of surface hydrophobicity.

### 3.4. Treatment of Mature Biofilms with Metal Cations

When a mature biofilm of *B. subtilis* B-1 is exposed to  $\text{Cu}^{2+}$  ions, the properties of the biofilm are changed a lot. However, different from the experiments described above, where the biofilm was exposed to cations during growth—the cations now do not change the composition of the biofilm. Instead, the metal ions lead to the formation of chelate complexes and thus introduce ionic crosslinks between the biofilm biomacromolecules.<sup>[37]</sup>

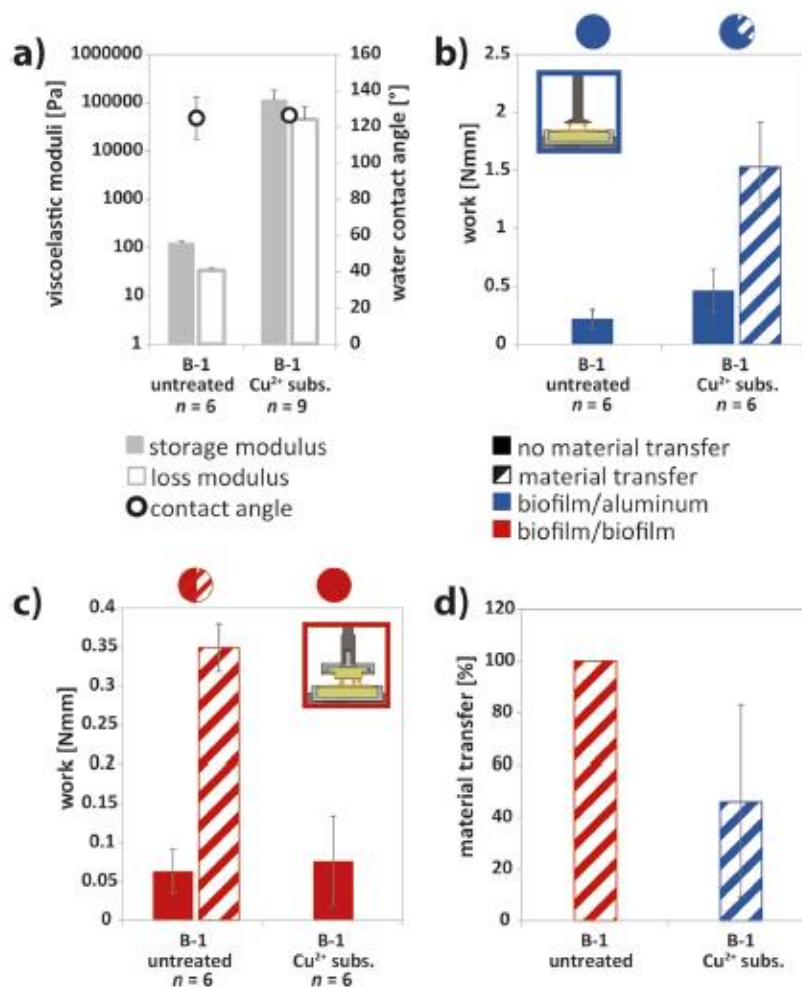


**Figure 4.** Material properties and detachment behavior of *B. subtilis* B-1 biofilms treated with metal ions during growth; data obtained for samples grown at standard conditions is shown as a reference. a) Viscoelastic properties and wetting behavior of the biofilms. Full bars denote the storage modulus and open bars the loss modulus. The contact angle is depicted with open circles when rose petal-like hydrophobic behavior is observed, and with dashed circles when partial rose-like and partial lotus-like hydrophobic behavior occurred. The separation work measured is depicted for the material pairing biofilm/aluminum b) and for the material pairing biofilm/biofilm c). Full bars denote absence of material transfer whereas striped bars indicate that material transfer did occur. The pie charts above the bars visualize how often material transfer occurred for a given sample type. The amount of biofilm material transferred during a detachment test is summarized in d). All data shown represent mean values; error bars denote the standard deviation. The number of different samples analyzed per condition is specified in the respective subfigures.

As demonstrated before,<sup>[34,37]</sup> such a formation of chelate complexes strongly increases the stiffness of the biofilm. And indeed, the same effect is observed here (Figure 5a): after exposure to Cu<sup>2+</sup> ions, the storage modulus of the biofilm sample is increased by three orders of magnitude to ~100 kPa. Yet, with this particular treatment, the wetting behavior of the biofilm remains unchanged.

For the material pairing biofilm/aluminum, most samples show the expected behavior, i.e., detachment without material transfer and a slightly higher separation work than for untreated B-1 biofilms. In line with our argumentation above, both features can be explained by the increased stiffness of the

biofilm material. Interestingly, some of those Cu<sup>2+</sup>-exposed B-1 biofilms show a qualitatively altered detachment behavior: in ~1/3 of the experiments, partial material transfer occurs; in contrast, untreated B-1 biofilm do not show any material transfer events (Figure 5b,d). In other words, now cohesive failure contributes as well. This change in the mode of fracture was unexpected since stiff biofilms—so far—showed mostly adhesive failure, and hydrophobic biofilms appeared to have a low stickiness toward aluminum. Yet, it is important to realize that, as a consequence of the treatment procedure applied here (where a CuCl<sub>2</sub> solution is poured onto the biofilm surface and then removed again after a certain incubation time), the biofilm

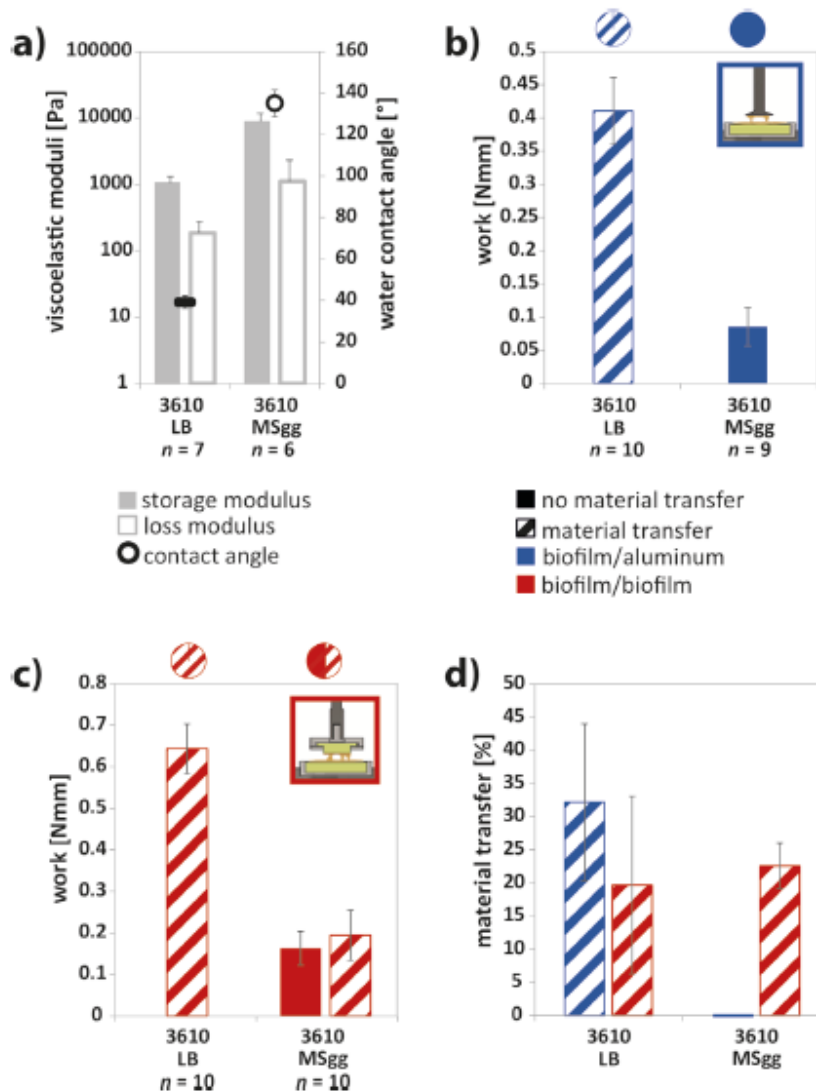


**Figure 5.** Material properties and detachment behavior of mature *B. subtilis* B-1 biofilms treated with a  $\text{CuCl}_2$  solution; data obtained for samples grown at standard conditions is shown as a reference. a) Viscoelastic properties and wetting behavior of the biofilms. Full bars denote the storage modulus and open bars the loss modulus. The contact angle is depicted with open circles for rose petal-like hydrophobic behavior. The separation work measured is depicted for the material pairing biofilm/aluminum b) and for the material pairing biofilm/biofilm c). Full bars denote absence of material transfer whereas striped bars indicate that material transfer did occur. The pie charts above the bars visualize how often material transfer occurred for a given sample type. The amount of biofilm material transferred during a detachment test is summarized in (d). All data shown represent mean values; error bars denote the standard deviation. The number of different samples analyzed per condition is specified in the respective subfigures.

surface is wetted. Remaining moisture on those biofilm samples could be responsible for those unexpected adhesion effects with the aluminum surface. Moreover, we also observe that the aluminum surface of the measuring head used for the rheology and detachment tests shows signs of corrosion (Figure S11, Supporting Information)—and we attribute this to direct contact of residual  $\text{Cu}^{2+}$  ions from the biofilm surface with the aluminum material: such residual  $\text{Cu}^{2+}$  ions on the biofilm surface may act as ionic cross-linkers with the aluminum surface thus giving rise to higher adhesion forces inducing material transfer. Alternatively, the partially corroded aluminum surface

exhibits a higher surface roughness promoting adhesion to the biofilm (Figure S11, Supporting Information). Consistent with any of those two possibilities, the measured separation work is strongly increased as a consequence of the  $\text{Cu}^{2+}$  exposure.

For the material pairing biofilm/biofilm (Figure 5c), a different picture emerges. Whereas untreated biofilms show material transfer in 50% of the measurements, this feature does not occur anymore when the *B. subtilis* B-1 biofilm is treated with  $\text{Cu}^{2+}$ . In other words, now adhesion failure dominates, which fully agrees with the line of argumentation we followed so far.



**Figure 6.** Material properties and detachment behavior of *B. subtilis* 3610 biofilms cultivated on MSgg agar, where nutrients are limited; data obtained for samples grown at standard conditions (=on LB agar) is shown as a reference. a) Viscoelastic properties and wetting behavior of the biofilms. Full bars denote the storage modulus and open bars the loss modulus. The contact angle is depicted with open circles when rose petal-like hydrophobic behavior is observed, and with filled symbols for hydrophilic behavior. The separation work measured is depicted for the material pairing biofilm/aluminum b) and for the material pairing biofilm/biofilm c). Full bars denote the absence of material transfer whereas striped bars indicate that material transfer did occur. The pie charts above the bars visualize how often material transfer occurred for a given sample type. The amount of biofilm material transferred during a detachment test is summarized in d). All data shown represent mean values; error bars denote the standard deviation. The number of different samples analyzed per condition is specified in the respective subfigures.

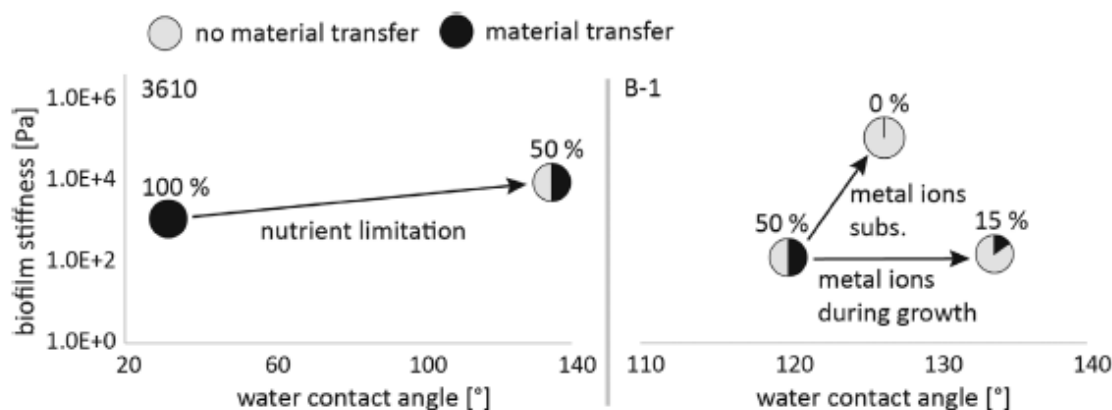
### 3.5. Biofilm Cultivation during Nutrient Limitation

The last option we explore to alter the physical properties of the biofilm is limiting the nutrient availability during biofilm growth. Different from B-1 biofilms (whose wetting behavior cannot be altered easily by this approach), *B. subtilis* 3610 biofilms exhibit wetting properties that sensitively depend on the

nutrient source.<sup>[54]</sup> This behavior is reproduced here: when grown on MSgg agar, those biofilms possess rose petal-like hydrophobicity (Figure 6a); at the same time, the stiffness of the biofilm is increased by one order of magnitude compared to cultivation on LB agar.

As consequence of these changes in the biofilm properties, we expect the biofilm to be less adhesive toward foreign





**Figure 7.** Relation between the material properties of the tested biofilms and the occurrence of material transfer during detachment tests conducted in the biofilm/biofilm configuration for 3610 biofilms (left) and B-1 biofilms (right). Data obtained at comparable conditions (similar biofilms, similar treatments, similar properties) were pooled. Black color denotes samples where material transfer occurred (and their fraction within a set of samples is referred to by the percentage values shown above the pie charts); gray color denotes samples, which did not show such material transfer.

surfaces and to be more difficult to rupture; in other words, we expect that those MSgg grown biofilm samples should tend to show adhesion failure without material transfer in the detachment tests. Indeed, this is what we observe for both, the material pairing biofilm/aluminum (Figure 6b) as well as the biofilm/biofilm configuration (Figure 6c). For the biofilm/aluminum pairing, no material transfer occurs anymore (this was always the case when the same biofilm was cultivated on LB agar) and adhesion failure clearly is the dominant mode of fracture. For the biofilm/biofilm pairing, we observe a similar trend—yet less pronounced: here, a material transfer occurs less often than when LB agar is used for biofilm cultivation, i.e., only in  $\approx 1/2$  of the experiments. Consistent with our expectation, we also find a cohesion failure here when no material transfer occurs; if such material transfer takes place, however, we find a mixed failure mode with only partial material transfer (Figure 6d). We interpret this finding such that the strong alteration in wetting behavior is mainly responsible for the observed alteration in biofilm adhesion and failure mode; of course, the increase in biofilm stiffness that accompanies the alteration in wetting may also contribute.

In summary, we could show that the measurement technique developed here is suitable for characterizing adhesive properties of bacterial biofilms toward metal surfaces and other biofilm surfaces alike. Two advantages of the method presented here are that this technique applies a uniform stress to the biofilm surface by controlling the normal force acting on the biofilm sample; this approach is very similar to established test protocols used for measuring the tensile strength of technical adhesives, and allows for characterizing the adhesive properties of biofilms *in situ*. Moreover, the experiments conducted here demonstrated that the adhesive properties and the fracture behavior of different biofilms generated by *B. subtilis* can be altered by changing the biofilm growth conditions or by exposing mature biofilms to cross-linking metal ions. Overall, we observed that two material properties of biofilms, i.e., the biofilms stiffness and the wetting behavior of the biofilm surface, affect the detailed adhesion behavior and failure

mode: Biofilms with a low stiffness and hydrophilic surfaces tend to exhibit a material transfer and thus mostly cohesion fractures whereas biofilms with a high stiffness and hydrophobic surfaces tend to show no material transfer and thus adhesion fractures (Figure 7).

At this point of research, there is no suitable theoretical model available to quantitatively rationalize the results obtained here. This is due to two main reasons: first, the intrinsic complexity of the material response of bacterial biofilms (which tend to show different types of nonlinear effects at large stress levels) is high;<sup>[38,40]</sup> second, the detailed configuration of our measurement setup would need to be accounted for in such a model, and this is not trivial either. For instance, the stress distribution across the biofilm layer (which is located between the two counterparts of the experimental setup) is dependent on various factors, such as the mechanical load distribution and the stiffness of the involved counterparts. To account for the latter two issues, probably a whole different set of experiments will be necessary – most likely also involving FE-based simulations.

Even though we here focused on biofilms generated by *B. subtilis* in combination with either other biofilm layers or aluminum surfaces exposed to air, the presented method can easily be extended further to study other material pairings or environments. For instance, the custom-made measuring head cannot only be equipped with an agar layer, but can also be adjusted to hold other materials such as ceramics or polymer materials (used in medical engineering), hydroxyapatite (as a model for teeth) or even tissue samples. Similarly, also the bottom sample holder of the rheometer could be modified to such that it holds biofilm samples harvested from their natural environment—provided that the substrate carrying the biofilm layer is sufficiently flat. Moreover, the measuring setup could be complemented with a cylindrical chamber such that the detachment process is conducted in a liquid environment; this would make it possible to test the adhesive properties of biofilms grown under water, e.g., those generated from marine bacteria. Finally, conducting those detachment tests on a

commercial research rheometer makes it also easily possible to control selected environmental conditions, such as changes the ambient temperature or humidity.

#### 4. Conclusion

Very often, biofilms are problematic for humans; for example, when they induce clogging or corrosion of pipes.<sup>[10,11]</sup> However, biofilms can also perform beneficial tasks, e.g., in wastewater treatment where they remove specific pollutants from the water.<sup>[56]</sup> Whether combating unwanted biofilms or when trying to employ them for human purposes, it is helpful to assess principles that govern the surface adhesion behavior of biofilms. With such knowledge and suitable, standardizable measurement protocols that quantify this material property, it should be possible to develop strategies that either enhance or reduce the adhesion properties of biofilms and other, slimy biomaterials.

#### Supporting Information

Supporting Information is available from the Wiley Online Library or from the author.

#### Acknowledgements

This project was funded by the Deutsche Forschungsgemeinschaft (DFG, German Research Foundation)—SFB 863, Projekt B11—111166240. The authors thank Bernardo Miller Naranjo for conducting pilot experiments.

Open access funding enabled and organized by Projekt DEAL.

#### Conflict of Interest

The authors declare no conflict of interest.

#### Author Contributions

M.K. and O.L. planned the experiments, which were conducted and analyzed by M.K. and C.A.S. The manuscript was written by M.K. and O.L.

#### Keywords

bacterial slime, biofilms, biomaterials, cohesion, detachment process, in situ test

Received: September 21, 2020

Revised: December 18, 2020

Published online:

[1] G. O'Toole, H. B. Kaplan, R. Kolter, *Annu. Rev. Microbiol.* **2000**, *54*, 49.

[2] H. Vlamakis, Y. Chai, P. Beauregard, R. Losick, R. Kolter, *Nat. Rev. Microbiol.* **2013**, *11*, 157.

- [3] H. C. Flemming, J. Wingender, U. Szewzyk, P. Steinberg, S. A. Rice, S. Kjelleberg, *Nat. Rev. Microbiol.* **2016**, *14*, 563.
- [4] A. Marguier, N. Poulin, C. Soraru, L. Vonna, S. Hajjar-Garreau, P. Kunemann, A. Airoudj, G. Mertz, J. Bardon, M. Delmée, V. Roucoules, D. Ruch, L. Ploux, *Adv. Mater. Interfaces* **2020**, *7*, 2000179.
- [5] H. Cao, O. Habimana, A. Safari, R. Heffernan, Y. Dai, E. Casey, *npj Biofilms Microbiomes* **2016**, *2*, 1.
- [6] S. C. Booth, I. F. S. George, D. Zannoni, M. Cappelletti, G. E. Duggan, H. Ceri, R. J. Turner, *Metallomics* **2013**, *5*, 723.
- [7] A. Bridier, R. Briandot, V. Thomas, F. Dubois-Brissonet, *Biofouling* **2011**, *27*, 1017.
- [8] S. Aggarwal, R. M. Hazalski, *Langmuir* **2012**, *28*, 2812.
- [9] A. W. Cense, E. A. G. Peeters, B. Gottenbos, F. P. T. Baaijens, A. M. Nuijs, M. E. H. van Dongen, *J. Microbiol. Methods* **2006**, *67*, 463.
- [10] I. B. Beech, J. Sunner, *Curr. Opin. Biotechnol.* **2004**, *15*, 181.
- [11] A. Vigneron, E. B. Alsop, B. Chambers, B. P. Lomans, I. M. Head, N. Tsesmezis, *Appl. Environ. Microbiol.* **2016**, *82*, 2545.
- [12] M. Wilson, *Sci. Prog.* **2001**, *84*, 235.
- [13] L. Liu, H. Shi, H. Yu, S. Yan, S. L. Biomater, *Science* **2020**, *8*, 4074.
- [14] G. Zhang, X. Zhang, Y. Yang, H. Zhang, J. Shi, X. Yao, X. Zhang, *Adv. Mater. Interfaces* **2020**, *7*, 1901706.
- [15] Q. Xie, H. Zeng, Q. Peng, C. Bressy, C. Ma, G. Zhang, *Adv. Mater. Interfaces* **2019**, *6*, 1900535.
- [16] R. D. Monds, G. A. O'Toole, *Trends Microbiol.* **2009**, *17*, 73.
- [17] E. S. Gloag, G. K. German, P. Stoodley, D. J. Wozniak, *Sci. Rep.* **2018**, *8*, 1.
- [18] H.-C. Flemming, J. Wingender, *Nat. Rev. Microbiol.* **2010**, *8*, 623.
- [19] S. S. Branda, A. Vik, L. Friedmann, R. Kolter, *Trends Biotechnol.* **2005**, *13*, 20.
- [20] I. W. Sutherland, *Trends Biotechnol.* **2001**, *9*, 222.
- [21] P. S. Stewart, J. W. Costerton, *Lancet* **2001**, *358*, 135.
- [22] C. B. Whitchurch, T. Tolker-Nielsen, P. C. Ragas, J. S. Mattick, *Science* **2002**, *295*, 1487.
- [23] Y. Liu, S. F. Yang, Y. Li, H. Xu, L. Qin, J. H. Tay, *J. Biotechnol.* **2004**, *110*, 251.
- [24] H. Fan, Z. Guo, *Biomater. Sci.* **2020**, *8*, 1502.
- [25] F. Alam, S. Kumar, K. M. Varadarajan, *ACS Biomater. Sci. Eng.* **2019**, *5*, 2093.
- [26] M. A. M. van Loosdrecht, J. Lyklema, W. Norde, A. J. B. Zehnder, *Microb. Ecol.* **1989**, *17*, 1.
- [27] R. Helbig, D. Günther, J. Friedrichs, F. Röbler, A. Lasagni, C. Werner, *Biomater. Sci.* **2016**, *4*, 1074.
- [28] W. M. Dunne, *Clinical Microbiology Reviews* **2002**, *15*, 155.
- [29] T. R. Garret, M. Bhakoo, Z. Zhang, *Prog. Nat. Sci.* **2008**, *18*, 1049.
- [30] I. Klapper, J. Dockery, *Phys. Rev. E* **2006**, *74*, 031902.
- [31] M. G. Mazza, *J. Phys. D: Appl. Phys.* **2016**, *49*, 203001.
- [32] S. Tsuneda, H. Aikwa, H. Hayashi, A. Yuasa, A. Hirata, *FEMS Microbiol. Lett.* **2003**, *223*, 287.
- [33] A. Harimawan, Y. P. Tin, *Colloids Surf., B* **2016**, *146*, 459.
- [34] S. Grumbein, M. Opitz, O. Lielieg, *Metallomics* **2014**, *6*, 1441.
- [35] S. Kesel, S. Grumbein, I. Gümperlein, M. Tallawi, A.-K. Marel, O. Lielieg, M. Opitz, *Appl. Environ. Microbiol.* **2016**, *82*, 2424.
- [36] M. Klotz, M. Kretschmer, A. Goetz, S. Ezedam, O. Lielieg, M. Opitz, *RSC Adv.* **2019**, *9*, 11521.
- [37] M. Kretschmer, O. Lielieg, *Biomater. Sci.* **2020**, *8*, 1923.
- [38] O. Lielieg, M. Caldara, R. Baumgärtel, K. Ribbeck, *Soft Matter* **2011**, *7*, 3307.
- [39] A. Di Stefano, E. D'Aurizio, O. Trubiani, R. Grande, E. Di Campi, M. Di Giulio, S. Di Bartolomeo, P. Sozio, A. Iannitelli, A. Nostro, L. Cellini, *Microb. Biotechnol.* **2009**, *2*, 634.
- [40] S. Jana, S. G. V. Charlton, L. E. Eland, J. G. Burgess, A. Wipart, T. P. Curtis, J. Chen, *npj Biofilms Microbiomes* **2020**, *6*, 1.
- [41] L. Pavlovsky, J. G. Younger, M. J. Solomon, *Soft Matter* **2013**, *9*, 122.
- [42] G. Habonicht, *Kleben: Grundlagen, Technologien, Anwendungen*, Springer, Berlin **2006**.

- [43] DIN EN Vol. 15870, Klebstoffe—Bestimmung der Zugfestigkeit von Stumpfklebungen (ISO 6922:1987 modifiziert), Deutsche Fassung, p. 2009-08.
- [44] DIN EN 1465, Klebstoffe—Bestimmung der Zugscherfestigkeit von Überlappungsklebungen, Deutsche Fassung, p. 2009-07.
- [45] ISO 11003-Vol. 2:2019-06, Adhesives—Determination of shear behaviour of structural adhesives: Part 2. Tensile test method using thick adherends.
- [46] ISO 10033-1:2011-04, Laminated Veneer Lumber (LVL)—Bonding quality: Part 1. Test methods.
- [47] M. J. Chen, Z. Zhang, T. R. Bott, *Biotechnol. Tech.* **1998**, *12*, 875.
- [48] J. Yan, A. Moreau, S. Khodaparast, A. Perazzo, J. Feng, C. Fei, S. Mao, S. Mukherjee, A. Košmrlj, N. S. Wingreen, B. L. Bassler, H. A. Stone, *Adv. Mater.* **2018**, *30*, 1804153.
- [49] S. S. Branda, J. E. González-Pastor, S. Ben-Yehuda, R. Losick, R. Kolter, *Proc. Natl. Acad. Sci. USA* **2001**, *98*, 11621.
- [50] M. Morikawa, M. Ito, T. Imanaka, *J. Ferment. Bioeng.* **1992**, *74*, 255.
- [51] A. Goto, M. K. Bioscience, *Biotechnol. Biochem.* **1992**, *56*, 1031.
- [52] A. F. Stalder, G. Kulik, D. Sage, L. Barbieri, P. Hoffmann, *Colloids Surf., A* **2006**, *286*, 92.
- [53] C. F. Garcia, F. Stangl, A. Götz, W. Zhao, S. A. Sieber, M. Opitz, O. Lieleg, *Biomater. Sci.* **2019**, *7*, 220.
- [54] M. Werb, C. F. Garcia, N. C. Bach, S. Grumbein, S. A. Sieber, M. Opitz, O. Lieleg, *npj Biofilms Microbiomes* **2017**, *3*, 1.
- [55] C. F. Garcia, M. Kretschmer, C. N. Lozano-Andrade, M. Schönleitner, A. Dragoš, Á. T. Kovács, O. Lieleg, *npj Biofilms Microbiomes* **2020**, *6*, 1.
- [56] W. K. Shieh, J. D. Keenan, *Bioproducts*, Springer, Berlin **1986**.

A.3.1 Supplementary information for: *Biofilm adhesion to surfaces is modulated by biofilm wettability and stiffness*

Supplemental information for

**Biofilm Adhesion to Surfaces is Modulated  
by Biofilm Wettability and Stiffness**

*Martin Kretschmer<sup>1,2</sup>, Carina Anke Schüßler<sup>1,2</sup> and Oliver Lieleg<sup>1,2,\*</sup>*

<sup>1</sup> Department of Mechanical Engineering and Munich School of Bioengineering,  
Technical University of Munich,  
Boltzmannstraße 11, 85748 Garching, Germany

<sup>2</sup> Center for Protein Assemblies (CPA),  
Technical University of Munich,  
Ernst-Otto-Fischer Straße 8, 85747, Garching, Germany

\* Corresponding author:

Prof. Dr. Oliver Lieleg  
Department of Mechanical Engineering and Munich School of Bioengineering,  
Technical University of Munich,  
Boltzmannstraße 11, 85748 Garching, Germany  
e-mail: [oliver.lieleg@tum.de](mailto:oliver.lieleg@tum.de)  
phone: +49 89 289 10952, fax: + 49 89 289 10801

*Keywords:* cohesion, detachment, bacterial slime, in situ test

### 1. Technical drawings of the custom made components for the detachment test

All of the technical drawings (Figure S1 – S5) were created with Autodesk inventor Professional 2020 (Autodesk Corp., San Rafael, USA).

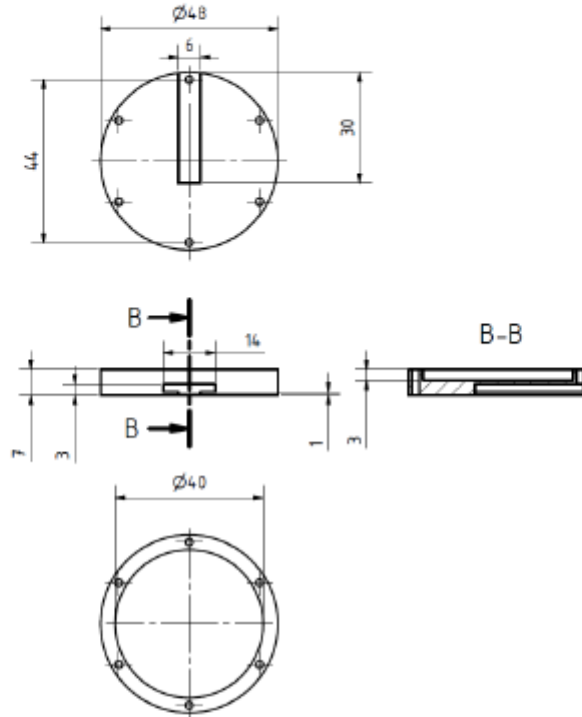


Figure S1: PTFE cup as used for the detachment tests. All measures are given in millimeters.

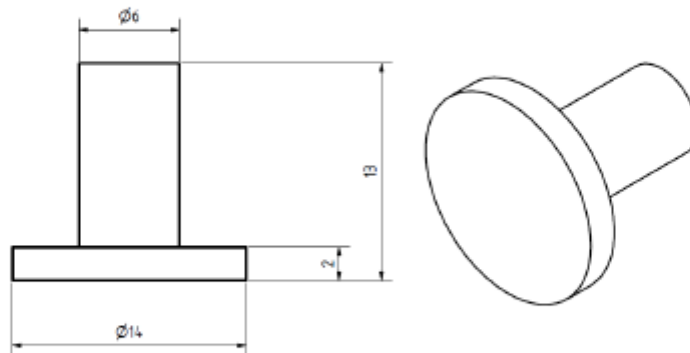
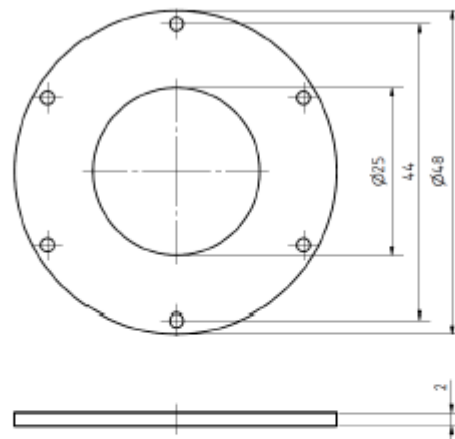
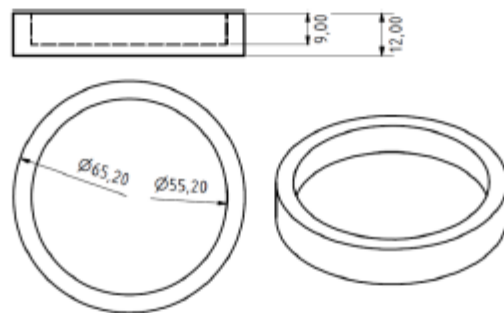


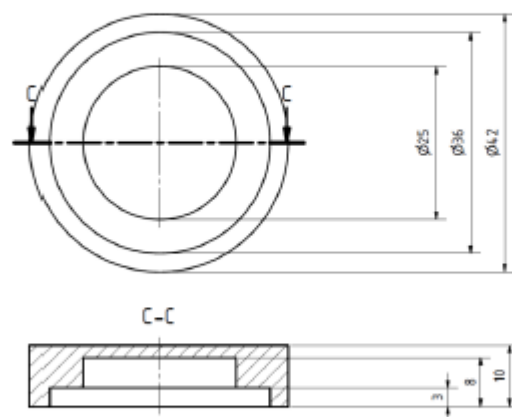
Figure S2: PTFE pin as used for the detachment tests. All measures are given in millimeters.



**Figure S3: PTFE ring as used for the detachment tests. All measures are given in millimeters.**



**Figure S4: PTFE bottom plate as used for the detachment tests. All measures are given in millimeters.**



**Figure S5: PTFE form to solidify agar hats as used for the detachment tests. All measures are given in millimeters.**

## 2. Influence of treating a *B. subtilis* B-1 biofilms (grown either in petri dishes or on hat-shaped agar layers) with a $\text{CuCl}_2$ solution

Figure S6 depicts the viscoelastic moduli of *B. subtilis* B-1 biofilms before and after treatment with a  $\text{CuCl}_2$  solution. Biofilms grown on agar layers generated in petri dishes and on dedicated hat-shaped samples had to be treated differently with the  $\text{CuCl}_2$  solution (see main text for details). However, both treatment variants returned highly similar outcomes.

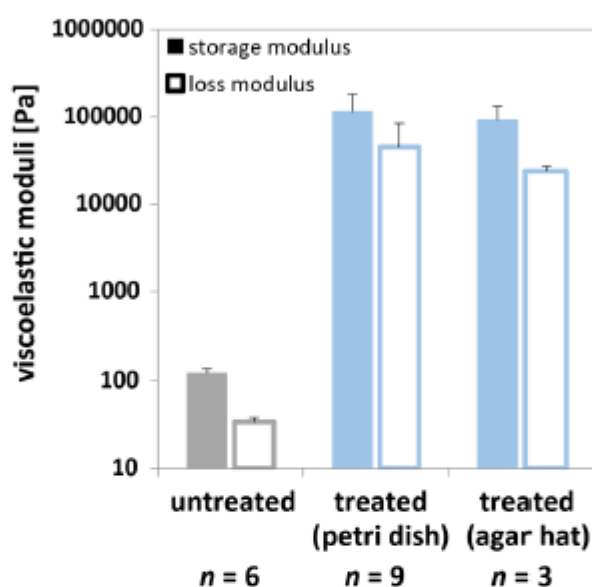
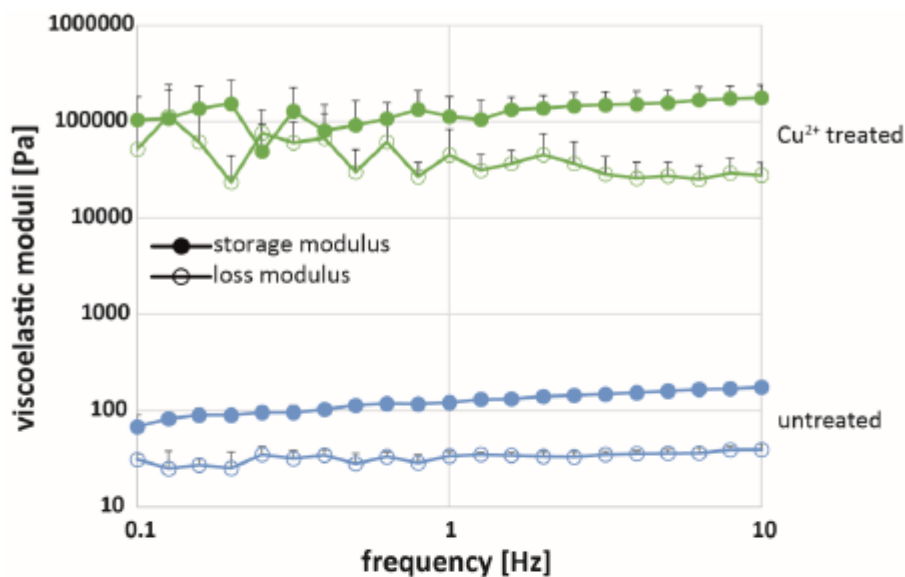


Figure S6: Viscoelastic properties of *B. subtilis* B-1 biofilms before (grey bars) and after (blue bars) treatment with a  $\text{CuCl}_2$  solution. Full bars denote the storage modulus,  $G'$ , and open bars the loss modulus,  $G''$ . All data shown represent mean values; error bars denote the standard deviation as obtained from at least three independent samples as specified in the figure.

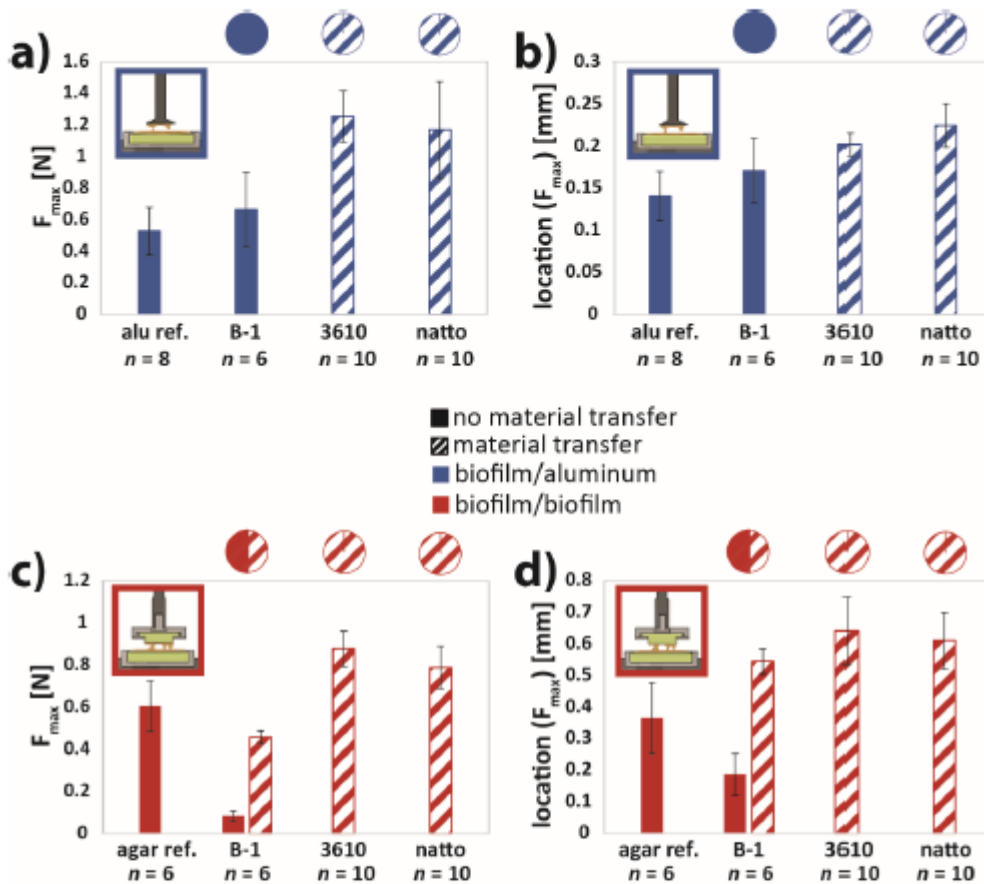
### 3. Exemplary frequency spectra obtained for *B. subtilis* B-1 biofilms



**Figure S7:** Viscoelastic response of *B. subtilis* B-1 biofilms grown on LB agar. Frequency spectra are shown for untreated *B. subtilis* B-1 biofilms (blue data) and *B. subtilis* B-1 biofilms treated with  $\text{CuCl}_2$  ions after biofilm cultivation (green data). In either case, there is only a very weak dependency of the measured moduli on the probing frequency. Full symbols denote the storage modulus,  $G'$ , and open symbols denote the loss modulus,  $G''$ . The values shown represent the mean obtained from six independent measurements. The corresponding samples were generated from two biological replicates. The error bars (which are sometimes smaller than the symbol size) represent the standard deviation.




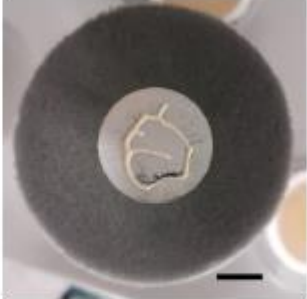

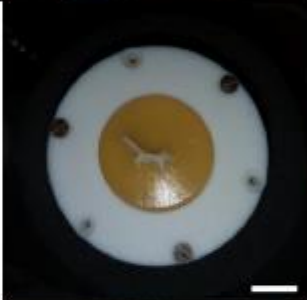

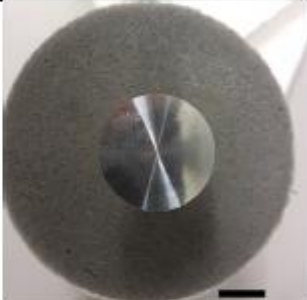

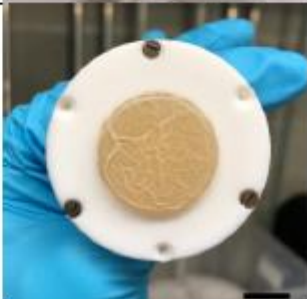
4. Maximal force and the corresponding separation distance as obtained from of the detachment tests with *B. subtilis* biofilms and reference samples



**Figure S8: Maximal force a), c) and position of this force peak b), d) as obtained from detachment tests.** Biofilms generated from *B. subtilis* B-1, *B. subtilis* 3610 and *B. subtilis natto* are compared. Data obtained for 'empty' material pairings (where no biofilms were grown on the agar layers) are depicted as references. For data shown in a) and b), the biofilm/aluminum configuration was used, data shown in c) and d) was obtained in the biofilm/biofilm configuration. Full bars denote absence of material transfer whereas striped bars indicate that material transfer did occur. The pie charts above the bars visualize how often material transfer occurred for a given sample type. All data shown represents mean values; error bars denote the standard deviation. The number of different samples analyzed per condition is specified in the respective subfigures.

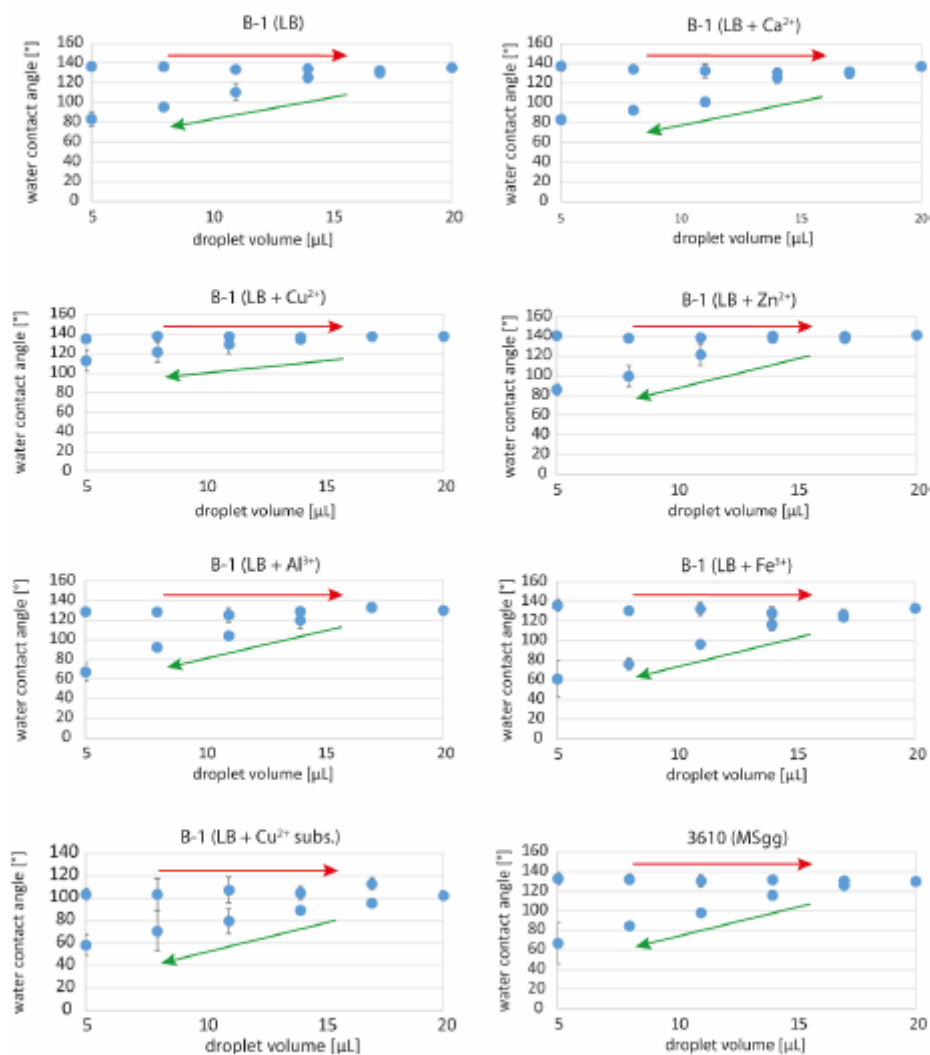
5. Example images of biofilms showing different types of fracture behavior

Table S1: The images shown below depict the surfaces of the respective partners used in the two material pairings after the detachment tests. The scale bars shown in the images represent 1 cm.

<i>sample</i>	<i>bottom layer</i>	<i>measuring head</i>	<i>fracture type</i>
biofilm/ aluminum: <i>B. subtilis natto</i> (grown on LB agar)			cohesion failure (material transfer)
biofilm/biofilm: <i>B. subtilis natto</i> (grown on LB agar)			cohesion failure (material transfer)
biofilm/ aluminum: <i>B. subtilis</i> 3610 (grown on MSgg agar)			adhesion failure (no material transfer)
biofilm/biofilm: <i>B. subtilis</i> B-1 (grown on LB agar)			adhesion failure (no material transfer)

## 6. Contact angle hysteresis measurements on different biofilms

To specify the type of superhydrophobicity the different biofilm variants exhibit, contact angle hysteresis measurements were conducted. Here, as shown in Figure S9, the volume of a wetting water droplet was increased from initially 5  $\mu\text{L}$  to 20  $\mu\text{L}$  and then reduced to 5  $\mu\text{L}$  again (in increments of 3  $\mu\text{L}$ ). Three independent samples were investigated, and the mean value together with the corresponding standard deviation was calculated, accordingly.



**Figure S9: Contact angle hysteresis measurements for all superhydrophobic biofilm variants.** Red arrows indicate an advancing droplet volume and green arrows a receding droplet volume. All data shown represent mean values; error bars denote the standard deviation as obtained from three independent samples each.

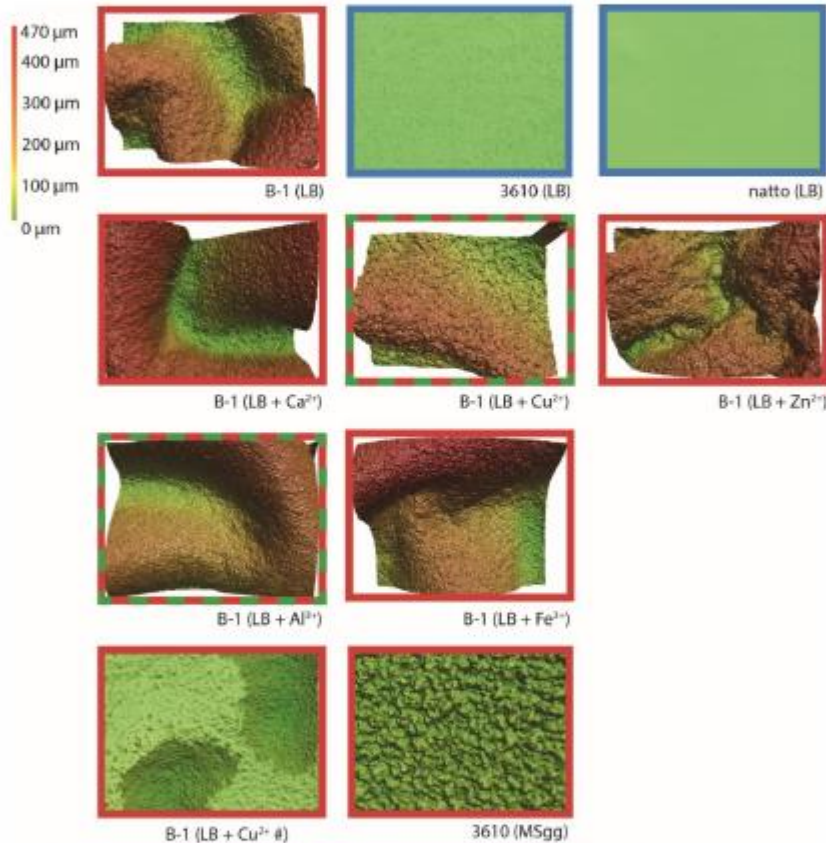
Based on those hysteresis measurements, the difference between the contact angles determined at the first and last step of those dynamic wetting tests (mean value with corresponding standard deviation of the  $\Delta CA$ ), was calculated from three independent samples of each sample type. The results are compiled in Table S2:

**Table S2: Contact angle hysteresis values as calculated from the data shown in Figure S1.** The difference between the initial and final contact angle,  $\Delta CA$ , is depicted for each biofilm variant tested in this study. Values shown depict averages from three independent wetting hysteresis tests; error values represent the corresponding standard deviation. The hash (#) symbol indicates conditions where the  $Cu^{2+}$  ions were not added to the agar layer during growth, but where an ion solution was added to the fully grown, mature biofilm from above (see main text for details).

<i>bacterial strain</i>	B-1	B-1	B-1	B-1	B-1	B-1	B-1	3610
<i>growth media</i>	LB	LB	LB	LB	LB	LB	LB	MSgg
<i>added ion</i>	-	$Ca^{2+}$	$Cu^{2+}$	$Zn^{2+}$	$Al^{3+}$	$Fe^{3+}$	$Cu^{2+}$ (#)	-
$\Delta CA$ [°]	$53 \pm 5$	$54 \pm 5$	$22 \pm 9$	$55 \pm 4$	$62 \pm 8$	$75 \pm 14$	$45 \pm 4$	$66 \pm 26$

## 7. Topographical characterization of the biofilm surfaces with laser scanning profilometry

To investigate the surface structure of the different biofilm variants, topographical images were obtained with laser scanning profilometry (Figure S10). Profilometric images were obtained with a 3D laser scanning confocal microscope (VK-X1000 series, Keyence Corporation, Osaka, Japan) at 20x magnification resulting in an image size of 705  $\mu\text{m}$  x 529  $\mu\text{m}$ . The topographical data was then evaluated with the software MultiFileAnalyzer (Version 2.1.3.89, Keyence).



**Figure S10: Topographical images of biofilm surfaces obtained with laser scanning profilometry.** One representative image is shown for each biofilm variant studied in this manuscript. The dimensions of each figure are 705  $\mu\text{m}$  x 529  $\mu\text{m}$ . All pictures of biofilms that were characterized as superhydrophobic (red frames: rose-like; green/red frames: partial lotus-like and partial rose like) show roughness features both on the micro- and nanoscale. In contrast, hydrophilic biofilms (blue frames) have very smooth surfaces. The hash (#) symbol indicates conditions where the  $\text{Cu}^{2+}$  ions were not added to the agar layer during growth, but where an ion solution was added to the fully grown, mature biofilm from above (see main text for details).

10

From the topographical images depicted in Figure S10, metrological parameters were calculated to quantify the surface roughness of the different biofilm variants. Here, two parameters defined in the ISO 25178 norm were used: First, the root mean square surface roughness ( $Sq$ ),

$$Sq = \sqrt{\frac{1}{A} \iint_A z^2(x,y) dx dy} \quad (1)$$

and, second, the developed interfacial area ratio ( $Sdr$ ),

$$Sdr = \frac{1}{A} \left[ \iint_A \left( \sqrt{\left[ 1 + \left( \frac{\partial z(x,y)}{\partial x} \right)^2 + \left( \frac{\partial z(x,y)}{\partial y} \right)^2 \right]} - 1 \right) dx dy \right] \quad (2)$$

For each biofilm variant, the  $Sq$  value and  $Sdr$  parameter of three independent samples were determined, and the mean value together with the corresponding standard deviation was calculated, accordingly. The obtained results are compiled in Table S3 shown below:

**Table S3: Metrological roughness parameters as calculated from three topographical images each.** Values shown depict averages; error values represent the corresponding standard deviation. The hash (#) symbol indicates conditions where the  $\text{Cu}^{2+}$  ions were not added to the agar layer during growth, but where an ion solution was added to the fully grown, mature biofilm from above (see main text for details).

<i>bacterial strain</i>	<i>growth media</i>	<i>added ion</i>	<i>Sdr</i> [%]	<i>Sq</i> [ $\mu\text{m}$ ]
B-1	LB	-	607 $\pm$ 412	116 $\pm$ 7
3610	LB	-	3.0 $\pm$ 0.7	1.9 $\pm$ 1.1
<i>natto</i>	LB	-	0.06 $\pm$ 0.02	1.7 $\pm$ 0.9
B-1	LB	$\text{Ca}^{2+}$	1037 $\pm$ 574	159 $\pm$ 30
B-1	LB	$\text{Cu}^{2+}$	1246 $\pm$ 666	128 $\pm$ 25
B-1	LB	$\text{Zn}^{2+}$	534 $\pm$ 276	96 $\pm$ 30
B-1	LB	$\text{Fe}^{3+}$	1842 $\pm$ 1566	156 $\pm$ 22
B-1	LB	$\text{Al}^{3+}$	792 $\pm$ 738	107 $\pm$ 34
B-1	LB	$\text{Cu}^{2+}$ (#)	18 $\pm$ 4	17 $\pm$ 5
3610	MSgg	-	160 $\pm$ 11	8.8 $\pm$ 0.3

This metrological analysis revealed, that all hydrophilic biofilms (*B. subtilis* 3610 (LB) and *B. subtilis natto* (LB)) exhibit a very smooth and featureless surface. In contrast, all hydrophobic biofilms exhibit multi-scale roughness on the micro- and nanolevel. In addition, for all B-1 biofilms we detected additional, mesoscopic waviness features on their surface. Such waviness is absent for *B. subtilis* 3610 biofilm cultivated on MSgg agar and reduced for the B-1 biofilm treated with a  $\text{Cu}^{2+}$  solution subsequent to its cultivation. Together, this indicates that the micro- and nanoscale roughness features are highly relevant for establishing

superhydrophobic properties; in contrast, the mesoscopic waviness is less important for the wetting behavior of the biofilms.

We determined the largest  $Sdr$  and  $Sq$  values for biofilms of B-1 grown on LB agar enriched with  $Ca^{2+}$ ,  $Cu^{2+}$ ,  $Fe^{3+}$  or  $Al^{3+}$ . Partial lotus-like superhydrophobic behavior was found for B-1 biofilms grown on LB agar enriched with  $Cu^{2+}$  or  $Al^{3+}$ , which is in agreement with their very high surface roughness. B-1 biofilms grown on LB agar enriched with  $Ca^{2+}$  or  $Fe^{3+}$ , however, showed rose-like superhydrophobicity. In those cases, the very high surface roughness values we measured are most likely due to the high waviness features present on those two biofilm variants. As argued above, this mesoscopic waviness is, however, less relevant for the wetting behavior of a biofilm than its micro- and nanoscale roughness.

### 8. Corrosion of the aluminum measuring head used in the detachment tests conducted with $\text{CuCl}_2$ treated *B. subtilis* B-1 biofilms

Figure S11 depicts an image of the aluminum measuring head used for the biofilm detachment tests with  $\text{CuCl}_2$ -treated *B. subtilis* biofilms. Here, clear signs of corrosion are visible with the naked eye. A profilometric analysis demonstrates that the surface roughness of such a corroded aluminum measuring head (as quantified by the root mean square height,  $S_q$ ) is almost twice as high as the corresponding value obtained for a new, unused measuring head. The profilometric images were obtained with a 3D laser scanning confocal microscope (VK-X1000 series, Keyence Corporation, Osaka, Japan). The images were obtained at 10x magnification resulting in an image size of  $1412 \mu\text{m} \times 1059 \mu\text{m}$ . The obtained topographical data was then evaluated with the software MultiFileAnalyzer (Version 2.1.3.89, Keyence).

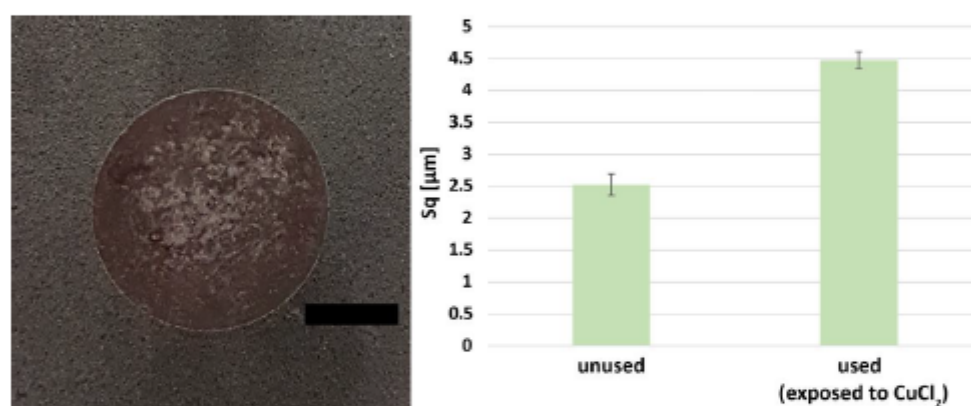


Figure S11: Photographic image (left) and roughness analysis (right) of an aluminum measuring head that was used for conducting detachments tests with *B. subtilis* B-1 biofilm samples that were exposed to a  $\text{CuCl}_2$  solution. The scale bar in the photograph represents 1 cm. Data shown in the right subfigure depicts the average roughness value as calculated from three topographical images obtained at different locations of the measuring head surface; the error bars represent the standard deviation.



## A.4 Viscoelastic behavior of chemically fueled supramolecular hydrogels under load and influence of reaction side products

# communications materials

ARTICLE



<https://doi.org/10.1038/s43246-021-00202-6>

OPEN

## Viscoelastic behavior of chemically fueled supramolecular hydrogels under load and influence of reaction side products

Martin Kretschmer <sup>1,2</sup>, Benjamin Winkeljann <sup>1,2</sup>✉, Brigitte A. K. Kriebisch <sup>3,4</sup>, Job Boekhoven <sup>3,4</sup> & Oliver Lieleg <sup>1,2</sup>✉

About ten years ago, chemically fueled systems have emerged as a new class of synthetic materials with tunable properties. Yet, applications of these materials are still scarce. In part, this is due to an incomplete characterization of the viscoelastic properties of those materials, which has – so far – mostly been limited to assessing their linear response under shear load. Here, we fill some of these gaps by comparing the viscoelastic behavior of two different, carbodiimide fueled Fmoc-peptide systems. We find that both, the linear and non-linear response of the hydrogels formed by those Fmoc-peptides depends on the amount of fuel driving the self-assembly process – but hardly on the direction of force application. In addition, we identify the concentration of accumulated waste products as a novel, so far neglected parameter that crucially affects the behavior of such chemically fueled hydrogels. With the mechanistic insights gained here, it should be possible to engineer a new generation of dynamic hydrogels with finely tunable material properties that can be tailored precisely for such applications, where they are challenged by mechanical forces.

<sup>1</sup>Department of Mechanical Engineering and Munich School of Bioengineering, Technical University of Munich, Boltzmannstraße 15, 85748 Garching, Germany. <sup>2</sup>Center for Protein Assemblies (CPA), Ernst-Otto-Fischer Straße 8, 85748 Garching, Germany. <sup>3</sup>Department of Chemistry, Technical University of Munich, Lichtenbergstrasse 4, 85748 Garching, Germany. <sup>4</sup>Institute for Advanced Study, Technical University of Munich, Lichtenbergstrasse 2a, 85748 Garching, Germany. ✉email: [benjamin.winkeljann@tum.de](mailto:benjamin.winkeljann@tum.de); [oliver.lieleg@tum.de](mailto:oliver.lieleg@tum.de)

Inspired by the dynamic assembly and disassembly of biomolecules at the expense of chemical energy<sup>1,2</sup>, intensive research has been conducted to understand the molecular mechanisms driving this self-assembly process to develop artificial analogs<sup>3–10</sup>. Both, biological and man-made, chemically fueled dynamic materials dramatically differ from in-equilibrium materials as they exist outside of thermodynamic equilibrium; in other words, a driving force is necessary to obtain and maintain these materials in their non-equilibrium state<sup>11,12</sup>. One strategy to achieve such a dynamic behavior is by using fuel-driven reaction cycles<sup>13–21</sup>. Here, the energy required to keep the material out of equilibrium is generated by the irreversible conversion of a “fuel” molecule. In nature, a prominent example for such a fuel-based assembly process can be found in the cytoskeleton<sup>22</sup> here, the building blocks of the actin cortex (i.e., G-actin subunits) assemble into filaments (F-actin) by consuming energy provided by the hydrolysis of ATP<sup>23,24</sup>. Pioneering work in synthetically recreating this reaction was done in the 2010s by van Esch and co-workers, who presented a chemical reaction cycle that catalyzes the hydrolysis of methylating agents<sup>25</sup>. Since then, various other strategies and reaction cycles have been introduced<sup>18</sup>. Whereas the main idea remains the same in all those examples, many different, fascinating systems have been presented including pulsating micelles<sup>26</sup>, self-assembling metal-organic framework systems<sup>27</sup>, or loadable, DNA-based actuators<sup>28</sup>.

In 2017, Tena-Solsona et al. introduced chemically fueled materials based on fluorenylmethyloxycarbonyl (Fmoc)-protected peptides<sup>29</sup>. Here, self-assembly is driven by the hydration of a carbodiimide fuel. In such Fmoc-based peptide systems, the properties of the self-assembled materials are broadly tunable, and this is achieved by a tailored variation of the conjugated amino acid sequence<sup>29</sup>. In detail, supramolecular structures with tunable shape, size, and lifetime could be created. Although the reaction kinetics governing the lifecycle of such assembled structures have been investigated extensively, one detail remains partially neglected: the role of waste products. Compared to biological systems, where the concentrations of the contributing molecular components are strictly regulated by the cellular machinery, such control is difficult to achieve in closed, artificial systems; here, waste products accumulate over the lifetime of the material. It was speculated previously that the reaction waste products might interact with the supramolecular structures and disturb their assembly process<sup>30</sup>. To avoid such interference by waste accumulation effects, Sorrenti et al. created dynamic self-assemblies in a membrane reactor which allowed waste molecules to leave the microcompartment<sup>31</sup>.

The micro- and mesoscopic properties of such supramolecular assemblies, especially fiber-forming peptides, also directly impact macroscopic material characteristics. Specifically, a dynamic transition from a solution into a gel (and back) was observed, and those transitions were shown to follow the kinetics of the molecular assembly process<sup>29,32</sup>. Depending on the detailed structures generated during the self-assembly procedure, the lifetime of such macroscopic gels can be broadly tunable. Yet, so far, experimental studies investigating the mechanical properties of such out-of-equilibrium materials were limited to the linear response regime<sup>32–34</sup>. The nonlinear behavior of these chemically fueled materials has been underexplored. Partially this might be caused by the fact that both the exact point where Hooke’s law does not hold true anymore and the type of nonlinear material response setting in beyond this point cannot easily be predicted; instead, both items require separate investigations using the specialized methodology. Such nonlinear material properties are, however, relevant when a material is exposed to a large mechanical load—be it shear or compression forces. Depending on the application area such (or similar) self-assembling, dynamic materials might

be further developed; in the future, such material behavior under load can be highly important.

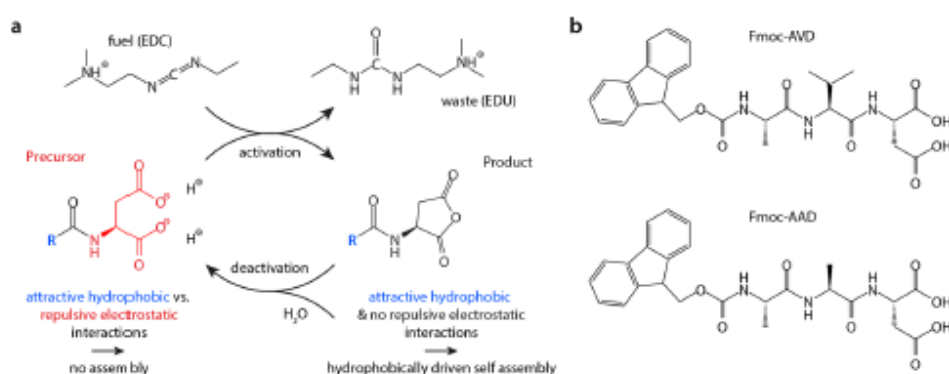
Here, we investigate the macroscopic material properties of hydrogels formed by two different self-assembling (Fmoc)-protected peptides derivatives. We first characterize both, the linear and nonlinear viscoelastic properties of these two systems with respect to initial fuel concentration and time. Then, we assess the failure behavior of the hydrogel materials when exposed to different levels of mechanical stress. We demonstrate how the waste products generated by the fuel conversion affects the mechanical properties of the hydrogels—both, when added to the system prior to gel formation and when accumulating within the system over time. By comparing results obtained with the full waste product to data obtained with waste-mimetics, we identify hydrophobic and (to a lower extent) electrostatic interactions between the Fmoc-based peptides and the waste molecules to be the critical forces that challenge the assembly process. Furthermore, our results suggest that the molecular design of the peptide sequence plays a critical role for how waste accumulation influences the dynamic self-assembly/disassembly process.

## Results and discussion

**Peptide design and dynamic assembly process.** Dynamic self-assembling hydrogels based on Fmoc-protected peptides (Fmoc-aa) derivatives have been introduced previously<sup>29</sup>. When solubilized in a suitable aqueous buffer system, the anionic peptides repel each other through electrostatic forces established by the dicarboxylate groups. The peptides are designed to react with a carbodiimide-based fuel in an activation reaction. Upon activation, the dicarboxylate-based precursor is converted into its corresponding cyclic anhydride at the expense of 1-ethyl-3-(3-dimethylaminopropyl)carbodiimid-hydrochlorid (EDC) which is converted in 1-[3-(dimethylamino)propyl]-3-ethylurea (EDU). In the aqueous environment, the activated anhydride state is not stable and will spontaneously hydrolyze to yield its precursor state (Fig. 1a). Thus, when fuel is added to the precursor, a population of transiently activated anhydride product is obtained. In this anhydride state, the electrostatic repulsion between the molecules is eliminated, which results in their assembly. However, due to the transient nature of the anhydride, a dynamic assembly is created which is regulated through the kinetics of activation and deactivation. When a finite amount of fuel is added, assemblies emerge with a finite lifetime. The range of assemblies that can be obtained by using EDC as fuel includes colloids<sup>35</sup>, vesicles<sup>36</sup>, oil-based<sup>37,38</sup> and coacervate-based<sup>39,40</sup> droplets, and hydrogel-forming fibers<sup>32</sup>.

In the peptide design, the repulsive and attractive forces must be balanced such that the precursor remains in solution but the product assembles. Two possible peptide sequences that allow for such controlled self-assembly of Fmoc-peptide-conjugates into supramolecular structures are Fmoc-alanine-valine-aspartic acid (Fmoc-AVD) and Fmoc-alanine-alanine-aspartic acid (Fmoc-AAD) (Fig. 1b). Here, the substitution of valine with alanine slightly reduces the hydrophobic character of the tripeptide. As a consequence of this small modification, a larger proportion of the Fmoc-constructs can be expected to switch into the disassembled state thus rendering supramolecular aggregates less pronounced<sup>41</sup>. Furthermore, as demonstrated previously using confocal microscopy and cryo-TEM imaging, this modification also alters the morphology of the assembled structures from wide, flat fibers (obtained for Fmoc-AVD) into thinner, more twisted helical structures (observed for Fmoc-AAD)<sup>41</sup>.

**Rheological behavior of dynamic peptide-based hydrogels.** When we investigate the time-dependent viscoelastic moduli of



**Fig. 1** Schematic illustration of the reaction cycle and peptide precursors used in this study. **a** In the activation reaction, aspartic acid derivatives of the precursor peptide react in the presence of a suitable fuel (here: EDC) and are converted into their corresponding anhydride product; at the same time, a waste product (here: EDU) is generated. In the deactivation reaction, the aspartic acid anhydride derivative is hydrolyzed again. Through the correct design of the Fmoc-peptides, attractive and repulsive forces can be balanced such that a hydrophobically driven self-assembly process is enabled—but only in the product state. Hydrophobic sidechains are depicted in blue and anionic ones in red. **b** Structural formula of the two synthetic Fmoc-peptides used here.

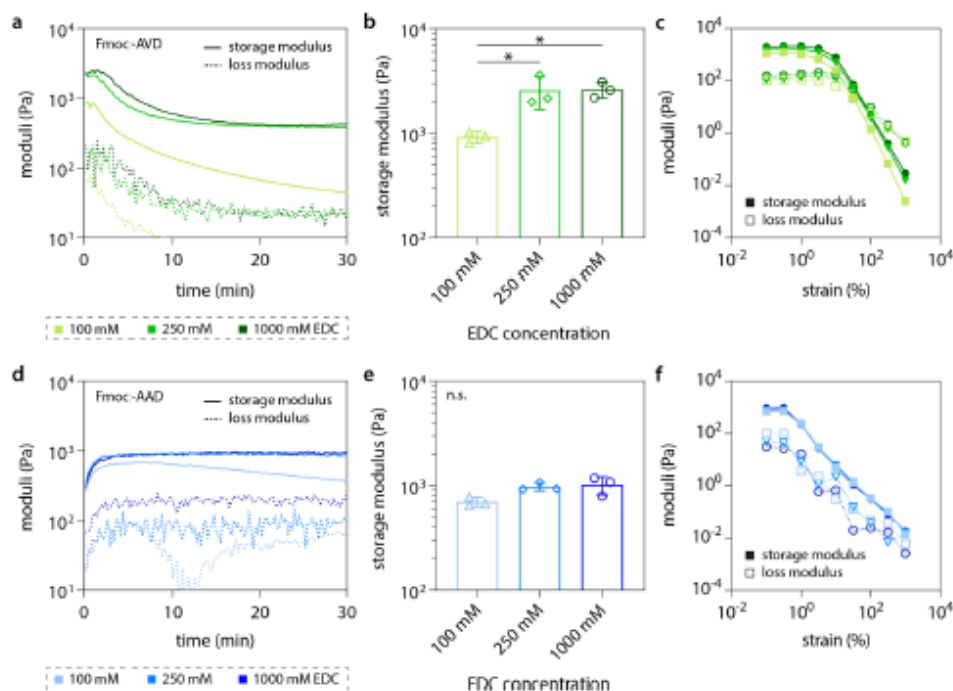
the Fmoc-AVD hydrogels, we observe a behavior consistent with the underlying reaction cycle driving the dynamic self-assembly of the system: When the Fmoc-AVD samples are premixed with the “fuel”, the system is already in a hydrogel state when the rheological characterization starts, i.e., the material is dominated by elastic properties as represented by the storage modulus  $G'$ . Then, we observe a quick increase in both viscoelastic moduli, which reach their respective maxima within the first 2 min of the measurement. Afterward, both viscoelastic moduli slowly decrease over time and reach plateaus after ~15–20 min (Fig. 2a). Further changes in the viscoelastic properties of this system are not observable—even when the moduli are tracked for up to 120 min (Supplementary Results Section 1.1 and Supplementary Fig. 1). Macroscopically, the formation of supramolecular structures can be visualized by a transition from clear to turbid samples. In addition, confocal images give insight into the size and shape of the supramolecular clusters formed in the hydrogels (Fig. 2). Over time, the turbidity of samples created with low (100 mM) or medium (250 mM) EDC concentrations slightly decreases; however, inverted tube tests confirm the ongoing presence of an elastically dominated material (Supplementary Results Section 1.1 and Supplementary Fig. 2).

In previous work, it was shown that the time point, at which such a dynamic peptide hydrogel system reaches its highest elasticity, corresponds to the moment when the maximal anhydride concentration is present in the system<sup>29</sup>. The subsequent hydrolysis of this anhydride is responsible for a slow disassembly of the gel, which causes both viscoelastic moduli to decline. Yet, a certain amount of the Fmoc-AVD molecules remains trapped in self-assembled fibers even though they have returned into their initial, self-repelling precursor state. Thus, we hypothesize that such kinetically trapped fibers are responsible for the remaining elastic-dominated properties of the system, which persist even though all the fuel can be expected to be consumed.

Consistent with previous results obtained with similar systems<sup>29</sup>, the amount of fuel that is initially present affects the viscoelastic properties of the assembled hydrogel in two ways: first, increasing the fuel concentration from 100 to 250 mM extends the lifetime of the gel, i.e., it increases the time span beyond which the elastic properties of the system start to decrease (Fig. 2a). Second, such an increase in the fuel concentration also boosts the maximal elasticity of the gel (Fig. 2b).

However, further increasing the fuel concentration to 1000 mM only slightly affects the properties of the assembled hydrogel by weakly increasing its lifetime (Fig. 2a) without significantly increasing the maximal gel stiffness. This finding indicates that, at those particular conditions, the conversion reaction from precursor to anhydride has probably reached its maximum yield<sup>29</sup>. So far, we have assessed the viscoelastic properties of the Fmoc-AVD system in the linear response regime, i.e., a small mechanical load where Hooke's law holds. When we probe the nonlinear properties of the same set of samples by large amplitude oscillatory shear (LAOS) measurements (where we continuously increase the oscillatory strain applied to the samples while tracking the viscoelastic moduli; see Methods section “LAOS measurements” for details), we find that all three Fmoc-AVD hydrogel variants show linear material response up to strain levels of  $\sim\gamma = 1\text{--}2\%$  (Fig. 2c). At this critical point, where the nonlinear response regime of the hydrogels is left, strain weakening sets in. The corresponding maximal stress levels we determine around those critical points range from  $26 \pm 5$  Pa (determined for 100 mM fuel) to  $82 \pm 8$  Pa (determined for 1000 mM fuel) (Supplementary Results Section 1.1 and Supplementary Fig. 3a).

Next, we use a similar approach to assess the viscoelastic properties of a system generated from a slightly different Fmoc-variant conjugated to the tripeptide AAD. In contrast to the Fmoc-AVD system discussed above, the AAD peptide provides the respective Fmoc-conjugate with significantly slower reaction kinetics<sup>29</sup>. Consequently, upon gelation, this system reaches its maximal elasticity a bit later than Fmoc-AVD, i.e., ~4–5 min after the addition of fuel. Moreover, the absolute values of the moduli reached here are lower than for Fmoc-AVD. This can be rationalized by differences in the attractive forces acting in both Fmoc-systems: by replacing the amino acid valine with alanine, the hydrophobicity of the peptide core part is decreased. This replacement should slightly shift the delicate balance between hydrophobic attractive and electrostatic repulsive forces towards the attractive forces. In addition, as discussed above, this replacement also entails a structural change of the supramolecular motifs generated by the Fmoc-peptides. Together, we consider this structural change and the increase in hydrophobic attractive forces to be one reason for the increased mechanical stability of Fmoc-AVD gels compared to Fmoc-AAD gels.



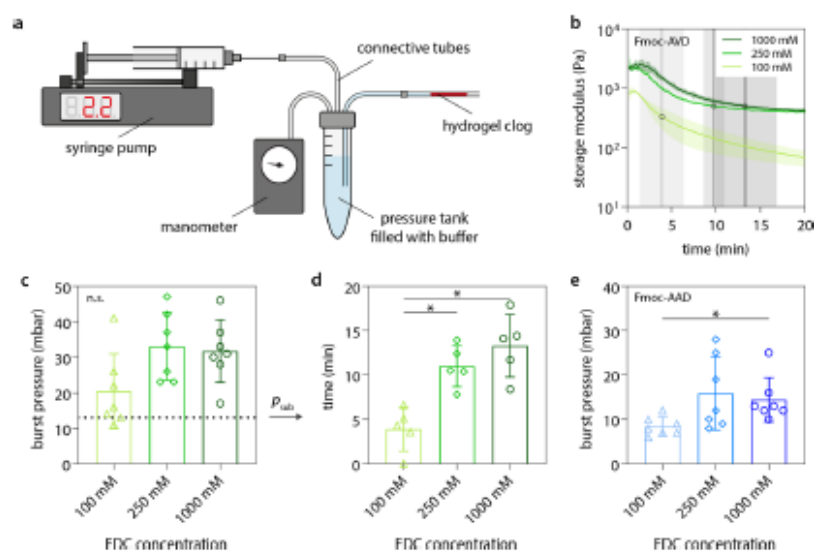
**Fig. 2** Viscoelastic properties of self-assembled hydrogels. The fuel concentration affects the time-dependent viscoelastic properties (a), the maximal storage modulus obtained during the reaction process (b), and the nonlinear mechanical properties (c) of self-assembled Fmoc-AVD hydrogels. The Fmoc-AAD system is influenced by different fuel concentrations in a similar manner (d–f); yet, the viscoelastic moduli stay in a plateau-like state once the gel is formed (d). Gelation curves (a, d) and LAOS measurements (c, f) show the mean of data obtained from  $n = 3$  independent samples. Bar plots in panels (b, e) represent the mean together with the standard deviation ( $n = 3$ ; significance level  $p < 0.05$  as determined by ordinary one-way ANOVA and Tukey post hoc tests). Fmoc-AVD data is depicted in green and Fmoc-AAD data is in blue. Bright colors represent an EDC concentration of 100 mM, medium bright colors correspond to 250 mM, and dark colors to 1000 mM. Solid lines represent the storage modulus and dashed lines the loss modulus. Individual data points are depicted with triangles (100 mM EDC), rhombuses (250 mM EDC), and circles (1000 mM).

Moreover, once a stable gel is formed, we only observe a slight (if at all) decline in the viscoelastic properties over time (Fig. 2d). Also, here, the turbidity changes and the inverted tube tests and fluorescent images support our observations from the rheological investigations (Supplementary Results Section 1.1 and Supplementary Fig. 4). Based on previous studies, we expect this good stability of the hydrogel to originate from the fact that, when fuel is abundant, most of the supramolecular structures formed by Fmoc-AAD remain in their assembled state—even when the anhydride component is hydrolyzed into its precursor state<sup>41</sup>. Overall, the Fmoc-AAD system has properties that only weakly depend on the fuel concentration—both in the linear and nonlinear response regime (Fig. 2d–f). Similar to the Fmoc-AVD gels, also the Fmoc-AAD gel variants show strain weakening at strain levels above  $\gamma = 1$ –2%, and the maximal stress levels, the samples withstand during this type of nonlinear shear rheology measurements, are all in the range of 2.5–3 Pa (Supplementary Fig. 3b).

**Mechanical failure of hydrogel clogs in tubings.** Up to now, we have assessed the mechanical properties of the two Fmoc-systems when exposed to either low or high shear forces. We found that the shear resistance of Fmoc-AVD gels depends on the amount of fuel present in the system. In contrast, the viscoelastic properties of the Fmoc-AAD system exhibit only a weak dependence on the fuel concentration. In possible application scenarios, however, it is unlikely that the material will be exposed to shear forces

exclusively. Thus, in the next step, we aim at testing the same set of gels in an environment, where they can be exposed to normal load. For this purpose, we developed a fluidic system, which can be temporarily sealed using hydrogel clogs generated by the two Fmoc-based peptides. When injected into this fluidic system, the hydrogel clog can be exposed to an adjustable fluid pressure, which creates a defined normal load onto the hydrogel material (Fig. 3a, see Methods section “Transient clogging of fluidic systems” for details).

When determining the stress resistance of such dynamic hydrogel clogs, it is important to consider that two parameters affect the stability of the gels in the presence of mechanical load: the viscoelastic properties of the system as determined by the initial fuel concentration and the intrinsic lifetime of the created hydrogel system. For consistency, we test the maximal pressure resistance of each gel variant at the particular time point when the gel reaches its highest elasticity. When we seal the tubing with a Fmoc-AVD hydrogel clog containing 100 mM fuel and then continuously increase the applied fluid pressure, we observe clog failure at a “burst pressure” of  $\sim 20$  mbar. When increasing the fuel concentration to 250 mM, the stress resistance of the hydrogel clog is increased such that it withstands pressures up to  $\sim 30$  mbar (Fig. 3c). This result agrees well with the differences we observed in the maximum elastic moduli determined for those two Fmoc-AVD hydrogel variants in the linear response regime, i.e.,  $G'_{100} = 0.9 \pm 0.1$  kPa for 100 mM of fuel and  $G'_{250} = 2.6 \pm 0.9$  kPa for 250 mM of fuel (Fig. 2b). Interestingly,



**Fig. 3 | Transient clogging of tubings.** Schematic illustration of the fluidic system used to conduct the clogging experiments (a). The pressure resistance of clogs formed by Fmoc-AVD and Fmoc-AAD hydrogels in macroscopic tubings depends on the fuel concentration (c, e). If Fmoc-AVD hydrogel clogs are exposed to a subcritical pressure (black dashed line in c), they withstand this mechanical load for a certain, fuel-dependent time span (d). This time span reflects the time point in the gelation curves where the gel stiffness falls below a critical value (circles in b). Data shown represents the mean and the standard deviation as obtained from  $n = 3$  (b),  $n = 7$  (c, e), and  $n = 5$  (d) independent samples. The level of significance was set to  $p < 0.05$  and determined by ordinary one-way ANOVA and Tukey post hoc test (c, d) or Kruskal-Wallis test in combination with the Dunn's multiple comparisons test (e). Fmoc-AVD data is depicted in green and Fmoc-AAD data in blue. Bright colors represent an EDC concentration of 100 mM, medium bright colors correspond to 250 mM, and dark colors to 1000 mM. Individual data points are depicted with triangles (100 mM EDC), rhombuses (250 mM EDC), and circles (1000 mM).

further increasing the fuel concentration from 250 to 1000 mM has almost no impact on the maximum elasticity of the Fmoc-AVD system ( $G'_{1000} = 2.6 \pm 0.5$  kPa)—and similarly, also the pressure resistance of a Fmoc-AVD hydrogel clog generated with 250 mM fuel is not further enhanced when the amount of fuel is increased (Fig. 3c). With the measured burst pressure values and the peak values of the elastic moduli determined for the different hydrogel variants, we estimate critical strain levels (which correspond to the respective burst events) ranging between  $\sim 1$  and 2% (Supplementary Results Section 1.2 and Supplementary Table 1). Those estimated critical strain values agree reasonably well with the results from the LAOS experiments, where we observed that the samples enter nonlinear behavior at those strain levels. In other words, this result implies that failure of the hydrogel clogs occurs as soon as the linear response regime of the material is left, i.e., when the hydrogels start to get damaged.

When using a dynamic hydrogel system for a clogging test as we conduct it here, the maximal elasticity of the hydrogel clog is not the only relevant parameter to consider; instead, the intrinsic lifetime of the gel can also be expected to contribute to the failure process of such a hydrogel clog. To test this notion, we next apply a subcritical pressure to the hydrogel clogs, i.e., a pressure level that is smaller than the burst pressure levels we determined above. When such a (constant) subcritical pressure level (here, selected 13 mbar) is applied to a Fmoc-AVD hydrogel clog fueled with 100 mM EDC, we observe clog failure after  $\sim 4$ –5 min (Fig. 3d). Using the time-dependent viscoelasticity properties determined before, we find that this time point corresponds to an elasticity range of  $G'_{crit} \sim 120$ –760 Pa (Fig. 3b). With this result, we expect that the failure of the hydrogel clog should be delayed, when the fuel concentration is increased from 100 to 250 mM: At this higher fuel concentration, the lifetime of the hydrogel is

extended such that a similarly low level of hydrogel elasticity is not reached within the first 5 min. Indeed, failure of this hydrogel clog occurs a bit later, i.e., around  $\sim 11$ –12 min, which is in line with our expectation. Accordingly, another (yet small) increase in the clog lifetime is obtained when even larger amounts of fuel (i.e., 1000 mM EDC) are used (Fig. 3d). Also, this result is in good agreement with the time-dependent viscoelastic properties of this hydrogel variant, which requires even more time to soften up to levels in the range of a few hundreds of Pa (Fig. 3b).

When we use the same setup to test the pressure resistance of softer Fmoc-AAD-based gels, the obtained results are in good agreement with the viscoelastic properties of those gels as we discussed above. For instance, we observe that the burst pressure values we determine for such Fmoc-AAD clogs only weakly depends on the fuel concentration used to generate those hydrogels. Similar to the maximal shear moduli determined in the linear response regime, this burst pressure only increases when the fuel concentration is increased from 100 mM to 250 mM—but not beyond that (Fig. 3e). Also here, based on the measured burst pressures, we estimate a critical strain of  $\sim 1$ –2% (Supplementary Table 1) upon which clog failure is triggered—and this critical strain level agrees well with the LAOS measurements we described for those Fmoc-AAD hydrogels above. In other words, all hydrogel clog variants fail at such conditions where the linear response regime ends. Here, the hydrogels can no longer withstand the mechanical load they are exposed to; depending on the measuring setup used, this results in either strain weakening or clog failure.

#### Influence of reaction waste products on the hydrogel lifetime.

So far, we have discussed the influence of mechanical load and the intrinsic lifetime of the dynamic hydrogels on the viscoelastic

properties of the self-assembled materials. As mentioned above, increasing the fuel concentration from 250 to 1000 mM neither increases the maximal stiffness of the hydrogels nor their intrinsic lifetime. Based on this result, one might assume that 250 mM of fuel is sufficient to generate the highest anhydride concentration possible—at least for a short time period. This idea would be consistent with our observation that the Fmoc-systems fueled with this particular EDC concentration show a similarly high maximal elastic modulus as the same system fueled with 1000 mM EDC. However, as the cyclic EDC conversion reaction drives the assembly process of the Fmoc-conjugates, any excess EDC molecules should be able to immediately reactivate the hydrolyzed (and thus disassembling) variants of the Fmoc-anhydrides. As a consequence, hydrogel samples containing 1000 mM fuel should show a prolonged regime where a near-maximal elastic modulus is present. Why is this not the case?

The EDC-based reaction cycle is rather simple, and the only molecular component we neglected in our considerations so far is the reaction waste product EDU (Fig. 4a). One possible explanation as to why larger EDC concentrations return unexpected results could be that an accumulation of this “waste” product within the sample might negatively affect the ongoing conversion reaction of the Fmoc-precursors to the anhydride. To test this idea, we add 1000 mM EDU to a Fmoc-AVD sample (which already contains 1000 mM EDC) and again track the development of its viscoelastic properties. Interestingly, the presence of EDU seems to prevent the formation of a hydrogel: the system now remains dominated by its viscous properties, and we do not detect any sign of gelation (Fig. 4b).

To obtain a better understanding of how EDU might interact with the microscopic mechanism of the self-assembling system, we choose two additional molecules, which mimic different parts of the chemical structure of EDU: First, urea—this molecule is selected to mimic the urea group of EDU. Second, methyl 3-(dimethylamino)propionate (MDP)—at the pH value used for our experiments, MDP contains a slightly hydrophobic and positively charged carbon chain, which approximates the carbon chain of EDU (Fig. 4a). In the aqueous environment used here, the hydrolysis of the ester MDP into its carboxylic acid and methanol is rather slow (Supplementary Results Section 1.3 and Supplementary Fig. 5); thus, such an MDP hydrolysis should not significantly impact our experiments. When we add one of those two EDU-mimetics, i.e., urea or MDP, to the same Fmoc-AVD sample tested before, we obtain the following results: Whereas even high concentrations of urea (i.e., 3000 mM) do not affect the gelation process of Fmoc-AVD at all, the presence of MDP prevents gelation (Fig. 4b).

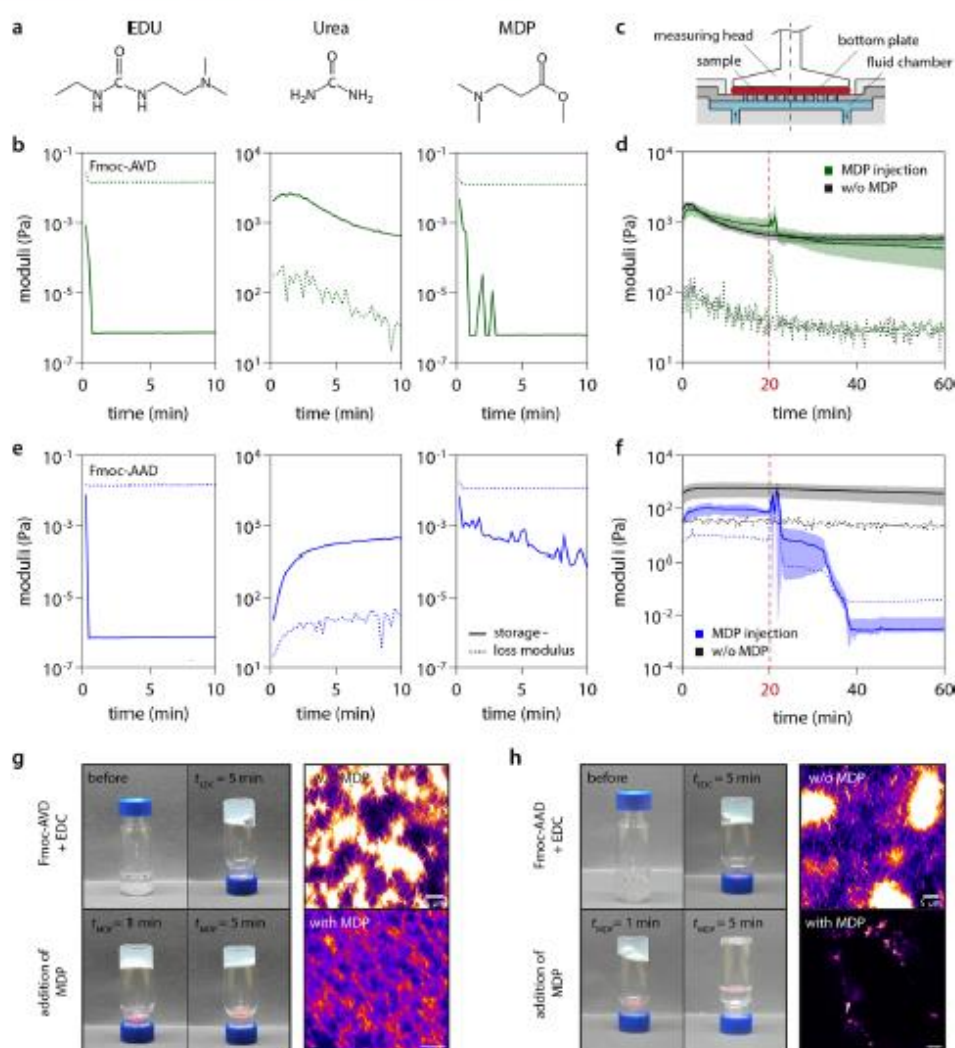
Together, those results suggest that the carbon chain of EDU (or MDP) interacts with the Fmoc-system such that its self-assembly process is disturbed. At this point, it is important to recall that the carbon chains of both, EDU and MDP, combine hydrophobic as well as cationic properties, and the latter originate from the tertiary amine groups present in the molecules. Thus, EDU, as well as MDP, could interact with the Fmoc-conjugates via cation- $\pi$  interactions between these tertiary amine groups of MDP/EDU and the Fmoc-group, and/or via electrostatic interactions between the tertiary amine groups of MDP/EDU and the anionic carboxyl group of the Fmoc-precursor. Either of those interactions could disturb the self-assembly process of the system and inhibit the formation of fibers and thus hydrogels.

Of course, the conditions we created for this particular set of tests, i.e., mixing the precursor with both, fuel and waste molecules, do not correctly reproduce the scenario present in the dynamically self-assembling gels: here, at the beginning of the experiment, the concentration of waste molecules is close to zero but increases over time while the reaction cycle converts EDC. To

better mimic this dynamic scenario, we change the setting of our rheological measurements. In detail, we switch to a custom-made setup, where we can expose a preformed hydrogel to waste molecules *in situ*<sup>42</sup> (see the schematic in Fig. 4c and the Methods section “Measurements with a perforated plate setup” for technical details). As this complex setup can have small influences on the absolute values of the measured viscoelastic moduli, we first set a new baseline by again measuring the gelation behavior of Fmoc-AVD samples without the addition of any interfering agents. Overall, as expected, the time-dependent behavior of the chemically fueled hydrogels is successfully reproduced (Supplementary Results Section 1.4 and Supplementary Fig. 6). Then, once more, we observe the gelation behavior of a Fmoc-AVD hydrogel fueled with 1000 mM EDC; however, this time, the fluid chamber is filled with only 1000 mM EDC dissolved in 200 mM 2-(*N*-morpholino)ethanesulfonic acid (MES) buffer at the beginning of this measurement. After recording the viscoelastic properties of the sample for 20 min (the corresponding time point is indicated by the red dashed line in Fig. 4d), the fluid in the reservoir is replaced with a solution containing 1000 mM MDP in addition to 1000 mM EDC.

Interestingly, for the preformed Fmoc-AVD hydrogel, this exposure to MDP only results in a small measuring artifact, which is created by a sudden increase in pressure in the reservoir chamber (this pressure increase is generated when the pump is started to exchange the fluid in this reservoir). In contrast, for Fmoc-AAD hydrogels, similar sudden exposure to MDP does affect the viscoelastic properties of the system. Here, after observing a similar artifact induced by the buffer exchange process (which is more strongly pronounced for the softer Fmoc-AAD hydrogel than for the stiffer Fmoc-AVD gel), we detect full liquefaction of the system: in other words, the system returns into its liquid state that is dominated by the loss modulus (Fig. 4f). This difference in the hydrogel behavior is very interesting as an immediate exposure of Fmoc-AAD conjugates to EDU, urea, or MDP prior to gel formation returns virtually identical results (Fig. 4e) as what we described for Fmoc-AVD above. Consistently, a preformed Fmoc-AVD gel maintains its supramolecular structures upon MDP addition: here, the sample turbidity persists after MDP addition, and confocal microscopy images show similar supramolecular structures as in the absence of MDP (Fig. 4g). In contrast, just minutes after MDP was added to the test tube, turbid Fmoc-AAD gels are reverted into clear samples. Accordingly, fluorescent images obtained for such MDP-enriched Fmoc-AAD systems show the disintegration of the previously present supramolecular structures (Fig. 4h). To visualize the dynamic structural changes in the gels, time-lapse movies (Supplementary Movies 1–4) of both peptide systems with and without the addition of MDP were obtained using confocal microscopy (those are available as electronic SI). To quantify the turbidity of the gels, light absorption measurements were conducted. Also here, the gels are initially turbid indicating a successfully formed gel structure (Supplementary Results Section 1.5 and Supplementary Fig. 7a–f). Upon addition of MDP, we observe a loss of turbidity for preformed gels generated from Fmoc-AAD, but not for those generated from Fmoc-AVD (Supplementary Fig. 7g, h).

Together, we interpret those results as follows: As mentioned above, hydrophobic attractive forces are responsible for driving the self-assembly of both variants of Fmoc-conjugates into supramolecular structures and, consequently, the formation of macroscopic hydrogels. When the Fmoc-derivates are brought into contact with the waste product EDU prior to gelation, the EDU molecules might bind to (and thus shield) the hydrophobic domains of the anhydride thus preventing self-assembly. Yet, when the Fmoc-derivates are already present in their self-



**Fig. 4** Influence of reaction side products on the viscoelastic properties of chemically fueled hydrogels. The waste product of the reaction cycle (EDU) and its structural mimetics (**a**) affect the gelation behavior of Fmoc-AVD (green) and Fmoc-AAD (blue) differently (**b, e**). Custom-made rheological setup to assess the behavior of preformed gels when brought into contact with the waste-mimetic MDP (**c**): here, the viscoelastic properties of a preformed Fmoc-AVD gel exposed to MDP after 20 min (dashed red line) remain virtually unaffected (**d**). However, a preformed Fmoc-AAD gel disintegrates upon exposure to MDP (**f**). Reference measurements without the addition of MDP are illustrated in gray for both peptide systems. Data shown represents the mean as obtained from  $n \geq 3$  independent samples. Error bands (**d, f**) depict the standard deviation. Inverted tube tests and fluorescent imaging of Fmoc-AVD (**g**) and Fmoc-AAD (**h**) samples further illustrate gel formation and gel (in)stability after MDP addition.

assembled state (e.g., as fibers) the strength of the stabilizing interactions determines if those supramolecular structures can be disintegrated by EDU. Based on the molecular architecture of the tripeptides conjugated to the Fmoc-groups, it is reasonable to assume that the hydrophobic forces responsible for self-assembly are weaker for Fmoc-AAD than for Fmoc-AVD. Thus, preformed Fmoc-AAD gels are more sensitive to EDU addition than Fmoc-AVD, which is why the former liquefy and the latter do not.

For other, less dynamic hydrogel systems, similar effects of molecular additives on the gel properties were observed previously and were used to adjust the gel properties in a controlled manner<sup>43,44</sup>. Owing to their ability to aggregate in water and to interact with hydrophobic gel structures,

hydrophobic additives are especially well suited for this purpose. For instance, by adding poly(lactic acid) it is possible to generate porous hydrogels<sup>45</sup>, and the swelling behavior of certain gel systems can be modified by the addition of hydrophobic additives such as benzoic acid or pheno<sup>146</sup>. Moreover, using molecular additives, the viscoelastic properties of hydrogels can be tuned: when poly(ethylene glycol) is added to poly(vinyl pyrrolidone) hydrogels, this reduces the gel stiffness; in contrast, the addition of poly(ethylene oxide) increases the elasticity of this gel variant<sup>47</sup>. In addition to affecting the lifetime of self-assembling peptide systems as we demonstrate here, such other molecular additives could be used in the future to further tailor the properties of chemically fueled hydrogels.

## Conclusions

We demonstrate that the chemically fueled peptide conjugates Fmoc-AVD and Fmoc-AAD offer tunable mechanical properties both in the linear and nonlinear response regime. In addition, we demonstrate that the lifetime of the emerging supramolecular materials depends not only on the amount of fuel available for creating assembly-competent molecules but also on the concentration of accumulated waste products, which can destabilize the assembled structures. Future developments of this class of materials have to take this additional parameter into account when designing molecular features of the self-assembling Fmoc-peptides. In brief, such dynamic hydrogels do not only come with intrinsic, preprogrammed material properties, they also allow for externally influencing the lifetime of the self-assembled structures. The possibility to combine adjustable mechanical properties with an a priori programmable and a posteriori tunable lifetime opens up a broad range of future applications for such dynamic materials: we expect that similar systems could be used as pre-programmable sealings for (micro)-fluidic systems, or as components in soft actuators and micro-robotics.

## Materials and methods

**Chemicals.** The following commercial chemicals were used for the synthesis of the Fmoc-tripeptides: deuterated dimethyl sulfoxide (DMSO- $d_6$ ), *N,N'*-diisopropylcarbodiimide (DIC), ethyl (hydroxyimino)cyanoacetate (oxyma) (Nova-biochem<sup>®</sup>), piperidine (99%), protected amino acids alanine (Fmoc-A-OH) and valine (Fmoc-V-OH), solvents (acetonitrile (ACN), *N,N*-dimethylformamide (DMF), dichloromethane, double distilled water (MilliQ<sup>®</sup> Direct 8), trifluoroacetic acid (99%, TFA), triisopropylsilane (TIPS), and preloaded Fmoc-Asp(OrBu)-Wang resin (100–200 mesh, loading  $0.67 \text{ mmol g}^{-1}$ ). The chemicals were purchased from Sigma-Aldrich (St. Louis, USA) and used without any further purification unless indicated otherwise. For the rheological measurements, the hydrogel dog tests in tubings, the inverted tube tests, and confocal microscopy, the following commercial chemicals were used: 1-ethyl-3-(3-dimethylamino propyl)carbodiimid-hydrochlorid (EDC) (Carl Roth GmbH & Co. KG, Karlsruhe, Germany), 1-[3-(dimethylamino)propyl]-3-ethylurea (EDU) (Alfa Aesar, Ward Hill, USA), Urea (Carl Roth GmbH & Co. KG), methyl 3-(dimethylamino)propionate (MDP) (Sigma-Aldrich, St. Louis, USA). For the confocal microscopy, additionally, the dye Nile red (Sigma-Aldrich, St. Louis, USA) was used.

**Peptide synthesis and purification.** Peptides were synthesized using standard fluorenylmethoxycarbonyl (Fmoc) solid-phase peptide synthesis on preloaded Fmoc-Asp(OrBu)-Wang resin (100–200 mesh, loading  $0.67 \text{ mmol g}^{-1}$ ). Peptide synthesis was conducted on a 0.5 mmol scale using a CEM Liberty microwave-assisted peptide synthesizer, and the Liberty Blue Application Software (Copyright © CEM Corporation 2015, Version: 1.45.5794.20265). Preloaded Fmoc-Asp(OrBu)-Wang resin (100–200 mesh, loading  $0.67 \text{ mmol g}^{-1}$ ) was swelled 30 min in 10 mL DMF at room temperature. Next, the preloaded Fmoc-Asp(OrBu)-Wang resin (100–200 mesh, loading  $0.67 \text{ mmol g}^{-1}$ ) was put into the automated peptide synthesizer. Before the following amino acid-coupling, a 20% (v/v) solution of piperidine ( $1 \times 10 \text{ mL}$ ) in DMF was used to remove the *N*-terminal Fmoc protecting group. The reaction mixture was heated in the microwave ( $1 \times \text{min}$ ,  $90^\circ \text{C}$ ). This step was repeated. Next, the resin was washed with DMF ( $2 \times 10 \text{ mL}$ ). The coupling was achieved by using four equivalents (eq.) of Fmoc-V-OH respectively Fmoc-A-OH in DMF (0.2 M, 10 mL), 4 eq. of DIC (0.5 M, 4 mL), and 4 eq. of oxyma (1 M, 2 mL). This resin solution was heated in the microwave ( $1 \times \text{min}$ ,  $90^\circ \text{C}$ ). To increase the yield, this amino acid coupling step was repeated. After the two coupling steps, the resin was washed with DMF ( $2 \times 10 \text{ mL}$ ). The  $2 \times$  Fmoc-deprotection, washing,  $2 \times$  coupling, the washing cycle was carried out to couple also the last amino acid Fmoc-A-OH of the respective peptide sequence Fmoc-alanine-valine-aspartic acid (AVD), and Fmoc-alanine-alanine-aspartic acid (AAD), respectively. Then, the peptide was cleaved from the resin by reacting the resin with a solution of 2.5% MQ-water, 2.5% TIPS, and 95% TFA for 1 h under continuous agitation at room temperature. Rotary evaporation by co-distillation with dichloromethane removed the solvent, and the crude product was dried under reduced pressure. Next, the crude peptides Fmoc-AVD and Fmoc-AAD were dissolved in  $\pm 50\%$  acetonitrile in MQ-water and then purified using reversed-phase high-performance liquid chromatography (RP-HPLC, Thermo Fisher Dionex Ultimate 3000, Hypersil Gold 5  $\mu\text{m}$ , length 250 mm, ID 20 mm), with gradient elution from 40 to 98% acetonitrile (with 0.1% TFA) in MQ-water (with 0.1% TFA) and a flow rate of 20 mL/min. UV-Vis detection at 254 nm was applied to detect the peptide. The purified peptide was lyophilized (Lyophilite: Alpha L Dplus, Christ) and stored at  $-20^\circ \text{C}$  until further use. <sup>1</sup>H-NMR spectroscopy (Supplementary Results Section 1.6 and Supplementary Fig. 8), Electrospray ionization mass spectrometry (ESI-MS, positive mode) on an LCQ

Fleet Ion Trap Mass Spectrometer (Thermo Scientific, Supplementary Table 2), as well as analytical HPLC (ThermoFisher Dionex Ultimate 3000, Hypersil Gold, Diameter (mm)  $250 \times 4.6$ ), eluted with a gradient of 0.1% TFA in MQ-water: ACN from 98:2 to 2:98 in 14 min, (Supplementary Fig. 9) was used to analyze the purity of the peptides Fmoc-AVD and Fmoc-AAD. <sup>1</sup>H-NMR spectra were recorded on a Bruker 500 MHz NMR. Chemical shifts are reported as  $\delta$ -values in parts per million (ppm) relative to the deuterated solvent peak: DMSO- $d_6$  ( $\delta$ H: 2.50). For the denotation of the observed signal multiplicities, the following abbreviations were used: d (doublet), dd (doublet of doublets), and m (multiplet).

## Rheological characterizations

**Gelation tests.** To determine the gelation behavior of the hydrogels<sup>43</sup>, rheological measurements were performed using a commercial shear rheometer (MCR 302, Anton Paar, Graz, Austria) and a plate-plate geometry (bottom plate P-PTD 200/ AIR, Anton Paar; 25 mm steel measuring head: PP25, 79044, Anton Paar). The sample volume was 200  $\mu\text{L}$  for each measurement; the plate separation was set to 0.3 mm and kept constant during all measurements. A solvent trap (a chamber containing a water-soaked paper towel, covered with a lid), as well as temperature control of the bottom plate (set to  $21^\circ \text{C}$ ), was used for all measurements. With this configuration, sample dehydration can be avoided for up to 6 h (Supplementary Results Section 1.7 and Supplementary Fig. 10).

To obtain the gels, the first 50  $\mu\text{L}$  of an EDC stock solution ( $c_{\text{EDC}} = 400, 1000$ , or  $4000 \text{ mM}$  solubilized in 200 mM MES, pH = 6) was homogeneously spread onto the bottom plate of the rheometer; then 150  $\mu\text{L}$  of the respective Fmoc-conjugate solution ( $c_{\text{Fmoc}} = 13.3 \text{ mM}$ , solubilized in 200 mM MES, pH = 6) was added on top. No further mixing was conducted to ensure that structures self-assembling *in situ* were not disrupted. With this method, the gels do not need to be transferred, which minimizes mechanical perturbation prior to their characterization. Then, the measuring head was lowered, and the test was started immediately afterwards. To ensure linear material response during the gelation process of the samples, the measurements were performed in torque-controlled mode (by applying small torques of  $0.5 \mu\text{Nm}$  and a constant oscillation frequency of 1 Hz). The storage and loss moduli were determined for at least 30 min, and one measurement point was recorded every 15 s. For determining the influence of EDU, urea, and MDP on the gelation behavior of the Fmoc-samples, the respective substance was added to the EDC stock solution (here, always  $c_{\text{EDC}} = 4000 \text{ mM}$  in 200 mM MES, pH = 6; then, either:  $c_{\text{EDU}} = 4000 \text{ mM}$ , or  $c_{\text{urea}} = 12000 \text{ mM}$ , or  $c_{\text{MDP}} = 4000 \text{ mM}$ ) and the procedure was conducted the same way as described above. For urea, a high concentration, close to the limit of solubility ( $1200 \text{ g L}^{-1}$ , Haynes 2016<sup>40</sup>) was tested to see if it has an effect on the gelation behavior at all. For each sample type, three independent samples were created and characterized *in situ*.

**LAOS measurements.** For assessing the onset of nonlinear material response, LAOS experiments were performed using the same setup and sample preparation protocol as described above. As LAOS tests slowly but steadily increase the applied shear strain, they are well suitable to investigate the nonlinear behavior of viscoelastic solids such as the hydrogels used here. At the same time, since LAOS makes use of an oscillatory strain application, it is still possible to determine the storage modulus and loss modulus as well as the point where material failure takes place. The linear elastic regime is valid for small strains only. In this regime, Hooke's law applies and a linear relation between stress and strain is observed. At larger mechanical loads, either strain weakening or strain hardening sets in<sup>40</sup> and Hooke's law is not valid anymore. The storage and loss moduli were determined in strain-controlled mode, and the applied shear strain was increased logarithmically from 0.1 to 1000% (using a constant oscillation frequency of 1 Hz and collecting two data points in each strain decade). For all Fmoc-AVD samples, the tests were started immediately after the samples were placed on the bottom plate; this was necessary as those samples reach their maximal stiffness quite rapidly after the different molecular components are brought together. In contrast, the Fmoc-AAD samples were allowed to rest for 3 min after the components were brought together; here, this was necessary since those samples require  $\sim 3 \text{ min}$  to reach their maximal stiffness (this was determined in the gelation measurements, which were conducted prior to the LAOS tests). For each sample type, three independent samples were created and characterized *in situ*.

**Measurements with a perforated plate setup.** To test the effect of MDP on pre-formed hydrogels, a custom-made rheological setup was used; this setup allows for bringing the sample in contact with a liquid reservoir located below the sample plane (Fig. 4c). This dedicated setup was enabled in the same commercial shear rheometer (MCR 302, Anton Paar) used for the other tests; also here, a commercial measuring head (PP25, 79044, Anton Paar) was employed. Yet, an in-house developed, perforated bottom plate (from now on referred to as "hole-y plate") and first described in Yan et al., 2019<sup>44</sup> was used. This hole-y plate can be mounted onto the commercial bottom plate of the rheometer (P-PTD200/80-1, Anton Paar) and comprises 19 regularly orientated holes with a diameter of 1.5 mm each. This design allows fluid to diffuse from a reservoir chamber located below the measurement gap into the actual sample. The sample and the reservoir of the hole-y plate were separated by a polycarbonate membrane (Whatman Nuclepore track-etch membrane, pore size: 50 nm, GE Healthcare, Chalfont St Giles, Great Britain) to prevent the sample from leaking into the fluid chamber while allowing small



molecules (such as EDU or MDP) to penetrate the membrane and to enter the sample.

First tests without the addition of MDP were conducted to validate the measurement setup. Before the measurement, the reservoir was filled with 200 mM MES buffer (pH 6) containing the same EDC concentration as of the investigated Fmoc-based sample (i.e.,  $c_{\text{EDC}} = 100, 250, \text{ or } 1000 \text{ mM}$ ). For these tests, the inlet and outlet of the chamber was closed, so that no additional fluid exchange is possible, and the sample interacts only with the static reservoir. In the next step, the inlet and outlet of the fluid chamber was used for the addition of MDP ( $c_{\text{MDP}} = 1000 \text{ mM}$  added to 200 mM MES containing 1000 mM EDC, pH 6) by using a syringe pump (LA 100, Landgraf Laborsysteme HLL GmbH, Langenhagen, Germany) after the sample has formed a gel. Here only the highest EDC concentration was investigated, resulting in the most stable gel. In all cases, sample preparation on top of the membrane was conducted in the same way as described for the gelation experiments above. Furthermore, the same measurement parameters as during the standard gelation tests were applied. Only the solvent trap could not be used in this setup, due to the inlet and outlet of the hole-y plate. Here, the liquid reservoir prevents the draining of the samples. For each sample type, three independent samples were created and characterized in situ.

**Confocal fluorescence microscopy.** Confocal fluorescence microscopy was performed on a Leica TCS SP8 confocal microscope using a 63x water immersion objective with a numerical aperture of 1.2. Samples with a total reaction volume of 20  $\mu\text{L}$  were prepared directly in an ibidi  $\mu$ -slide angiogenesis well plate. About 25  $\mu\text{M}$  Nile red was added as a dye before the fluid EDC was added. Samples were excited with a 552 nm laser and imaged at 577–656 nm. A laser intensity of 0.3 or 1.0%, and a pinhole of either 23.92, 39.61, 79.22, or 111.3  $\mu\text{m}$  ( $\lambda_{\text{excitation}} = 580 \text{ nm}$ ) was used to image the samples. The software ImageJ 1.52p (Java 1.8.0\_172, 64-bit) was used to analyze all recorded images. Imaging was conducted at 22 °C.

**Macroscopic images of gels.** Samples of 10 mM Fmoc-AAD / 10 mM Fmoc-AVD with a total reaction volume of 500  $\mu\text{L}$  were prepared in 1.5 mL screw cap HPLC vials. The samples were imaged after EDC addition with a high-definition camera.

**Transient clogging of fluidic systems.** To test the ability of the self-assembled hydrogels to transiently clog a tubing, we used a custom-made setup, which comprises a syringe pump (LA 100, Landgraf Laborsysteme HLL GmbH, Langenhagen, Germany) and a small pressure regulation tank. In combination, those two items allowed for applying a controlled pressure onto a fluid-filled outlet tube. Furthermore, a manometer (GDH 13 AN, Greisinger Electronic GmbH, Regenstauf, Germany) was attached to the pressure tank to monitor the pressure in the system. The outlet tube comprised an exchangeable, 10 cm long silicon test tube (inner diameter = 1 mm, Rotilabo, Carl Roth, Karlsruhe, Germany) which was intentionally clogged in the experiments (Fig. 3a). To generate such a clog, 60  $\mu\text{L}$  of a Fmoc-peptide solution ( $c_{\text{AVD}} = c_{\text{AAD}} = 13.3 \text{ mM}$  in 200 mM MES pH = 6) and 20  $\mu\text{L}$  of an EDC solution ( $c_{\text{EDC}} = 400, 1000, \text{ or } 4000 \text{ mM}$ ; all solutions were prepared in 200 mM MES at pH = 6) were combined using a 100  $\mu\text{L}$  Hamilton syringe and immediately injected into the outlet tube. The hydrogel clog was then allowed to form in situ and was left to rest for 90 s to ensure that the system reaches its maximal mechanical stability. Then, an increasing pressure was applied (at a rate of 1 mbar/s) to this hydrogel clog until it failed; the corresponding pressure level at which this clog failure occurred is referred to as “burst pressure” in the main text. To test the stability of a hydrogel clog in the presence of constant, subcritical pressure, a pressure level of 14 mbar was selected and applied to the clog; then, the time point was determined at which the hydrogel clog failed.

**Data analysis.** Prior to statistical analysis, we tested for the normal distribution of the measured values by using the Shapiro–Wilk test. To detect statistical differences between more than two groups, ordinary one-way ANOVA (for normally distributed samples) and Kruskal–Wallis test (for non-normal distribution) were conducted. Multi-comparisons were performed using the Tukey post hoc test or the Dunn’s multiple comparisons test, respectively. Professional software (Prism 8, GraphPad Software, San Diego, CA, USA) was used to conduct all statistical calculations. The level for the significant difference was set to  $p < 0.05$ , and significant differences were marked with an asterisk where applicable. Where no significant difference was found, the abbreviation n.s. was used.

#### Data availability

The authors declare that the experimental and theoretical data supporting the findings of this study are available within the paper (and its supplementary information files). However, more data that support the findings of this study are available from the corresponding authors upon reasonable request.

Received: 22 April 2021; Accepted: 1 September 2021;

Published online: 17 September 2021

#### References

- Philp, D. & Stoddart, J. F. Self-assembly in natural and unnatural systems. *Angew. Chem. Int. Ed.* **35**, 1154–1196 (1996).
- Fialkowski, M. et al. Principles and implementations of dissipative (dynamic) self-assembly. *J. Phys. Chem. B* **110**, 2482–2496 (2006).
- Honorato-Rios, C. & Lagerwall, J. P. F. Interrogating helical nanorod self-assembly with fractionated cellulose nanocrystal suspensions. *Commun. Mater.* **1**, 1–11 (2020).
- Freeman, R. et al. Reversible self-assembly of superstructured networks. *Science* **362**, 808–813 (2018).
- Sutar, P. et al. Binder driven self-assembly of metal-organic cubes towards functional hydrogels. *Nat. Commun.* **9**, 1–12 (2018).
- Hua, M. et al. Strong tough hydrogels via the synergy of freeze-casting and salting out. *Nature* **590**, 594–599 (2021).
- Panja, S. & Adams, D. J. Gel to gel transitions by dynamic self-assembly. *Chem. Commun.* **55**, 10154–10157 (2019).
- Panja, S., Patterson, C. & Adams, D. J. Temporally-programmed transient supramolecular gels. *Macromol. Rapid Commun.* **40**, 1900251 (2019).
- Singh, N. et al. Devising synthetic reaction cycles for dissipative nonequilibrium self-assembly. *Adv. Mater.* **32**, 1906834 (2020).
- Astumian, R. D. Kinetics asymmetry allows macromolecular catalysts to drive an information ratchet. *Nat. Commun.* **10**, 1–14 (2019).
- Pezzato, C. & Prins, L. J. Transient signal generation in a self-assembled nanosystem fueled by ATP. *Nat. Commun.* **6**, 1–8 (2015).
- te Brinke, E. et al. Dissipative adaptation in driven self-assembly leading to self-dividing fibrils. *Nat. Nanotechnol.* **13**, 849–855 (2018).
- Mairé, S. et al. Dissipative self-assembly of vesicular nanoreactors. *Nat. Chem.* **8**, 725–731 (2016).
- Dhiman, S., Jain, A. & George, S. J. Transient helicity: Fuel-driven temporal control over conformational switching in a supramolecular polymer. *Angew. Chem. Int. Ed.* **129**, 1349–1353 (2016).
- De, S. & Klajn, R. Dissipative self-assembly driven by the consumption of chemical fuels. *Adv. Mater.* **30**, 1706750 (2018).
- della Sala, F. et al. Transient self-assembly of molecular nanostructures driven by chemical fuels. *Curr. Opin. Biotechnol.* **46**, 27–33 (2017).
- Zhang, B. et al. Chemically fueled covalent crosslinking of polymer materials. *Chem. Commun.* **55**, 2086–2089 (2019).
- Wang, G. & Liu, S. Strategies to construct a chemical-fuel-driven self-assembly. *ChemSystemsChem* **2**, e1900046 (2020).
- Ragazzo, G. & Prins, L. J. Energy consumption in chemical fuel-driven self-assembly. *Nat. Nanotechnol.* **13**, 882–889 (2018).
- Leira-Iglesias, J. et al. Oscillations, travelling fronts and patterns in a supramolecular system. *Nat. Nanotechnol.* **13**, 1021–1027 (2018).
- Singh, N. et al. Re-programming hydrogel properties using a fuel-driven reaction cycle. *J. Am. Chem. Soc.* **142**, 4083–4087 (2020).
- Falzone, T. T. et al. Assembly kinetics determine the architecture of  $\alpha$ -actinin crosslinked F-actin networks. *Nat. Commun.* **3**, 1–9 (2012).
- Levin, M. et al. Kinetics of actin networks formation measured by time resolved particle-tracking micro-rheology. *Soft Matter* **16**, 7869–7876 (2020).
- Deshpande, S. & Pfohl, T. Hierarchical self-assembly of actin in micro-confinements using microfluidics. *Biomicrofluidics* **6**, 034120 (2012).
- Boekhoven, J. et al. Dissipative self-assembly of a molecular gelator by using a chemical fuel. *Angew. Chem. Int. Ed.* **122**, 4935–4938 (2010).
- Hao, X. et al. Pulsating polymer micelles via ATP-fueled dissipative self-assembly. *ACS Macro Lett.* **6**, 1151–1155 (2017).
- Wood, C. S. et al. Fuel-controlled reassembly of metal–organic architectures. *ACS Cent. Sci.* **1**, 504–509 (2015).
- Del Grosso, E. et al. Dissipative synthetic DNA-based receptors for the transient loading and release of molecular cargo. *Angew. Chem. Int. Ed.* **57**, 10489–10493 (2018).
- Tena-Solsona, M. et al. Non-equilibrium dissipative supramolecular materials with a tunable lifetime. *Nat. Commun.* **8**, 1–8 (2017).
- Rieß, B., Grötsch, R. K. & Boekhoven, J. The design of dissipative molecular assemblies driven by chemical reaction cycles. *Chem* **6**, 552–578 (2020).
- Sorrenti, A. et al. Non-equilibrium steady states in supramolecular polymerization. *Nat. Commun.* **8**, 1–8 (2017).
- Dai, K. et al. Regulating chemically fueled peptide assemblies by molecular design. *J. Am. Chem. Soc.* **142**, 14142–14149 (2020).
- Orbach, R. et al. The rheological and structural properties of Fmoc-peptide-based hydrogels: the effect of aromatic molecular architecture on self-assembly and physical characteristics. *Langmuir* **28**, 2015–2022 (2012).
- Adams, D. J. et al. Relationship between molecular structure, gelation behaviour and gel properties of Fmoc-dipeptides. *Soft Matter* **6**, 1971–1980 (2010).
- Rieß, B. et al. Dissipative assemblies that inhibit their deactivation. *Soft Matter* **14**, 4852–4859 (2018).
- Wanke, C. et al. Dynamic vesicles formed by dissipative self-assembly. *ChemSystemsChem* **2**, e1900044 (2020).

37. Tena-Solsona, M. et al. Accelerated ripening in chemically fueled emulsions. *ChemSystemsChem* **3**, e2000034 (2021).
38. Wanzke, C. et al. Active droplets in a hydrogel release drugs with a constant and tunable rate. *Mater. Horiz.* **7**, 1397–1403 (2020).
39. Späth, F. et al. Molecular design of chemically fueled peptide–polyelectrolyte coacervate-based assemblies. *J. Am. Chem. Soc.* **143**, 4782–4789 (2021).
40. Donau, C. et al. Active coacervate droplets as a model for membraneless organelles and protocells. *Nat. Commun.* **11**, 1–10 (2020).
41. Kriebisch, B. A. K. et al. Reciprocal coupling in chemically fueled assembly: a reaction cycle regulates self-assembly and vice versa. *J. Am. Chem. Soc.* **142**, 20837–20844 (2020).
42. Yan, H. et al. Immune-informed mucin hydrogels evade fibrotic foreign body response in vivo. *Adv. Funct. Mater.* **29**, 1902581 (2019).
43. Mishra, G. P., Tamboli, V. & Mitra, A. K. Effect of hydrophobic and hydrophilic additives on sol–gel transition and release behavior of simvastatin from polycaprolactone-based hydrogel. *Colloid Polym. Sci.* **289**, 1553–1562 (2011).
44. Semmling, B. et al. Development of hydrophobized alginate hydrogels for the vessel-simulating flow-through cell and their usage for bio-relevant drug-eluting stent testing. *AAPS PharmSciTech* **14**, 1209–1218 (2013).
45. Zhang, X.-Z., Chu, C.-C. & Zhuo, R.-X. Using hydrophobic additive as pore-forming agent to prepare macroporous PNIPAAm hydrogels. *J. Polym. Sci. A Polym. Chem.* **43**, 5490–5497 (2005).
46. Koga, S., Sasaki, S. & Maeda, H. Effect of hydrophobic substances on the volume-phase transition of N-isopropylacrylamide gels. *J. Phys. Chem. B* **105**, 4105–4110 (2001).
47. Luglo, A. B., Rogero, S. O. & Malmonge, S. M. Rheological behaviour of irradiated wound dressing poly(vinyl pyrrolidone) hydrogels. *Radiat. Phys. Chem.* **63**, 543–546 (2002).
48. Schnitter, F. et al. Synthesis and characterization of chemically fueled supramolecular materials driven by carbodiimide-based fuels. *Nat. Protoc.* **16**, 3901–3932 (2021).
49. Haynes, W. M. *CRC handbook of chemistry and physics* (Taylor & Francis Group, LLC, 2017).
50. Lieleg, O. & Bausch, A. R. Cross-linker unbinding and self-similarity in bundled cytoskeletal networks. *Phys. Rev. Lett.* **99**, 158105 (2007).

### Acknowledgements

This project was funded by the Deutsche Forschungsgemeinschaft (DFG, German Research Foundation)—SFB 863, Projekt B11—111166340. The authors thank Marvin Ertel for helpful discussions regarding the structure of EDU mimetics. B.A.K.K. is grateful for a Kekulé Stipendium by the Verband der Chemischen Industrie.

### Author contributions

M.K., B.W., B.A.K.K., J.B. and O.L. planned the experiments, which were conducted and analyzed by M.K., B.W. and B.A.K.K. The manuscript was written by contributions of all authors.

### Funding

Open Access funding enabled and organized by Projekt DEAL.

### Competing interests

The authors declare no competing interest.

### Additional information

**Supplementary information** The online version contains supplementary material available at <https://doi.org/10.1038/s43246-021-00202-6>.

**Correspondence** and requests for materials should be addressed to Benjamin Winkelmann or Oliver Lieleg.

**Peer review information** *Communications Materials* thanks the anonymous reviewers for their contribution to the peer review of this work. Primary Handling Editor: John Plummer.

**Reprints and permission information** is available at <http://www.nature.com/reprints>

**Publisher's note** Springer Nature remains neutral with regard to jurisdictional claims in published maps and institutional affiliations.



**Open Access** This article is licensed under a Creative Commons Attribution 4.0 International License, which permits use, sharing, adaptation, distribution and reproduction in any medium or format, as long as you give appropriate credit to the original author(s) and the source, provide a link to the Creative Commons license, and indicate if changes were made. The images or other third party material in this article are included in the article's Creative Commons license, unless indicated otherwise in a credit line to the material. If material is not included in the article's Creative Commons license and your intended use is not permitted by statutory regulation or exceeds the permitted use, you will need to obtain permission directly from the copyright holder. To view a copy of this license, visit <http://creativecommons.org/licenses/by/4.0/>.

© The Author(s) 2021

*A.4.1 Supplementary information for: Viscoelastic behavior of chemically fueled supramolecular hydrogels under load and influence of reaction side products*

Supplementary Information  
for

**Viscoelastic behavior of chemically fueled supramolecular hydrogels  
under load and influence of reaction side products**

Martin Kretschmer<sup>1,2</sup>, Benjamin Winkeljann<sup>1,2,\*</sup>, Brigitte A. K. Kriebisch<sup>3,4</sup>, Job Boekhoven<sup>3,4</sup>, and Oliver Lieleg<sup>1,2,\*</sup>

<sup>1</sup> Department of Mechanical Engineering and Munich School of Bioengineering,  
Technical University of Munich, Boltzmannstraße 15, 85748 Garching, Germany

<sup>2</sup> Center for Protein Assemblies (CPA), Ernst-Otto-Fischer Straße 8, 85748, Garching, Germany

<sup>3</sup> Department of Chemistry, Technical University of Munich, Lichtenbergstrasse 4, 85748 Garching,  
Germany

<sup>4</sup> Institute for Advanced Study, Technical University of Munich, Lichtenbergstrasse 2a, 85748  
Garching, Germany

\*correspondence:

Prof. Dr. Oliver Lieleg  
Department of Mechanical Engineering and Munich School of Bioengineering,  
Technical University of Munich,  
Ernst-Otto-Fischer Straße 8, 85748 Garching, Germany  
e-mail: oliver.lieleg@tum.de,  
phone: +49 89 289 10952, fax: + 49 89 289 10801

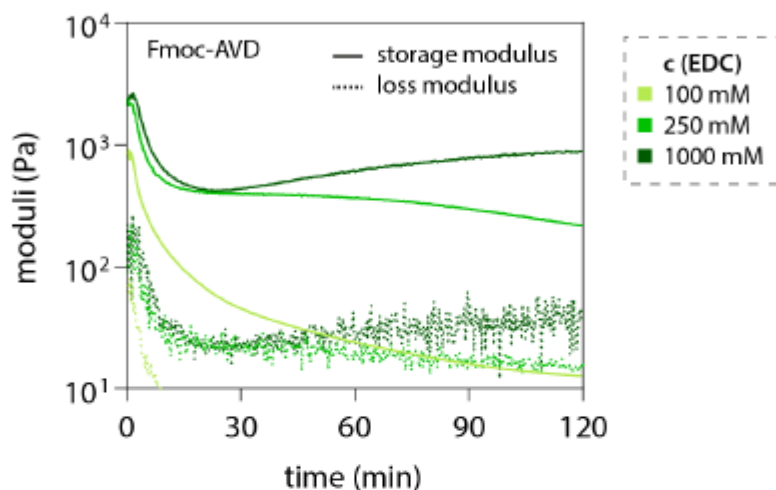
Dr. Benjamin Winkeljann  
Department of Mechanical Engineering and Munich School of Bioengineering,  
Technical University of Munich,  
Ernst-Otto-Fischer Straße 8, 85748 Garching, Germany  
e-mail: benjamin.winkeljann@tum.de,  
phone: +49 89 289 10952, fax: + 49 89 289 10801

*keywords: non-linear rheology, supramolecular chemistry, self-assembly, dynamic materials*

## 1 1 Supplementary Results

### 2 1.1 Viscoelastic behavior of dynamic Fmoc-based systems

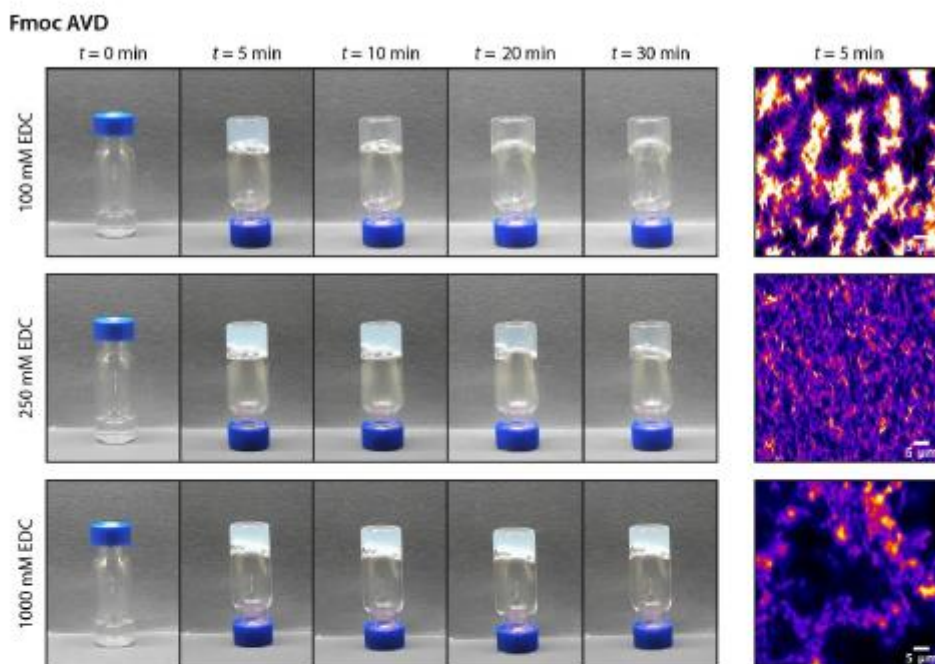
3 The stiffness of Fmoc-AVD hydrogels reach their maxima within the first 2 min; afterwards both  
4 viscoelastic moduli slowly decrease over time and reach plateaus after ~15-20 min. Further changes in  
5 the viscoelastic properties of the system are not observable (**Supplementary Figure 1**).



**Supplementary Figure 1:** Viscoelastic properties of Fmoc-AVD hydrogels at different EDC concentrations tracked over 120 min. Bright colors represent an EDC concentration of 100 mM, medium bright colors correspond to 250 mM and dark colors to 1000 mM. Data represent the mean as obtained from  $n=3$  samples.

6

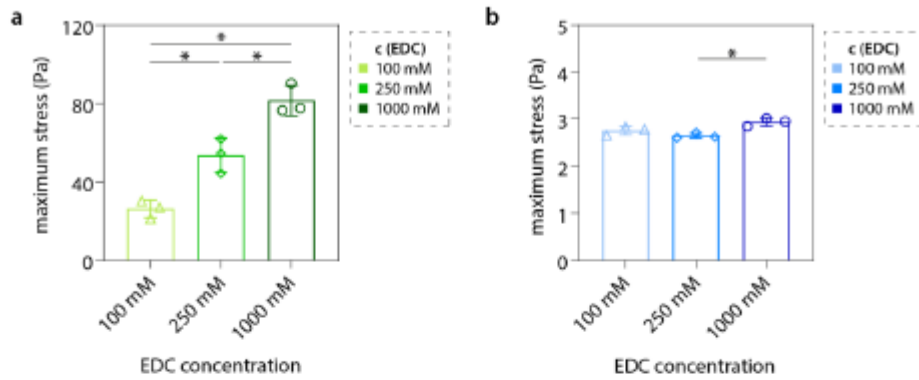
7 In **Supplementary Figure 2**, the formation of supramolecular structures of Fmoc-AVD is visible by a  
8 transition from clear to turbid samples. Further, confocal images illustrate the size and shape of the  
9 supramolecular clusters formed in the hydrogels.



**Supplementary Figure 2:** Inverted tube test and fluorescence imaging for Fmoc-AVD hydrogels at different fuel concentrations and time-points.

10

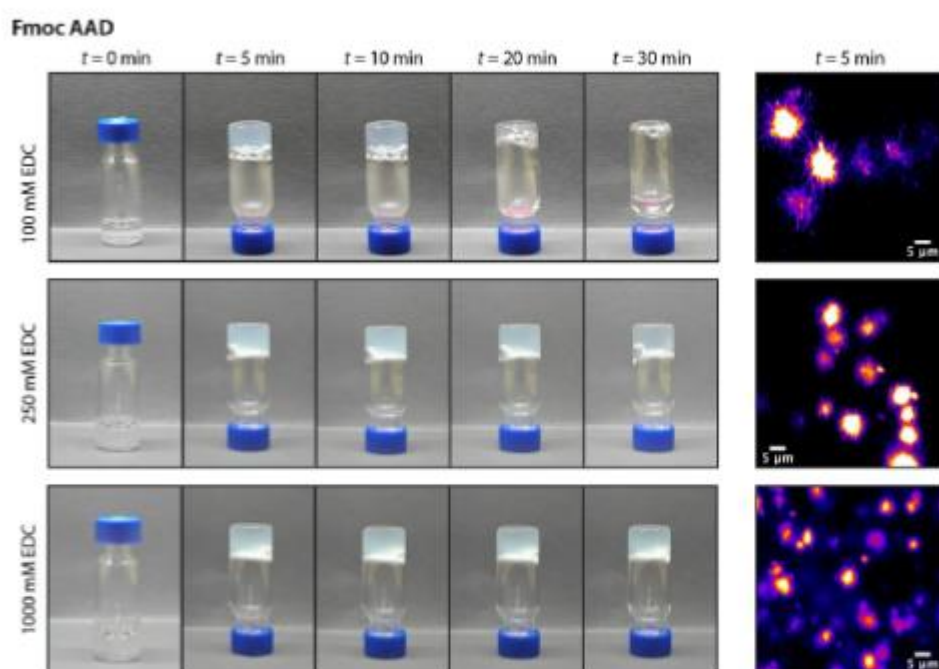
- 11 The maximum shear stress of the fully assembled Fmoc-based hydrogels is depicted in **Supplementary**  
 12 **Figure 3.**



**SupplementaryFigure 3:** Maximum shear stress the fully assembled Fmoc-AVD (green) (a) and Fmoc-AAD (blue) (b) hydrogels can withstand before they are irreversibly mechanically damaged. Bright colors represent an EDC concentration of 100 mM, medium bright colors correspond to 250 mM and dark colors to 1000 mM. Bar plots depict the mean and standard deviation ( $n=3$ ). Asterisks indicate statistically significant differences (as determined by ordinary one-way ANOVA and Tukey Post Hoc tests) using a significance level of  $p < 0.05$ .

13

14 In **Supplementary Figure 4**, the formation of supramolecular structures of Fmoc-AAD is visible by a  
15 transition from clear to turbid samples. Further, confocal images illustrate the size and shape of the  
16 supramolecular clusters formed in the hydrogels.



**Supplementary Figure 4:** Inverted tube test and fluorescence imaging for Fmoc-AAD hydrogels at different fuel concentrations and time-points.

17

18 **1.2 Strain at burst pressure in the clogging experiments**

19 The strain at burst pressure ( $\gamma_{burst}$ ) of the investigated hydrogels in the clogging experiments is shown in  
 20 **Supplementary Table 1**. The values were calculated with *Equation 1*, from the burst pressures ( $\sigma_{burst}$ )  
 21 measured in the clogging experiments and the sample elasticity values that correspond to the shear  
 22 moduli ( $G'$ ) measured in the linear response regime during the gelation experiments.

23 
$$\gamma_{burst} = \frac{\sigma_{burst}}{G'} \quad (1)$$

24

25 **Supplementary Table 1:** Strain at burst pressure. Those values were calculated from the burst pressures measured  
 26 in the clogging experiments ( $n = 7$ ) by assuming sample elasticity values that correspond to the shear moduli  
 27 measured in the linear response regime ( $n = 3$ ). Error values represent the standard deviation.

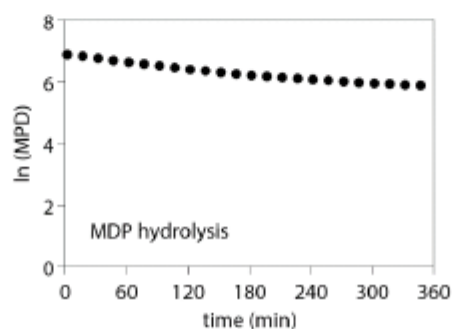
Sample	Maximum storage modulus $G'$ [kPa]	Burst pressure $\sigma_{burst}$ [mbar]	Calculated strain $\gamma_{burst}$ at burst pressure [%]
Fmoc-AVD 100 mM EDC	0.9 ± 0.1	20 ± 11	2.2
Fmoc-AVD 250 mM EDC	2.6 ± 0.9	33 ± 10	1.3
Fmoc-AVD 1000 mM EDC	2.6 ± 0.5	32 ± 9	1.2
Fmoc-AAD 100 mM EDC	0.70 ± 0.07	8 ± 2	1.2
Fmoc-AAD 250 mM EDC	0.98 ± 0.09	16 ± 8	1.6
Fmoc-AAD 1000 mM EDC	1.0 ± 0.2	14 ± 5	1.4

28



29 **1.3 MDP hydrolysis**

30 <sup>1</sup>H-NMR spectroscopy was used to determine the hydrolysis rate constant of MDP (methyl 3-  
31 (dimethylamino)propanoate) in 200 mM MES buffer, pH 6.0. <sup>1</sup>H-NMR spectra were recorded on a Varian  
32 Inova 300 (300 MHz). An inner tube with an internal hydroquinone standard (50 mM) dissolved in D<sub>2</sub>O  
33 was used as a reference. The <sup>1</sup>H-NMR spectra were recorded with water suppression. MDP hydrolysis was  
34 determined by comparing the integral of the CH<sub>3</sub> group of the decreasing MDP at 3.57 ppm to the  
35 integral of the internal hydroquinone standard at 6.65 ppm. The MDP concentration was calculated  
36 based on the arising MeOH signal at 3.22 ppm. Analysis of all recorded NMR spectra was performed using  
37 MestReNova© software (Version 11.0.0.-17609). **Supplementary Figure 5** shows the hydrolysis  
38 behavior of MDP.



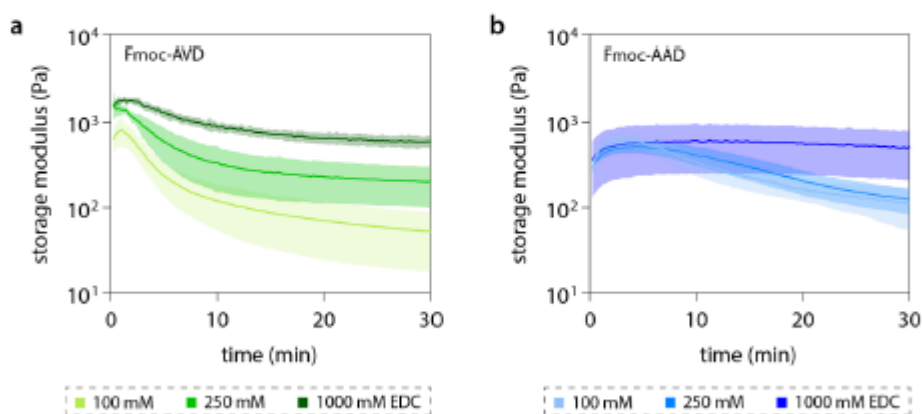
**Supplementary Figure 5:** Hydrolysis rate constant of methyl 3-(dimethylamino)propanoate (MDP):  $5.0 \times 10^{-5} \text{ s}^{-1}$ .

39

40 **1.4 Viscoelastic behavior of dynamic Fmoc-based systems determined with the hole-y plate**  
41 **setup**

42 For the validation of the custom made hole-y plate, the viscoelastic behavior of the Fmoc-based systems  
43 was investigated with this setup (**Supplementary Figure 6**).

44

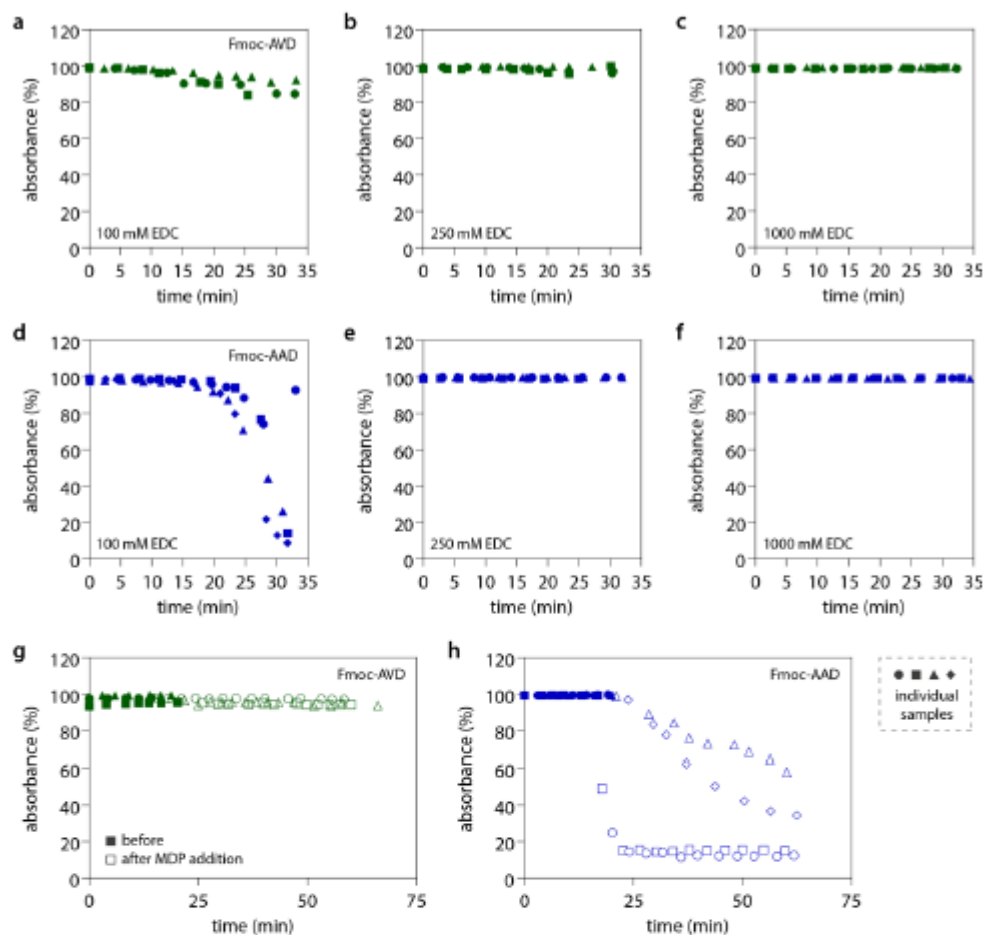


**Supplementary Figure 6:** Viscoelastic properties of Fmoc-AVD (green) (a) and Fmoc-AAD (blue) (b) hydrogels at different EDC concentrations as determined with the hole-y plate setup. Bright colors represent an EDC concentration of 100 mM, medium bright colors correspond to 250 mM and dark colors to 1000 mM. Data shown represents the mean and standard deviation as obtained from  $n = 3$  independent samples.

45

46 **1.5 Turbidity measurements**

47 The turbidity of Fmoc-based samples was tracked using a Litesizer 500 (Anton Paar, Graz, Austria)  
48 (**Supplementary Figure 7**). To prepare the samples, 75  $\mu\text{L}$  of the respective Fmoc-conjugate stock  
49 solution ( $C_{\text{AVD}} = C_{\text{AAD}} = 13.3 \text{ mM}$ ; dissolved in 200 mM MES, pH = 6) were mixed with 25  $\mu\text{L}$  of an EDC ( $C_{\text{EDC}}$   
50 = 400, 1000, or 4000 mM in 200 mM MES, pH = 6) solution. Mixing was conducted using a 100  $\mu\text{L}$  capillary  
51 piston, and 50  $\mu\text{L}$  of the mixed sample were injected into a low volume cuvette (Univette, Anton Paar).  
52 The amount of light absorbed by the sample was determined for 30 min. To investigate the effect of  
53 MDP, the procedure was slightly modified: First, the hydrogel sample was prepared as described above;  
54 then, after 20 min, 20  $\mu\text{L}$  of an EDC/MDP ( $C_{\text{EDC}} = 4000 \text{ mM}$ ,  $C_{\text{MDP}} = 4000 \text{ mM}$ , dissolved in 200 mM MES, pH  
55 = 6) solution was added on top without any further mixing and the sample was measured for additional  
56 40 min.



**Supplementary Figure 7:** Sample turbidity as observed by light absorption measurements for Fmoc-AVD samples (green) containing 100 mM EDC (a), 250 mM EDC (b), or 1000 mM EDC (c, g) as well as Fmoc-AAD samples (blue) containing 100 mM EDC (d), 250 mM EDC (e), or 1000 mM EDC (f, h). The addition of 1000 mM MDP has no effect on the turbidity of Fmoc-AVD gels (g), but rapidly and strongly increases the transparency of Fmoc-AAD (h). Data shown represents individual data points as obtained from  $n \geq 3$  independent samples.

57

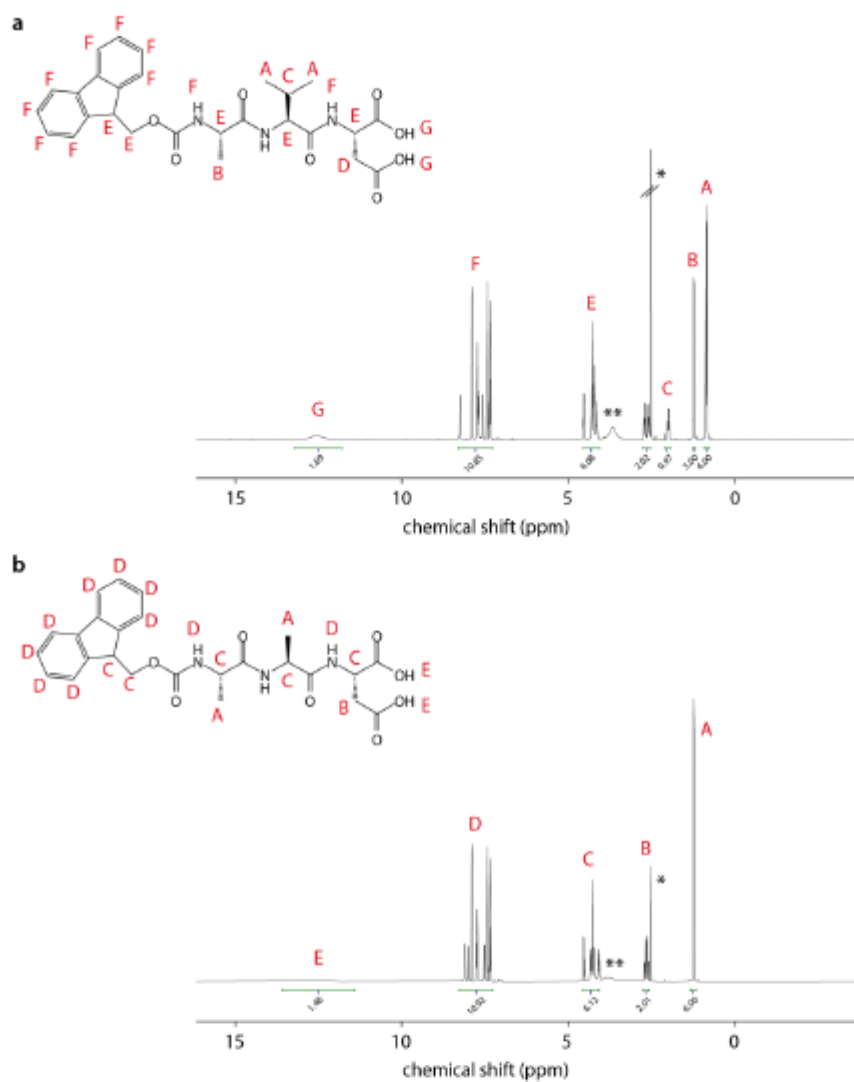
58 **1.6 Characterization of Fmoc-amino acid conjugates**

59 The synthesis of the Fmoc-amino acid conjugates was characterized to determine possible influences  
60 on the material behavior (**Supplementary Table 2**). Further <sup>1</sup>H-NMR spectroscopy and HPLC was used  
61 to analyze the purity of the Fmoc-amino acid conjugates (**Supplementary Figures 8-9**).

62

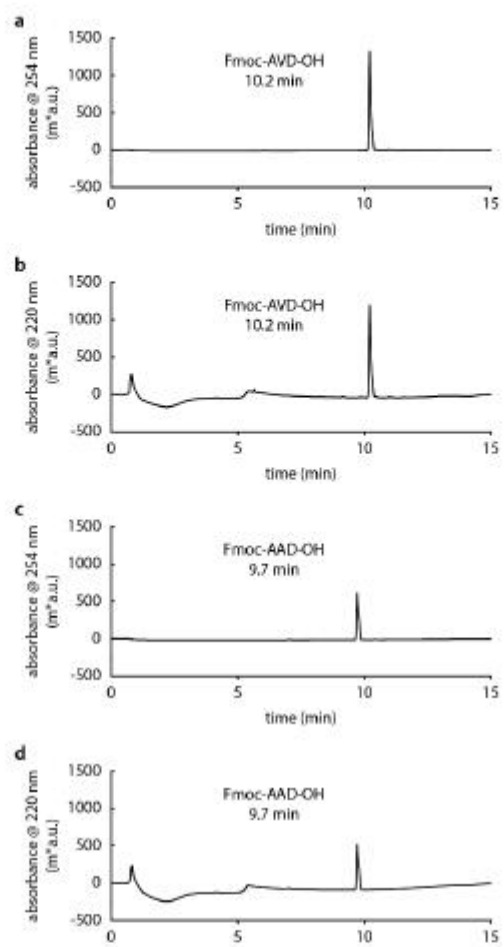
63 **Supplementary Table 2:** Characterization of the synthesized Fmoc-AVD and Fmoc-AAD conjugates.

name (purity)	calculated mass [g mol <sup>-1</sup> ]	determined mass [g mol <sup>-1</sup> ]	retention time [min]
Fmoc-AVD (97%)	$M_w = 525.21$ $C_{27}H_{31}N_3O_6$	526.00 ( $M_w + H^+$ ) 548.32 ( $M_w + Na^+$ )	10.2
Fmoc-AAD (97%)	$M_w = 497.18$ $C_{25}H_{27}N_3O_6$	497.98 ( $M_w + H^+$ ) 520.31 ( $M_w + Na^+$ )	9.7



**Supplementary Figure 8:**  $^1\text{H-NMR}$  spectrum (500 MHz NMR, Bruker) of Fmoc-AVD (a) and Fmoc-AAD (b) in DMSO- $d_6$ .

- a: Fmoc-AVD  $^1\text{H-NMR}$  (500 MHz, DMSO- $d_6$ )  $\delta$  (ppm) = 12.51 (s, 2H, HG), 8.29-7.26 (m, 11H, HF), 4.54-4.06 (m, 6H, HE), 2.77-2.55 (m, 2H, HD), 2.11-1.91 (m, 1H, HC), 1.20 (d, 3H, HB), 0.89 (dd, 6H, HA). \* = DMSO- $d_6$   $\delta$  (ppm) = 2.50, \*\* =  $\text{H}_2\text{O}$   $\delta$  (ppm) = 3.50.
- b: Fmoc-AAD  $^1\text{H-NMR}$  (500 MHz, DMSO- $d_6$ )  $\delta$  (ppm) = 12.50 (s, 2H, H<sub>i</sub>), 8.27-7.26 (m, 11H, H<sub>i</sub>), 4.56-4.07 (m, 6H, H<sub>j</sub>), 2.75-2.57 (m, 2H, H<sub>i</sub>), 1.234 (d, 6H, H<sub>k</sub>). \* = DMSO- $d_6$   $\delta$  (ppm) = 2.50, \*\* =  $\text{H}_2\text{O}$   $\delta$  (ppm) = 3.50

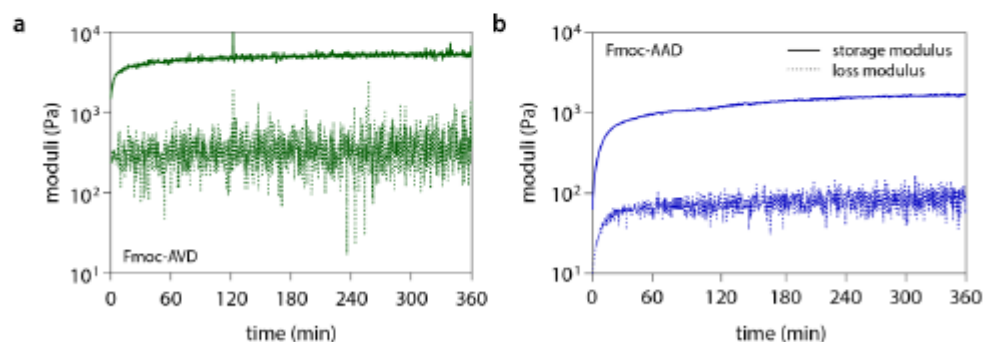


**Supplementary Figure 9:** HPLC-chromatogram of Fmoc-AVD 254 nm (a) and 220nm (b) and of Fmoc-AAD at 254 nm (c) and 220 nm (d) after purification. Injection volume: 1  $\mu$ L.

65 **1.7 Rheology of static hydrogels assembled from Fmoc-amino acid conjugates**

66 To assess putative sample drying effects, rheological measurements were conducted for 6 h using static  
67 Fmoc-AVD and Fmoc-AAD hydrogels, respectively. Here, gelation was induced by the addition of  
68 500 mM HCl. As depicted in **Supplementary Figure 10**, both samples reach a plateau stiffness after  
69  $\approx 10$  min. Owing to the solvent trap used in our measurements (see Methods section "Gelation tests" of  
70 the main paper), no indications of drying effects were detected.

71



**Supplementary Figure 10:** Viscoelastic properties of static Fmoc-AVD (green) (a) and Fmoc-AAD (blue) (b) gels over a time range of 6 hours. Data shown represents the mean as obtained from  $n = 3$  independent samples.

72





## B. Licenses for publications

### B.1 Importance of the biofilm matrix for the erosion stability of *Bacillus subtilis* NCIB 3610 biofilms



This is a License Agreement between Martin Kretschmer ("User") and Copyright Clearance Center, Inc. ("CCC") on behalf of the Rightsholder identified in the order details below. The license consists of the order details, the CCC Terms and Conditions below, and any Rightsholder Terms and Conditions which are included below.  
All payments must be made in full to CCC in accordance with the CCC Terms and Conditions below.

Order Date	02-Nov-2021	Type of Use	Republish in a thesis/dissertation
Order License ID	1158795-1	Publisher Portion	RSC Publishing Chapter/article
ISSN	2046-2069		

#### LICENSED CONTENT

Publication Title	RSC advances	Publication Type	e-Journal
Article Title	Importance of the biofilm matrix for the erosion stability of <i>Bacillus subtilis</i> NCIB 3610 biofilms	Start Page	11521
		End Page	11529
		Issue	20
Date	01/01/2011	Volume	9
Language	English	URL	<a href="http://pubs.rsc.org/en/Journals/JournalIssues/RA">http://pubs.rsc.org/en/Journals/JournalIssues/RA</a>
Country	United Kingdom of Great Britain and Northern Ireland		
Rightsholder	Royal Society of Chemistry		

#### REQUEST DETAILS

Portion Type	Chapter/article	Rights Requested	Main product and any product related to main product
Page range(s)	11521-11529	Distribution	Worldwide
Total number of pages	9	Translation	Original language of publication
Format (select all that apply)	Print, Electronic	Copies for the disabled?	No
Who will republish the content?	Author of requested content	Minor editing privileges?	No
Duration of Use	Life of current edition	Incidental promotional use?	No
Lifetime Unit Quantity	Up to 499	Currency	EUR

#### NEW WORK DETAILS

Title	Material Properties of Bacterial Biofilms and Bioinspired Synthetic Hydrogels	Institution name	Technical University of Munich
Instructor name	Prof. Dr. Oliver Lieleg	Expected presentation date	2022-01-01

#### ADDITIONAL DETAILS

Order reference number	N/A	The requesting person / organization to appear on the license	Martin Kretschmer
------------------------	-----	---	-------------------

## REUSE CONTENT DETAILS

Title, description or numeric reference of the portion(s)	Importance of the biofilm matrix for the erosion stability of <i>Bacillus subtilis</i> NCIB 3610 biofilms	Title of the article/chapter the portion is from	Importance of the biofilm matrix for the erosion stability of <i>Bacillus subtilis</i> NCIB 3610 biofilms
Editor of portion(s)	Ezendam, S.; Goetz, A.; Klotz, M.; Kretschmer, M.; Lieleg, O.; Opitz, M.	Author of portion(s)	Ezendam, S.; Goetz, A.; Klotz, M.; Kretschmer, M.; Lieleg, O.; Opitz, M.
Volume of serial or monograph	9	Issue, if republishing an article from a serial	20
Page or page range of portion	11521-11529	Publication date of portion	2019-01-01

## SPECIAL RIGHTSHOLDER TERMS AND CONDITIONS

Thank you for your email. The Royal Society of Chemistry hereby grants permission for the use of the material specified below under the Creative Commons CC-BY-NC licence in the work described and in all subsequent editions of the work for distribution throughout the world, in all media including electronic and microfilm. You may use the material in conjunction with computer-based electronic and information retrieval systems, grant permissions for photocopying, reproductions and reprints, translate the material and to publish the translation, and authorize document delivery and abstracting and indexing services. The Royal Society of Chemistry is a signatory to the STM Guidelines on Permissions (available on request). Please note that if the material specified below or any part of it appears with credit or acknowledgement to a third party then you must also secure permission from that third party before reproducing that material. Please ensure that the published article carries a credit to The Royal Society of Chemistry (see <http://rsc.li/permissions> for details) and that any electronic version of the work includes a hyperlink to the article on the Royal Society of Chemistry website.

## CCC Terms and Conditions

1. Description of Service; Defined Terms. This Republication License enables the User to obtain licenses for republication of one or more copyrighted works as described in detail on the relevant Order Confirmation (the "Work(s)"). Copyright Clearance Center, Inc. ("CCC") grants licenses through the Service on behalf of the rightsholder identified on the Order Confirmation (the "Rightsholder"). "Republication", as used herein, generally means the inclusion of a Work, in whole or in part, in a new work or works, also as described on the Order Confirmation. "User", as used herein, means the person or entity making such republication.
2. The terms set forth in the relevant Order Confirmation, and any terms set by the Rightsholder with respect to a particular Work, govern the terms of use of Works in connection with the Service. By using the Service, the person transacting for a republication license on behalf of the User represents and warrants that he/she/it (a) has been duly authorized by the User to accept, and hereby does accept, all such terms and conditions on behalf of User, and (b) shall inform User of all such terms and conditions. In the event such person is a "freelancer" or other third party independent of User and CCC, such party shall be deemed jointly a "User" for purposes of these terms and conditions. In any event, User shall be deemed to have accepted and agreed to all such terms and conditions if User republishes the Work in any fashion.
3. Scope of License; Limitations and Obligations.
  - 3.1. All Works and all rights therein, including copyright rights, remain the sole and exclusive property of the Rightsholder. The license created by the exchange of an Order Confirmation (and/or any invoice) and payment by User of the full amount set forth on that document includes only those rights expressly set forth in the Order Confirmation and in these terms and conditions, and conveys no other rights in the Work(s) to User. All rights not expressly granted are hereby reserved.

- 3.2. General Payment Terms: You may pay by credit card or through an account with us payable at the end of the month. If you and we agree that you may establish a standing account with CCC, then the following terms apply: Remit Payment to: Copyright Clearance Center, 29118 Network Place, Chicago, IL 60673-1291. Payments Due: Invoices are payable upon their delivery to you (or upon our notice to you that they are available to you for downloading). After 30 days, outstanding amounts will be subject to a service charge of 1-1/2% per month or, if less, the maximum rate allowed by applicable law. Unless otherwise specifically set forth in the Order Confirmation or in a separate written agreement signed by CCC, invoices are due and payable on "net 30" terms. While User may exercise the rights licensed immediately upon issuance of the Order Confirmation, the license is automatically revoked and is null and void, as if it had never been issued, if complete payment for the license is not received on a timely basis either from User directly or through a payment agent, such as a credit card company.
- 3.3. Unless otherwise provided in the Order Confirmation, any grant of rights to User (i) is "one-time" (including the editions and product family specified in the license), (ii) is non-exclusive and non-transferable and (iii) is subject to any and all limitations and restrictions (such as, but not limited to, limitations on duration of use or circulation) included in the Order Confirmation or invoice and/or in these terms and conditions. Upon completion of the licensed use, User shall either secure a new permission for further use of the Work(s) or immediately cease any new use of the Work(s) and shall render inaccessible (such as by deleting or by removing or severing links or other locators) any further copies of the Work (except for copies printed on paper in accordance with this license and still in User's stock at the end of such period).
- 3.4. In the event that the material for which a republication license is sought includes third party materials (such as photographs, illustrations, graphs, inserts and similar materials) which are identified in such material as having been used by permission, User is responsible for identifying, and seeking separate licenses (under this Service or otherwise) for, any of such third party materials; without a separate license, such third party materials may not be used.
- 3.5. Use of proper copyright notice for a Work is required as a condition of any license granted under the Service. Unless otherwise provided in the Order Confirmation, a proper copyright notice will read substantially as follows: "Republished with permission of [Rightsholder's name], from [Work's title, author, volume, edition number and year of copyright]; permission conveyed through Copyright Clearance Center, Inc. " Such notice must be provided in a reasonably legible font size and must be placed either immediately adjacent to the Work as used (for example, as part of a by-line or footnote but not as a separate electronic link) or in the place where substantially all other credits or notices for the new work containing the republished Work are located. Failure to include the required notice results in loss to the Rightsholder and CCC, and the User shall be liable to pay liquidated damages for each such failure equal to twice the use fee specified in the Order Confirmation, in addition to the use fee itself and any other fees and charges specified.
- 3.6. User may only make alterations to the Work if and as expressly set forth in the Order Confirmation. No Work may be used in any way that is defamatory, violates the rights of third parties (including such third parties' rights of copyright, privacy, publicity, or other tangible or intangible property), or is otherwise illegal, sexually explicit or obscene. In addition, User may not conjoin a Work with any other material that may result in damage to the reputation of the Rightsholder. User agrees to inform CCC if it becomes aware of any infringement of any rights in a Work and to cooperate with any reasonable request of CCC or the Rightsholder in connection therewith.
4. Indemnity. User hereby indemnifies and agrees to defend the Rightsholder and CCC, and their respective employees and directors, against all claims, liability, damages, costs and expenses, including legal fees and expenses, arising out of any use of a Work beyond the scope of the rights granted herein, or any use of a Work which has been altered in any unauthorized way by User, including claims of defamation or infringement of rights of copyright, publicity, privacy or other tangible or intangible property.
5. Limitation of Liability. UNDER NO CIRCUMSTANCES WILL CCC OR THE RIGHTSHOLDER BE LIABLE FOR ANY DIRECT, INDIRECT, CONSEQUENTIAL OR INCIDENTAL DAMAGES (INCLUDING WITHOUT LIMITATION DAMAGES FOR LOSS OF BUSINESS PROFITS OR INFORMATION, OR FOR BUSINESS INTERRUPTION) ARISING OUT OF THE USE OR INABILITY

TO USE A WORK, EVEN IF ONE OF THEM HAS BEEN ADVISED OF THE POSSIBILITY OF SUCH DAMAGES. In any event, the total liability of the Rightsholder and CCC (including their respective employees and directors) shall not exceed the total amount actually paid by User for this license. User assumes full liability for the actions and omissions of its principals, employees, agents, affiliates, successors and assigns.

6. Limited Warranties. THE WORK(S) AND RIGHT(S) ARE PROVIDED "AS IS". CCC HAS THE RIGHT TO GRANT TO USER THE RIGHTS GRANTED IN THE ORDER CONFIRMATION DOCUMENT. CCC AND THE RIGHTSHOLDER DISCLAIM ALL OTHER WARRANTIES RELATING TO THE WORK(S) AND RIGHT(S), EITHER EXPRESS OR IMPLIED, INCLUDING WITHOUT LIMITATION IMPLIED WARRANTIES OF MERCHANTABILITY OR FITNESS FOR A PARTICULAR PURPOSE. ADDITIONAL RIGHTS MAY BE REQUIRED TO USE ILLUSTRATIONS, GRAPHS, PHOTOGRAPHS, ABSTRACTS, INSERTS OR OTHER PORTIONS OF THE WORK (AS OPPOSED TO THE ENTIRE WORK) IN A MANNER CONTEMPLATED BY USER; USER UNDERSTANDS AND AGREES THAT NEITHER CCC NOR THE RIGHTSHOLDER MAY HAVE SUCH ADDITIONAL RIGHTS TO GRANT.
7. Effect of Breach. Any failure by User to pay any amount when due, or any use by User of a Work beyond the scope of the license set forth in the Order Confirmation and/or these terms and conditions, shall be a material breach of the license created by the Order Confirmation and these terms and conditions. Any breach not cured within 30 days of written notice thereof shall result in immediate termination of such license without further notice. Any unauthorized (but licensable) use of a Work that is terminated immediately upon notice thereof may be liquidated by payment of the Rightsholder's ordinary license price therefor; any unauthorized (and unlicensable) use that is not terminated immediately for any reason (including, for example, because materials containing the Work cannot reasonably be recalled) will be subject to all remedies available at law or in equity, but in no event to a payment of less than three times the Rightsholder's ordinary license price for the most closely analogous licensable use plus Rightsholder's and/or CCC's costs and expenses incurred in collecting such payment.
8. Miscellaneous.
  - 8.1. User acknowledges that CCC may, from time to time, make changes or additions to the Service or to these terms and conditions, and CCC reserves the right to send notice to the User by electronic mail or otherwise for the purposes of notifying User of such changes or additions; provided that any such changes or additions shall not apply to permissions already secured and paid for.
  - 8.2. Use of User-related information collected through the Service is governed by CCC's privacy policy, available online here:<https://marketplace.copyright.com/rs-ui-web/mp/privacy-policy>
  - 8.3. The licensing transaction described in the Order Confirmation is personal to User. Therefore, User may not assign or transfer to any other person (whether a natural person or an organization of any kind) the license created by the Order Confirmation and these terms and conditions or any rights granted hereunder; provided, however, that User may assign such license in its entirety on written notice to CCC in the event of a transfer of all or substantially all of User's rights in the new material which includes the Work(s) licensed under this Service.
  - 8.4. No amendment or waiver of any terms is binding unless set forth in writing and signed by the parties. The Rightsholder and CCC hereby object to any terms contained in any writing prepared by the User or its principals, employees, agents or affiliates and purporting to govern or otherwise relate to the licensing transaction described in the Order Confirmation, which terms are in any way inconsistent with any terms set forth in the Order Confirmation and/or in these terms and conditions or CCC's standard operating procedures, whether such writing is prepared prior to, simultaneously with or subsequent to the Order Confirmation, and whether such writing appears on a copy of the Order Confirmation or in a separate instrument.
  - 8.5. The licensing transaction described in the Order Confirmation document shall be governed by and construed under the law of the State of New York, USA, without regard to the principles thereof of conflicts of law. Any case, controversy, suit, action, or proceeding arising out of, in connection with, or related to such licensing transaction shall be brought, at CCC's sole discretion, in any federal or state court located in the County of New York, State of New York, USA, or in any federal or state court whose geographical jurisdiction covers the location of the Rightsholder set forth in the Order Confirmation. The parties

expressly submit to the personal jurisdiction and venue of each such federal or state court. If you have any comments or questions about the Service or Copyright Clearance Center, please contact us at 978-750-8400 or send an e-mail to [support@copyright.com](mailto:support@copyright.com).

v 1.1



## B.2 Chelate chemistry governs ion-specific stiffening of *Bacillus subtilis* B-1 and *Azotobacter vinelandii* biofilms



This is a License Agreement between Martin Kretschmer ("User") and Copyright Clearance Center, Inc. ("CCC") on behalf of the Rightsholder identified in the order details below. The license consists of the order details, the CCC Terms and Conditions below, and any Rightsholder Terms and Conditions which are included below.

All payments must be made in full to CCC in accordance with the CCC Terms and Conditions below.

Order Date	02-Nov-2021	Type of Use	Republish in a thesis/dissertation
Order License ID	1158794-1	Publisher Portion	Royal Society of Chemistry Chapter/article
ISSN	2047-4830		

### LICENSED CONTENT

Publication Title	Biomaterials science	Rightsholder	Royal Society of Chemistry
Article Title	Chelate chemistry governs ion-specific stiffening of <i>Bacillus subtilis</i> B-1 and <i>Azotobacter vinelandii</i> biofilms.	Publication Type	Journal
		Start Page	1923
		End Page	1933
		Issue	7
Author/Editor	Kyoto Daigaku.Bushitsu-Saibō Tōgō Shisutemu Kyoten, Royal Society of Chemistry (Great Britain)	Volume	8
Date	01/01/2013		
Language	English		
Country	United Kingdom of Great Britain and Northern Ireland		

### REQUEST DETAILS

Portion Type	Chapter/article	Rights Requested	Main product and any product related to main product
Page range(s)	1923-1933	Distribution	Worldwide
Total number of pages	11	Translation	Original language of publication
Format (select all that apply)	Print, Electronic	Copies for the disabled?	No
Who will republish the content?	Author of requested content	Minor editing privileges?	No
Duration of Use	Life of current edition	Incidental promotional use?	No
Lifetime Unit Quantity	Up to 499	Currency	EUR

### NEW WORK DETAILS

Title	Material Properties of Bacterial Biofilms and Bioinspired Synthetic Hydrogels	Institution name	Technical University of Munich
Instructor name	Prof. Dr. Oliver Lieleg	Expected presentation date	2022-01-01

## ADDITIONAL DETAILS

Order reference number	N/A	The requesting person / organization to appear on the license	Martin Kretschmer
------------------------	-----	---	-------------------

## REUSE CONTENT DETAILS

Title, description or numeric reference of the portion(s)	Chelate chemistry governs ion-specific stiffening of <i>Bacillus subtilis</i> B-1 and <i>Azotobacter vinelandii</i> biofilms.	Title of the article/chapter the portion is from	Chelate chemistry governs ion-specific stiffening of <i>Bacillus subtilis</i> B-1 and <i>Azotobacter vinelandii</i> biofilms.
Editor of portion(s)	Kretschmer, Martin; Lieleg, Oliver	Author of portion(s)	Kretschmer, Martin; Lieleg, Oliver
Volume of serial or monograph	8	Issue, if republishing an article from a serial	7
Page or page range of portion	1923-1933	Publication date of portion	2020-01-01

## SPECIAL RIGHTSHOLDER TERMS AND CONDITIONS

The Royal Society of Chemistry (RSC) hereby grants permission for the use of your paper(s) specified below in the printed and microfilm version of your thesis. You may also make available the PDF version of your paper(s) that the RSC sent to the corresponding author(s) of your paper(s) upon publication of the paper(s) in the following ways: in your thesis via any website that your university may have for the deposition of theses, via your university's Intranet or via your own personal website. We are however unable to grant you permission to include the PDF version of the paper(s) on its own in your institutional repository. The Royal Society of Chemistry is a signatory to the STM Guidelines on Permissions (available on request). Please note that if the material specified below or any part of it appears with credit or acknowledgement to a third party then you must also secure permission from that third party before reproducing that material. Please ensure that the thesis includes the correct acknowledgement (see <http://rsc.li/permissions> for details) and a link is included to the paper on the Royal Society of Chemistry's website. Please also ensure that your co-authors are aware that you are including the paper in your thesis.

## CCC Terms and Conditions

1. Description of Service; Defined Terms. This Republication License enables the User to obtain licenses for republication of one or more copyrighted works as described in detail on the relevant Order Confirmation (the "Work(s)"). Copyright Clearance Center, Inc. ("CCC") grants licenses through the Service on behalf of the rightsholder identified on the Order Confirmation (the "Rightsholder"). "Republication", as used herein, generally means the inclusion of a Work, in whole or in part, in a new work or works, also as described on the Order Confirmation. "User", as used herein, means the person or entity making such republication.
2. The terms set forth in the relevant Order Confirmation, and any terms set by the Rightsholder with respect to a particular Work, govern the terms of use of Works in connection with the Service. By using the Service, the person transacting for a republication license on behalf of the User represents and warrants that he/she/it (a) has been duly authorized by the User to accept, and hereby does accept, all such terms and conditions on behalf of User, and (b) shall inform User of all such terms and conditions. In the event such person is a "freelancer" or other third party independent of User and CCC, such party shall be deemed jointly a "User" for purposes of these terms and conditions. In any event, User shall be deemed to have accepted and agreed to all such terms and conditions if User republishes the Work in any fashion.
3. Scope of License; Limitations and Obligations.
  - 3.1. All Works and all rights therein, including copyright rights, remain the sole and exclusive property of the Rightsholder. The license created by the exchange of an Order Confirmation (and/or any invoice) and payment by User of the full amount set forth on that document includes only those rights expressly set



forth in the Order Confirmation and in these terms and conditions, and conveys no other rights in the Work(s) to User. All rights not expressly granted are hereby reserved.

- 3.2. General Payment Terms: You may pay by credit card or through an account with us payable at the end of the month. If you and we agree that you may establish a standing account with CCC, then the following terms apply: Remit Payment to: Copyright Clearance Center, 29118 Network Place, Chicago, IL 60673-1291. Payments Due: Invoices are payable upon their delivery to you (or upon our notice to you that they are available to you for downloading). After 30 days, outstanding amounts will be subject to a service charge of 1-1/2% per month or, if less, the maximum rate allowed by applicable law. Unless otherwise specifically set forth in the Order Confirmation or in a separate written agreement signed by CCC, invoices are due and payable on "net 30" terms. While User may exercise the rights licensed immediately upon issuance of the Order Confirmation, the license is automatically revoked and is null and void, as if it had never been issued, if complete payment for the license is not received on a timely basis either from User directly or through a payment agent, such as a credit card company.
  - 3.3. Unless otherwise provided in the Order Confirmation, any grant of rights to User (i) is "one-time" (including the editions and product family specified in the license), (ii) is non-exclusive and non-transferable and (iii) is subject to any and all limitations and restrictions (such as, but not limited to, limitations on duration of use or circulation) included in the Order Confirmation or invoice and/or in these terms and conditions. Upon completion of the licensed use, User shall either secure a new permission for further use of the Work(s) or immediately cease any new use of the Work(s) and shall render inaccessible (such as by deleting or by removing or severing links or other locators) any further copies of the Work (except for copies printed on paper in accordance with this license and still in User's stock at the end of such period).
  - 3.4. In the event that the material for which a republication license is sought includes third party materials (such as photographs, illustrations, graphs, inserts and similar materials) which are identified in such material as having been used by permission, User is responsible for identifying, and seeking separate licenses (under this Service or otherwise) for, any of such third party materials; without a separate license, such third party materials may not be used.
  - 3.5. Use of proper copyright notice for a Work is required as a condition of any license granted under the Service. Unless otherwise provided in the Order Confirmation, a proper copyright notice will read substantially as follows: "Republished with permission of [Rightsholder's name], from [Work's title, author, volume, edition number and year of copyright]; permission conveyed through Copyright Clearance Center, Inc. " Such notice must be provided in a reasonably legible font size and must be placed either immediately adjacent to the Work as used (for example, as part of a by-line or footnote but not as a separate electronic link) or in the place where substantially all other credits or notices for the new work containing the republished Work are located. Failure to include the required notice results in loss to the Rightsholder and CCC, and the User shall be liable to pay liquidated damages for each such failure equal to twice the use fee specified in the Order Confirmation, in addition to the use fee itself and any other fees and charges specified.
  - 3.6. User may only make alterations to the Work if and as expressly set forth in the Order Confirmation. No Work may be used in any way that is defamatory, violates the rights of third parties (including such third parties' rights of copyright, privacy, publicity, or other tangible or intangible property), or is otherwise illegal, sexually explicit or obscene. In addition, User may not conjoin a Work with any other material that may result in damage to the reputation of the Rightsholder. User agrees to inform CCC if it becomes aware of any infringement of any rights in a Work and to cooperate with any reasonable request of CCC or the Rightsholder in connection therewith.
4. Indemnity. User hereby indemnifies and agrees to defend the Rightsholder and CCC, and their respective employees and directors, against all claims, liability, damages, costs and expenses, including legal fees and expenses, arising out of any use of a Work beyond the scope of the rights granted herein, or any use of a Work which has been altered in any unauthorized way by User, including claims of defamation or infringement of rights of copyright, publicity, privacy or other tangible or intangible property.

5. **Limitation of Liability.** UNDER NO CIRCUMSTANCES WILL CCC OR THE RIGHTSHOLDER BE LIABLE FOR ANY DIRECT, INDIRECT, CONSEQUENTIAL OR INCIDENTAL DAMAGES (INCLUDING WITHOUT LIMITATION DAMAGES FOR LOSS OF BUSINESS PROFITS OR INFORMATION, OR FOR BUSINESS INTERRUPTION) ARISING OUT OF THE USE OR INABILITY TO USE A WORK, EVEN IF ONE OF THEM HAS BEEN ADVISED OF THE POSSIBILITY OF SUCH DAMAGES. In any event, the total liability of the Rightsholder and CCC (including their respective employees and directors) shall not exceed the total amount actually paid by User for this license. User assumes full liability for the actions and omissions of its principals, employees, agents, affiliates, successors and assigns.
6. **Limited Warranties.** THE WORK(S) AND RIGHT(S) ARE PROVIDED "AS IS". CCC HAS THE RIGHT TO GRANT TO USER THE RIGHTS GRANTED IN THE ORDER CONFIRMATION DOCUMENT. CCC AND THE RIGHTSHOLDER DISCLAIM ALL OTHER WARRANTIES RELATING TO THE WORK(S) AND RIGHT(S), EITHER EXPRESS OR IMPLIED, INCLUDING WITHOUT LIMITATION IMPLIED WARRANTIES OF MERCHANTABILITY OR FITNESS FOR A PARTICULAR PURPOSE. ADDITIONAL RIGHTS MAY BE REQUIRED TO USE ILLUSTRATIONS, GRAPHS, PHOTOGRAPHS, ABSTRACTS, INSERTS OR OTHER PORTIONS OF THE WORK (AS OPPOSED TO THE ENTIRE WORK) IN A MANNER CONTEMPLATED BY USER; USER UNDERSTANDS AND AGREES THAT NEITHER CCC NOR THE RIGHTSHOLDER MAY HAVE SUCH ADDITIONAL RIGHTS TO GRANT.
7. **Effect of Breach.** Any failure by User to pay any amount when due, or any use by User of a Work beyond the scope of the license set forth in the Order Confirmation and/or these terms and conditions, shall be a material breach of the license created by the Order Confirmation and these terms and conditions. Any breach not cured within 30 days of written notice thereof shall result in immediate termination of such license without further notice. Any unauthorized (but licensable) use of a Work that is terminated immediately upon notice thereof may be liquidated by payment of the Rightsholder's ordinary license price therefor; any unauthorized (and unlicensable) use that is not terminated immediately for any reason (including, for example, because materials containing the Work cannot reasonably be recalled) will be subject to all remedies available at law or in equity, but in no event to a payment of less than three times the Rightsholder's ordinary license price for the most closely analogous licensable use plus Rightsholder's and/or CCC's costs and expenses incurred in collecting such payment.
8. **Miscellaneous.**
  - 8.1. User acknowledges that CCC may, from time to time, make changes or additions to the Service or to these terms and conditions, and CCC reserves the right to send notice to the User by electronic mail or otherwise for the purposes of notifying User of such changes or additions; provided that any such changes or additions shall not apply to permissions already secured and paid for.
  - 8.2. Use of User-related information collected through the Service is governed by CCC's privacy policy, available online here: <https://marketplace.copyright.com/rs-ui-web/mp/privacy-policy>
  - 8.3. The licensing transaction described in the Order Confirmation is personal to User. Therefore, User may not assign or transfer to any other person (whether a natural person or an organization of any kind) the license created by the Order Confirmation and these terms and conditions or any rights granted hereunder; provided, however, that User may assign such license in its entirety on written notice to CCC in the event of a transfer of all or substantially all of User's rights in the new material which includes the Work(s) licensed under this Service.
  - 8.4. No amendment or waiver of any terms is binding unless set forth in writing and signed by the parties. The Rightsholder and CCC hereby object to any terms contained in any writing prepared by the User or its principals, employees, agents or affiliates and purporting to govern or otherwise relate to the licensing transaction described in the Order Confirmation, which terms are in any way inconsistent with any terms set forth in the Order Confirmation and/or in these terms and conditions or CCC's standard operating procedures, whether such writing is prepared prior to, simultaneously with or subsequent to the Order Confirmation, and whether such writing appears on a copy of the Order Confirmation or in a separate instrument.
  - 8.5. The licensing transaction described in the Order Confirmation document shall be governed by and construed under the law of the State of New York, USA, without regard to the principles thereof of conflicts

of law. Any case, controversy, suit, action, or proceeding arising out of, in connection with, or related to such licensing transaction shall be brought, at CCC's sole discretion, in any federal or state court located in the County of New York, State of New York, USA, or in any federal or state court whose geographical jurisdiction covers the location of the Rightsholder set forth in the Order Confirmation. The parties expressly submit to the personal jurisdiction and venue of each such federal or state court. If you have any comments or questions about the Service or Copyright Clearance Center, please contact us at 978-750-8400 or send an e-mail to [support@copyright.com](mailto:support@copyright.com).

v 1.1



### *B.3 Biofilm adhesion to surfaces is modulated by biofilm wettability and stiffness*

#### JOHN WILEY AND SONS LICENSE TERMS AND CONDITIONS

Nov 02, 2021

---

---

This Agreement between Mr. Martin Kretschmer ("You") and John Wiley and Sons ("John Wiley and Sons") consists of your license details and the terms and conditions provided by John Wiley and Sons and Copyright Clearance Center.

License Number	5180740776146
License date	Nov 02, 2021
Licensed Content Publisher	John Wiley and Sons
Licensed Content Publication	Advanced Materials Interfaces
Licensed Content Title	Biofilm Adhesion to Surfaces is Modulated by Biofilm Wettability and Stiffness
Licensed Content Author	Martin Kretschmer, Carina Anke Schüßler, Oliver Lieleg
Licensed Content Date	Jan 15, 2021
Licensed Content Volume	8
Licensed Content Issue	5
Licensed Content Pages	13
Type of use	Dissertation/Thesis
Requestor type	Author of this Wiley article

Format	Print and electronic
Portion	Full article
Will you be translating?	No
Title	Material Properties of Bacterial Biofilms and Bioinspired Synthetic Hydrogels
Institution name	Technical University of Munich
Expected presentation date	Jan 2022
Requestor Location	Mr. Martin Kretschmer Anton-Zwengauer-Weg 13  Poing, other 85586 Germany Attn: Mr. Martin Kretschmer
Publisher Tax ID	EU826007151
Total	0.00 EUR
Terms and Conditions	

#### TERMS AND CONDITIONS

This copyrighted material is owned by or exclusively licensed to John Wiley & Sons, Inc. or one of its group companies (each a "Wiley Company") or handled on behalf of a society with which a Wiley Company has exclusive publishing rights in relation to a particular work (collectively "WILEY"). By clicking "accept" in connection with completing this licensing transaction, you agree that the following terms and conditions apply to this transaction (along with the billing and payment terms and conditions established by the Copyright Clearance Center Inc., ("CCC's Billing and Payment terms and conditions"), at the time that you opened your RightsLink account (these are available at any time at <http://myaccount.copyright.com>).

#### Terms and Conditions

- The materials you have requested permission to reproduce or reuse (the "Wiley Materials") are protected by copyright.
- You are hereby granted a personal, non-exclusive, non-sub licensable (on a stand-alone basis), non-transferable, worldwide, limited license to reproduce the Wiley Materials for the purpose specified in the licensing process. This license, and any **CONTENT (PDF or image file) purchased as part of your order**, is for a one-time use only and limited to any maximum distribution number specified in the license. The first instance of republication or reuse granted by this license must be completed within two years of the date of the grant of this license (although copies prepared before the end date may be distributed thereafter). The Wiley Materials shall not be used in any other manner or for any other purpose, beyond what is granted in the license. Permission is granted subject to an appropriate acknowledgement given to the author, title of the material/book/journal and the publisher. You shall also duplicate the copyright notice that appears in the Wiley publication in your use of the Wiley Material. Permission is also granted on the understanding that nowhere in the text is a previously published source acknowledged for all or part of this Wiley Material. Any third party content is expressly excluded from this permission.
- With respect to the Wiley Materials, all rights are reserved. Except as expressly granted by the terms of the license, no part of the Wiley Materials may be copied, modified, adapted (except for minor reformatting required by the new Publication), translated, reproduced, transferred or distributed, in any form or by any means, and no derivative works may be made based on the Wiley Materials without the prior permission of the respective copyright owner. **For STM Signatory Publishers clearing permission under the terms of the [STM Permissions Guidelines](#) only, the terms of the license are extended to include subsequent editions and for editions in other languages, provided such editions are for the work as a whole in situ and does not involve the separate exploitation of the permitted figures or extracts,** You may not alter, remove or suppress in any manner any copyright, trademark or other notices displayed by the Wiley Materials. You may not license, rent, sell, loan, lease, pledge, offer as security, transfer or assign the Wiley Materials on a stand-alone basis, or any of the rights granted to you hereunder to any other person.
- The Wiley Materials and all of the intellectual property rights therein shall at all times remain the exclusive property of John Wiley & Sons Inc, the Wiley Companies, or their respective licensors, and your interest therein is only that of having possession of and the right to reproduce the Wiley Materials pursuant to Section 2 herein during the continuance of this Agreement. You agree that you own no right, title or interest in or to the Wiley Materials or any of the intellectual property rights therein. You shall have no rights hereunder other than the license as provided for above in Section 2. No right, license or interest to any trademark, trade name, service mark or other branding ("Marks") of WILEY or its licensors is granted hereunder, and you agree that you shall not assert any such right, license or interest with respect thereto
- **NEITHER WILEY NOR ITS LICENSORS MAKES ANY WARRANTY OR REPRESENTATION OF ANY KIND TO YOU OR ANY THIRD PARTY, EXPRESS, IMPLIED OR STATUTORY, WITH RESPECT TO THE MATERIALS OR THE ACCURACY OF ANY INFORMATION CONTAINED IN THE MATERIALS, INCLUDING, WITHOUT LIMITATION, ANY IMPLIED**

WARRANTY OF MERCHANTABILITY, ACCURACY, SATISFACTORY QUALITY, FITNESS FOR A PARTICULAR PURPOSE, USABILITY, INTEGRATION OR NON-INFRINGEMENT AND ALL SUCH WARRANTIES ARE HEREBY EXCLUDED BY WILEY AND ITS LICENSORS AND WAIVED BY YOU.

- WILEY shall have the right to terminate this Agreement immediately upon breach of this Agreement by you.
- You shall indemnify, defend and hold harmless WILEY, its Licensors and their respective directors, officers, agents and employees, from and against any actual or threatened claims, demands, causes of action or proceedings arising from any breach of this Agreement by you.
- IN NO EVENT SHALL WILEY OR ITS LICENSORS BE LIABLE TO YOU OR ANY OTHER PARTY OR ANY OTHER PERSON OR ENTITY FOR ANY SPECIAL, CONSEQUENTIAL, INCIDENTAL, INDIRECT, EXEMPLARY OR PUNITIVE DAMAGES, HOWEVER CAUSED, ARISING OUT OF OR IN CONNECTION WITH THE DOWNLOADING, PROVISIONING, VIEWING OR USE OF THE MATERIALS REGARDLESS OF THE FORM OF ACTION, WHETHER FOR BREACH OF CONTRACT, BREACH OF WARRANTY, TORT, NEGLIGENCE, INFRINGEMENT OR OTHERWISE (INCLUDING, WITHOUT LIMITATION, DAMAGES BASED ON LOSS OF PROFITS, DATA, FILES, USE, BUSINESS OPPORTUNITY OR CLAIMS OF THIRD PARTIES), AND WHETHER OR NOT THE PARTY HAS BEEN ADVISED OF THE POSSIBILITY OF SUCH DAMAGES. THIS LIMITATION SHALL APPLY NOTWITHSTANDING ANY FAILURE OF ESSENTIAL PURPOSE OF ANY LIMITED REMEDY PROVIDED HEREIN.
- Should any provision of this Agreement be held by a court of competent jurisdiction to be illegal, invalid, or unenforceable, that provision shall be deemed amended to achieve as nearly as possible the same economic effect as the original provision, and the legality, validity and enforceability of the remaining provisions of this Agreement shall not be affected or impaired thereby.
- The failure of either party to enforce any term or condition of this Agreement shall not constitute a waiver of either party's right to enforce each and every term and condition of this Agreement. No breach under this agreement shall be deemed waived or excused by either party unless such waiver or consent is in writing signed by the party granting such waiver or consent. The waiver by or consent of a party to a breach of any provision of this Agreement shall not operate or be construed as a waiver of or consent to any other or subsequent breach by such other party.
- This Agreement may not be assigned (including by operation of law or otherwise) by you without WILEY's prior written consent.
- Any fee required for this permission shall be non-refundable after thirty (30) days from receipt by the CCC.
- These terms and conditions together with CCC's Billing and Payment terms and conditions (which are incorporated herein) form the entire agreement between you and



WILEY concerning this licensing transaction and (in the absence of fraud) supersedes all prior agreements and representations of the parties, oral or written. This Agreement may not be amended except in writing signed by both parties. This Agreement shall be binding upon and inure to the benefit of the parties' successors, legal representatives, and authorized assigns.

- In the event of any conflict between your obligations established by these terms and conditions and those established by CCC's Billing and Payment terms and conditions, these terms and conditions shall prevail.
- WILEY expressly reserves all rights not specifically granted in the combination of (i) the license details provided by you and accepted in the course of this licensing transaction, (ii) these terms and conditions and (iii) CCC's Billing and Payment terms and conditions.
- This Agreement will be void if the Type of Use, Format, Circulation, or Requestor Type was misrepresented during the licensing process.
- This Agreement shall be governed by and construed in accordance with the laws of the State of New York, USA, without regards to such state's conflict of law rules. Any legal action, suit or proceeding arising out of or relating to these Terms and Conditions or the breach thereof shall be instituted in a court of competent jurisdiction in New York County in the State of New York in the United States of America and each party hereby consents and submits to the personal jurisdiction of such court, waives any objection to venue in such court and consents to service of process by registered or certified mail, return receipt requested, at the last known address of such party.

## **WILEY OPEN ACCESS TERMS AND CONDITIONS**

Wiley Publishes Open Access Articles in fully Open Access Journals and in Subscription journals offering Online Open. Although most of the fully Open Access journals publish open access articles under the terms of the Creative Commons Attribution (CC BY) License only, the subscription journals and a few of the Open Access Journals offer a choice of Creative Commons Licenses. The license type is clearly identified on the article.

### **The Creative Commons Attribution License**

The [Creative Commons Attribution License \(CC-BY\)](#) allows users to copy, distribute and transmit an article, adapt the article and make commercial use of the article. The CC-BY license permits commercial and non-

### **Creative Commons Attribution Non-Commercial License**

The [Creative Commons Attribution Non-Commercial \(CC-BY-NC\) License](#) permits use, distribution and reproduction in any medium, provided the original work is properly cited and is not used for commercial purposes.(see below)

### **Creative Commons Attribution-Non-Commercial-NoDerivs License**

The [Creative Commons Attribution Non-Commercial-NoDerivs License \(CC-BY-NC-ND\)](#)

permits use, distribution and reproduction in any medium, provided the original work is properly cited, is not used for commercial purposes and no modifications or adaptations are made. (see below)

**Use by commercial "for-profit" organizations**

Use of Wiley Open Access articles for commercial, promotional, or marketing purposes requires further explicit permission from Wiley and will be subject to a fee.

Further details can be found on Wiley Online Library <http://olabout.wiley.com/WileyCDA/Section/id-410895.html>

**Other Terms and Conditions:**

v1.10 Last updated September 2015

Questions? [customercare@copyright.com](mailto:customercare@copyright.com) or +1-855-239-3415 (toll free in the US) or +1-978-646-2777.



## B.4 Viscoelastic behavior of chemically fueled supramolecular hydrogels under load and influence of reaction side products



Viscoelastic behavior of chemically fueled supramolecular hydrogels under load and influence of reaction side products

Author: Martin Kretschmer et al

Publication: Communications Materials

Publisher: Springer Nature

Date: Sep 17, 2021

Copyright © 2021, The Author(s)

**SPRINGER NATURE**

### Creative Commons

This is an open access article distributed under the terms of the [Creative Commons CC BY](#) license, which permits unrestricted use, distribution, and reproduction in any medium, provided the original work is properly cited.

You are not required to obtain permission to reuse this article.

To request permission for a type of use not listed, please contact [Springer Nature](#)



## C. Full list of publications

### C.1 Peer-reviewed

Klotz, M., **M. Kretschmer**, A. Goetz, S. Ezendam, O. Lieleg, and M. Opitz, Importance of the bio-film matrix for the erosion stability of *Bacillus subtilis* NCIB 3610 biofilms. *RSC Advances*, 2019. 9(20): p. 11521-11529.

**Kretschmer, M.**, and O. Lieleg, Chelate chemistry governs ion-specific stiffening of *Bacillus subtilis* B-1 and *Azotobacter vinelandii* biofilms. *Biomaterials Science*, 2020. 8(7): p. 1923-1933.

García, C. F., **M. Kretschmer**, C. N. Lozano-Andrade, M. Schönleitner, A. Dragoș, Á. T. Kovács, and O. Lieleg, Metal ions weaken the hydrophobicity and antibiotic resistance of *Bacillus subtilis* NCIB 3610 biofilms. *NPJ Biofilms and Microbiomes*, 2020. 6(1): p. 1-11.

**Kretschmer, M.**, C. A. Schüßler, and O. Lieleg, Biofilm adhesion to surfaces is modulated by bio-film wettability and stiffness. *Advanced Materials Interfaces*, 2021. 8(5): p. 2001658.

**Kretschmer, M.**, B. Winkeljann, B. A. Kriebisch, J. Boekhoven, and O. Lieleg, Viscoelastic behavior of chemically fueled supramolecular hydrogels under load and influence of reaction side products. *Communications Materials*, 2021. 2(1): p. 1-10.

Hayta, E. N., M. J. Ertelt, **M. Kretschmer**, and O. Lieleg, Bacterial materials: applications of natural and modified biofilms. *Advanced Materials Interfaces*, 2021. 8: p. 2101024.

### C.2 Not peer-reviewed yet

**Kretschmer, M.**, E. N., Hayta, M. J. Ertelt, M. A., Würbser, J. Boekhoven, and O. Lieleg, A rotating bioreactor for the production of biofilms at the solid-air interface. In review process, *Biotechnology and Bioengineering*.



## D. Bibliography

1. Vlamakis, H., et al., *Sticking together: building a biofilm the Bacillus subtilis way*. Nature Reviews Microbiology, 2013. **121**: p. 1-58.
2. Costerton, J.W., P.S. Stewart, and E.P. Greenberg, *Bacterial biofilms: A common cause of persistent infections*. Science, 1999. **17**: p. 1318-1322.
3. Schultz, M.P., et al., *Economic impact of biofouling on a naval surface ship*. Biofouling, 2011. **27**: p. 87-98.
4. Bhatia, R., D. Gulati, and G. Sethi, *Biofilms and nanoparticles: applications in agriculture*. Folia Microbiologica, 2021. **66**: p. 159-170.
5. Gauri, S.S., S.M. Mandal, and B.R. Pati, *Impact of Azotobacterexopolysaccharides on sustainable agriculture*. Applied Microbiology and Biotechnology, 2012. **95**: p. 331-338.
6. Nicolella, C., M.C.M. van Loosdrecht, and J.J. Heijnen, *Wastewater treatment with particulate biofilm reactors*. Journal of Biotechnology, 2000. **80**: p. 1-33.
7. Lewandowski, Z. and J.P. Boltz, *Biofilms in water and wastewater treatment*, in *Treatise on Water Science*, P. Wilderer, Editor. 2011, Academic Press: Oxford. p. 529-570.
8. Flemming, H.-C. and J. Wingender, *The biofilm matrix*. Nature reviews microbiology, 2010. **8**: p. 623-633.
9. Sauer, K., A.H. Rickard, and D.G. Davies, *Biofilms and Biocomplexity*. Microbe-American Society for Microbiology, 2007. **2**: p. 347-353.
10. Thompson, R.C., et al., *Differences in photosynthetic marine biofilms between sheltered and moderately exposed rocky shores*. Marine Ecology Progress Series, 2005. **296**: p. 53-63.
11. Siqueira Jr., J.F., I.N. Rôças, and D. Ricucci, *Biofilms in endodontic infection*. Endodontic Topics, 2012. **22**: p. 33-49.
12. Pandit, A., et al., *Microbial biofilms in nature: unlocking their potential for agricultural applications*. Journal of Applied Microbiology, 2020. **129**: p. 199-211.
13. Salta, M., et al., *Marine biofilms on artificial surfaces: structure and dynamics*. Environmental Microbiology, 2013. **15**: p. 2879-2893.
14. Yu, J., D. Kim, and T. Lee, *Microbial diversity in biofilms on water distribution pipes of different materials*. Water Science and Technology, 2010. **61**: p. 163-171.
15. Herb, S., et al., *Characterization of biofilms on corroded concrete surfaces in drinking water reservoirs*. Water Science and Technology, 1995. **32**: p. 141-147.
16. Roehling, S., et al., *In vitro biofilm formation on titanium and zirconia implant surfaces*. Journal of Periodontology, 2017. **88**: p. 298-307.
17. Gominet, M., et al., *Central venous catheters and biofilms: where do we stand in 2017?* Apmis, 2017. **125**: p. 365-375.
18. Kryazhevskikh, N.A., et al., *Reactivation of dormant and nonculturable bacterial forms from paleosoils and subsoil permafrost*. Microbiology, 2012. **81**: p. 435-445.
19. Konings, W.N., et al., *The cell membrane plays a crucial role in survival of bacteria and archaea in extreme environments*. Antonie van Leeuwenhoek, 2002. **81**: p. 61-72.
20. Branda, S.S., et al., *Fruiting body formation by Bacillus subtilis*. Proceedings of the National Academy of Sciences, 2001. **98**: p. 11621-11626.

21. Morikawa, M., M. Ito, and T. Imanaka, *Isolation of a new surfactin producer Bacillus punilus A-1, and cloning and nucleotide sequence of the regulator gene, psf-1*. Journal of Fermentation and Bioengineering, 1992. **74**(5): p. 255-261.
22. Goto, A. and M. Kunioka, *Biosynthesis and hydrolysis of poly( $\gamma$ -glutamic acid) from Bacillus subtilis IFO3335*. Bioscience, biotechnology, and biochemistry, 1992. **56**(7): p. 1031-1035.
23. Zhang, N., et al., *A new bioorganic fertilizer can effectively control banana wilt by strong colonization with Bacillus subtilis N11*. Plant and Soil, 2011. **344**: p. 87-97.
24. Dang, H., et al., *Cross-ocean distribution of Rhodobacterales bacteria as primary surface colonizers in temperate coastal marine waters*. Applied and environmental microbiology, 2008. **74**: p. 52-60.
25. Wilking, J.N., et al., *Biofilms as complex fluids*. Materials research society, 2011. **36**: p. 385-391.
26. Seymour, J.D., et al., *Magnetic resonance microscopy of biofilm structure and impact on transport in a capillary bioreactor*. Journal of magnetic resonance, 2004. **167**: p. 322-327.
27. Kolodkin-Gal, I., et al., *D-amino acids trigger biofilm disassembly*. Science, 2010. **328**: p. 627-629.
28. Russel, R.R.B., *Bacterial polysaccharides in dental plaque*, in *Bacterial polysaccharides: current innovations and future trends*, M. Ullrich, Editor. 2009, Caister Academic Press: Bremen, Germany.
29. Branda, S.S., et al., *A major protein component of the Bacillus subtilis biofilm matrix*. Molecular microbiology, 2006. **59**: p. 1229-1238.
30. Romero, D., et al., *Amyloid fibers provide structural integrity to Bacillus subtilis biofilms*. Proceedings of the National Academy of Sciences, 2010. **107**: p. 2230-2234.
31. Romero, D., et al., *An accessory protein required for anchoring and assembly of amyloid fibres in B. subtilis biofilms*. Molecular Microbiology, 2011. **80**: p. 1155-1168.
32. Morikawa, M., et al., *Biofilm formation by a Bacillus subtilis strain that produces  $\gamma$ -polyglutamate*. Microbiology, 2006. **152**: p. 2801-2807.
33. Grumbein, S., M. Opitz, and O. Lieleg, *Selected metal ions protect Bacillus subtilis biofilms from erosion*. Metallomics, 2014. **6**(8): p. 1441-1450.
34. Rehm, B.H.A., *Alginate: biology and applications*. 2009, Berlin, Heidelberg: Springer-Verlag.
35. Wloka, M., et al., *Rheological properties of viscoelastic biofilm extracellular polymeric substances and comparison to the behavior of calcium alginate gels*. Colloid and Polymer Science, 2004. **282**(10): p. 1067-1076.
36. Mayer, C., et al., *The role of intermolecular interactions: studies on model systems for bacterial biofilms*. International journal of biological macromolecules, 1999. **26**: p. 3-16.
37. Hayta, E.N., et al., *Bacterial materials: applications of natural and modified biofilms*. Advanced Materials Interfaces, 2021. **8**: p. 2101024.
38. Lieleg, O., et al., *Mechanical robustness of Pseudomonas aeruginosa biofilms*. Soft matter, 2011. **7**(7): p. 3307-3314.
39. Shen, Y., et al., *Effect of divalent ions and a polyphosphate on composition, structure, and stiffness of simulated drinking water biofilms*. Npj Biofilms and Microbiomes, 2018. **4**: p. 1-9.



40. Jana, S., et al., *Nonlinear rheological characteristics of single species bacterial biofilms*. Npj Biofilms and Microbiomes, 2020. **6**: p. 1-11.
41. Hohne, D.N., J.G. Younger, and M.J. Solomon, *Flexible microfluidic device for mechanical property characterization of soft viscoelastic solids such as bacterial biofilms*. Langmuir, 2009. **25**: p. 7743-7751.
42. Vilain, S., et al., *DNA as an adhesin: Bacillus cereus requires extracellular DNA to form biofilms*. Applied and Environmental Microbiology, 2009. **75**: p. 2861-2868.
43. Ma, L., et al., *Assembly and development of the Pseudomonas aeruginosa biofilm matrix*. PLoS pathogens, 2009. **5**: p. e1000354.
44. Morikawa, M., *Beneficial biofilm formation by industrial bacteria Bacillus subtilis and related species*. Journal of bioscience and bioengineering, 2006. **101**(1): p. 1-8.
45. Epstein, A.K., et al., *Bacterial biofilm shows persistent resistance to liquid wetting and gas penetration*. Proceedings of the National Academy of Sciences, 2011. **108**: p. 995-1000.
46. García, C.F., et al., *Topographical alterations render bacterial biofilms susceptible to chemical and mechanical stress*. Biomaterials Science, 2019. **7**: p. 220-232.
47. Werb, M., et al., *Surface topology affects wetting behavior of Bacillus subtilis biofilms*. npj Biofilms and Microbiomes, 2017. **3**(1): p. 1-10.
48. Kobayashi, K. and M. Iwano, *BslA(YuaB) forms a hydrophobic layer on the surface of Bacillus subtilis biofilms*. Molecular microbiology, 2012. **85**: p. 51-66.
49. Wösten, H.A.B., *Hydrophobins: multipurpose proteins*. Annual Reviews in Microbiology, 2001. **55**: p. 625-646.
50. García, C.F., et al., *Metal ions weaken the hydrophobicity and antibiotic resistance of Bacillus subtilis NCIB 3610 biofilms*. NPJ Biofilms and Microbiomes, 2020. **6**(1): p. 1-11.
51. Singh, S., et al., *Understanding the mechanism of bacterial biofilms resistance to antimicrobial agents*. The open microbiology journal, 2017. **11**: p. 53-62.
52. Stewart, P.S., *Mechanisms of antibiotic resistance in bacterial biofilms*. International journal of medical microbiology, 2002. **292**: p. 107-113.
53. Nichols, W.W., *Biofilms, antibiotics and penetration*. Reviews in Medical Microbiology, 1991. **2**: p. 177-181.
54. van Hullebusch, E.D., M.H. Zandvoort, and P.N.L. Lens, *Metal immobilisation by biofilms: mechanisms and analytical tools*. Reviews in Environmental Science and Biotechnology, 2004. **0**: p. 1-25.
55. Hall-Stoodley, L., J.W. Costerton, and P. Stoodley, *Bacterial biofilms: from the natural environment to infectious diseases*. Nature reviews microbiology, 2004. **2**: p. 95-108.
56. Oliver, A., et al., *High frequency of hypermutable Pseudomonas aeruginosa in cystic fibrosis lung infection*. Science, 2000. **288**: p. 1251-1253.
57. Vishwakarma, V., *Impact of environmental biofilms: Industrial components and its remediation*. Journal of basic microbiology, 2019. **60**: p. 198-206.
58. Brooks, J.D. and S.H. Flint, *Biofilms in the food industry: problems and potential solutions*. International journal of food science & technology, 2008. **43**: p. 2163-2176.
59. Kumar, C.G. and S. Anand, *Significance of microbial biofilms in food industry: a review*. International journal of food microbiology, 1998. **42**: p. 9-27.

60. Galié, S., et al., *Biofilms in the food industry: health aspects and control methods*. *Frontiers in microbiology*, 2018. **9**: p. 898.
61. Beech, I.B. and J. Sunner, *Biocorrosion: towards understanding interactions between biofilms and metals*. *Current opinion in biotechnology*, 2004. **15**: p. 181-186.
62. Yao, J. and C. Allen, *The plant pathogen *Ralstonia solanacearum* needs aerotaxis for normal biofilm formation and interactions with its tomato host*. *Journal of Bacteriology*, 2007. **189**: p. 6415-6424.
63. Rudrappa, T., M.L. Biedrzycki, and H.P. Bais, *Causes and consequences of plant-associated biofilms*. *FEMS microbiology ecology*, 2008: p. 153-166.
64. Walker, T.S., et al., *Pseudomonas aeruginosa-plant root interactions. Pathogenicity, biofilm formation, and root exudation*. *Plant Physiology*, 2004. **134**: p. 320-331.
65. Fung, T.C., C.A. Olson, and E.Y. Hsiao, *Interactions between the microbiota, immune and nervous systems in health and disease*. *Nature Neuroscience*, 2017. **20**: p. 145-155.
66. Macfarlane, S., *Microbial biofilm communities in the gastrointestinal tract*. *Journal of clinical gastroenterology*, 2008. **42**: p. S142-S143.
67. Macfarlane, S., B. Bahrami, and G.T. Macfarlane, *Mucosal biofilm communities in the human intestinal tract*. *Advances in applied microbiology*, 2011. **75**: p. 111-143.
68. Dimidi, E., et al., *Fermented foods: definitions and characteristics, impact on the gut microbiota and effects on gastrointestinal health and disease*. *Nutrients*, 2019. **11**: p. 1806.
69. Hasan, M.N., M.Z. Sultan, and M. Mar-E-Um, *Significance of fermented food in nutrition and food science*. *Journal of Scientific Research*, 2014. **6**: p. 373-386.
70. Hu, Y., et al., *Characterization of fermented black soybean natto inoculated with *Bacillus natto* during fermentation*. *Journal of the Science of Food and Agriculture*, 2010. **90**: p. 1194-1202.
71. Burns Jr., T.A., P.E. Bishop, and D.W. Irsrael, *Enhanced nodulation of leguminous plant roots by mixed cultures of *Azotobacter vinelandii* and *Rhizobium**. *Plant and soil*, 1981. **62**: p. 399-412.
72. Dabral, S., et al., *Synergistic inoculation of *Azotobacter vinelandii* and *Serendipita indica* augmented rice growth*. *Symbiosis*, 2020. **81**: p. 139-148.
73. Zuo, R. and T.K. Wood, *Inhibiting mild steel corrosion from sulfate-reducing and iron-oxidizing bacteria using gramicidin-S-producing biofilms*. *Applied microbiology and biotechnology*, 2004. **65**: p. 747-753.
74. Liu, T., et al., *Marine bacteria provide lasting anticorrosion activity for steel via biofilm-induced mineralization*. *ACS applied materials & interfaces*, 2018. **10**: p. 40317-40327.
75. Ødegaard, H., *Innovations in wastewater treatment:—the moving bed biofilm process*. *Water Science and Technology*, 2006. **53**: p. 17-33.
76. Wingender, J. and K.-E. Jaeger, *Extracellular enzymes in biofilms*, in *Encyclopedia of environmental microbiology.*, G. Bitton, Editor. 2003, John Wiley & Sons, Inc.: New York, USA.
77. Schaffner, M., et al., *3D printing of bacteria into functional complex materials*. *Science Advances*, 2017. **3**: p. eaao6804.
78. Demirci, A., A.L. Pometto III, and K.E. Johnson, *Lactic acid production in a mixed-culture biofilm reactor*. *Applied and Environmental Microbiology*, 1993. **59**: p. 203-207.

79. Demirci, A., A.L. Pometto III, and K.L.G. Ho, *Ethanol production by Saccharomyces cerevisiae in biofilm reactors*. Journal of Industrial Microbiology and Biotechnology, 1997. **19**: p. 299-304.
80. Rainieri, S. and C. Zambonelli, *Organisms associated with acetic acid bacteria in vinegar production*, in *Vinegars of the world*, L. Solieri and P. Giudici, Editors. 2009, Springer-Verlag Italia: Milan, Italy.
81. Grumbein, S., et al., *Hydrophobic properties of biofilm-enriched hybrid mortar*. Advanced Materials, 2016. **28**: p. 8138-8143.
82. Ertelt, M.J., et al., *Bacterial additives improve the water resistance of mortar*. ACS Sustainable Chemistry & Engineering, 2020. **8**: p. 5704-5715.
83. Ertelt, M.J., et al., *Bacterial spores as hydrophobizing agents in mortar*. Cement and Concrete Composites, 2021. **120**: p. 104002.
84. Qureshi, N., et al., *Biofilm reactors for industrial bioconversion processes: employing potential of enhanced reaction rates*. Microbial Cell Factories, 2005. **4**: p. 1-21.
85. Rittmann, B.E., *Comparative performance of biofilm reactor types*. Biotechnology and Bioengineering, 1982. **24**: p. 1341-1370.
86. Arvin, E. and P. Harremoës, *Concepts and models for biofilm reactor performance*. Water Science and Technology, 1990. **22**: p. 171-192.
87. Tallawi, M., M. Opitz, and O. Lieleg, *Modulation of the mechanical properties of bacterial biofilms in response to environmental challenges*. Biomaterials science, 2017. **5**: p. 887-900.
88. Lattif, A.A., et al., *Characterization of biofilms formed by Candida parapsilosis, C. metapsilosis, and C. orthopsilosis*. International Journal of Medical Microbiology, 2010. **300**: p. 265-270.
89. Chen, M.J., Z. Zhang, and T. Bott, R, *Direct measurement of the adhesive strength of biofilms in pipes by micromanipulation*. Biotechnology Techniques, 1998. **12**(12): p. 875-880.
90. Yan, J., et al., *Bacterial biofilm material properties enable removal and transfer by capillary peeling*. Advanced Materials, 2018. **30**: p. 1-10.
91. Rupp, F., L. Scheideler, and J. Geis-Gerstorfer, *Effect of heterogenic surfaces on contact angle hysteresis: dynamic contact angle analysis in material sciences*. Chemical Engineering & Technology: Industrial Chemistry–Plant Equipment–Process Engineering–Biotechnology, 2002. **25**: p. 877-882.
92. Bajaj, I. and R. Singhal, *Poly (glutamic acid) – An emerging biopolymer of commercial interest*. Bioresource Technology, 2011. **102**: p. 5551-5561.
93. Shi, Z., et al., *Double network bacterial cellulose hydrogel to build a biology–device interface*. Nanoscale, 2014. **6**: p. 970-977.
94. Azeredo, H.M.C., et al., *Bacterial cellulose as a raw material for food and food packaging applications*. Frontiers in Sustainable Food Systems, 2019. **3**: p. 1-14.
95. Lee, K.Y. and D.J. Mooney, *Alginate: Properties and biomedical applications*. Progress in Polymer Science, 2012. **37**: p. 106-126.
96. Wang, P., et al., *Biomimetic poly ( $\gamma$ -glutamic acid) hydrogels based on iron (III) ligand coordination for cartilage tissue engineering*. International Journal of Biological Macromolecules, 2021. **167**: p. 1508-1516.

97. Smidsrød, O. and G. Skjåk-Bræk, *Alginate as immobilization matrix for cells*. Trends in biotechnology, 1990. **8**: p. 71-78.
98. Morris, E.R., D.A. Rees, and D. Thom, *Chiroptical and stoichiometric evidence of a specific, primary dimerisation process in alginate gelation*. Carbohydrate research, 1978. **66**: p. 145-154.
99. Amin, M.C.I.M.A., et al., *Synthesis and characterization of thermo- and pH-responsive bacterial cellulose/acrylic acid hydrogels for drug delivery*. Carbohydrate Polymers, 2012. **88**: p. 465-473.
100. Hogley, L., et al., *BslA is a self-assembling bacterial hydrophobin that coats the Bacillus subtilis biofilm*. Proceedings of the National Academy of Sciences, 2013. **110**: p. 13600-13605.
101. Diehl, A., et al., *Structural changes of TasA in biofilm formation of Bacillus subtilis*. Proceedings of the National Academy of Sciences, 2017. **115**: p. 3237-3242.
102. Falzone, T.T., et al., *Assembly kinetics determine the architecture of  $\alpha$ -actinin crosslinked F-actin networks*. Nature Communications, 2012. **3**: p. 1-9.
103. Levin, M., et al., *Kinetics of actin networks formation measured by time resolved particle-tracking microrheology*. Soft Matter, 2020. **16**: p. 7869-7876.
104. Deshpande, S. and T. Pfohl, *Hierarchical self-assembly of actin in micro-confinements using microfluidics*. Biomicrofluidics, 2012. **6**: p. 034120.
105. Pollard, T.D., *Mechanism of actin filament self-assembly and regulation of the process by actin-binding proteins*. Biophysical Journal 1986. **49**: p. 149-151.
106. Korn, E.D., M.-F. Carlier, and D. Pantaloni, *Actin polymerization and ATP hydrolysis*. Science, 1987. **238**: p. 638-644.
107. Murakami, K., et al., *Structural basis for actin assembly, activation of ATP hydrolysis, and delayed phosphate release*. Cell, 2010. **143**: p. 275-287.
108. Pezzato, C. and L.J. Prins, *Transient signal generation in a self-assembled nanosystem fueled by ATP*. Nature Communications, 2015. **6**: p. 1-8.
109. te Brinke, E., et al., *Dissipative adaptation in driven self-assembly leading to self-dividing fibrils*. Nature Nanotechnology, 2018. **13**: p. 849-855.
110. Tena-Solsona, M., et al., *Non-equilibrium dissipative supramolecular materials with a tunable lifetime*. Nature Communications, 2017. **8**: p. 1-8.
111. Wang, G. and S. Liu, *Strategies to construct a chemical-fuel-driven self-assembly*. ChemSystemsChem, 2020. **2**: p. e1900046.
112. De, S. and R. Klajn, *Dissipative self-assembly driven by the consumption of chemical fuels*. Advanced Materials, 2018. **30**: p. 1706750.
113. della Sala, F., et al., *Transient self-assembly of molecular nanostructures driven by chemical fuels*. Current opinion in biotechnology, 2017. **46**: p. 27-33.
114. Ragazzon, G. and L.J. Prins, *Energy consumption in chemical fuel-driven self-assembly*. Nature Nanotechnology, 2018. **13**: p. 882-889.
115. Singh, N., et al., *Re-programming hydrogel properties using a fuel-driven reaction cycle*. Journal of the American Chemical Society, 2020. **142**: p. 4083-4087.
116. Dai, K., et al., *Regulating chemically fueled peptide assemblies by molecular design*. Journal of the American Chemical Society, 2020. **142**: p. 14142-14149.

117. Rieß, B., et al., *Dissipative assemblies that inhibit their deactivation*. *Soft Matter*, 2018. **14**: p. 4852-4859.
118. Wanzke, C., et al., *Dynamic vesicles formed by dissipative self-assembly*. *ChemSystemsChem*, 2020. **2**: p. e1900044.
119. Sano, K.I., et al., *Self-repairing filamentous actin hydrogel with hierarchical structure*. *Biomacromolecules*, 2011. **12**: p. 4173-4177.
120. Parente, E., et al., *Alginate production by Azotobacter vinelandii DSM576 in batch fermentation*. *Journal of Industrial Microbiology and Biotechnology*, 1998. **20**: p. 171-176.
121. Takesada, H., H. Yamazaki, and A. Wada, *Nature of Cu (II)-poly(glutamic acid) complex in aqueous solution*. *Biopolymers: Original Research on Biomolecules*, 1966. **4**(7): p. 713-721.
122. Huheey, J.E., E. Keiter, and R. Keiter, *Anorganische Chemie*. 2014, Berlin, Boston: Walter de Gruyter.
123. Kriebisch, B.A.K., et al., *Reciprocal coupling in chemically fueled assembly: A reaction cycle regulates self-assembly and vice versa*. *Journal of the American Chemical Society*, 2020. **142**: p. 20837-20844.
124. Arrojo, B., et al., *Aerobic granulation with industrial wastewater in sequencing batch reactors*. *Water Research*, 2004. **38**: p. 3389-3399.
125. Xu, P., *Analytical solution for a hybrid Logistic-Monod cell growth model in batch and continuous stirred tank reactor culture*. *Biotechnology and Bioengineering*, 2019. **117**: p. 873-878.
126. Mallikarjuna, C. and R.R. Dash, *A review on hydrodynamic parameters and biofilm characteristics of inverse fluidized bed bioreactors for treating industrial wastewater*. *Journal of Environmental Chemical Engineering*, 2020. **8**: p. 104233.
127. Devarapalli, M., et al., *Ethanol production during semi-continuous syngas fermentation in a trickle bed reactor using Clostridium ragsdalei*. *Bioresource Technology*, 2016. **209**: p. 56-65.
128. Jensen, M.B., et al., *Selecting carrier material for efficient biomethanation of industrial biogas-CO<sub>2</sub> in a trickle-bed reactor*. *Journal of CO<sub>2</sub> Utilization*, 2021. **51**: p. 101611.
129. Renaudie, M., et al., *Intensification and optimization of continuous hydrogen production by dark fermentation in a new design liquid/gas hollow fiber membrane bioreactor*. *Chemical Engineering Journal*, 2021. **416**: p. 129068.
130. Mezger, T., *Das Rheologie-Handbuch: für Anwender von Rotations- und Oszillations-Rheometern*. 2000, Hannover, Germany: Curt R. Vincentz Verlag.
131. Pottier, B., et al., *High frequency linear rheology of complex fluids measured from their surface thermal fluctuations*. *Journal of Rheology*, 2013. **57**: p. 441-455.
132. Hyun, K., et al., *A review of nonlinear oscillatory shear tests: Analysis and application of large amplitude oscillatory shear (LAOS)*. *Progress in Polymer Science*, 2011. **26**: p. 1697-1753.
133. Hyun, K., et al., *Large amplitude oscillatory shear as a way to classify the complex fluids*. *Journal of Non-Newtonian Fluid Mechanics*, 2002. **107**: p. 51-65.
134. Parthasarathy, M. and D.J. Klingenberg, *Large amplitude oscillatory shear of ER suspensions*. *Journal of Non-Newtonian Fluid Mechanics*, 1999. **81**: p. 83-104.

135. Sim, H.G., K.H. Ahn, and S.J. Lee, *Three-dimensional dynamics simulation of electrorheological fluids under large amplitude oscillatory shear flow*. Journal of Rheology, 2003. **47**: p. 879-895.
136. Mason, T.G. and D.A. Weitz, *Linear viscoelasticity of colloidal hard sphere suspensions near the glass transition*. Physical Review Letters, 1995. **75**: p. 2770-2773.
137. Bossard, F., M. Moan, and T. Aubry, *Linear and nonlinear viscoelastic behavior of very concentrated plate-like kaolin suspensions*. Journal of Rheology, 2007. **51**: p. 1253-1270.
138. Wyss, H.M., et al., *Strain-rate frequency superposition: A rheological probe of structural relaxation in soft materials*. Physical Review Letters, 2007. **98**: p. 238303.
139. Tirtaatmadja, V., K.C. Tam, and R.D. Jenkins, *Rheological properties of model alkali-soluble associative (HASE) polymers: Effect of varying hydrophobe chain length*. Macromolecules, 1997. **30**: p. 3271-3282.
140. Habenicht, G., *Kleben: Grundlagen, Technologien, Anwendungen*. Vol. 5. 2006, Berlin, Germany: Springer.
141. Lee, H.J. and S. Michielsen, *Lotus effect: Superhydrophobicity*. Journal of the Textile Institute, 2006. **97**: p. 455-462.
142. Wang, J., et al., *Investigation on hydrophobicity of lotus leaf: Experiment and theory*. Plant Science, 2009. **176**: p. 687-695.
143. Bhushan, B. and M. Nosonovsky, *The rose petal effect and the modes of superhydrophobicity*. Philosophical Transactions of the Royal Society A: Mathematical, Physical and Engineering Sciences, 2010. **368**: p. 4713-4728.
144. Klotz, M., et al., *Importance of the biofilm matrix for the erosion stability of Bacillus subtilis NCIB 3610 biofilms*. RSC Advances, 2019. **9**: p. 11521-11529.
145. Kretschmer, M. and O. Lieleg, *Chelate chemistry governs ion-specific stiffening of Bacillus subtilis B-1 and Azotobacter vinelandii biofilms*. Biomaterials Science, 2020. **8**(7): p. 1923-1933.
146. Kretschmer, M., C.A. Schübler, and O. Lieleg, *Biofilm adhesion to surfaces is modulated by biofilm wettability and stiffness*. Advanced Materials Interfaces, 2021. **8**: p. 2001658.
147. Keskin, T., L. Giusti, and N. Azbar, *Continuous biohydrogen production in immobilized biofilm system versus suspended cell culture*. International Journal of Hydrogen Energy, 2012. **37**: p. 1418-1424.
148. Lewis, K., *Persister cells and the riddle of biofilm survival*. Biochemistry (Moscow), 2005. **70**: p. 267-274.
149. Yan, J. and B.L. Bassler, *Surviving as a community: antibiotic tolerance and persistence in bacterial biofilms*. Cell Host & Microbe, 2019. **26**: p. 15-21.
150. Dai, M., et al., *Analysis and imitation of organic sanhetu concrete discovered in an ancient Chinese tomb of Qing dynasty*. Journal of Archaeological Science: Reports, 2019. **26**: p. 101918.
151. Stark, J. and B. Wicht, *Geschichte der Baustoffe*. 1998, Berlin: Bauverlag.
152. Irvine, R.L. and L.H. Ketchum Jr, *Sequencing batch reactors for biological wastewater treatment*. Critical Reviews in Environmental Science and Technology, 1989. **18**: p. 255-294.
153. Münch, E.V., P. Lant, and J. Keller, *Simultaneous nitrification and denitrification in bench-scale sequencing batch reactors*. Water Research, 1996. **30**: p. 277-284.

154. Kunduru, M.R. and A.L. Pometto, *Continuous ethanol production by Zymomonas mobilis and Saccharomyces cerevisiae in biofilm reactors*. Journal of Industrial Microbiology, 1996. **16**: p. 249-256.
155. Ramasamy, E.V. and S.A. Abbasi, *Energy recovery from dairy waste-waters: impacts of biofilm support systems on anaerobic CST reactors*. Applied Energy, 2000. **65**: p. 91-98.
156. Tyagi, R.D. and T.K. Ghose, *Studies on immobilized Saccharomyces cerevisiae. I. Analysis of continuous rapid ethanol fermentation in immobilized cell reactor*. Biotechnology and Bioengineering, 1982. **24**: p. 781-795.
157. Özkaya, B., et al., *Fluidized bed reactor biotechnology for multiple environmental engineering solutions*. Water Research, 2019. **150**: p. 452-465.
158. Sahu, A.K., et al., *Biological perchlorate reduction in packed bed reactors using elemental sulfur*. Environmental Science & Technology, 2009. **43**: p. 4466-4471.
159. Shen, Y., R.C. Brown, and Z. Wen, *Syngas fermentation by Clostridium carboxidivorans P7 in a horizontal rotating packed bed biofilm reactor with enhanced ethanol production*. Applied Energy, 2017. **187**: p. 585-594.
160. Shieh, W.K. and J.D. Keenan, *Fluidized bed biofilm reactor for wastewater treatment*. Bioproducts. 1986, Berlin, Heidelberg: Springer.
161. Tsapekos, P., et al., *Pilot-scale biomethanation in a trickle bed reactor: Process performance and microbiome functional reconstruction*. Energy Conversion and Management, 2021. **244**: p. 114491.
162. Costa, F., B. Silva, and T. Tavares, *Biofilm bioprocesses*. Current Developments in Biotechnology and Bioengineering, 2017: p. 143-175.
163. Melo, L.F., *Biofilm formation and its role in fixed film processes*, in *Handbook of Water and Wastewater Microbiology*, M. Duncan and H. Nigel, Editors. 2003: London, UK. p. 337-349.
164. Taşkan, B., H. Hasar, and C.-H. Lee, *Effective biofilm control in a membrane biofilm reactor using a quenching bacterium (Rhodococcus sp. BH4)*. Biotechnology and Bioengineering, 2019. **117**: p. 1012-1023.
165. Lackner, S., et al., *Enhancing the formation and shear resistance of nitrifying biofilms on membranes by surface modification*. Water Research, 2009. **43**: p. 3469-3478.
166. Terada, A., et al., *Enhancement of biofilm formation onto surface-modified hollow-fiber membranes and its application to a membrane-aerated biofilm reactor*. Water Science and Technology, 2004. **49**: p. 263-268.
167. Yamamoto, K., et al., *Direct solid-liquid separation using hollow fiber membrane in an activated sludge aeration tank*. Water Science and Technology, 1989. **21**: p. 43-54.
168. Muffler, K., et al., *Application of biofilm bioreactors in white biotechnology*, in *Productive Biofilms*, K. Muffler and R. Ulber, Editors. 2014, Springer-Verlag: Berlin Heidelberg. p. 123-161.
169. Bric, J.M., R.M. Bostock, and S.E. Silverstone, *Rapid in situ assay for indoleacetic acid production by bacteria immobilized on a nitrocellulose membrane*. Applied and Environmental Microbiology, 1991. **57**: p. 535-538.
170. Mohammad, A.W., et al., *Hybrid processes: membrane bioreactor*, in *Membrane separation principles and applications*, C.F. Poole, Editor. 2019, Elsevier: Amsterdam. p. 401-470.
171. Ryzhkov, N.V., et al., *Polyelectrolyte substrate coating for controlling biofilm growth at solid-air interface*. Advanced Materials Interfaces, 2021. **8**: p. 2001807.

172. Sarjit, A., S.M. Tan, and G.A. Dykes, *Surface modification of materials to encourage beneficial biofilm formation*. AIMS Bioengineering, 2015. **2**: p. 404-422.
173. Adinarayana, K., et al., *Optimization of process parameters for cephalosporin C production under solid state fermentation from Acremonium chrysogenum*. Process Biochemistry, 2003. **39**: p. 171-177.
174. Godtfredsen, W.O., et al., *Metabolites of Fusidium coccineum*. Tetrahedron, 1979. **35**: p. 2419-2431.
175. Ezra, D., W.M. Hess, and G.A. Strobel, *New endophytic isolates of Muscodor albus, a volatile-antibiotic-producing fungus*. Microbiology, 2004. **150**: p. 4023-4031.
176. Strobel, G., *Muscodor albus and its biological promise*. Journal of Industrial Microbiology and Biotechnology, 2006. **33**: p. 514-522.
177. Bano, N., et al., *Production of bioactive secondary metabolites from endophytic fungi*. International Research Journal of Engineering and Technology, 2016. **3**: p. 1859-1866.
178. Shukla, S.T., et al., *Endophytic microbes: a novel source for biologically/pharmacologically active secondary metabolites*. Asian Journal of Pharmacology and Toxicology, 2014. **2**: p. 1-16.
179. Coban, I. and S. Sargin, *Production of Trichoderma micropropagules as a biocontrol agent in static liquid culture conditions by using an integrated bioreactor system*. Biocontrol Science and Technology, 2019. **29**: p. 1197-1214.
180. Coşkuntuna, A. and N. Özer, *Biological control of onion basal rot disease using Trichoderma harzianum and induction of antifungal compounds in onion set following seed treatment*. Crop Protection, 2007. **27**: p. 330-336.
181. Lee, S.-Y., et al., *Cultivation of entomopathogenic fungi for the search of antibacterial compounds*. Mycopathologia, 2005. **160**: p. 321-325.
182. Zimmermann, G., *Review on safety of the entomopathogenic fungus Metarhizium anisopliae*. Biocontrol Science and Technology, 2007. **17**: p. 879-920.
183. Kretschmer, M., et al., *Viscoelastic behavior of chemically fueled supramolecular hydrogels under load and influence of reaction side products*. Communications Materials, 2021. **2**: p. 1-10.
184. Rieß, B., R.K. Grötsch, and J. Boekhoven, *The design of dissipative molecular assemblies driven by chemical reaction cycles*. Chem, 2020. **6**: p. 552-578.
185. Orbach, R., et al., *The rheological and structural properties of Fmoc-peptide-based hydrogels: The effect of aromatic molecular architecture on self-assembly and physical characteristics*. Langmuir, 2012. **28**: p. 2015-2022.
186. Adams, D.J., et al., *Relationship between molecular structure, gelation behaviour and gel properties of Fmoc-dipeptides*. Soft Matter, 2010. **6**: p. 1971-1980.
187. Boekhoven, J., et al., *Transient assembly of active materials fueled by a chemical reaction*. Science, 2015. **349**: p. 1075-1079.
188. Sorrenti, A., et al., *Non-equilibrium steady states in supramolecular polymerization*. Nature Communications, 2017. **8**: p. 1-8.
189. Bridier, A., et al., *Resistance of bacterial biofilms to disinfectants: a review*. Biofouling, 2011. **27**: p. 1017-1032.
190. Hayta, E.N. and O. Lieleg, *Biopolymer-enriched B. subtilis NCIB 3610 biofilms exhibit increased erosion resistance*. Biomaterials science, 2019. **7**: p. 4675-4686.



191. Pavlovsky, L., J.G. Younger, and M.J. Solomon, *In situ rheology of Staphylococcus epidermidis bacterial biofilms*. *Soft Matter*, 2013. **9**: p. 122-131.
192. Di Stefano, A., et al., *Viscoelastic properties of Staphylococcus aureus and Staphylococcus epidermidis mono-microbial biofilms*. *Microbial Biotechnology*, 2009. **2**(6): p. 634-641.
193. Stojković, B., et al., *Viscoelastic properties of levan-DNA mixtures important in microbial biofilm formation as determined by micro-and macrorheology*. *Biophysical Journal*, 2015. **108**: p. 758-765.
194. Graham, M.V., et al., *Development of antifouling surfaces to reduce bacterial attachment*. *Soft Matter*, 2013. **9**: p. 6235-6244.
195. Shen, L., et al., *Efficient surface ionization and metallization of TFC membranes with superior separation performance, antifouling and anti-bacterial properties*. *Journal of Membrane Science*, 2019. **586**: p. 84-97.
196. Winkeljann, B., et al., *Covalent mucin coatings form stable anti-biofouling layers on a broad range of medical polymer materials*. *Advanced Materials Interfaces*, 2020. **7**: p. 1902069.
197. Clasen, A. and A.B. Kesel, *Microstructural surface properties of drifting seeds—a model for non-toxic antifouling solutions*. *Biomimetics*, 2019. **4**: p. 1-14.
198. Kargar, M., et al., *Controlling bacterial adhesion to surfaces using topographical cues: a study of the interaction of Pseudomonas aeruginosa with nanofiber-textured surfaces*. *Soft Matter*, 2012. **8**: p. 10254-10259.
199. Srinivasan, R., I.M. Nambi, and J. Senthilnathan, *Liquid crystal display electrode assisted bio-reactor for highly stable and enhanced biofilm attachment for wastewater treatment—a sustainable approach for e-waste management*. *Chemical Engineering Journal*, 2019. **358**: p. 1012-1021.
200. Hadjiev, D., et al., *Enhancement of the biofilm formation on polymeric supports by surface conditioning*. *Enzyme and microbial technology*, 2006. **40**: p. 840-848.
201. Busscher, H.J. and A.H. Weerkamp, *Specific and non-specific interactions in bacterial adhesion to solid substrata*. *FEMS Microbiology Reviews*, 1987. **46**: p. 165-173.
202. Andersson, S., et al., *Biofilm formation and interactions of bacterial strains found in wastewater treatment systems*. *FEMS Microbiology Letters*, 2008. **283**: p. 83-90.
203. Giraud, N., et al., *Passivation of hydrated cement*. *ACS Sustainable Chemistry & Engineering*, 2018. **6**: p. 727-737.
204. Glasser, F.P., J. Marchand, and E. Samson, *Durability of concrete—Degradation phenomena involving detrimental chemical reactions*. *Cement and Concrete Research*, 2008. **38**: p. 226-246.
205. von der Ecken, J., et al., *Structure of the F-actin-tropomyosin complex*. *Nature*, 2015. **519**: p. 114-117.
206. Shi, L., et al., *Self-healing polymeric hydrogel formed by metal–ligand coordination assembly: design, fabrication, and biomedical applications*. *Macromolecular Rapid Communications*, 2019. **40**: p. 1800837.
207. Li, Q., et al., *Controlling hydrogel mechanics via bio-inspired polymer–nanoparticle bond dynamics*. *ACS Nano*, 2015. **10**: p. 1317-1324.
208. Shi, L., et al., *Dynamic coordination chemistry enables free directional printing of biopolymer hydrogel*. *Chemistry of Materials* 2017. **29**: p. 5816-5823.

209. Nejadnik, M.R., et al., *Self-healing hybrid nanocomposites consisting of bisphosphonated hyaluronan and calcium phosphate nanoparticles*. *Biomaterials*, 2014. **35**: p. 6918-6929.
210. Grindy, S.C., et al., *Control of hierarchical polymer mechanics with bioinspired metal-coordination dynamics*. *Nature Materials*, 2015. **14**: p. 1210-1216.
211. Casuso, P., et al., *Injectable and self-healing dynamic hydrogels based on metal (I)-thiolate/disulfide exchange as biomaterials with tunable mechanical properties*. *Biomacromolecules*, 2015. **16**: p. 3552-3561.
212. Wei, Z., et al., *Autonomous self-healing of poly (acrylic acid) hydrogels induced by the migration of ferric ions*. *Polymer Chemistry*, 2013. **4**: p. 4601-4605.
213. Holten-Andersen, N., et al., *pH-induced metal-ligand cross-links inspired by mussel yield self-healing polymer networks with near-covalent elastic moduli*. *Proceedings of the National Academy of Sciences*, 2011. **108**: p. 2651-2655.
214. Wang, W., et al., *Zinc induced polyelectrolyte coacervate bioadhesive and its transition to a self-healing hydrogel*. *RSC Advances*, 2015. **5**: p. 66871-66878.
215. Gao, Z., et al., *Mussel-inspired tough hydrogels with self-repairing and tissue adhesion*. *Applied Surface Science*, 2018. **427**: p. 74-82.

## **E. Acknowledgements**

An dieser Stelle möchte ich mich bei allen bedanken, die mich bei meiner Dissertation unterstützt und auf meinem Weg begleitet haben.

Ein besonderer Dank gilt meinem Doktorvater Prof. Dr. Oliver Lieleg. Ich bedanke mich für den großen fachlichen Input und die vielen konstruktiven Diskussionen. Jedes Projekt hatte seine eigenen Höhen und Tiefen, und ich möchte mich für die Motivierung und Unterstützung in jeder Lage bedanken, ohne die ich vermutlich noch heute an dem ersten Paper arbeiten würde. Ich bedanke mich auch für die intensiven sprachlichen Hilfestellungen, die mir geholfen haben meine Englischkenntnisse deutlich zu verbessern.

Des Weiteren bedanke ich mich bei meinen Kollegen der AG Lieleg für die gemeinsame und unvergessliche Zeit, ohne euch wäre meine Doktorandenzeit nicht halb so schön gewesen. Auch für die fachlichen Konversationen und Hilfestellungen, vielen Dank Maria Bauer, Marvin Ertelt, Dr. Carolina Falcón García, Elif Nur Hayta, Ceren Kimna, Theresa Lutz, Matthias Marczynski, Carolin Rickert, Dr. Jian Song und Dr. Benjamin Winkeljann! Ein besonderer Dank gilt hierbei den Kollegen, mit denen gemeinsame Projekte und Veröffentlichungen realisiert wurden. Für die gute Zusammenarbeit möchte ich mich bei Benjamin, Carolina, Marvin und Elif bedanken!

Für die gute Zusammenarbeit in den unterschiedlichsten Projekten bedanke ich mich auch bei Dr. Alexandra Götz und Prof. Dr. Madeleine Opitz von der LMU, bei Brigitte Kriebisch, Michaela Würbser, Dr. Jennifer Rodon-Fores und Prof. Dr. Job Boekhoven vom Chemiedepartment der TUM, sowie bei Dr. Hongji Yan und Prof. Dr. Thomas Crouzier von der KTH.

Darüber hinaus möchte ich mich für die praktischen und administrativen Hilfestellungen bei Iris König-Decker, Christine Braig, Gabriele Kronenwetter, Tobias Fuhrmann und Rudolf Lehrhuber bedanken.

Ein besonderer Dank geht auch an die Studierenden Jonas Reinelt, Bernardo Miller Naranjo und Carina Schüssler, die ich bei ihren Studienarbeiten begleiten durfte und die mich mit ihren Arbeiten bei meinen Projekten unterstützt haben. Besonders freut mich, dass Bernardo den Entschluss gefasst hat für seine Promotion in der Arbeitsgruppe weiterzumachen. Ich wünsche euch an dieser Stelle viel Erfolg für euren weiteren Weg!

Schließlich gilt ein weiterer großer Dank meiner Familie für die großartige Unterstützung während meines gesamten Werdegangs und dass ihr immer an mich geglaubt habt. Ohne eure Motivationen und Aufheiterungen wäre das alles nicht möglich gewesen!